

## Table of Contents

16 September 2005

Volume 309

Number 5742



### NEW THIS WEEK:

[Science in Iran](#)

[Adaptive Insect Immunity?](#)

[Stronger Hurricanes to Come?](#)

[Mouse Hormone Prolongs Life](#)

▶ [Editors' Choice](#)

▶ [NetWatch](#)

▶ [ScienceScope](#)

▶ [Random Samples](#)

▶ [New Products](#)

▶ [Science Online Contents](#)

### Research

[This Week in Science](#)

[Brevia](#)

[Research Articles](#)

[Reports](#)

### News

[News Summaries](#)

[News of the Week](#)

[News Focus](#)

### Commentary

[Editorial](#)

[Letters](#)

[Policy Forum](#)

[Book Reviews](#)

[Perspectives](#)

## RESEARCH

### This Week in *Science*

Blow Me Down \* Klotho for Eternal Youth? \* Right After the Burst \* Stronger Under Pressure \* Adaptive Immunity in Insects? \* Rings of Uranium \* Connecting Craters \* Evolving Sequence and Expression \* Protein Sequence Structure Prediction \* Temporal Controls in Inflammatory Responses \* SARS Spike, Up Close and Personal \* New Salt \* Two Ways to Longer Life (for Yeast) \* DNA Damage Comes to Light  
1785

### Editors' Choice: Highlights of the recent literature

MATERIALS SCIENCE: Large Nanotemplates \* IMMUNOLOGY: Diabetes on Display \* BIOCHEMISTRY: Some Like It Briny \* PSYCHOLOGY: A Cooling-Off Period \* ECOLOGY/EVOLUTION: Bleaching in Hot Water \* CHEMISTRY: Site-Specific Catalysis \* STKE: Fateful Feedback 1790

### Brevia

#### Characterization of a *Phytophthora* Mating Hormone

Jianhua Qi, Tomoyo Asano, Masashi Jinno, Kouhei Matsui, Keisuke Atsumi, Youji Sakagami, and Makoto Ojika 1828.

### Research Article

#### Suppression of Aging in Mice by the Hormone Klotho

Hiroshi Kurosu, Masaya Yamamoto, Jeremy D. Clark, Johanne V. Pastor, Animesh Nandi, Prem Gurnani, Owen P. McGuinness, Hiroataka Chikuda, Masayuki Yamaguchi, Hiroshi Kawaguchi, Iichiro Shimomura, Yoshiharu Takayama, Joachim Herz, C. Ronald Kahn, Kevin P. Rosenblatt, and Makoto Kuro-o 1829-1833.

### Reports

#### Bright X-ray Flares in Gamma-Ray Burst Afterglows

D. N. Burrows, P. Romano, A. Falcone, S. Kobayashi, B. Zhang, A. Moretti, P. T. O'Brien, M. R. Goad, S. Campana, K. L. Page, L. Angelini, S. Barthelmy, A. P. Beardmore, M. Capalbi, G. Chincarini, J. Cummings, G. Cusumano, D. Fox, P. Giommi, J. E. Hill, J. A. Kennea, H. Krimm, V. Mangano, F. Marshall, P. Mészáros, D. C. Morris, J. A. Nousek, J. P. Osborne, C. Pagani, M. Perri, G. Tagliaferri, A. A. Wells, S. Woosley, and N. Gehrels 1833-1835.

#### Molecular Octa-Uranium Rings with Alternating Nitride and Azide Bridges

William J. Evans, Stosh A. Kozimor, and Joseph W. Ziller 1835-1838.

#### Ultra-high Strength in Nanocrystalline Materials Under Shock Loading

Eduardo M. Bringa, Alfredo Caro, Yinmin Wang, Maximo Victoria, James M. McNaney, Bruce A. Remington, Raymond F. Smith, Ben R. Torralva, and Helena Van Swygenhoven 1838-1841.

#### Influence of the Atlantic Subpolar Gyre on the Thermohaline Circulation

Hjálmar Hátún, Anne Britt Sandø, Helge Drange, Bogi Hansen, and Heðinn Valdimarsson 1841-1844.

#### Changes in Tropical Cyclone Number, Duration, and Intensity in a Warming Environment

P. J. Webster, G. J. Holland, J. A. Curry, and H.-R. Chang 1844-1846.

### The Origin of Planetary Impactors in the Inner Solar System

Robert G. Strom, Renu Malhotra, Takashi Ito, Fumi Yoshida, and David A. Kring 1847–1850.

### Parallel Patterns of Evolution in the Genomes and Transcriptomes of Humans and Chimpanzees

Philipp Khaitovich, Ines Hellmann, Wolfgang Enard, Katja Nowick, Marcus Leinweber, Henriette Franz, Gunter Weiss, Michael Lachmann, and Svante Pääbo 1850–1854.

### Achieving Stability of Lipopolysaccharide-Induced NF- $\kappa$ B Activation

Markus W. Covert, Thomas H. Leung, Jahlionais E. Gaston, and David Baltimore 1854–1857.

### Stimulus Specificity of Gene Expression Programs Determined by Temporal Control of IKK Activity

Shannon L. Werner, Derren Barken, and Alexander Hoffmann 1857–1861.

### *HST2* Mediates *SIRT2*-Independent Life-Span Extension by Calorie Restriction

Dudley W. Lamming, Magda Latorre-Esteves, Oliver Medvedik, Stacy N. Wong, Felicia A. Tsang, Chen Wang, Su-Ju Lin, and David A. Sinclair 1861–1864.

### Structure of SARS Coronavirus Spike Receptor-Binding Domain Complexed with Receptor

Fang Li, Wenhui Li, Michael Farzan, and Stephen C. Harrison 1864–1868.

### Toward High-Resolution de Novo Structure Prediction for Small Proteins

Philip Bradley, Kira M. S. Misura, and David Baker 1868–1871.

### Azathioprine and UVA Light Generate Mutagenic Oxidative DNA Damage

Peter O'Donovan, Conal M. Perrett, Xiaohong Zhang, Beatriz Montaner, Yao-Zhong Xu, Catherine A. Harwood, Jane M. McGregor, Susan L. Walker, Fumio Hanaoka, and Peter Karran 1871–1874.

### Extensive Diversity of Ig-Superfamily Proteins in the Immune System of Insects

Fiona L. Watson, Roland Püttmann-Holgado, Franziska Thomas, David L. Lamar, Michael Hughes, Masahiro Kondo, Vivienne I. Rebel, and Dietmar Schmucker 1874–1878.

## COMMENTARY

### Editorial

#### Climate Equity for All

Chris Huntingford and John Gash 1789.

### Letters

A Strongly Held, But Wrong Conviction *Richard G. Pearson* ; Early Uses of the Ivory-Billed Woodpecker *Alex Barker* ; Are Polar Bears Threatened? *Oystein Wiig* ; Using Words Carefully *William H. Danforth and William B. Neaves* ; The Slide of Education *Leonid Teytelman* ; An Archaeological Dilemma *David I. Owen* ; Corrections and Clarifications 1814.

### Policy Forum

#### CLIMATE:

#### Enhanced: A Madisonian Approach to Climate Policy

David G. Victor, Joshua C. House, and Sarah Joy 1820–1821.

### Books *et al.*

#### ASTRONOMY:

#### People, Stars, and Scopes

Vera Rubin 1817–1818.

#### GEOLOGY:

#### The Grand Question

John C. Schmidt 1818–1819.

Books Received 1818.

### Perspectives

#### STRUCTURAL BIOLOGY:

#### Adaptation of SARS Coronavirus to Humans

Kathryn V. Holmes 1822–1823.

#### CHEMISTRY:

#### Bridging a Gap in Actinide Chemistry

Carol J. Burns 1823–1824.

#### CHEMISTRY:

#### Palladium-Catalyzed Oxidation of Organic Chemicals with O<sub>2</sub>

Shannon S. Stahl 1824–1826.

#### IMMUNOLOGY:

#### Insects Diversify One Molecule to Serve Two Systems

Louis Du Pasquier 1826–1827.

## NEWS

### News of the Week

#### TEACHING EVOLUTION:

#### ID Goes on Trial This Month in Pennsylvania School Case

Constance Holden 1796.

#### INTELLECTUAL PROPERTY:

#### Court Tightens Patent Rules on Gene Tags

Eli Kintisch 1797–1799.

**PLANETARY SCIENCE:**

**Beaming to Itokawa**

Richard A. Kerr 1797.

**RESEARCH MISCONDUCT:**

**China Science Foundation Takes Action Against 60 Grantees**

Gong Yidong 1798-1799.

**RUSSIAN SCIENCE:**

**Government Offers Pay Raise, but Demands Reform**

Andrey Allakhverdov and Vladimir Pokrovsky 1798.

**PEDIATRIC MEDICINE:**

**Europe Follows U. S. in Testing Drugs for Children**

Xavier Bosch 1799.

**PLANETARY SCIENCE:**

**Another Hint of Planetary Marauders**

Richard A. Kerr 1800.

**BIOETHICS:**

**Pellegrino to Succeed Kass on U. S. Panel**

Constance Holden 1800.

**THEORETICAL PHYSICS:**

**To Escape From Quantum Weirdness, Put the Pedal to the Metal**

Adrian Cho 1801.

**News Focus**

**SCIENCE IN IRAN:**

**An Islamic Science Revolution?**

Richard Stone 1802-1804.

**SCIENCE IN IRAN:**

**Attack of the Killer Jellies**

Richard Stone 1805-1806.

**SCIENCE IN IRAN:**

**The Sturgeon's Last Stand**

Richard Stone 1806.

**ATMOSPHERIC SCIENCE:**

**Is Katrina a Harbinger of Still More Powerful Hurricanes?**

Richard A. Kerr 1807.

**HURRICANE KATRINA:**

**Scientists Weigh Options for Rebuilding New Orleans**

John Bohannon and Martin Enserink 1808-1809.

**HURRICANE KATRINA:**

**Questioning the 'Dutch Solution'**

Martin Enserink and John Bohannon 1809.

**AMERICAN CHEMICAL SOCIETY MEETING:**

**Safer Alternative Could Replace Widespread Contaminant**

Robert F. Service 1810.

**AMERICAN CHEMICAL SOCIETY MEETING:**

**New Techniques Aim to Thwart Terrorists**

Yudhijit Bhattacharjee 1810-1811.

**AMERICAN CHEMICAL SOCIETY MEETING:**

**New Routes Toward Practical Hydrogen?**

Robert F. Service 1811.

**Products**

**New Products** 1879.

**NetWatch**

**DATABASE: To Know the Worm \* COMMUNITY SITE: Focus on a Killer \* RESOURCES: Breaking the Patent Barrier \* RESOURCES: Making Light Coherent \* DATABASE: Eating Pollution** 1795

**ScienceScope**

**Audit Slams French Research \* U. S. to Bar Caviar \* EPA Revises Pesticide Human Testing Rules \* Hall In ... \* ... Dale Too ... \* ... And Klausner Out** 1799

**Random Samples**

**Egypt in China \* Crème de la Crème \* A Choir of Wrens \* Renewables in the Doldrums \* Survivors \* Politics \* Awards \* They Said It** 1812

## Climate Equity for All

**R**ecent natural catastrophes have catapulted climate into the headlines again. As we witness the devastation wreaked by Hurricane Katrina, we are also reminded of numerous floods, droughts, and storms seen across the world in recent years. Are these linked to climate change? Questions about climate change, its global effects, and whether and how we can tackle this issue can no longer be avoided. Fortunately, this summer at the G8 Summit in Scotland, the leaders of the world's major industrialized nations agreed on the need to reduce carbon emissions; and although there is argument about the mechanism and timing, the case for moving to a low-carbon economy is essentially won. But we are faced with a rapidly changing global economy. As developing countries industrialize—China and India in Asia and Brazil and Mexico in Latin America—greenhouse gas-related climate stresses are expected to increase. At the same time, the environments, economies, and societies of the least-developed countries, such as those in Africa, are the most vulnerable to climate change because their ability to adapt is poor. Reaching international agreement on actions to minimize the dangerous impacts of climate change requires not only negotiations among developed nations but dialogue with the developing world. How do we involve these developing countries in the ongoing climate change discussions, and what information is needed to inform both developing-country policies and international decisions?

Local scientists could help formulate developing-country perspectives on climate change by conducting regional climate model experiments. These are essentially high-resolution weather forecast models that are used to calculate the environmental impacts of predicted changed weather patterns. Only when there are estimates of the economic and social impacts of changes in flood and drought frequency can possible increases in global mean temperature be translated into estimates of changes in food security and livelihoods. Scientists in the developing countries concerned are best placed to undertake these detailed local analyses. This work would also provide incentives to governments to maintain the long-term climate data sets that are needed for verification of climate simulations at the present levels of greenhouse gas concentrations.

Technologies to run modeling experiments are now being made available to scientists in developing countries. But this initial technical capacity is of little use without the human scientific capacity to design and interpret the experiments. Creating this expertise is a long process that, for each individual, requires continual personal development in a vibrant research environment. There is strong argument for concentrating scientists at centers of excellence in the developing world. When Carlos Nobre directed the Brazilian Center for Weather Forecasting and Climate Research in the 1990s, he initiated collaborations with experts in the United Kingdom and United States, building a critical mass of local expertise. As a result, Brazil now includes climate change in its long-term planning for economic and land use development.

Earlier this year, speakers at a Royal Society meeting in London indicated that climate change is likely to increase the frequency of crop failure in Africa. Other research presented this month at the British Association's Festival of Science in Dublin warned that an extra 50 million people will be at risk of hunger by 2050, and the majority of these will be in Africa. This alarming forecast begs for an Africa-based research program to investigate the possible impacts of regional climate change.

This need to strengthen climate change research in the developing world can be filled by establishing regional centers of excellence in developing countries and arranging training, staff exchanges, and shared research projects with developed nations. The Global Environment Facility, which provides grants to developing countries for projects that benefit the environment, has a mandate to address the issue of climate change. It is well placed to fund this initiative by either financing new institutions or strengthening and expanding existing organizations. The African Centre of Meteorological Application for Development, a pan-African center located in Niger, is one clear candidate for this role.

Developing countries need to become more engaged and empowered in the international negotiations on managing global climate change. This should be done quickly if we are to outrun the pace of that change.

**Chris Huntingford and John Gash**

Chris Huntingford and John Gash are at the Centre for Ecology and Hydrology, Wallingford, UK.



## Klotho for Eternal Youth?

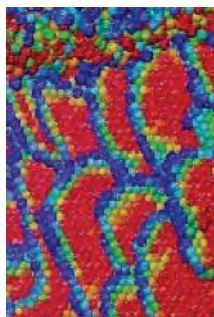
A defect in Klotho gene expression in mice leads to a syndrome resembling aging. **Kurosu *et al.*** (p. 1829, published online 25 August 2005; see the 26 August news story by **Couzin**) now find that Klotho overexpression extends life span in mice. Klotho protein functions as a circulating hormone that binds to a cell-surface receptor and suppresses insulin and insulin-like growth factor-1 (IGF-1) signaling in an evolutionarily conserved mechanism for extending life span in worms, flies, and mice. Furthermore, perturbing insulin/IGF-1 signaling slows aging in Klotho-deficient mice. Thus, it appears that Klotho protein may function as an antiaging hormone.

## Right After the Burst

Apart from the Big Bang, gamma-ray bursts are the most powerful explosions in the universe and are thought to be massive stars collapsing to form black holes. Such events are followed by an extended afterglow over a range of wavelengths from x-rays down to radio frequencies. In the past, the afterglows were only detected several hours after the event, which resulted in missed opportunities to study this important phase of the burst. **Burrows *et al.*** (p. 1833, published online 18 August 2005) report their detection of energetic x-ray flares in the afterglows of recent gamma-ray bursts with the Swift x-ray telescope. The flares appear to be evidence of strong shock waves and extended activity in the central region of the burst.

## Stronger Under Pressure

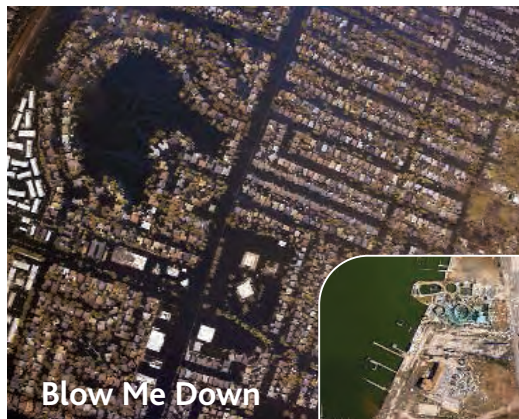
For certain applications, materials need to be designed to sustain extreme shocks, as might be experienced, for example, at national ignition facilities; some nanocrystalline materials are showing promise. **Bringa *et al.*** (p. 1838) report molecular dynamics simulations on nanocrystalline copper subjected to shock loading. At high pressures, the active deformation mechanisms change from those that are thermally activated to those that are pressure mediated. The results show that the copper strengthens because grain boundary sliding is suppressed by the pressure. Experiments on nanocrystalline nickel confirm the behavior seen in the simulations.



## Adaptive Immunity in Insects?

Refined and complex genetic mechanisms generate huge levels of diversity in the B cell and T cell receptors of the adaptive immune system, but this diversity generation has been thought to be restricted to some higher vertebrates. **Watson *et al.*** (p. 1874, published online 18 August 2005; see the Perspective by **Du Pasquier**) now describe a mechanism of alternative splicing

of *Dscam*, a single gene locus in insects, that has the potential to generate an exceptional level of protein diversity. Originally identified as a neuronal receptor, splice products of this gene were also found in various immune tissues of *Drosophila*. Functional studies suggest that some isotypes of *Dscam* could assist in the phagocytosis of bacteria, pointing to a direct and adaptable form of insect immunity.



Blow Me Down

It has been suggested that global warming could lead to an increase in the general level of storminess. Evidence that such an effect is occurring has been elusive, however, and the links between increasing atmospheric and sea surface temperatures and hurricane activity have been debated. **Webster *et al.*** (p. 1844; see news story by **Kerr**) examine the frequency and strength of tropical storms and hurricanes worldwide during the past 35 years. Although there has not been an increase in the number or frequency of events, the proportion of hurricanes reaching the most energetic categories increased significantly, particularly in the Pacific and Indian Oceans.



## Rings of Uranium

The actinide elements are well known for their nuclear instability, which leads to radioactivity and atomic energy applications. However, they also engage in unusual chemical bonding, resulting from their occupied f-orbitals and the relativistic effects of their high nuclear charge, allowing unusual compounds to be formed and studied. **Evans *et al.*** (p. 1835; see the Perspective by **Burns**) have isolated and characterized a ring of eight uranium atoms connected through alternating nitride and azide ( $N_3$ ) groups. Prepared by mixing an organo-uranium precursor with sodium azide in solution, the compound sheds light on molecular uranium-nitride bonding and also models the electronics of extended lattice uranium nitride materials.

## Connecting Craters

The record of impact cratering observed on the Moon and Mars, calibrated with age determinations from Apollo samples, is the primary means for dating surfaces on the terrestrial planets. **Strom *et al.*** (p. 1847; see news story by **Kerr**) have reexamined the distribution of sizes of craters, inferred the sizes of causative asteroids, and show that an older population of craters, before about 3.8 billion years ago, has the same distribution as observed asteroids in the main asteroid belt. Younger craters seem to be caused by near-Earth asteroids. These data imply that a process early in the history of the solar system, perhaps outward migration of the giant planets, ejected asteroids from the main belt, but that this process ceased about 3.8 billion years ago.

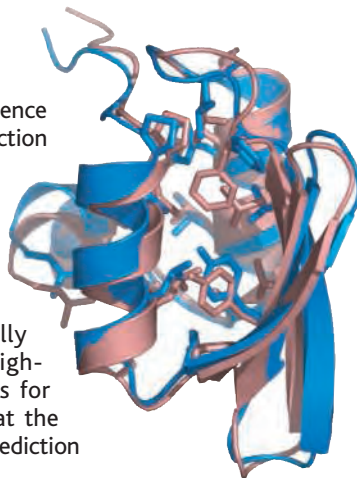
CONTINUED ON PAGE 1787

## Evolving Sequence and Expression

An analysis of the evolution of both gene sequences and expression patterns in humans and chimpanzees by **Khaitovich *et al.*** (p. 1850, published online 1 September 2005; see the 2 September Editorial by **Jolly**, the Perspectives by **Hauser** and by **McConkey and Varki**, and the news story by **Culotta**) show that in the brain, heart, liver, kidneys, and testes, the general patterns of evolution conform to a neutral theory. Similar patterns of selection were seen for protein sequence and gene expression. Genes that are expressed in more tissues have diverged less between species than genes expressed in fewer tissues, which suggests neutral evolution with negative selections, but genes on the X chromosome that are expressed in testes showed evidence of positive selection. Surprisingly, genes expressed in the brain have changed more on the human lineage than on the chimpanzee lineage, not only in terms of gene expression but also in terms of amino acid sequences.

## Protein Sequence Structure Prediction

It has long been known that the amino acid sequence of a protein defines its structure; however, the prediction of structure from sequence remains a challenge. Now **Bradley *et al.*** (p. 1868) have achieved high-resolution structure prediction (<1.5 angstrom) for 5 sequences in a test set of 16 small protein domains (<85 residues). These results were obtained using a combination of improved conformational sampling methods, a physically realistic all-atom free-energy function, and high-performance computing. The free-energy basins for native structures are very narrow, suggesting that the primary bottleneck to consistent high-resolution prediction is conformational sampling.



## Temporal Controls in Inflammatory Responses

Understanding control of cellular regulation requires not only a description of the signaling events and mediators involved, but also an understanding of the temporal properties of how signals are generated and sensed. **Covert *et al.*** (p. 1854) and **Werner *et al.*** (p. 1857) now provide insight into temporal control of signals that control the activity of a key mediator of inflammatory responses, the transcription factor NF- $\kappa$ B. Signals from the receptor for the inflammatory cytokine tumor necrosis factor or from the Toll-like receptor 4 (TLR4), which recognizes bacterial lipopolysaccharide, result in either oscillating or stable patterns of NF- $\kappa$ B activity, respectively, which in turn lead to distinct patterns of gene expression. Computational models and biochemical analysis reveal the regulatory events that produce the distinct temporal patterns of NF- $\kappa$ B activity. The stable signal produced by activation of TLR4 appears to result from activation of two signaling pathways—a rapid one, and a slower one that requires protein synthesis and autocrine signaling.

## SARS Spike, Up Close and Personal

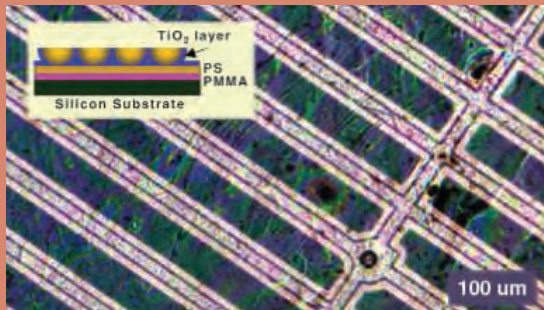
The SARS coronavirus causes severe acute respiratory syndrome (SARS), which has a fatality rate of about 10%. Attachment to human cells is through a spike protein on the viral surface that binds to a cell-surface zinc peptidase, angiotensin-converting enzyme (ACE2). Now **Li *et al.*** (p. 1864; see the Perspective by **Holmes**) have determined the structure of the SARS coronavirus spike protein receptor-binding domain bound to the peptidase domain of human ACE2 at 2.9 angstrom resolution. The details of the interface suggest how a few residue changes led to efficient cross-species infection and human-to-human transmission in the 2002–2003 SARS outbreak. The structure could guide design of receptor-binding domain variants in the development of an effective SARS vaccine.

edited by Gilbert Chin

### MATERIALS SCIENCE

#### Large Nanotemplates

A nanoscale template (for making materials and devices) can be created by coating an array of closely packed particles, but it often is difficult to handle such a film without tearing it, because it is, in essence, a thin ceramic sheet. Wang *et al.* report on the formation of transferable and reusable TiO<sub>2</sub> "nanobowl" templates. They coated a silicon substrate with a 300-nm-thick film of poly(methyl methacrylate) (PMMA) and then applied a 100-nm-thick film of polystyrene (PS). Next, a monolayer of 500-nm-diameter PS spheres was loaded onto the composite film from a water surface, and topped off with a 25-nm-thick coating of TiO<sub>2</sub> via atomic layer deposition. Ion milling removed the top half of the spheres, and the PMMA was dissolved with acetone to free the film from the silicon substrate. Finally, the nanobowl film could be freed completely by removing the PS with toluene. These films (as large as 10 mm<sup>2</sup>) were lifted with a copper mesh support and examined in a transmission electron microscope, which revealed that the bottoms of the TiO<sub>2</sub> bowls have a 100-nm opening. The films could then be used as templates to create a regular array of 100-nm gold dots, spaced 500 nm apart. — PDS



A nanobowl sheet on a copper grid and a schematic (inset) of the fabrication.

*Nano. Lett.* 10.1021/nl051389x (2005).

7 January 2005). This enzyme reversibly adopts three quaternary structures: (i) a 104-kD monomer in standard buffer; (ii) a heterodimer of 21- and 85-kD chains upon disulfide reduction; and (iii) a 325-kD trimer under high pressure (20 MPa), high salt (3.5 M NaCl), and a reducing agent. In a fashion consistent with the ionic and anoxic conditions 3500 m below sea level, the activity of the trimer is maximal and about 700 times that of the monomer. Furthermore, in terms of its potential use in chemical synthesis, O.16 is stable in a variety of nonpolar and polar solvents. — GJC

*Chem. Biol.* 12, 895 (2005).

### PSYCHOLOGY

#### A Cooling-Off Period

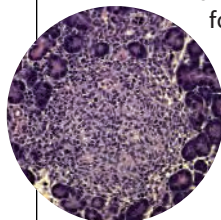
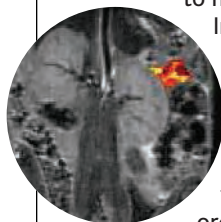
In interpersonal situations, conflicts are inevitable and tempers can flare, sometimes with long-lasting and deleterious consequences for one's psyche. Coming to grips with emotional upset has been pursued via talk-based therapies, and Kross *et al.* suggest one way that these interventions might be focused for greater benefit. Translating negative experiences into abstract or intellectualized representations may run the risk of suppressing and avoiding the very reasons for the distress, yet opening the door to reliving the emotionally troubling events may lead to destructive and iterative rumination. In two experiments, the authors show that adopting the viewpoint of an observer while continuing to attend fully to the affective components of the experience can help to process negative emotions, perhaps by yoking the autonomic arousal system (hot) to cognitive control circuits (cool). — GJC

*Psychol. Sci.* 16, 709 (2005).

### IMMUNOLOGY

#### Diabetes on Display

Autoimmune conditions, such as type 1 diabetes, are unpredictable and difficult to manage.



Pancreatic infiltration (top) and islet histology (bottom).

Improvements in treatment will depend on better noninvasive monitoring of those at risk in order to enable forecasting of disease onset, sensitive and accurate screening for changes in disease status,

and prediction of how the condition in a given individual might respond to treatment. Turvey *et al.* used magnetic resonance imaging (MRI) of mouse models of type 1

diabetes, in which the accumulation of a biocompatible superparamagnetic nanoparticle was used to detect changes in microvascular permeability that accompany autoimmune-induced pancreatic inflammation. In the NOD mouse, MRI measures of increased vascular leakage correlated with diabetes close to the time of disease onset, but were not as useful in longer-range prognosis. In a therapeutic setting in which T cell tolerance was achieved using antibody to CD3, prediction of therapeutic efficacy was possible, with low vascular leakage values corresponding to a favorable response to therapy, reflected by normal-range blood glucose levels. Similar noninvasive monitoring using magnetic nanoparticles is already being assessed in the clinic for lymph node metastases, and these experimental studies suggest that their use in organ-specific autoimmune conditions may also be feasible. — SJS

*J. Clin. Invest.* 115, 2454 (2005).

### BIOCHEMISTRY

#### Some Like It Briny

Recent expeditions have exploited the power of metagenomics to prospect in harsh and hazardous environments for unusual and useful microbial molecules. Ferrer *et al.* have sampled a deep-sea hypersaline anoxic basin (DHAB) in the eastern Mediterranean, and then nurtured microbial growth by feeding with Arabian light crude. They have isolated a remarkable esterase, cataloged as O.16 (for more on DHAB microbes, see van der Wielen *et al.*, Reports, p. 121,

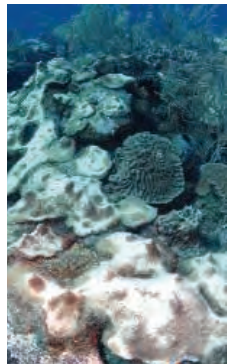


The RV *Urania*.

## ECOLOGY/EVOLUTION

### Bleaching in Hot Water

When corals lose their symbiotic algae, they bleach. Coral bleaching is known to be caused by a number of factors such as increased salinity, disease, or increased sea surface temperature (SST). The relationship with SST, in particular, has raised concerns that global warming could trigger more frequent and widespread episodes of bleaching. Because of its potentially serious effects on the



Bleached coral.

productivity of reef systems and the biota they support, this relationship has been researched closely in a number of tropical reef systems. Despite clear evidence that increased SST can trigger bleaching, it has proven hard to predict from

individual reef-based or laboratory studies how SST influences bleaching at the regional scale.

McWilliams *et al.* have assembled coral bleaching data from two decades of research in the Caribbean, at the scale of cells of 1° of latitude and longitude, and examined their relation with SST anomalies over the period. They find an exponential increase in the extent and

intensity of bleaching episodes with increasing frequency of SST anomalies, such that 100% bleaching is reached with SST increases of slightly less than 1°C—well within the predicted temperature rise for the rest of this century. — AMS

*Ecology* 86, 2055 (2005).

## CHEMISTRY

### Site-Specific Catalysis

Chemical patterning of surfaces has traditionally been achieved by zapping a reactive coating with light or electron beams. More recently, “dip pen” techniques have used atomic force microscope (AFM) probes to plant molecules in selected surface locations. Davis *et al.* show that AFM probes can also be used as spatially selective catalysts. They capped the silicon nitride probe tips with palladium nanoparticles, which catalyzed the Suzuki coupling of aryl boronic acids to a layer of aryl bromides that were bound through sulfide linkages to a gold surface. After submerging the film in a methanol solution of the boronic acid and a base, they maneuvered the probe to the desired reaction site and induced coupling by applying 20 to 25 nN of force between tip and surface. Reducing the force to the 1- to 5-nN range allowed imaging of the patterned surface without further catalysis. For verification of spatial selectivity, coupling was performed with amine-substituted boronic acid substrates, which were subsequently labeled with fluorescent dye. — JSY

*J. Am. Chem. Soc.* 10.1021/ja043235+ (2005).

## HIGHLIGHTED IN SCIENCE'S SIGNAL TRANSDUCTION KNOWLEDGE ENVIRONMENT



### Fateful Feedback

Control of cell differentiation is thought to result from bistable regulatory networks that allow a transient developmental signal to instruct cells to adopt a differentiated state. In the nematode *Caenorhabditis elegans*, Johnston *et al.* examined a network that determines the alternative fates of two taste receptor neurons, known as ASE left (ASEL) and ASE right (ASER). These neurons are bilaterally symmetric but express distinct sets of chemoreceptors that are necessary for the worm's navigation in search of food. The authors find through genetic analysis that two key transcription factors, DIE-1 and COG-1, which promote the expression of genes specific to ASEL and ASER neurons, respectively, act in a feedback loop in which they are linked by two microRNAs (miRNAs) encoded by *lgy-6* and *mir-273*. Expression of *lgy-6* is enhanced by DIE-1, and the *lgy-6* miRNA inhibits the expression of ASER-promoting factor COG-1, which in turn promotes the expression of *mir-273* miRNA, which closes the loop by inhibiting expression of the ASEL-inducing gene *die-1*. Although the stimulus that causes switching of this loop to favor production of one or the other transcription factor remains unknown, the results provide the essence of a miRNA-containing transcriptional feedback loop that can account for the stabilized expression of terminal cell fate in the ASER and ASEL neurons. — LBR

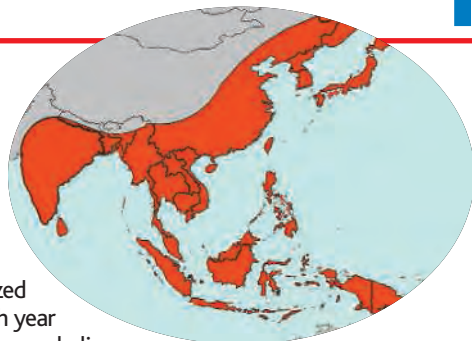
*Proc. Natl. Acad. Sci. U.S.A.* 102, 12449 (2005).



## COMMUNITY SITE

### Focus on a Killer

West Nile virus has monopolized the media's attention, but each year its cousin that causes Japanese encephalitis infects about 50,000 people. Some 10,000 die, mainly children. The new portal Japanese Encephalitis Prevention Network (JEPN) will allow researchers, health officials, and others to swap information about the mosquito-borne disease that's endemic to Asia. Hosted by the Seattle-based nonprofit PATH, the growing site already offers resources such as the latest news on research and outbreaks and a tutorial on the disease's epidemiology and control. Tools allow visitors to graph and map cases and deaths. JEPN's creators hope that other nations will add information for more countries and years. Above, the distribution of the disease.



[www.jepn.org](http://www.jepn.org)

## RESOURCES

### Breaking the Patent Barrier

Biotech patents can stymie researchers in the developing world who are trying to solve local problems. BioForge, launched earlier this year, creates a forum in which scientists from north and south can collaborate to devise alternatives. The site is part of the BIOS initiative, which aims to apply the open-source model that has fostered software innovation to problems such as food production and environmental degradation. The idea is to get visitors to brainstorm about biotechnologies that would be available to anyone who promises to share any improvements. BioForge also links to resources such as the PatentLens, a database of more than 1.5 million life science patents and patent applications.

[www.bioforge.org](http://www.bioforge.org)

## RESOURCES

### Making Light Coherent

When laser experts talk about an upper-state lifetime, they aren't discussing how long people in Montana live. The term refers to how long atoms remain excited, as you can discover at The Encyclopedia of Laser Physics and Technology, written by physicist Rüdiger Paschotta of RP Photonics Consulting in Zurich, Switzerland. The reference explains more than 400 concepts including laser physics, nonlinear optics, quantum effects, and related fields. For example, you can learn about so-called eye-safe lasers, which emit wavelengths of light that peter out before they reach the retina. The site, which assumes that readers have a basic physics background, also furnishes graphs, animations, and links to papers.

[www.rp-photonics.com/encyclopedia.html](http://www.rp-photonics.com/encyclopedia.html)



## DATABASE

### Eating Pollution

To us, the molecule cyclohexane is a noxious solvent for making products such as rubber and wood stains.

But to the bacterium *Brachymonas petroleovorans*, it's dinner. A strain of the bug can break down cyclohexane and use it as a source of carbon.

Researchers hoping to harness microbial metabolism for environmental cleanup should visit the Biocatalysis/Biodegradation Database at the University of Minnesota. The site displays the biochemical pathways that allow various

kinds of bacteria to disassemble a long list of pollutants, from the carcinogen carbon tetrachloride to the pesticide parathion.

[umbdd.ahc.umn.edu](http://umbdd.ahc.umn.edu)



## DATABASE

### To Know the Worm

About 20,000 genes orchestrate a nematode's development and keep it squirming throughout its life. To tease out each gene's role, scientists are deploying RNA interference (RNAi), a technique for silencing genes. Worm fans can track the results of these studies at The RNAi Database, maintained by Kris Gunsalus, Philip MacMenamin, and Fabio Piano of New York University.

Housing results from the WormBase genome database and the researchers' own lab, the site records experiments on more than 18,000 genes. Users can uncover the consequences of blocking a particular gene or search for studies that elicited a specific defect, such as slow growth or sterility. A new feature called PhenoBlast corrals genes whose disruption induced the same range of abnormalities. To help users visualize what goes wrong with the animals, many of the entries furnish photos and movies. Pictured are early development for a wild-type embryo (top row) and an embryo treated with RNAi against the gene for the protein actin. The actin-deprived embryo can't divide properly, but its chromosomes keep replicating, so it becomes a single cell with multiple nuclei.

[www.rnai.org](http://www.rnai.org)

Send site suggestions to [netwatch@aaas.org](mailto:netwatch@aaas.org). Archive: [www.sciencemag.org/netwatch](http://www.sciencemag.org/netwatch)



### TEACHING EVOLUTION

## ID Goes on Trial This Month in Pennsylvania School Case

In 1925, John Scopes was found guilty of teaching evolution to Tennessee schoolchildren in “the trial of the century.” On 26 September, a court in Harrisburg, Pennsylvania, will look at the flip side of the controversy—whether a local school district can require that students be told about intelligent design (ID) as an alternative to Darwinian evolution.

The stakes are high: Although defenders of Darwin believe they have both the facts and the law on their side, a loss could be a disaster. “If we prevail, it’s not going to be a knockout punch,” says Witold Walczak, a lawyer with the American Civil Liberties Union. But “if we lose, ... you’re going to see intelligent design taught in schools all across the country.”

The suit was brought last December by 11 parents of children in the 3700-student Dover district after its school board, on a 6–3 vote, became the first in the country to instruct teachers not only to inform students of “gaps/problems in Darwin’s Theory” but to tell them about “other theories of evolution including, but not limited to, intelligent design.” Dover High School’s seven biology teachers refused to play ball. So twice this year, in January and June, the district’s top two administrators went around to biology classrooms and read a 1-minute statement explaining that Darwin’s was only “a theory” (*Science*, 28 January, p. 505). They pointed students to books in the school library—in particular *Of Pandas and People*—that could enlighten them about ID.

In their suit, the Dover parents claim that teaching ID is an unconstitutional establishment of religion. The plaintiffs have lined

up 25 possible witnesses, including experts in philosophy, theology, science education, and mathematics as well as two veterans of the ID wars, Brown University biologist



**Squaring off.** Brown’s Ken Miller (left) and Lehigh’s Michael Behe (above, center) are veterans of the evolution debate who are scheduled to testify.



Kenneth Miller and paleoanthropologist Kevin Padian of the University of California, Berkeley.

The defense is now down to two scientists: Lehigh University biologist Michael J. Behe and Scott Minnich, a microbiologist at the University of Idaho in Moscow. Neither would comment on the pending trial. Two prominent figures who agreed to be witnesses—Stephen C. Meyer of the Discovery Institute, a think tank that

promotes ID, and mathematician William Dembski, a Discovery fellow—pulled out before they could be deposed, reportedly on orders from Discovery leadership. John West, associate director of the institute’s Center for Science and Culture, would say only that there were “differences of opinion between lawyers.”

But ID opponents think they know what’s going on. “Discovery has been very cagey—they’re worried about a big court defeat,” says Joseph Conn of Americans United for Separation of Church and State, one of the groups supporting the plaintiffs. Eugenie Scott of the National Center for Science Education in Oakland, California, says that the appearance of Dembski, editor of the latest edition of *Of Pandas and People*, would have allowed the plaintiffs to introduce the book into the trial and put ID front and center. Instead, Miller expects the defense to “present as small a target as possible,” arguing that “the board did not teach ID and that they didn’t even endorse it.”

Darwin’s critics make much of a distinction between “teaching the controversy”—that is, highlighting what they see as scientific discrepancies in Darwinian theory—and teaching ID. “We oppose any effort to require teaching about ID. ... We think that simply politicizes [intelligent] design,” says West, adding that Discovery is keen on teaching “scientific” criticisms of evolution. But Miller calls this point “a distinction without a difference. ... ID is nothing except these arguments against evolution.”

Although a win by the school board seems unlikely, all seem to agree it would be significant. “I believe school boards all across the country will, in the interest of good science, start mentioning intelligent design as an alternative theory,” says defense counsel Richard Thompson of the Christian-oriented Thomas More Law Center in Ann Arbor, Michigan.

Adding to the tension is a local school board race this fall. Seven pro-ID members of the nine-member board are running for election in November. They are being opposed by seven who believe ID is unscientific. Observers say the races are too close to call.

—CONSTANCE HOLDEN

#### Evolution in the Courts

- 1925:** John Scopes is convicted of teaching evolution in Tennessee (later reversed).
- 1968:** In *Epperson v. Arkansas*, the Supreme Court rules that laws banning the teaching of evolution violate the First Amendment.
- 1982:** In *McLean v. Arkansas* (dubbed *Scopes II*), a U.S. district court strikes down “equal time” law for creation science.
- 1987:** In *Edwards v. Aguillard*, the Supreme Court rules that equal time laws are unconstitutional. States are barred from requiring the teaching of creationism in public schools but allowed to teach alternatives to Darwin’s theory of origins.

1802

What future for science in Iran?



1807

More powerful hurricanes on the way?



1808

Rebuilding New Orleans

## INTELLECTUAL PROPERTY

# Court Tightens Patent Rules on Gene Tags

Slamming shut what Nobelist Paul Berg once called a genetic Pandora's box, a federal appeals court ruled last week that researchers cannot patent DNA strands that bind genes whose function is unknown. The ruling,\* in a case brought by agbiotech giant Monsanto involving strings of corn DNA, puts an end to more than a decade of uncertainty about the patentability of a basic research tool.

The roots of the case reach back to 1991, when the National Institutes of Health (NIH), based on work by J. Craig Venter, submitted the first of thousands of patent applications for gene-grabbing tools called expressed sequence tags (ESTs). The U.S. Patent and Trademark Office (PTO) rejected the application, NIH chose not to fight, and subsequent applications for ESTs for which the underlying gene was unknown were put on hold or denied.

Last week's 2-1 decision by the U.S. Court of Appeals for the Federal Circuit upholds a 2001 ruling by PTO that Monsanto's application for corn ESTs fell short of the requirement that any innovation be "use-



**Getting an earful.** Court tells Monsanto that its corn ESTs can't be patented.

ful." In its ruling, the court calls Monsanto's ESTs "only tools to be used along the way" in exploring an organism's genes. Inventions must have both a "significant and presently available [and] well-defined" benefit to receive a patent, it added.

Although most pending patents on genetic sequences now include adequate information on function, according to PTO, observers were

worried that a victory for Monsanto could restrict scientific inquiry, especially as the infringement exemption for basic research has come under recent fire. An amici brief filed by the National Academy of Sciences and several biotech and drug companies and medical societies raised the specter of infringement suits and other legal hurdles that could "preempt other

scientists from entire fields of research."

In his dissent, federal Judge Randall Rader said the decision to set a high bar for patenting ESTs will harm research by denying deserved patents for early-stage "research tools [that] provide a cognizable benefit for society." It also sets up a potential legal battle over the increasingly popular argument by some applicants seeking to patent new genes that usefulness should be based on homology—base-pair similarity with better-known genes. "I've seen pretty strong homology rejected on utility grounds," says patent agent Sherri Oslick of McDonnell Boehnen Hulbert & Berghoff LLP in Chicago, Illinois. "How much homology is enough?"

PTO worked with Monsanto to arrange what both sides acknowledge was a test case. In 2001, PTO had rejected Monsanto's patent application for the ESTs because they lacked a "real world" context of use." Monsanto argued that several applications—including finding DNA regulatory regions called promoters—made the ESTs useful. But the appellate court said that Monsanto needed to lay out more "specific" uses: the identification of particular promoters, for example.

Monsanto officials say the decision brings much-needed "clarity" to the issue, although the company may still request a rehearing before the appellate court. In the meantime, researchers can breathe easier knowing that the court has cleared away a potentially large obstacle to their bench research. —**ELI KINTISCH**

\* [www.fedcir.gov/opinions/04-1465.pdf](http://www.fedcir.gov/opinions/04-1465.pdf)

## PLANETARY SCIENCE

# Beaming to Itokawa

The Japanese spacecraft Hayabusa arrived at near-Earth asteroid Itokawa on 11 September after traveling 28 months on a beam of high-speed ions. Hayabusa's ion-drive engine is just one part of a technologically ambitious attempt to bring home the first sample collected from an asteroid.

So far, the ion drive and the laser-guided autonomous navigation have worked flawlessly. During the next several months, a robot named Minerva will be deployed to the surface. There, it should hop around taking pictures, because the 0.6-kilometer-long Itokawa's gravity is too feeble—at less than one hundred-thousandth

that of Earth—for wheels to work.

Up to three times during the mission, Hayabusa itself will land momentarily to blast a sample into a collector for return to Earth in

June 2007. That sample could finally explain why the most common type of asteroid looks different—spectroscopically more red—from the most common type of meteorite. Apparently, some sort of "space weathering" is reddening the surface of S-type asteroids. The NEAR Shoemaker mission to orbit another S-type relied on remote sensing and never quite nailed down the meteorite-asteroid connection (*Science*, 14 December 2001, p. 2276). Hayabusa could do it.

—**RICHARD A. KERR**



NEAR Shoemaker mission to orbit another S-type relied on remote sensing and never quite nailed down the meteorite-asteroid connection (*Science*, 14 December 2001, p. 2276). Hayabusa could do it.

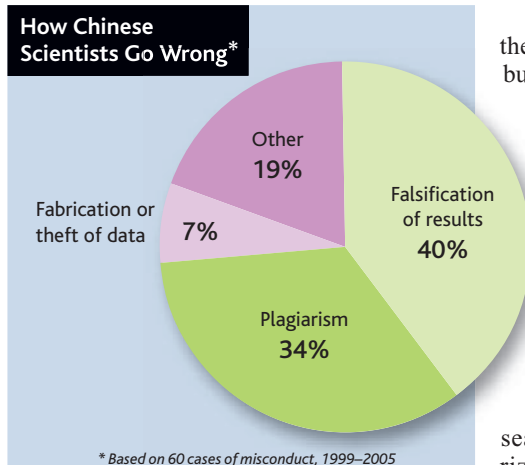
CREDITS (TOP TO BOTTOM): DOUG WILSON/ARS/USDA; JAXA

## RESEARCH MISCONDUCT

# China Science Foundation Takes Action Against 60 Grantees

BEIJING—As part of a campaign to improve ethical behavior among China's rapidly growing scientific community, the country's leading basic research agency has disclosed the names of three scientists being punished for misconduct. In the past 2 years, some 60 scientists funded by the National Science Foundation of China (NSFC) have been found guilty of misconduct, but the Web posting (nsfc.gov.cn) late last month is the first time that any names or institutions have been identified.

"This is a good start to reverse the prevalence of scientific misconduct in China," says Zou Chenglu, a biophysicist at the Chinese Academy of Sciences who follows misconduct issues closely. In December 1998, NSFC formed a 19-member committee of distinguished scientists to investigate allegations of scientific misconduct. Since then, the committee has opened files on 542 cases, most of them flagged by anonymous tipsters. More than 10% of them led to a finding of misconduct, from plagiarism to falsifying data on a grant application (see pie chart, above). Some 40 cases of misconduct were resolved last year without any public announcement. The second round includes 16 cases in which only the general nature of the mis-



**Assigning blame.** Some 60 scientists funded by China's NSF have committed misconduct since 1999, the agency says.

conduct was disclosed, plus the three in which detailed information was released.

Under a 29-paragraph regulation published in April, the investigations committee has the right to circulate an internal notice of criticism or move it to its public Web site. "The main purpose of making public the scientific misconduct is not to expose the errors but to help the relevant

scientists correct faults," says Meng Hui, an official with the Chinese Academy of Sciences who has followed the issue closely. "For this reason, the privacy of those who have committed less serious misdeeds needs to be protected."

In the three cases detailed last month, the scientists have been ordered to reimburse the agency and are barred for up to 4 years from submitting new grant proposals. The agency was the sole body that conducted an investigation, and none of those found guilty elected to appeal the decision. Zou says that the facts must be "irrefutable" for the agency to act.

The first case involves Su Bingyin, a neurologist at the Third Military Medical University in Chongqing. The committee concluded that Su added ghost researchers to his grant proposal, plagiarized material from other applications, and altered biographical information. At Jilin University, Cui Jianwei, a postgraduate student in accounting, was found to have lifted a thesis from the Web site of the University of Pennsylvania's Wharton Business School, translated it into Chinese, and published it in a Chinese magazine. In the third instance, the committee found that Li Guibao, who resigned recently as director of the Water Environment Security Lab at China's Institute of Water Resources and Hydropower Research in Beijing, plagiarized material ▶

## RUSSIAN SCIENCE

## Government Offers Pay Raise, but Demands Reform

MOSCOW—The Russian government is offering scientists both carrot and stick in its long-delayed plan to reform Russian science, including the bloated and moribund Russian Academy of Sciences (RAS). The carrot is a fivefold boost in a researcher's average monthly paycheck, to \$1050. The sticks are the replacement of lifetime jobs with fixed-term contracts, limits on the amount of time scientists can work abroad, and mandatory retirement ages.

Once a shining star of the Soviet system, RAS's fortunes have declined precipitously since the end of the Cold War, leaving many of its hundreds of institutes empty or rented out for office space. Many of the best researchers have emigrated, and some have taken other jobs as inflation has made their RAS salaries worthless. So this month's announcement by the Ministry of Science and Education is being hailed as an important step in restoring the academy's reputation. "The most important thing is Putin's proposal to substantially raise salaries. This is an

essential breakthrough," says former science minister Vladimir Fortov.

Although the pay raises evoke the halcyon days of generous Soviet funding, the decision to limit researchers' ability to work abroad, to 3 months per year or less, stirs up less pleasant memories of the old regime. "They will sweeten the pill for researchers by raising their salary but then will tie them tightly to the motherland like peasants in the times of serfdom," says human rights campaigner Alexander Podrabinek. RAS Vice President Gennady Mesyats dismisses such fears, telling a Moscow radio station that "the president told us when he met with us that there will be no return to old times."

Ministry officials say the new policy is simply intended to prevent scientists from earning two salaries. "A researcher must not get lost abroad for most of the time," the ministry's Dmitry Livanov told the ITAR-TASS press agency. Adds Mesyats, "If a person goes to do experiments, for example to CERN or anywhere else, he gets his salary

there. We do not pay him for this period."

Once the new salary increases go into effect by 2008, the ministry plans to introduce limited-term contracts and to assess all the staff at least once every 3 years. Highly valued researchers may get 5-year contracts, but only the most outstanding will be given open-ended contracts. "It will be necessary to put strict limitations [on contracts], as a mere increase of a salary may not lead to expected results," Livanov says.

The ministry also wants to cull older staff members by forcing lab chiefs to retire at age 60 and institution directors at 65. But there will be exceptions, says another RAS vice president, Valery Kozlov. "We do not plan to fire researchers at the pension age if they actively participate in the scientific life. But if a young researcher has lost interest in science, he will be laid off."

—ANDREY ALLAKHVERDOV AND  
VLADIMIR POKROVSKY

Andrey Allakhverdov and Vladimir Pokrovsky are writers in Moscow.

from another grant proposal. All three declined comment.

NSFC was founded in 1986 and has an annual budget of \$332 million. Last year, it received more than 40,000 applications and made about 8000 awards, with an average annual grant size of \$9500 for

single investigators. Shen Wenqing, deputy director of NSFC, says the agency is also on guard against unethical conduct among its reviewers and grants administrators as well as its grantees.

—GONG YIDONG

Gong Yidong writes for *China Features* in Beijing.

## PEDIATRIC MEDICINE

# Europe Follows U.S. in Testing Drugs for Children

**BARCELONA, SPAIN**—The European Parliament approved a law last week that will compel drug companies to investigate whether new drugs will benefit children and submit results for consideration with drug applications. Researchers hope this will boost research into pediatric drugs and lead to a more formal drug authorization process.

Between 50% and 90% of drugs used by adults have never been tested or licensed for use in children (from newborns to 18-year-olds). The result is that physicians treating the 100 million children in the European Union often prescribe off-label products or unauthorized drugs and so risk ineffectiveness or adverse reactions. The new law, passed on 7 September, aims to create a more rational approach; it mirrors the United States' "pediatric rule," which encourages clinical trials in children and has stimulated the development of drugs designed specifically for children.

Central to the new European legislation will be a 35-member advisory committee. Before any new drug can be approved, a company must submit a pediatric investigation plan to this Pediatric Committee and present the outcome of the research with any subsequent drug application. (The committee can approve waivers or deferrals of pediatric studies if, for example, the disease in question only affects adults.) The committee, administered by the European Medicines Agency (EMA), will be independent of industry. "The critical piece in the jigsaw for the new regulation is the pediatric advisory committee to the EMA. ... I hope we get an expert committee of people with relevant skills," says Bruce Morland, chair of the United Kingdom Children's Cancer Study group. The new regulation also calls for a network of clinical researchers and research centers, a database of ongoing and terminated pediatric drug trials, and a free scientific advice service for industry provided by EMA.

A child-centered approach "was absolutely necessary," says clinical pharmacologist Josep-Maria Arnau of Vall d'Hebró University Hospital in Barcelona, Spain. Pediatric pharmacologist Gerard Pons of the René Descartes University in Paris says that the regulation "is very important not only in terms of public health but also in terms of economy, as an E.U. network for research of children's drugs should attract



**Get 'em young.** New European legislation will encourage drug companies to research new drugs for children.

drug manufacturers to the E.U."

The new law, expected to get final approval from the European Council this year, also calls for the E.U. to provide funding to research drugs that are not patent protected. This Medicines Investigation for the Children of Europe program will aim to get off-patent drugs for children authorized, normally a difficult task because of the slim profits.

As in the United States, drug companies can win a 6-month extension of their patent protection if they have carried out a pediatric investigation plan. The law "is a key opportunity for Europe's children and for Europe's pharmaceutical science base," says Brian Ager, director general of the European Federation of Pharmaceutical Industries and Associations. —XAVIER BOSCH  
Xavier Bosch is a science writer in Barcelona, Spain.

## ScienceScope

### Audit Slams French Research

**PARIS**—France's system of managing research requires "urgent, significant reform," says a 170-page draft report by an independent audit authority. According to an article in *Le Figaro*, the document deplores poor accounting rules, inadequate evaluation, and insufficiently coordinated resources to compete internationally.

A group of university presidents welcomed proposals in the report to rectify the problems, including a call for greater university independence. But Cochin Institute biologist Alain Trautmann, spokesperson for the long-running researcher protest movement (*Science*, 16 April 2004, p. 368), says more autonomy for universities without getting rid of rife cronyism "would be a catastrophe."

—BARBARA CASASSUS

### U.S. to Bar Caviar

Nearly 5 years after activists first petitioned the U.S. Fish and Wildlife Service to stop importing beluga sturgeon from the Caspian Sea, the agency has decided to do just that. The countries bordering the sea have failed to present a plan to stop the 200-million-year-old fish's decline, due to overfishing, in the past 2 decades (see p. 1806). The United States has been the biggest importer of beluga caviar, which can fetch more than \$6600 a kilogram. "The U.S. will set an important example," says Lisa Speer of the U.S. environmental coalition Caviar Emptor.

—CHRISTOPHER PALA

### EPA Revises Pesticide Human Testing Rules

The Environmental Protection Agency (EPA) last week released a draft rule for considering toxicity studies in which volunteers are intentionally dosed with pesticides.

In July, lawmakers criticized an early version of the rules as ethically lax (*Science*, 8 July, p. 232), and a spending bill ordered the agency to modify the rules. The new rule, if adopted, would bar the use of any dosing studies of pregnant women or children and create a Human Studies Review Board to vet research proposals. CropLife America, a pesticide trade group, welcomed the rule, but Richard Wiles of the Environmental Working Group, an advocacy organization in Washington, D.C., worries that it won't bar studies in which children are exposed to pesticides, such as CHEERS, which EPA spiked in April due to congressional concerns. The rule is open for comment for 90 days, and EPA hopes to finalize it by Congress's January deadline.

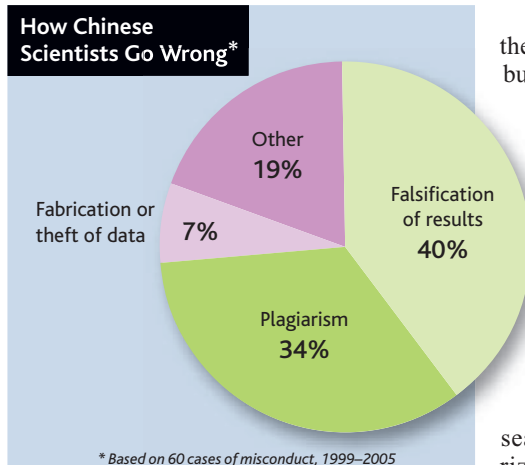
—ERIK STOKSTAD

## RESEARCH MISCONDUCT

# China Science Foundation Takes Action Against 60 Grantees

BEIJING—As part of a campaign to improve ethical behavior among China's rapidly growing scientific community, the country's leading basic research agency has disclosed the names of three scientists being punished for misconduct. In the past 2 years, some 60 scientists funded by the National Science Foundation of China (NSFC) have been found guilty of misconduct, but the Web posting (nsfc.gov.cn) late last month is the first time that any names or institutions have been identified.

"This is a good start to reverse the prevalence of scientific misconduct in China," says Zou Chenglu, a biophysicist at the Chinese Academy of Sciences who follows misconduct issues closely. In December 1998, NSFC formed a 19-member committee of distinguished scientists to investigate allegations of scientific misconduct. Since then, the committee has opened files on 542 cases, most of them flagged by anonymous tipsters. More than 10% of them led to a finding of misconduct, from plagiarism to falsifying data on a grant application (see pie chart, above). Some 40 cases of misconduct were resolved last year without any public announcement. The second round includes 16 cases in which only the general nature of the mis-



**Assigning blame.** Some 60 scientists funded by China's NSF have committed misconduct since 1999, the agency says.

conduct was disclosed, plus the three in which detailed information was released.

Under a 29-paragraph regulation published in April, the investigations committee has the right to circulate an internal notice of criticism or move it to its public Web site. "The main purpose of making public the scientific misconduct is not to expose the errors but to help the relevant

scientists correct faults," says Meng Hui, an official with the Chinese Academy of Sciences who has followed the issue closely. "For this reason, the privacy of those who have committed less serious misdeeds needs to be protected."

In the three cases detailed last month, the scientists have been ordered to reimburse the agency and are barred for up to 4 years from submitting new grant proposals. The agency was the sole body that conducted an investigation, and none of those found guilty elected to appeal the decision. Zou says that the facts must be "irrefutable" for the agency to act.

The first case involves Su Bingyin, a neurologist at the Third Military Medical University in Chongqing. The committee concluded that Su added ghost researchers to his grant proposal, plagiarized material from other applications, and altered biographical information. At Jilin University, Cui Jianwei, a postgraduate student in accounting, was found to have lifted a thesis from the Web site of the University of Pennsylvania's Wharton Business School, translated it into Chinese, and published it in a Chinese magazine. In the third instance, the committee found that Li Guibao, who resigned recently as director of the Water Environment Security Lab at China's Institute of Water Resources and Hydropower Research in Beijing, plagiarized material ▶

## RUSSIAN SCIENCE

## Government Offers Pay Raise, but Demands Reform

MOSCOW—The Russian government is offering scientists both carrot and stick in its long-delayed plan to reform Russian science, including the bloated and moribund Russian Academy of Sciences (RAS). The carrot is a fivefold boost in a researcher's average monthly paycheck, to \$1050. The sticks are the replacement of lifetime jobs with fixed-term contracts, limits on the amount of time scientists can work abroad, and mandatory retirement ages.

Once a shining star of the Soviet system, RAS's fortunes have declined precipitously since the end of the Cold War, leaving many of its hundreds of institutes empty or rented out for office space. Many of the best researchers have emigrated, and some have taken other jobs as inflation has made their RAS salaries worthless. So this month's announcement by the Ministry of Science and Education is being hailed as an important step in restoring the academy's reputation. "The most important thing is Putin's proposal to substantially raise salaries. This is an

essential breakthrough," says former science minister Vladimir Fortov.

Although the pay raises evoke the halcyon days of generous Soviet funding, the decision to limit researchers' ability to work abroad, to 3 months per year or less, stirs up less pleasant memories of the old regime. "They will sweeten the pill for researchers by raising their salary but then will tie them tightly to the motherland like peasants in the times of serfdom," says human rights campaigner Alexander Podrabinek. RAS Vice President Gennady Mesyats dismisses such fears, telling a Moscow radio station that "the president told us when he met with us that there will be no return to old times."

Ministry officials say the new policy is simply intended to prevent scientists from earning two salaries. "A researcher must not get lost abroad for most of the time," the ministry's Dmitry Livanov told the ITAR-TASS press agency. Adds Mesyats, "If a person goes to do experiments, for example to CERN or anywhere else, he gets his salary

there. We do not pay him for this period."

Once the new salary increases go into effect by 2008, the ministry plans to introduce limited-term contracts and to assess all the staff at least once every 3 years. Highly valued researchers may get 5-year contracts, but only the most outstanding will be given open-ended contracts. "It will be necessary to put strict limitations [on contracts], as a mere increase of a salary may not lead to expected results," Livanov says.

The ministry also wants to cull older staff members by forcing lab chiefs to retire at age 60 and institution directors at 65. But there will be exceptions, says another RAS vice president, Valery Kozlov. "We do not plan to fire researchers at the pension age if they actively participate in the scientific life. But if a young researcher has lost interest in science, he will be laid off."

—ANDREY ALLAKHVERDOV AND  
VLADIMIR POKROVSKY

Andrey Allakhverdov and Vladimir Pokrovsky are writers in Moscow.

from another grant proposal. All three declined comment.

NSFC was founded in 1986 and has an annual budget of \$332 million. Last year, it received more than 40,000 applications and made about 8000 awards, with an average annual grant size of \$9500 for

single investigators. Shen Wenqing, deputy director of NSFC, says the agency is also on guard against unethical conduct among its reviewers and grants administrators as well as its grantees.

—GONG YIDONG

Gong Yidong writes for *China Features* in Beijing.

## PEDIATRIC MEDICINE

# Europe Follows U.S. in Testing Drugs for Children

**BARCELONA, SPAIN**—The European Parliament approved a law last week that will compel drug companies to investigate whether new drugs will benefit children and submit results for consideration with drug applications. Researchers hope this will boost research into pediatric drugs and lead to a more formal drug authorization process.

Between 50% and 90% of drugs used by adults have never been tested or licensed for use in children (from newborns to 18-year-olds). The result is that physicians treating the 100 million children in the European Union often prescribe off-label products or unauthorized drugs and so risk ineffectiveness or adverse reactions. The new law, passed on 7 September, aims to create a more rational approach; it mirrors the United States' "pediatric rule," which encourages clinical trials in children and has stimulated the development of drugs designed specifically for children.

Central to the new European legislation will be a 35-member advisory committee. Before any new drug can be approved, a company must submit a pediatric investigation plan to this Pediatric Committee and present the outcome of the research with any subsequent drug application. (The committee can approve waivers or deferrals of pediatric studies if, for example, the disease in question only affects adults.) The committee, administered by the European Medicines Agency (EMA), will be independent of industry. "The critical piece in the jigsaw for the new regulation is the pediatric advisory committee to the EMA. ... I hope we get an expert committee of people with relevant skills," says Bruce Morland, chair of the United Kingdom Children's Cancer Study group. The new regulation also calls for a network of clinical researchers and research centers, a database of ongoing and terminated pediatric drug trials, and a free scientific advice service for industry provided by EMA.

A child-centered approach "was absolutely necessary," says clinical pharmacologist Josep-Maria Arnau of Vall d'Hebró University Hospital in Barcelona, Spain. Pediatric pharmacologist Gerard Pons of the René Descartes University in Paris says that the regulation "is very important not only in terms of public health but also in terms of economy, as an E.U. network for research of children's drugs should attract



**Get 'em young.** New European legislation will encourage drug companies to research new drugs for children.

drug manufacturers to the E.U."

The new law, expected to get final approval from the European Council this year, also calls for the E.U. to provide funding to research drugs that are not patent protected. This Medicines Investigation for the Children of Europe program will aim to get off-patent drugs for children authorized, normally a difficult task because of the slim profits.

As in the United States, drug companies can win a 6-month extension of their patent protection if they have carried out a pediatric investigation plan. The law "is a key opportunity for Europe's children and for Europe's pharmaceutical science base," says Brian Ager, director general of the European Federation of Pharmaceutical Industries and Associations. —XAVIER BOSCH  
Xavier Bosch is a science writer in Barcelona, Spain.

## ScienceScope

### Audit Slams French Research

**PARIS**—France's system of managing research requires "urgent, significant reform," says a 170-page draft report by an independent audit authority. According to an article in *Le Figaro*, the document deplores poor accounting rules, inadequate evaluation, and insufficiently coordinated resources to compete internationally.

A group of university presidents welcomed proposals in the report to rectify the problems, including a call for greater university independence. But Cochin Institute biologist Alain Trautmann, spokesperson for the long-running researcher protest movement (*Science*, 16 April 2004, p. 368), says more autonomy for universities without getting rid of rife cronyism "would be a catastrophe."

—BARBARA CASASSUS

### U.S. to Bar Caviar

Nearly 5 years after activists first petitioned the U.S. Fish and Wildlife Service to stop importing beluga sturgeon from the Caspian Sea, the agency has decided to do just that. The countries bordering the sea have failed to present a plan to stop the 200-million-year-old fish's decline, due to overfishing, in the past 2 decades (see p. 1806). The United States has been the biggest importer of beluga caviar, which can fetch more than \$6600 a kilogram. "The U.S. will set an important example," says Lisa Speer of the U.S. environmental coalition Caviar Emptor.

—CHRISTOPHER PALA

### EPA Revises Pesticide Human Testing Rules

The Environmental Protection Agency (EPA) last week released a draft rule for considering toxicity studies in which volunteers are intentionally dosed with pesticides.

In July, lawmakers criticized an early version of the rules as ethically lax (*Science*, 8 July, p. 232), and a spending bill ordered the agency to modify the rules. The new rule, if adopted, would bar the use of any dosing studies of pregnant women or children and create a Human Studies Review Board to vet research proposals. CropLife America, a pesticide trade group, welcomed the rule, but Richard Wiles of the Environmental Working Group, an advocacy organization in Washington, D.C., worries that it won't bar studies in which children are exposed to pesticides, such as CHEERS, which EPA spiked in April due to congressional concerns. The rule is open for comment for 90 days, and EPA hopes to finalize it by Congress's January deadline.

—ERIK STOKSTAD

## PLANETARY SCIENCE

## Another Hint of Planetary Marauders

As scientists accumulate evidence that something battered the inner planets 3.9 billion years ago, some say they are homing in on what did the pummeling. On page 1847, Robert Strom, a professor emeritus at the University of Arizona, Tucson, and colleagues present evidence that the massive cratering seen on Earth and its neighbors originated in the asteroid belt. "I've been working 35 years on this problem," says Strom. "I was one of those who did not believe in a cataclysm. This has changed my view entirely."

The most obvious clues to the source of the so-called late heavy bombardment are the number of craters left behind and the sizes of the impactors responsible, as derived from crater size. Strom and his co-workers compiled Strom's published and unpublished crater counts from the most pockmarked planetary surfaces—such as the highlands of the moon. They did the same for younger, more lightly cratered areas, such as certain volcanic plains on Mars. They also calculated projectile sizes from crater diameters.

Relatively more small objects hit the younger surfaces, they found, a size distribution that matches that of the near-Earth asteroids that have drifted in from the main belt more recently. That makes sense because the



**A battering.** Outer planets may have rattled the asteroid belt, showering the moon with impactors.

forces that nudge asteroids out of the belt today, such as the Yarkovsky effect driven by solar heating (*Science*, 13 August 1999, p. 1002), favor smaller objects.

A bigger proportion of large impactors, by contrast, had cratered older terrains. As reported before, the breakdown of sizes

matched the distribution seen in main belt asteroids. That indicated that a very different mechanism must have driven the ancient bombardment—one that did not discriminate between large and small asteroids.

The group argues that the asteroids must have pummeled the inner solar system after a rearrangement of the outer planets. Perhaps Jupiter and Saturn teamed up to scatter asteroids gravitationally (*Science*, 3 December 2004, p. 1676), or Neptune and Uranus formed long after the rest of the planets. Such planetary shifts would have disturbed the planetesimals in the outer solar system as well as the main belt, they concede, but the weak, porous structure of icy planetesimals would have led to a different distribution of sizes from what they observed, says Strom.

Cratering specialists suspect that Strom and his colleagues are on to something, but they say the case remains open. Outer solar system planetesimals "can't be ruled out without further testing and evidence" to show that their size distribution really would have been different, says William Bottke of the Southwest Research Institute in Boulder, Colorado. Strom "could very well be right," he says, "but we have to be careful."

—RICHARD A. KERR

## BIOETHICS

## Pellegrino to Succeed Kass on U.S. Panel

A presidentially appointed bioethics panel might be slipping out of the limelight as its outspoken chair steps down. He will be replaced by an elder statesman of the field who is expected to be more of a consensus-builder.

President George W. Bush's decision to replace the 66-year-old Leon Kass with Edmund Pellegrino, an 85-year-old physician and bioethicist at Georgetown University, has some people wondering if the President's Council on Bioethics will assume more of a figurehead role. "I wouldn't be surprised if the council recedes into the background from now on," says Daniel Perry, head of the Coalition for the Advancement of Medical Research in Wash-



**New chair.** Catholic scholar Edmund Pellegrino will lead the President's Bioethics Council.

ington, D.C. "Pellegrino is not the lightning rod that Leon was."

Saying that "two [2-year] terms is enough," Kass plans to stay on as a member even as he returns to the University of Chicago, where he's a professor on the Committee on Social Thought. Kass insists that there will be "no diminution of the role of the council" after Pellegrino takes over on 30 September. But Dartmouth College neuroscientist Michael Gazzaniga, one of the most outspoken members of the council, says, "there is word that some members may resign due to other duties and probably waning interest."

There seems little doubt that the 18-member council will be quieter under Pellegrino. "Leon defined this council," says Kathy Hudson, director of the Johns Hopkins University Genetics and Public Policy Center. She expects that Pellegrino, renowned for his diplomatic skills,

will "rein in the council's recent activist tendencies" and "boost public confidence in the objectivity of this important body."

The Jesuit-trained Pellegrino is universally applauded for his scholarship. "There isn't an award that he hasn't been awarded," says Baruch Brody of Baylor University in Waco, Texas, including from groups that differ with him on matters such as abortion and when to withdraw treatment for the terminally ill. He's also held many administrative posts, including a 4-year stint as president of Catholic University in Washington, D.C.

Although Pellegrino declined comment, his writings appear to place him in the same camp as Kass in opposing research cloning—what scientists prefer to call somatic cell nuclear transfer—and other technologies promising to "enhance" humans. Acquaintances predict Pellegrino won't have a problem with the workload, which Kass found to be a full-time job. And he'll do it the old-fashioned way: When *Science* tried e-mailing his office, an automatic reply explained that "Dr. Pellegrino does not use E-Mail."

—CONSTANCE HOLDEN



# To Escape From Quantum Weirdness, Put the Pedal to the Metal

If you want to disentangle yourself, hit the accelerator. That sounds like the thinking of a runaway groom racing away from the chapel, but it's also a surprising insight into the realm of quantum physics. Acceleration unravels a weird connection between widely separated particles known as "entanglement," physicists calculate. The finding hints at a deeper connection between quantum mechanics and gravity.

The result is surprising because it means that whether two particles are entangled depends on the motion of the observer, says Samuel Braunstein, a theorist at the University of York, U.K. An observer who is not accelerating may find that two particles are entangled, whereas an observer who is accelerating will find that the same particles are not. "I don't quite know how to eat that and be happy," Braunstein says.

When two particles are entangled, fiddling with one of them instantly affects the other, even if it's light-years away. Suppose Alice has one electron on Earth, and Bob has another on a planet orbiting Betelgeuse.

The electrons spin like tops, and in principle they can be entangled so that if Alice measures hers and finds it spinning "up," she'll know instantly that Bob's is spinning "down" and vice versa—even though both electrons spin both ways at the same time until Alice makes her measurement. By measuring her electron, Alice instantly forces Bob's to adopt the opposite spin.

Previously, physicists had studied how entanglement is affected if Bob and Alice move at steady near-light speed relative to each other (*Science*, 10 January 2003, p. 185). They found that Alice and Bob will agree that the entanglement remains, although the details of the connection will change and may involve the particles' momenta. Acceleration affects entanglement more dramatically, report theorists Ivette Fuentes-Schuller of the University of Oxford, U.K., and Robert Mann of the University of Waterloo, Canada.

Fuentes-Schuller and Mann, who are also affiliated with the Perimeter Institute for Theoretical Physics in Waterloo, imagined

that Alice and Bob share pairs of photons from a source somewhere between them. The pairs of photons are entangled, so that if Alice spots a photon in her particle detector, she knows that Bob got one, too. If Alice does not get one, she knows that Bob didn't get one either. The same conditions apply to Bob. Suppose, however, that Alice accelerates away from Bob. Then Bob still finds that his measurements are perfectly entangled with Alice's. But Alice finds that her measurements are not completely entangled with Bob's, the researchers report in a paper to be published in *Physical Review Letters*.

The asymmetry arises from the "Unruh effect," which

makes Alice see particles that Bob does not. As Alice accelerates ever closer to light speed, light from some parts of space can never quite catch up to her.

That creates a "horizon" that cuts her off from part of the universe. At the same time, the vacuum roils with particle-antiparticle pairs that pop into existence and quickly annihi-

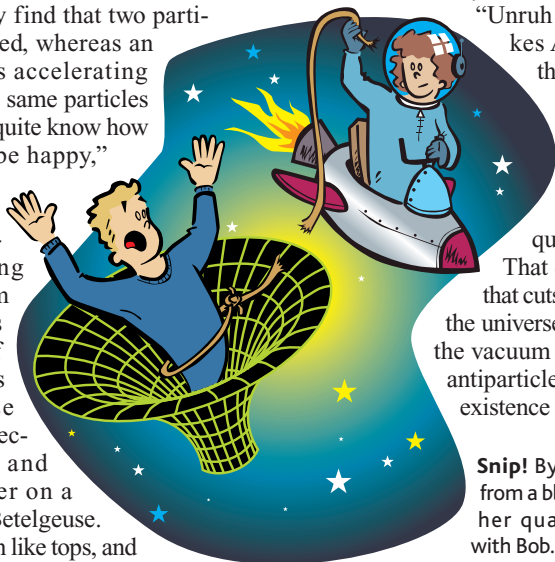
**Snip!** By accelerating away from a black hole, Alice severs her quantum connection with Bob.

late themselves. For Alice, some pairs appear just at the horizon, in which case the antiparticle slips beyond it, while the particle zooms into bona fide existence. The additional particles entangle with the photons from the source and obscure the original entanglement, Mann says.

The effect can obliterate the original entanglement entirely. If Bob falls into a black hole, he feels no acceleration and observes perfect entanglement with Alice. But if Alice fires a powerful rocket to accelerate away from the black hole and stay outside its "event horizon," she sees no entanglement at all.

Acceleration is linked to gravity through Einstein's general theory of relativity, so the result hints at a connection between gravity and entanglement, says Christoph Adami of the California Institute of Technology in Pasadena and the Keck Graduate Institute in Claremont. However, the tie between the two remains to be unraveled.

—ADRIAN CHO



## Hall In ...

Neuroscientist Zach Hall will be the first permanent president of California's new stem cell effort, the California Institute for Regenerative Medicine (CIRM). The interim president for the past 6 months, Hall said in June that he wasn't interested in a long-term position. His change of heart comes at a key time, with lawsuits delaying a bond sale and officials scrambling to pay for CIRM's first grants, for research training. "Zach has been terrific at getting things up and running," says stem cell researcher Evan Snyder of the Burnham Institute in La Jolla, California.

—CONSTANCE HOLDEN

## ... Dale Too ...

A lawyer is expected to win easy Senate confirmation as the next deputy NASA administrator. Shana Dale, who would be the first woman in such a NASA leadership position, is currently deputy director for homeland and national security at the White House Office of Science and Technology Policy. Dale, who is to replace former astronaut Frederick Gregory, will have her hands full: Hurricane Katrina damaged the Mississippi plant that builds the space shuttle's external tank. That means a \$1 billion cost increase, the latest in a series of budget and schedule overruns.

—ANDREW LAWLER

## ... And Klausner Out

Richard Klausner, former director of the National Cancer Institute (NCI), announced this week that he is stepping down at the end of the year as director of the Global Health Program at the \$29 billion Bill & Melinda Gates Foundation. A foundation spokesperson says Klausner's decision to leave after 3 years was "mutual." Klausner told *Science* that he's done "what I set out to do" and wants a job that requires less travel.

Klausner and the Seattle, Washington-based foundation deny the move is connected to recent reports that Congress has asked the Government Accountability Office to investigate whether NCI had adequate conflict-of-interest procedures in place when Klausner was director. Klausner had interviewed for two Harvard positions while NCI was developing a \$40 million contract that the university ultimately won. Klausner says he followed proper procedures, noting that the study is a general look at NCI policies. He says he was told that official recusals he signed while under consideration at Harvard applied only to "making decisions."

—JOCELYN KAISER

Iran is pouring money into world-class facilities for biotechnology, particle physics, and astronomy. But growing tensions with the West threaten a scientific community just coming into its own

## An Islamic Science Revolution?

**TEHRAN**—In a quiet suburb that seems light-years from the hubbub of downtown Tehran, Amir Mousavi beams with pride at a state-of-the-art gene gun for injecting DNA into cells. “It’s a dream of many universities in Iran to have one,” says Mousavi, a molecular biologist with the National Research Center for Genetic Engineering and Biotechnology (NRCGEB). The lab has become a magnet for young talent, filling up with researchers who in other times might have left Iran to make their mark in science.

The rising campus is a prime example of Iran’s recent push to create oases of elite science. Other brick-and-mortar initiatives include the country’s first world-class astronomical observatory, a linear accelerator, and a facility for international conferences. The sails of Iranian science have been filling with government support of several kinds—including a rapid expansion of foreign cooperation that embraces even “the Great Satan,” as the United States is still known in some circles here.

But some fear that Iranian science may be heading into the doldrums. President Mahmoud Ahmadinejad, an ultraconservative who took office last month on a promise to restore the values of the Islamic Revolution, has yet to express his views on R&D, although he has named a mathematician as his science minister. If the new government attempts to roll back the social reforms begun by Ahmadinejad’s predecessor Mohammad Khatami, academic freedom could become restricted, and science could suffer, says Shapour Etemad, director of the

National Research Institute for Science Policy in Tehran. “The mood in the scientific community is very poor,” he says. Moreover, Iran’s refusal to halt a nuclear fuel enrich-



**Thinking in many dimensions.** Physicist Hessemaddin Arfaei is the nucleus of IPM’s highly rated group of string theorists.

ment program may endanger collaborations with the West. Immunologist Mostafa Moin, an architect of scientific reforms in Iran and a presidential candidate who placed fifth in the first round of voting in elections last June, is concerned for the future. “All research is in danger,” he says.

### **Trials and tribulations**

What worries Iranian intellectuals most is a reprise of the scientific stagnation that followed the 1979 revolution. After a fundamentalist coup toppled the shah, universities were

closed for 3 years, and many research projects wilted. The Cultural Revolution “rejected science as a product of the West or endeavored to promote an ‘Islamic science’” focused on development, Iranian sociologist Farhad Khosrokhavar of the *École des Hautes Études en Sciences Sociales* in Paris wrote in the summer 2004 issue of *Critical Middle Eastern Studies*. That spurred an exodus of talented researchers. Hit hard were the prestigious Hamadan University and the Institute for Biochemistry and Biophysics in Tehran. Scientists who chose to stay, says Etemad, “often were suspected of being counter-revolutionaries.”

During this dark period, the remnants of an elite group of mathematicians and theoretical physicists struggled to prevent an implosion of Iranian science. Meeting weekly for a “Tuesday Gathering” at the University of Tehran’s Institute of Physics, the scientists “fought against the prevailing atmosphere and convinced the new generation to continue its efforts for the survival of scientific activity in Iran,” Khosrokhavar wrote. One safe haven was the Atomic Energy Center, the nerve center of Iran’s efforts to develop nuclear power—and, some Western analysts contend, atomic bombs.

The Tuesday Gathering lobbied the government hard to permit universities to train Ph.D.s. Its efforts paid off in 1988, soon after the Iran-Iraq war ended, when Sharif University of Technology launched Iran’s first science Ph.D. program, in physics. Moin, appointed minister of culture and higher education in 1989, says he sought to breathe life into the largely moribund universities. Since then, undergraduate enrollment has shot up 10-fold, to nearly 1 million. “People are thirsty for higher education,” says Mohammad Javad Rasaei, dean of medical sciences at Tarbiat Modarres University in Tehran. Meanwhile, science spending has climbed steadily, from about 0.2% of gross domestic product in 1990 to 0.65% this year.

Although few researchers have reached the highest echelons of their disciplines, Iran’s scientific leaders say their community is coalescing. “Scientific output has skyrocketed since 1993,” Rasaei says. In 2003, scientists in Iran published 3277 papers in international journals, a 30-fold increase over 1985, placing the country well ahead of Pakistan and on par with Egypt. Since 2000, the number of international collaborations has risen



**Home is where the lab is.** Modern facilities at the National Research Center for Genetic Engineering and Biotechnology in Tehran have persuaded some talented young biologists to stay in Iran.

CREDITS (TOP TO BOTTOM): R. STONE; NRCGEB



threefold, with chemistry, engineering, and physics leading the pack.

Iranian science has been bedeviled by shifting relations with the West. As higher education minister, Moin encouraged science students and faculty members to make a beeline for Western labs. NRCGEB's Mousavi, 36, is a star example. He won a Japanese government scholarship for his Ph.D. studies at the Nara Institute of Science and Technology in Japan. After a postdoc stint, he turned down a job offer from the University of California, San Diego, to return to Iran. "Many scientists love their country and come back," he says.

However, many others have stayed abroad. "It's hard to attract people back to meager facilities and meager salaries," says Yousef Sobouti, director of the Institute for Advanced Studies in Basic Sciences (IASBS) in Zanjan, a fast-growing center for graduate science education in the foothills of the Zāgros Mountains, 300 kilometers west of Tehran. That has prompted worries that Iran's push for foreign training has shortchanged its own growth. "We came to the conclusion that this is not a safe way to develop science," says Iran's deputy research minister Reza Mansouri.

### Bringing on big science

The science ministry has tried to shore up a weak infrastructure by showering money on a handful of institutes founded after the revolution. One beneficiary is the Institute for Studies in Theoretical Physics and Mathematics (IPM) in Tehran. "We go after people who can build a field," says Hessamaddin Arfaei, IPM's deputy director of research, who returned to Iran in 1979 after earning a Ph.D. at the University of California, Berkeley. His reputation as a top string theorist has enticed some of Iran's best young minds to work on the problem at IPM.

The institute's main focus is particle physics. Since 2001, IPM has been sending researchers to CERN, the European laboratory for particle physics near Geneva, Switzerland. "It took 10 years to get a green

light" from the Iranian government to proceed with the collaboration, says Arfaei. IPM scientists are helping construct the Compact Muon Solenoid, a detector for CERN's Large Hadron Collider due to come online in 2007.

The collider project is laying the groundwork for IPM's own dream: to start building an accelerator in the next decade that can infuse particles with 1 billion electron volts (GeV) of energy. Arfaei says such a machine "would allow us to do modern science," such as looking for violations of charge-parity symmetry, which would confirm that matter and antimatter are not always completely equivalent. As a dry run, IPM has begun constructing a 10-million-electron-volt linear accelerator. "You could go and buy one of these in Europe," Arfaei says. Instead, IPM staff members are devising superconducting magnets and other technologies on their own.

As further preparation for the GeV accelerator, the institute, under a deal inked last month and awaiting formal approval by Par-



**Looking outward.** Yousef Sobouti says Iran's planned new observatory will provide opportunities for foreign collaboration.

liament, will build magnets for boosting the power of the SESAME synchrotron in Jordan. IPM's longtime director Mohammad Javad Larijani, an influential conservative, is the brother of Iran's new nuclear negotiator, Ali Larijani. The institute should continue to fare well under Ahmadinejad, Etemad says.

Astronomers, too, are about to reap a reward. The government has begun site selection for an \$18 million observatory, likely to be dedicated to surveys for objects such as near-earth pulsars and extrasolar planets. Iranian astronomers began a campaign for the project in the 1970s, but it wasn't until 2004 that funds were allotted, thanks to a push from astrophysicist Mansouri. After specifications for the 2-meter optical and near-infrared telescope are drafted later this year, orders for components will go out to government factories.

In the meantime, scientists are surveying four sites—Kashan, Kerman, Khorosan, and Qom—in the running to host the observatory. The scope should see first light by 2010. "After so many years, we'll finally be able to make world-class observations in Iran," says Mansouri. The facility will create a wealth of new opportunities for foreign collaborations, adds Sobouti, an astrophysicist. "If you're in a position to offer something, you are in a position to be offered," he says. Centuries ago, in the early days of Islam, astronomers in Persia and Central Asia were at the vanguard of their profession. "We hope that cuts ice with the new government," says one scientist.

The darling of Iran's previous administration was biotechnology. Its largess included Tarbiat Modarres University, which has sunk millions of dollars into its labs in the last few years. "There is nothing we cannot buy," claims Rasaei. A recent purchase is a \$1 million nuclear magnetic resonance x-ray fluorescence microscope. Biotech is so popular, Rasaei says, that 700 undergrads vied for five positions in his lab, which recently succeeded in producing recombinant immunoglobulin from the Bactrian camel.

The first fruits of Iran's biotech boom are ripening. The Agricultural Biotechnology



**Tradition and change.** Akram Amani, a medicinal chemist and lab chief at the Pasteur Institute in Tehran, predicts that female scientists will continue to make gains.

Research Institute of Iran has completed field trials of a genetically modified variety of local rice called tarom molai. Risk assessments and biosafety studies of the rice, equipped with the gene for making a *Bacillus thuringiensis* protein that's toxic to insects, are under way. At NRCGEB, meanwhile, the plant biotechnology group is conducting field trials of virus-resistant sugar beets and herbicide-tolerant canola, and the industrial biotech department is scaling up, in a new pilot plant, production of recombinant human growth hormone.

In March 2004, NRCGEB's 170-strong staff relocated from cramped digs in downtown Tehran to the first of five wings of the new campus in Chitgar, 17 kilometers west of Tehran. When construction is completed, the institute will have onsite staff housing and childcare for a staff expected to grow fourfold, Mousavi says. NRCGEB is also the anchor of a budding science village. A short drive down Research Boulevard is a polymer research center, chemistry and forestry institutes, the botanical garden, and the agriculture faculty of Tarbiat Modarres.

### Gloomy outlook

Iranian scientists have a love-hate relationship with the world's most powerful scientific nation, which Iran's theocracy has branded an archenemy. On one hand, Iran has more collaborative projects with the United States than with any other nation. On the other hand, sanctions imposed by the United States after the revolution have taken a toll on science.

Sanctions forbid the direct sale of U.S.-made goods to Iran, impeding scientists here from obtaining certain specialized instruments and supplies. Although middlemen in places such as Dubai sell many of these items, their prices are inflated, and there is no after-sales service. "We train technicians to fix instruments," says Rasaei. "But spare parts are a problem."

New impediments to Iranian scientists are restrictions the United States imposed after the 11 September 2001 terror attacks and informal barriers thrown up after President George W. Bush labeled Iran a member of the so-called axis of evil in 2002. Iranians must obtain U.S. visas in a third country, and they are harder than ever to get. Rasaei would have preferred to spend an upcoming sabbatical in the United States, he says, but "I'm not going to humiliate myself by applying for a visa and not getting it." And one scientist says that at conferences, Westerners treat Chinese or Indian scientists with more respect than an Iranian with similar credentials. "Scientists endure many symbolic wounds due to their Iranian citizenship," Etemad notes.

Iran must overcome internal constraints as well. Only recently have universities created postdoc positions, primarily as a mechanism to try out talented young scientists for junior faculty positions. "Nobody wants to let a good graduate go," says Mohammad Reza Khajepour, deputy director of IASBS, which has earned a reputation as one of the most productive scientific centers in Iran, publishing more papers per staff member than any other institute. At the same time, Iran's own strict visa regime sharply constrains the amount of time that any foreign researcher can work in Iran. "China and Malaysia have asked to send postdocs [to IASBS], but we can't take them," Khajepour says. And although the government has raised scientists' salaries, many observers say the national science budget, about \$900 million, is not increasing fast enough.

People are waiting to see whether Ahmadinejad, the new president, will change the science agenda. After a restructuring earlier this year, a new High Commission for Science, Research, and Technology now controls the science budget. The commission, chaired by the president and

expected to meet in the fall, "will decide what will happen in science in the coming years," says Rasaei. Few scientists believe that Ahmadinejad's new science minister, mathematician Mohammad-Mehdi Zahedi of Shahid Bahonar University in Kerman, will radically alter course.

Rather, much hinges on whether the new government follows through on Ahmadinejad's vow to restore the values of the Islamic revolution, including greater segregation of the sexes. The ranks of women in academia swelled during Khatami's two terms: Of 28,000 scientists currently in Iranian universities, 5400 are women. Among the country's rising scientific stars is Akram Amani, a female lab chief at the Pasteur Institute in Tehran. Trained in medicinal chemistry in India, Amani returned to Tehran in 1996, just before Khatami came to power. She predicts that female scientists will continue to make gains under Ahmadinejad, who she says "did a very good job" as Tehran's mayor before becoming president. Others are pessimistic.

One pervasive fear is that academic freedom could be eroded. "I don't think the universities and research institutes can defend themselves" if conservatives grow more assertive, says Moin, president of the Immunology, Asthma, and Allergy Research Institute in Tehran. Rasaei adds that "if scientists cannot speak openly, and they don't want to keep quiet, they will probably prefer to leave Iran." Arfaei worries that funds for travel and hosting short-term visiting researchers may dwindle. "It could be like it was 20 years ago, when traveling abroad was a luxury," he says.

Not likely, says Mansouri, who is preparing to resign from the science ministry to pursue a sabbatical at McGill University in Montreal, Canada. He sees a bright future taking shape in the Dasht-e Kavir desert. There, in the Khoranagh oasis near the city of Yazd, the science ministry is refurbishing a 4000-year-old citadel and caravansary for hosting international workshops. The idea was born several years ago, when Mansouri and some colleagues were longing for a science retreat like the Snowmass Conference Center in Aspen, Colorado. "We need to bring more scientists from abroad to Iran," he says.

Khoranagh is the centerpiece of a new organization, the Center for International Research and Collaboration, formed under an agreement between the science ministry and the Abdus Salam International Center for Theoretical Physics in Trieste, Italy. The conference facility should be ready in about 5 years, Mansouri says. In the meantime, Iran's fragile scientific community will either continue to enjoy a renaissance or discover that, like the Khoranagh citadel, its vibrant days are already behind it.

—RICHARD STONE

CREDITS: STONE

# Attack of the Killer Jellies

A vicious alien is wreaking havoc in the Caspian Sea, but governments have not approved deployment of the only weapon likely to stop it

**BANDAR-E ANZALI, IRAN**—The invasion began 6 years ago, when an advance force slipped into the Caspian Sea. A massacre followed. Three-quarters of the zooplankton species in the southern Caspian were annihilated, sending a shock wave through the food chain that dealt the biggest blow to kilka, a favorite of Iran's fishing industry. The aggressor—one of the most feared and reviled invasive species, the comb jelly *Mnemiopsis leidyi*—had transformed the world's largest lake into a killing field.

The voracious jelly seemed to be an unstoppable menace. But it has been stopped before—in the Black Sea. In the late 1990s, another comb jelly, *Beroe ovata*, put an end to *Mnemiopsis*'s romp there by eating its cousins and bringing the population under control. Natural rivalry could be deployed against comb jellies again—except that in the Caspian, bordered by five nations, complex politics have thwarted the use of this silver bullet. Some decision-makers fear unexpected side effects, says ecologist Henri Dumont of Ghent University in Belgium. Yet with *Beroe*, he says, “we have a predator of *Mnemiopsis* that is such a specialized feeder that it is almost too good to be true.”

Any delay in joining battle with *Mnemiopsis* is bad news for the Caspian, where environmental degradation and overfishing imperil sturgeons, prized for their caviar (see sidebar, p. 1806), and a virus has hammered the endangered Caspian seal (*Science*, 18 January 2002, p. 430). Because the Caspian is landlocked, pollution accumulates, magnifying its effects. “We were already losing genetic resources before *Mnemiopsis* came along,” says Ali Asghar Khanipour, director of the Guilan Fisheries Research Center in Bandar-e Anzali, a port on the southern Caspian coast.

## Wipeout

Black-and-white photos in the Guilan center's zooplankton lab pay funereal homage to the victims. “Some species have entirely vanished,” including several varieties of copepods and Cladocera, says center biologist Siamak Bagheri. Of these, he says, only *Acartia* is left in high numbers.

The villain, rapacious and bioluminescent, can consume up to 15 times its body weight in a day. Within 2 weeks after birth, the hermaphrodite reaches sexual maturity and can produce thousands of eggs each day. Although its main food is zooplankton, *Mnemiopsis* also eats fish eggs and larvae. For time immemorial, it thrived in obscurity in its native waters off the East Coast of the United States. Then in the early 1980s, the jelly found its way to the Black



**Natural-born killer.** *Beroe ovata* are ferocious predators of another comb jelly, *Mnemiopsis leidyi*.

Sea in ship ballast water. Its first bloom, in 1989, was overwhelming: As many as 800 million tons of *Mnemiopsis* overran the Black Sea that summer—800 times the total fish catch in the Black Sea that year. Fisheries were decimated (*Science*, 30 August 2002, p. 1482).

The carnage continued until 1997, when *Mnemiopsis*'s nemesis from back home arrived serendipitously on the scene, probably in ballast water. *Beroe*, which appears to prey exclusively on *Mnemiopsis*, quickly brought the monster to heel. By 2001, numbers had ebbed so low that researchers had trouble finding specimens for analysis, says Ahmet Kideys of the Institute of Marine Sciences in Erdemli, Turkey. “Turkey didn't have to do anything,” says Bagheri. “They were lucky.”

*Mnemiopsis* stole into the Caspian, however, and an ecological nightmare began to

unfold in 1999, when the comb jelly was first spotted by Iranian and Russian fishers. Researchers assume that *Mnemiopsis* had stowed away a year or two earlier in ballast water taken on in the Black Sea or the Sea of Azov by ships that later entered the Caspian via the Volga-Don canal.

The invasion was swift. *Mnemiopsis* “has spread everywhere in the Caspian,” says Naser Agh, director of the Artemia and Aquatic Animals Research Institute in Orumiyyeh, Iran. Sampling has found more than 2000 individuals per square meter; they persist in high numbers for more than 6 months of the year, peaking in August. Although most comb jellies in the Caspian are less than 10 millimeters long—much smaller than those of the Black Sea—their appetites are by no means diminished.

“It's been a disaster,” says Hossein Negarestan, senior marine ecologist at the Iranian Fisheries Research Organization (IFRO) in Tehran. With zooplankton biomass reduced 10-fold, Iran's kilka fishery has plunged from 85,000 tons in 1999 to 15,000 tons in 2004. Azerbaijan and Russia have reported similar drop-offs. There are worrying signs that the Caspian seal, which feeds on kilka, also may become a casualty. Pollution, hunting, and recent outbreaks of canine distemper virus have already reduced the seal population by 83% over the past 50 years. And with zooplankton hobbled, their phytoplankton prey are living it up. Phytoplankton blooms can be seen from satellites, says Kideys, now on a 1-year sabbatical at the European Commission's Joint Research Centre in Ispra, Italy. “The consequences of such high levels of phytoplankton must be enormous,” he says.

Fishers are reeling. The most valuable of the Caspian's three kilka species, anchovy kilka, has been hit hardest. Hauls are smaller, and catch quality is poorer. In Iran alone, losses exceed \$125 million.

## To the rescue?

In 2001, Kideys and others organized a research program to test whether *Beroe* could be introduced into the Caspian. Four years later, it's still unclear whether *Beroe* is up to the job. In 2002, researchers shipped *Beroe* from Turkey to Iran to try rearing the critter in Caspian water, the salinity of which is between a third and two-thirds that of Black Sea water. The international team had a narrow window to work in: *Beroe* is found in the Black Sea only in late summer, when *Mnemiopsis* numbers peak; it crashes in sync with

## The Sturgeon's Last Stand

**RASHT, IRAN**—In a cavernous hall packed with naval-gray steel tanks, a precious commodity is being enriched and multiplied. No, this is not a hitherto undeclared uranium facility in Iran's nuclear program: It's a breeding facility for Caspian sturgeons. Each tank is filled with fish of various ages, from fingerlings, a few centimeters long with crocodilian snouts, to meter-long juveniles. Here at the International Sturgeon Research Institute (ISRI) in the northern town of Rasht, scientists are refining techniques for rearing fingerlings that may give the ancient but threatened species a better shot at surviving in the open sea. "If something happened in the Caspian and a wild population was lost, we could reconstitute it," says ISRI director Mohammad Pourkazemi.

ISRI may get a chance to test that claim: Deteriorating spawning grounds and unbridled poaching have reduced sturgeon stocks to a shadow of what they were a generation ago. With disaster looming, the two biggest fishing nations—Iran and Russia—are sparring over how many sturgeon are left and how to divvy up a declining catch. Amid the bickering, a new survey suggests that the sturgeon's free fall is continuing.

For most of the 20th century, Iran and the Soviet Union ran tight ships, at least on regulating sturgeon fisheries. The situation unraveled in 1991 when four Caspian states—Azerbaijan, Kazakhstan, Russia, and Turkmenistan—emerged from the Soviet collapse. Weak law enforcement and poverty along the Volga and Ural rivers, the northern spawning areas, have enabled poachers to take up to 10 times the legal catch. Despite the release of tens of millions of fingerlings each year, Caspian nations in 2004 caught only 760 tons of sturgeon, the smallest figure in a century, down from 26,600 tons in 1985.

Four Caspian sturgeon varieties—Russian, Persian, beluga, and stellate, or sevruga—supply 90% of the world's caviar. A fifth, the ship sturgeon, is so scarce that exporting its meat or caviar has been banned since 2002. Almost half of this year's caviar quota—51 of 105 tons—is Persian sturgeon, which mostly keeps to Iranian waters. Iranian officials attribute its relative robustness to government control of the caviar trade and zero tolerance for poaching.

But the Persian's rise has come at the expense of its kin, throwing the ecosystem off kilter, asserts marine ecologist Arash Javanshir of the University of Tehran. Besides fishing restrictions, he says, what's needed is a restoration program by the Caspian states that targets all sturgeon and their spawning grounds and many other organisms as well.

One big blind spot is that no one knows just how many of the living dinosaurs—the first sturgeon are believed to have lived 300 million years ago—ply the Caspian. Some experts, picking up on charges first leveled by the Wildlife Conservation Society 2 years ago, accuse Russia of exaggerating population sizes by low-balling the catch coefficient and high-balling the escape coefficient—the fraction of fish that are captured or are thought to escape capture on a sweep of the trawl net. "They produce statistics that are not in line with reality," claims Ali Asghar Khanipour, director of the Guilan Fisheries Research Center in Bandar-e Anzali.

The latest stock assessment, a monthlong exercise by Iranian and U.K. scientists that finished in early August, has not added clarity. For the first time, a camera was attached to trawl nets to try to better estimate the escape coefficient, but the water was too turbid. One stark fact was apparent, though, says Pourkazemi, a population geneticist: Sturgeon stocks are down 20% to 30% from last year.

Time is running out. The last 2 years has seen a precipitous decline in breeders, suggesting that mature sturgeon are getting fished out. According to the head of one of the two hatcheries on the Ural River, the beluga's spawning ground, neither hatchery was able to catch a single female this year—a first. "If illegal catch and environmental deterioration continue at the same pace," Pourkazemi predicts, "we will soon witness the extinction of sturgeon stocks in the Caspian." ISRI's tanks, now brimming with more than 10,000 sturgeons, may well become a Noah's ark for this antediluvian beast.

—R.S.

its prey. Although adult *Beroe* could adapt to brackish Caspian water, they hardly bred. Things went better the next summer in Sinop, Turkey, when the team was able to coax *Beroe* into reproducing, albeit feebly, in Caspian water. The only way to discover whether it will flourish in the Caspian is to put it there, says Negarestan: "We can't replicate the Caspian environment in a laboratory."

Some environmentalists, however, have warned that *Beroe*, once in the Caspian, might seek out prey other than *Mnemiopsis*. To test this possibility, Negarestan and colleagues put the two comb jellies and the zooplankton *Acartia* in tanks in various combinations. "We found that *Beroe* doesn't feed on the zooplankton at all," Negarestan says. And to his surprise, *Acartia* did better when cohabiting with *Beroe* than in the absence of either jelly. Researchers have also tested whether *Beroe* might carry unspecified pests into the Caspian. "Parasites die off, probably because of the change in salinity," Negarestan says, whereas the bacteria profiles of the two seas are similar.

Scientists first made their case for introducing *Beroe* at a February 2004 meeting in Tehran sponsored by IFRO and the Caspian Environment Programme, a World Bank and European Union initiative with representatives from the five littoral nations—Azerbaijan,

Iran, Kazakhstan, Russia, and Turkmenistan. Kazakhstan vetoed the project on scientific grounds. Then earlier this year, the researchers aired the proposal at the Commission of Aquatic Bio-resources of the Caspian Sea, a forum for the five nations to manage stocks of seals, kilka, and sturgeon. Again, Kazakhstan objected, and the commission took a pass. "We have gone down two dead ends," says Negarestan, who says action at the foreign ministry level, or higher, may be required for approval. Dumont, who chaired the meetings, says he's "frustrated" by the lack of action.

Although this year the kilka fishery has rebounded slightly, it's unknown whether that means *Mnemiopsis* numbers have climaxed. Some in Iran whisper about taking matters into their own hands. "It's not easy to pass a border with a jar of comb jellies," says Negarestan. And even if smuggling were successful, he says, "it's highly unlikely" that a fisher could adapt *Beroe* to the Caspian. But if frustration mounts, one of the littoral countries may well attempt an unofficial introduction. "It's something that a scientist could do," Negarestan says.

—RICHARD STONE



**Proud father.** Aquaculturist Hamid Reza Pourali cradles a young sturgeon at ISRI.

# Is Katrina a Harbinger of Still More Powerful Hurricanes?

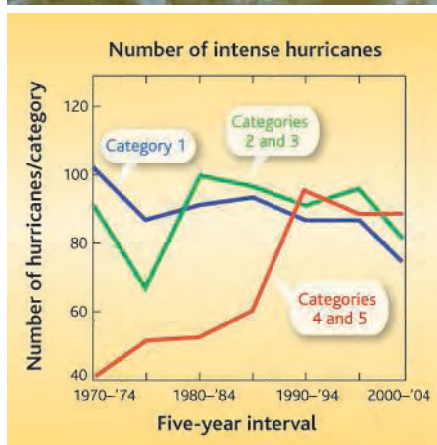
Mounting evidence suggests that tropical cyclones around the world are intensifying, perhaps driven by greenhouse warming, but humans still have themselves to blame for rising damage

Were New Orleans and coastal Mississippi victims of global warming? Greenhouse alarmists and the tabloids say yes, but until recently, most scientists would have answered no way. There was no evidence that global warming has had any effect on the planet's most powerful storms—dubbed hurricanes, typhoons, or cyclones depending on the ocean that spawns them.

Now, however, a connection is emerging between warming oceans and severe tropical cyclones. On page 1844, meteorologists report a striking 80% increase worldwide in the abundance of the most powerful tropical cyclones during the past 35 years. The study lends support to another, independent study published just last month that found a similar intensification in the Atlantic and western North Pacific. At the same time, the tropical oceans have been warming, driven, most researchers agree, by rising greenhouse gases. "There's a strong suggestion of a link" between the growing greenhouse and intensifying tropical cyclones, says meteorologist Kerry Emanuel of the Massachusetts Institute of Technology, sole author of the earlier paper.

But you still can't blame Katrina's damage on global warming, says Emanuel. There have been too few powerful storms striking densely populated coasts to declare with any confidence that intensifying storms are increasing the damage. And vulnerable coastal populations have swollen so much in recent decades that the increase in damage due to demographics is swamping any sign of increased damage due to storm intensification. But just wait until the second half of the century, he says.

Global warming and tropical cyclones are naturally linked by the storms' appetite for heat. Tropical storms are heat engines that draw their energy upward from warm ocean water to drive their winds before expelling waste heat to the upper atmosphere. So warming the tropical oceans—in effect throwing more wood on the fire—might be expected to spawn more frequent or more intense tropical cyclones. To find out whether warming has done that, meteorologist Peter Webster of the Georgia Institute of Technology in Atlanta and his colleagues examined satellite records of storms around the tropics, a history now 35 years long. The temperature contrast between a storm's eye and the adjacent cloud



**Bad trend rising.** The number of the most intense tropical cyclones is increasing worldwide.

tops provides a gauge of maximum wind speed, as calibrated in the Atlantic and western North Pacific against direct measurements of wind speeds by storm-penetrating aircraft.

Webster and colleagues seem to have been one for two in their search for warming effects. They found no long-term trend in the number of storms per year, only natural ups and downs, even as summer tropical sea surface temperatures rose 0.5°C. In the North Atlantic, where hurricane numbers have surged since 1995, such variability arises from changes in the strength of warm ocean currents (*Science*, 1 July, p. 41). But the researchers did find a sharp increase during the past 35 years in the number of category 4 and 5 tropical cyclones, the most intense storms that cause most of the

damage on landfall. Globally, category 4 and 5 storms climbed 57% from the first half of the period to the second.

That growing proportion of tropical cyclones in categories 4 and 5 "is very consistent with my results," says Emanuel. As he reported in the 4 August issue of *Nature*, he calculated the total power released during the life of Atlantic and western North Pacific storms (the Pacific spawns about five times as many storms as the Atlantic does) based on reported maximum sustained winds. Because of stronger winds and longer storms, this power dissipation index rose between 40% and 50% from the first half of the 45-year record to the second, in step with rising ocean temperatures. With two studies finding that the same trends correlate with sea surface temperatures in a half-dozen ocean basins, "it's fairly well established that the measure of hurricane intensity has been increasing," says Emanuel.

Perhaps predictably, that hasn't stopped other researchers from giving the two papers a guarded initial reception. Meteorologist Kevin Trenberth of the National Center for Atmospheric Research in Boulder, Colorado, notes inevitable reservations about such indirectly measured records. And modeler Thomas Knutson of the Geophysical Fluid Dynamics Laboratory in Princeton, New Jersey, says, "We would not have expected the signal [of storm intensification] to be detectable at the present time," based on theory and his modeling of storms under a growing greenhouse. That, he says, prompts the question, "Are these trends real?"

In any case, no one, including Webster and Emanuel, is claiming that these two positive results suffice to link global warming firmly to tropical cyclone intensification. Webster, for one, would first want to understand exactly how warming waters could trigger such a large response.

Even if global warming is driving a real intensification of tropical cyclones, notes climatologist Roger Pielke Jr. of the University of Colorado, Boulder, it shouldn't change anyone's plans. It's easy to see a rising trend in U.S. hurricane damage as people flock to the coasts, he says, and even the effects of the natural North Atlantic oscillation and of El Niño on hurricanes are recognizable in storm damage. But there's no sign of an effect of storm intensification. That's down in the noise and will be for many decades, he says.

A beach house owner on the southeast U.S. coast has plenty to worry about from current storm hazards, Emanuel agrees. But anyone operating globally on a half-century time scale or longer, such as some insurance companies, should expect to see big changes later this century, he says. Then global warming can start taking the blame. —RICHARD A. KERR

# Scientists Weigh Options For Rebuilding New Orleans

As experts ponder how best to rebuild the devastated city, one question is whether to wall off—or work with—the water

Even before the death toll from Hurricane Katrina is tallied, scientists are cautiously beginning to discuss the future of New Orleans. Few seem to doubt that this vital heart of U.S. commerce and culture will be restored, but exactly how to rebuild the city and its defenses to avoid a repeat catastrophe is an open question. Plans for improving its levees and restoring the barrier of wetlands around New Orleans have been on the table since 1998, but federal dollars needed to implement them never arrived. After the tragedy, that's bound to change, says John Day, an ecologist at Louisiana State University (LSU) in Baton Rouge. And if there is an upside to the disaster, he says, it's that "now we've got a clean slate to start from."

Many are looking for guidance to the Netherlands, a country that, just like bowl-shaped New Orleans, sits mostly below sea level, keeping the water at bay with a construction of amazing scale and complexity (see sidebar, p. 1809). Others, pointing to Venice's long-standing adaptations, say it's best to let water flow through the city, depositing sediments to offset geologic subsidence—a model that would require a radical rethinking of architecture. Another idea is to let nature help by restoring the wetland buffers between sea and city.

But before the options can be weighed, several unknowns will have to be addressed. One is precisely how the current defenses failed. To answer that, LSU coastal scientists Paul Kemp and Hassan Mashriqui are picking their way through the destroyed city and surrounding region, reconstructing the size of water surges by measuring telltale marks left on the sides of buildings and highway structures. They are feeding these data into a simulation of the wind and water around New Orleans during its ordeal.

"We can't say for sure until this job is done," says Day, "but the emerging picture is exactly what we've predicted for years." Namely, several canals—including the MRGO (pronounced Mister Go), which was



**Reconstruction.** Experts are piecing together how the current defenses failed in order to help design a new system to protect New Orleans from future storms.

built to speed shipping in the 1960s—have the combined effect

of funneling surges from the Gulf of Mexico right to the city's eastern levees and the lake system to the north. Those surges are to blame for the flooding. "One of the first things we'll see done is the complete backfilling of the MRGO canal," predicts Day, "which could take a couple of years."

The levees, which have been provisionally repaired, will be shored up further in the months to come, although their long-term fate is unclear. Better levees would probably have prevented most of the flooding in the city center. To provide further protection, a mobile dam system, much like a storm surge barrier in the Netherlands, could be used to close off the mouth of Lake Pontchartrain. But most experts agree that these are short-term fixes.

The basic problem for New Orleans and the Louisiana coastline is that the entire Mississippi River delta is subsiding and eroding, plunging the city deeper below sea level and removing a thick cushion of wetlands that once buffered the coastline from wind and waves. Part of the subsidence is geologic and unavoidable, but the rest stems from the levees that have hemmed in the Mississippi all the way to its mouth for nearly a century to prevent floods and facilitate shipping. As a result, river sediment is no longer spread across the delta but dumped into the Gulf of Mexico. Without a constant stream of fresh sediments, the barrier islands and marshes are disappearing rapidly, with a quarter, roughly the size of Rhode Island, already gone.

After years of political wrangling, a broad group pulled together by the Louisiana government in 1998 proposed a massive \$14 billion plan to save the Louisiana coasts, called Coast 2050 (now modified into a plan called the Louisiana Coastal Area project). Wetland restoration was a key component. "It's one of the best and cheapest hurricane defenses," says Day, who chaired its scientific advisory committee.

Although the plan was never given more than token funding, a team led by Day has been conducting a pilot study since 2000, diverting part of the Mississippi into the wetlands downstream of the city. "The results are as good as we could have hoped," he says, with land levels rising at about 1 centimeter per year—enough to offset rising sea levels, says Day.

Even if the wetlands were restored and new levees were built, the combination of geologic subsidence and rising sea levels will likely sink New Orleans another meter by 2100. The problem might be solved by another ambitious plan, says Roel Boumans, a coastal scientist at the University of Vermont in Burlington who did his Ph.D. at LSU: shoring up the lowest land with a slurry of sediments piped in from the river. The majority of the buildings in the flooded areas will have to be razed anyway, he says, "so why not take this opportunity to fix the root of the problem?" The river could deposit enough sediment to raise the bottom of the New Orleans bowl to sea level "in 50 to 60 years," he estimates. In the meantime, people could live in these areas Venice-style, with buildings built on stilts. Boumans even takes it a step further: "You would have to raise everything about 30 centimeters once every



## Questioning the 'Dutch Solution'

**KRAGGENBURG, THE NETHERLANDS**—Dutch scientists are making waves—literally. In a hangar here, researchers from Delft Hydraulics, a research and consulting institute, have built a 4-meter-wide slice of a dike at the end of a basin, used to mimic the North Sea crashing into the coast. Their goal: to test how different types of surface materials weather the thunderous onslaught.

Even after a millennium of hard-won experience, the Dutch are still perfecting the art of dike construction. They have little choice. More than half of the country—including Amsterdam, Rotterdam, and most of The Hague—lies below sea level and continues to sink, and the water is expected to rise as a result of climate change. Three major, often erratic, rivers compound the challenge. No wonder that many in the United States are wondering if the Dutch experience holds lessons for New Orleans.

Scientists in both countries agree that some of the technology developed here could be useful, and Dutch institutes and businesses are eager to help. But their offers come at a time when Dutch water management is increasingly questioned at home. Some scientists say the reliance on engineering prowess is not only ecologically harmful but has increased vulnerability in the long run. The national mindset shouldn't be exported without awareness of its downsides, cautions Toine Smits, a water management expert and professor at two universities.

The Dutch, too, learned their lessons the hard way. On 1 February 1953, a severe North Sea storm combined with a spring tide burst through neglected dikes in hundreds of places, killing more than



**Safety first.** The Delta Works, a response to the 1953 flood in the Netherlands, consists of a series of dams including a storm surge barrier across the Eastern Scheldt (*above, right*).

1800 people and flooding 2000 km<sup>2</sup> in the southwestern provinces. The answer, built over the subsequent 45 years, was The Delta Works, a series of dikes, dams, and other structures that closed off the major sea arms in the southwestern delta—destroying entire ecosystems in the process—and shortened the coastline by 600 kilometers.

Dikes that protect the most densely populated areas of the country are built to withstand all but storms expected once every 10,000 years, says Delft Hydraulics director Huib de Vriend.

Louisiana's geography is different, and no one is talking about damming the Mississippi Delta. Still, some Dutch solutions may work, says Bruce Good of the U.S. Geological Survey. After an intense political battle, for instance, the Dutch decided against permanently closing off one estuary; instead, the Eastern Scheldt was equipped with a "storm surge barrier" that shuts only in emergencies. Although pricey—the project cost more than \$1 billion—a similar solution could be used to block Lake Pontchartrain from the Gulf of Mexico while saving its ecology.

But in the end, protecting low-lying areas with dikes only is a "dead-end street" that should be avoided if possible, says Henk Saeijs, a former civil servant and professor at Erasmus University Rotterdam. When natural sedimentation stops and groundwater levels are kept low, the land sinks, requiring ever higher dikes and bigger pumps to get the water out. ("Pumping or drowning" is a national motto here.) Meanwhile, the illusion of safety lures people and investments, making future floods even more costly.

Although there is no turning back for built-up areas, it's "utterly crazy" to keep urbanizing areas far below sea level, as is still happening in the Netherlands, Saeijs says. Instead, he advocates "embracing the water"—an approach in which floods are not a major problem because people live on mounds, in higher areas, or "floating cities."

But Han Vrijling, a hydraulics engineer at Delft Technical University, says that in most cases, giving the water its freedom is a "romantic" notion that's not compatible with a modern economy. Besides, "we shouldn't be too nervous" about ever-higher dikes towering over a sinking country, he says.

—M.E. AND J.B.

30 years, so why not make the job easier by making houses that can float?"

Whether that is technically or politically feasible—Day, for one, calls it "not likely"—remains to be seen, especially because until now, the poorest residents lived in the lowest parts of the city. Any decision on how best to protect the city in the future will be tied to how many people will live there, and where. "There may be

a large contingent of residents and businesses who choose not to return," says Bill Good, an environmental scientist at LSU and manager of the Louisiana Geological Survey's Coastal Processes section. It is also not yet clear how decisions about the reconstruction will be made, says Good, "since there is no precedent of comparable magnitude." Every level of government is sure to be involved, and "the process is

likely to be ad hoc."

Even with the inevitable mingling of science and politics, we still have "a unique chance to back out of some bad decisions," says Good, who grew up in New Orleans. "I hope that we don't let this once-in-history opportunity slip through our fingers in the rush to rebuild the city."

—JOHN BOHANNON AND MARTIN ENSERINK  
John Bohannon is a writer in Berlin, Germany.

# Safer Alternative Could Replace Widespread Contaminant

Stain-resistant carpets, upholstery, and fabrics have a dark underside. A common coating that keeps them pristine has recently been found to break down into perfluorooctanoic acid, also known as PFOA or C8, a persistent compound that accumulates inside the body and has been fingered as a possible carcino-



**Green clean.** New polymers resist stains without breaking down into persistent compounds.

gen. Manufacturers have been scrambling to come up with alternatives, but none could rival C8-producing stain fighters. At the American Chemical Society (ACS) meeting, however, chemists from the University of North Carolina, Chapel Hill (UNC-CH), unveiled an alternative that repels stains with the best of them but that breaks down into compounds that don't accumulate in the body.

"It's a great step forward," says Tim Kropp, a toxicologist with the Environmental Working Group in Washington, D.C., who has closely followed C8 health concerns. Kropp notes that C8 is found in the blood of 96% of Americans and has been detected everywhere from the middle of the Pacific and Atlantic oceans to embedded in Arctic ice. Animal tests have suggested that the compound is a potential carcinogen, although that has yet to be confirmed in people. Still, the persistence of C8 has persuaded Canada to ban some of the compounds that break down to form C8 in the environment. C8 is also an industrial solvent in its own right, and manufacturers have begun to switch to other solvents and phase out its use. But many researchers suspect that textile and paper coatings, which are ubiquitous, are the largest environmental source of the chemical.

Current polymer fabric coatings owe their popularity to fluorine, an element that when added to polymers makes them strongly repel

both water and oil. The polymers consist of a long hydrocarbon backbone bristling with innumerable fluorine-containing arms, each containing eight carbons. Over time, the arms can break off and react with oxygen to form C8. That compound has a combination of size and chemical behavior that makes it readily taken up in the body but difficult for the body to break down and eliminate, says Joseph DeSimone, a UNC-CH chemist who led the effort to develop the new alternative.

DeSimone says that about 2 years ago, he and Paul Resnick, a polymer chemist formerly with DuPont and now at UNC-CH, noticed animal studies that suggested that fluorinated hydrocarbons with four instead of eight carbon atoms in the chains don't persist in the body. So they set out to make one with good stain-resistant qualities. Researchers at

3M had commercialized fluoropolymers with four carbons in the side chains for use as manufacturing solvents. But those compounds, the UNC-CH researchers found, did not repel water and oil as well as the longer chain compounds did. Part of the problem, DeSimone notes, is that the shorter side chains don't pack tightly around the hydrocarbon backbone. As a result, the backbone can more easily interact with oil and water, thereby making the chemicals less repellent.

To get around this problem, Ji Guo, a Ph.D. student in DeSimone's lab, doctored the C4 side chains, outfitting each with an extra pair of hydrocarbon groups called methylenes. The methylenes, DeSimone says, encouraged the side chains to pack tightly together, making a more formidable barrier around the hydrocarbon backbone. Tests of the new materials showed that they repel oil and water almost identically to the longer-side-chained polymers, Guo says. But because the new coatings are made from polymers with shorter side chains, even if they break down over time, there is no way that they can generate C8. DeSimone says he and his colleagues have applied for patents on the new materials and have already had several discussions with textile manufacturers interested in the technology. Kropp says the new compounds must be tested to make sure there are no unforeseen problems. How-

WASHINGTON, D.C.—About 13,000 chemists, physicists, and engineers gathered here from 28 August to 1 September to discuss research with applications including environmental protection, national security, and future energy sources.

ever, he adds, "it's always great to see scientists come up with an alternative to a problematic compound."

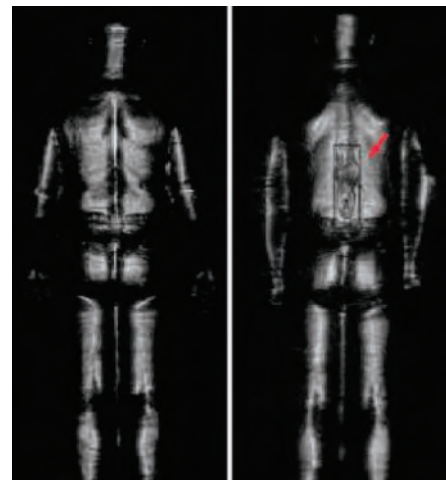
—ROBERT F. SERVICE

## New Techniques Aim To Thwart Terrorists

In more than a dozen sessions at the ACS meeting dedicated to defense and homeland security, researchers presented technologies aimed at countering every imaginable terrorist threat—from devices for sensing explosives strapped onto the body of a suicide bomber to sensors capable of detecting microscopic quantities of biotoxins injected into a city's water supply.

Not surprisingly, many talks focused on transportation security. The tools currently available to screeners at airports and subway stations—metal detectors, x-ray scanners, sniffer dogs, and manual pat-downs—can't detect explosives or nonmetallic weapons concealed inside luggage or on the body of a passenger. Two technologies presented at the meeting offer a solution to those problems, although they both have a way to go before they can be deployed.

One, developed by David Sheen and his colleagues at Pacific Northwest National Laboratory in Seattle, Washington, uses electromagnetic radiation of millimeter wavelength to see through clothing and other barriers. Ranging between 30 and 300 gigahertz in fre-



**Nailed.** Millimeter waves spot plastic explosive strapped to a tester's spine (right).

CREDITS (TOP TO BOTTOM): JUPITER IMAGES, JIM ZEY

quency, these are the same microwaves used for applications such as wireless access to the Internet. Different materials on a person's body reflect them to varying degrees, enabling a computer to generate a three-dimensional image showing the outlines of concealed objects. Because the waves are nonionizing, "they do not pose any health risks," Sheen says. The scan currently takes up to 10 seconds, during which the person must stand relatively still. Generating the image takes up to another 30 seconds. Sheen says his group is working to speed up the system.

A similar technology described by Robert Barat, a chemical engineer at the New Jersey Institute of Technology in Newark, uses waves of a shorter wavelength. Submillimeter (or terahertz) waves, familiar to radio astronomers, generate a spectrum when they interact with a material. They can also be transmitted farther than millimeter waves can. By harnessing those properties, Barat's group hopes to design scanners that would be capable of detecting weapons and bombs carried by a terrorist more than 5 meters away. The method "has the potential of not only showing the presence of a hidden substance but also of identifying the substance based on a transmission or reflection spectrum," says Barat, who has yet to build a prototype. Jehuda Yinon, an expert on explosives detection at the Weizmann Institute of Science in Rehovot, Israel, says the technology could be an invaluable tool for identifying suicide bombers in public places.

Other talks spotlighted new biosensors for detecting chemical and biological agents. Their common goal is to sniff out smaller and smaller doses of toxins in the environment with greater speed and accuracy. For example, a new sensing technique described by Jeffrey Mason, a researcher at the Armed Forces Institute of Pathology in Washington, D.C., can detect as few as 500 molecules of cholera or botulinum in a sample. That's 1000 times more sensitive than existing techniques.

The heart of the sensing device is a liposome—a molecular cylinder made up of lipids—with a DNA molecule encapsulated inside and a receptor molecule on the outside that attaches specifically to the toxin. The toxin molecules are first captured on a plate using antibodies that bind to the toxin. When the liposomes are added to this mix, the receptor molecules linked to them attach to the toxin as well. At the end of the assay, everything else is washed away, leaving only the liposomes that have been chained to the toxin molecules.

The researchers then split the liposomes open with an enzyme to release the DNA molecules and tally them with a standard polymerase chain reaction (PCR)—in effect, using the DNA molecules as a proxy for the toxin. And because PCR can detect tiny amounts of DNA (by making many copies of DNA molecules present in a sample), the technique can



**Cheaper gas?** Converting waste into H<sub>2</sub> could lower refining costs and spur a hydrogen economy.

sense extremely low concentrations of toxin. "What they've done is amplified the signal. It's really very clever," says James Robertson, a research biologist at the Federal Bureau of Investigation Laboratory in Quantico, Virginia.

—YUDHIJIT BHATTACHARJEE

## New Routes Toward Practical Hydrogen?

Hydrogen makes a tantalizing fuel. Water is its only byproduct when burned or run through a fuel cell to make electricity. It's also the most abundant element in the universe. But the downside is that earthly hydrogen is almost always bound to other elements, and liberating it requires much more energy than it releases as a fuel. At the meeting, two separate teams reported novel approaches to extracting hydrogen from waste products that could bring a sustainable hydrogen economy a step closer.

In the first, researchers from Pennsylvania and Georgia reported on a new catalyst that converts hydrogen sulfide (H<sub>2</sub>S)—an abundant contaminant in natural gas wells—to hydrogen gas (H<sub>2</sub>). In the other, researchers from Indiana revealed a new process for recovering H<sub>2</sub> from silicon-based compounds, which could open the door to new ways of generating and storing hydrogen.

Outsiders say it's too early to tell whether these approaches make economic sense. But they are "promising avenues," says Joseph Sadighi, a catalyst expert at the Massachusetts Institute of Technology in Cambridge.

Raiding industrial waste for useful chemicals is nothing new. H<sub>2</sub>S is routinely converted to sulfur dioxide (SO<sub>2</sub>) as part of a process to generate sulfuric acid, a widely used compound in the chemical industry. But although that reaction turns the sulfur in H<sub>2</sub>S into a valuable commodity, it misses an opportunity to do the same for hydrogen by instead converting it to water.

Using vanadium-based catalysts to convert H<sub>2</sub>S into SO<sub>2</sub> can generate H<sub>2</sub> instead of water, report Israel Wachs of Lehigh Univer-

sity in Bethlehem, Pennsylvania, and Andrew Gibson, who heads Gibson Technologies in Atlanta, Georgia. The conversion, Gibson explained, takes place in two steps. First, carbon monoxide (CO) reacts with H<sub>2</sub>S using a long-known reaction to generate H<sub>2</sub> and another compound called carbonyl sulfide (COS), a toxic byproduct. The COS is then fed to another chamber, where it reacts with oxygen over a vanadium oxide catalyst to form SO<sub>2</sub> and CO. The CO is then fed back into the first reaction to generate more H<sub>2</sub>.

Unlike the current technology used to convert H<sub>2</sub>S to H<sub>2</sub>, which extracts the CO needed for the hydrogen-generating reaction from expensive natural gas, the new approach continually generates CO by breaking down the toxic COS. Gibson notes that the process not only might fuel a future hydrogen economy but also could reduce the cost of refining gasoline by supplying H<sub>2</sub> needed to strip crude oil of sulfur.

Purdue University chemist Mahdi Abu-Omar and colleagues offered a very different scheme for generating hydrogen. They discovered it while looking for novel catalysts to convert organic silicon-based liquids called organosilanes into silanols, a more valuable class of compounds used in the chemical industry. The researchers were working with rhenium-based catalysts, which they added to organosilanes and water. They found that the rhenium catalysts not only readily converted their organosilanes into silanols but also generated large amounts of H<sub>2</sub>. Organosilanes may make an attractive way to store hydrogen for later use in fuel cells, Omar notes, because both they and the silanol "wastes" are liquids and easy to transport.

Abu-Omar acknowledges that the compounds are somewhat costly to produce and are generated industrially in only small quantities. At the meeting, Sadighi noted that related catalysts might also react with another silicon-based liquid, called PMHS, which is produced in large quantities as a byproduct of the silicone business. Turning this or other more abundant organic compounds into hydrogen could make hydrogen an even more tantalizing fuel.

—ROBERT F. SERVICE

# RANDOM SAMPLES

Edited by Constance Holden

## Egypt in China

Scholars in Beijing have unearthed ancient Egyptian treasures, collected by a diplomat of China's last emperor, that have lain forgotten for almost a century.

In 1906, ambassador Duan Fang, an antiquarian of some renown, purchased a number of Egyptian artifacts while passing through Cairo. In 1911, he was assassinated; his collection was later bought by the Chinese government.

Three years ago, Willy Clarysse of the Catholic University of Leuven in Belgium and Yan Haiying of Beijing University found some Egyptian funerary stelae with hieroglyphic texts in the Museum of Beijing University, registered under the name of Duan Fang. That set off a hunt for the rest of the collection. They ultimately found three sarcophagi, some 50 stone slabs, and more than 60 rubbings made from them at the museum, as well as in the storerooms of the Forbidden City and the National Library. The stelae range from the Old Kingdom to the early Christian Coptic period and have never been published, says Clarysse. He adds that most of the stelae are actually casts, but inscriptions by Duan Fang suggest that the originals must be somewhere in China: "So the search for the originals has just started."



The priestess Thenu, whose sarcophagus was made from a hollowed-out palm tree.

## Crème de la Crème

A stratospheric IQ predicts more worldly success than just a superhigh one, say researchers. That, they say, undermines the "threshold effect": the notion that IQ scores above, say, 130 don't matter because at those levels, other traits such as motivation and creativity distinguish people.

Scientists at Vanderbilt University in Nashville, Tennessee, looked at the careers of precocious youths who had aced the math SAT, an IQ-like test, at the age of 13. Using data collected when the subjects were 33, the researchers compared the top and bottom quartiles—covering about 1000 subjects—of those who scored in the top 1% of the math SAT on four indicators: advanced degrees, salaries, patents, and tenure at a top U.S. university.

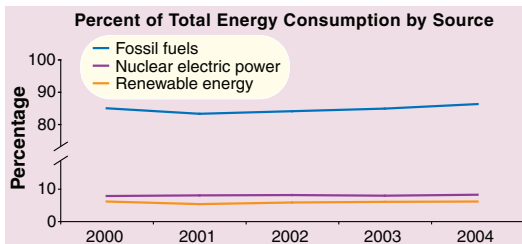
In a paper in press at the *Journal of Educational Psychology*, the researchers report that the top quartile usually come out ahead: 32.1% got Ph.D.s, compared with 20% in the bottom quartile. For patents, it was 7.5% versus 3.8%; for tenure, 3.2% versus 0.4%. The highest scorers also made more money. The findings make sense in view of the fact that "the top 1% contains one-third of the ability range," says Vander-

bilt's David Lubinski. For example, everything over 137 is in the top 1% of IQ scores, but IQs can go beyond 200.

Psychologist Joseph Renzulli of the University of Connecticut, Storrs, a proponent of the threshold effect, says he remains unconvinced. "Unless we can draw a perfect relationship between cognitive ability and creative productivity" in a wide range of people of above-average ability, "we must assume" that other factors are critical, he says.

## Renewables in the Doldrums

New figures from the Department of Energy show that despite billions in research into renewable energy sources over the past 3 decades, fossil fuels remain king.



Proponents of renewable energy sources say such sources could benefit from skyrocketing oil prices, but that government subsidies—which have helped the fossil fuel and nuclear industries—are needed to spur investment.



## A Choir of Wrens

The plain-tailed wrens of Ecuador may not look like much. But they do something unique in the bird world: synchronized antiphonal chorusing. Researchers have found that small groups of male and female wrens sing in such perfectly timed, alternating tweets that what emerges sounds like a call from a single bird.

A team led by Peter Slater, an ornithologist at St. Andrews University in Fife, U.K., found tight groups of the wrens singing in the underbrush during a 2002 survey in the Andes. Extensive subsequent recordings and observations, reported online 7 September in *Biology Letters*, revealed that each sex has a repertoire of about 20 phrases. When they sing together, members of each sex spontaneously choose the same two phrases, creating songs that can last up to 2 minutes. As many as seven birds can sound like a single chirper.

The reason for this complex vocalization is a mystery. One possibility is that, because the male and female wrens look alike—common in tropical birds—the group effort helps coordinate mating. Another is that the amplified song scares off intruders. The feathered choirs may help us understand how bird species acquire new songs, says Katharina Riebel, an ornithologist at Leiden University in the Netherlands. (For a sample song, go to [sciencenow.sciencemag.org/feature/data/Plain-tailed-wren.wav](http://sciencenow.sciencemag.org/feature/data/Plain-tailed-wren.wav))

Edited by Yudhijit Bhattacharjee

**POLITICS**

**Back in the fold.** Three years after cutting ties with its Iranian members, the Institute of Electrical and Electronics Engineers (IEEE) this week sent its president-elect to mend fences. Michael Lightner will reestablish the society's Iran section during his visit to Tehran and Shiraz, building upon a May ruling by the U.S.



Department of Commerce that allows IEEE to recognize members in Iran, Cuba, and Sudan—countries under a U.S. trade embargo.

IEEE still can't provide the section with any money, equipment, or services. But it can sponsor conferences and other events. The trip should help reduce the ill feeling caused by the society's 2002 decision to withdraw membership benefits (*Science*, 19 September 2003, p. 1646), says Farokh Marvasti, director of the Advanced Communications Research Center at Sharif University of Technology in Tehran. But IEEE's inability to fund events organized by

the Iran section makes the visit mostly a symbol of a better future, he says.

**Changing environment.** Iran's new president has brought a second scientist, and the first woman, into his inner circle. Last week, Mahmoud Ahmadinejad named paleontologist Fatemeh Javadi as one of nine new vice presidents in his cabinet. (Last month, mathematician Mohammad-Mehdi Zahedi was named science minister.)

Got any tips for this page?  
E-mail [people@aaas.org](mailto:people@aaas.org)

**SURVIVORS**

**Weathering Katrina.** For 10 days after Hurricane Katrina struck, New Orleans, Louisiana, zoo veterinarian Elizabeth Hammond slept in the reptile house and helped the zoo's 1500 animals cope with the disaster. She tended to an injured flamingo, helped evacuate 11 sea lions and otters to Texas due to fears that the zoo's water supply might be contaminated, and assisted in feeding the zoo's skeletal staff as well as its permanent residents. "It's a daily struggle, just providing for these animals," she said last week by cell phone from New Orleans.



Situated on high ground, the zoo escaped flooding but lost power before switching to a generator. Thanks to emergency plans, the zoo had several days' worth of supplies on hand. National Guard members living in dry zoo buildings are currently helping keep the zoo stocked.

Hammond, 31, eventually took a breather by driving to her family's home in Kentucky. But she plans to return to help the zoo survive.

**THEY SAID IT**

"[Scientists] are people who by definition live outside the norm, ... floating in zones that had never been reached before, ... people with strong egos and God complexes. That sounds like rock 'n' roll to me."

—Publisher Bob Guccione Jr., founder of *Spin* and soon-to-be owner of *Discover* magazine, comparing the worlds of music and science last week in *The New York Times*

**AWARDS**



**Love's reward.** It's said that love and work don't mix. But don't tell that to population biologists Rosemary and Peter Grant. This month, the married couple from Princeton University in New Jersey won an \$800,000 International Balzan Foundation prize for their 30-year study of the finches on the Galápagos Islands.

Married since 1962, the couple has avoided conflicts by carving out specialties within their field. "She is the expert on behavior and bird song, while I focus on measuring phenotypes," says Peter. And what will they do with the money? "I have no idea," says Rosemary, "but we're on cloud nine."

The Swiss-based foundation has also honored Russell Hemley and David Mao, mineralogists at the Carnegie Institution of Washington, D.C.; Lothar Ledderose, an art historian at Rupprechts Karls University in Heidelberg, Germany; and Peter Hall, a social historian at University College London, U.K.

CREDITS (TOP TO BOTTOM): ELIZABETH HAMMOND; IEEE; DENISE APPLEWHITE/PRINCETON UNIVERSITY OFFICE OF COMMUNICATIONS

## A Strongly Held, But Wrong Conviction

**IN SUPPORT OF PROPOSALS TO DROP SOME** evolution-related questions from school tests, Kathy Martin of the Kansas Board of Education recently told *Science* (“Kansas prepares new standards,” Y. Bhattacharjee, News of the Week, 19 Aug., p. 1163) that “some students have deeply held convictions about this topic, which puts them at a disadvantage while answering questions on a test.” I can sympathize with such students. During a mathematics exam some years ago, I recall being disadvantaged due to my deeply held conviction that  $3 \times 5$  equals 14. Thankfully, my teacher did not share this conviction.

One would have hoped that any person influencing the science education curriculum would support the requirement that all students are taught objective evidence-based thinking, regardless of their personal convictions.

**RICHARD G. PEARSON**

American Museum of Natural History, Central Park West at 79th Street, New York, NY 10024-5192, USA.

## Early Uses of the Ivory-Billed Woodpecker

**I READ WITH CONSIDERABLE PLEASURE THE** account of the ivory-billed woodpecker’s survival in “Ivory-billed woodpecker (*Campephilus principalis*) persists in continental North America” (J. W. Fitzpatrick *et al.*, Reports, 3 June, p. 1460) and “Rediscovery of the ivory-billed woodpecker” (D. S. Wilcove, Perspectives, 3 June, p. 1422). The relatively intensive use of ivory-bill skulls in specific items of Native American material culture may suggest that the very low population density and infrequent encounter rates noted for recent populations may not have applied, at least to the same degree, to ivory-bill populations in the past. The Ioway—a group from the American midcontinent not generally associated with the southeastern old-growth bottomland forests identified as the range of the ivory-bill—used the skull of female ivory-bills as central elements in a series of Buffalo clan-related pipe bundles (1). A single pipe stem associated with the Pigeon clan used seven male ivory-bill heads as decoration. Pileated woodpeckers (*Dryocopus pileatus*) are also sometimes used, and one pipe whose clan associations

are unclear included one male ivory-bill scalp, with the scalps of four pileated woodpeckers spaced along the shaft.

The ivory-bill’s widespread depictions in prehistoric art may also suggest that it was a more familiar sight than would be suggested by its relatively reclusive descendants. It appears, for example, on both engraved shell and ceramics from late prehistoric sites from Florida to Oklahoma (2); one particular style of engraved shell gorget, the so-called Cox Mound style, depicts four ivory-bills in rotation symmetry around the margins of the design, surrounding a looped square and cross-in-circle. Scholars differ regarding the meaning of the woodpecker heads (3). Although rarity may have been one factor in the selection of ivory-bill body parts for ceremonial objects, its use as a recognizable iconographic symbol suggests a greater degree of familiarity.

**ALEX BARKER**

Department of Anthropology, Milwaukee Public Museum, 800 West Wells Street, Milwaukee, WI 53233, USA.

### References

1. A. Skinner, *Ethnology of the Ioway Indians*, vol. 5 (Bulletin of the Milwaukee Public Museum, Milwaukee, WI, 1926).
2. J. P. Brain, P. Phillips, *Shell Gorgets: Styles of the Late Prehistoric and Protohistoric Southeast* (Peabody Museum Press, Cambridge, MA, 1996).
3. George Lankford has suggested they represent the four winds (4); Barker suggests sentinels (5).
4. G. Lankford, in *Hero Hawk and Open Hand: American Indian Art of the Ancient Midwest and South*, R. Townsend, Ed. (Yale Univ. Press, New Haven, CT, 2004), pp. 217–218.
5. A. Barker, *Archaeology* 55 (no. 4), 44 (2002).

## Are Polar Bears Threatened?

**NUNAVUT, CANADA, HAS INCREASED THE** harvest quota for the 12 subpopulations of polar bears found within the territory from 403 in 2004 to 518 in 2005 partly based on the perception by Inuit (not supported by scientific data) that some subpopulations have been increasing under the historical harvest regime (1). The subpopulation in Western Hudson Bay was allocated an increase in harvest from 47 to 56 bears. However, this population has experienced large changes in animal condition and reproductive rates associated with climate warming (2) and appears to be in decline (3). The recent 14th Working Meeting of



**Polar bear mother and cubs in Wapusk National Park, Manitoba, Canada.**

the IUCN/SSC Polar Bear Specialist Group recommended that appropriate management action be taken without delay (4).

The Baffin Bay population, shared with Greenland, was allocated an increase in harvest quota from 64 in 2004 to 105 in 2005. Based on a recent population estimate of 2074 (SE = 266), it was concluded that an assumed total harvest of 88 bears/year is sustainable (5). Greenland manages polar bears without a quota system, and the Greenland harvest from the Baffin Bay population has increased significantly over the last 10 years (6). A total harvest of 200 to 300 bears/year, based on a Nunavut harvest of 105 and a possible harvest of more than 150 bears by Greenland hunters, is much higher than is sustainable by this population. The 14th Working Meeting of the IUCN Polar Bear Specialist Group classified the population as decreasing.

The Group recommended that increases in harvest levels or estimates of subpopulation sizes should not be based on traditional knowledge without support from sound scientific data (7). In addition, the Group concluded that the IUCN Red List classification of the polar bear should be upgraded from “Least Concern” to “Vulnerable” based on the likelihood of an overall decline in the size of the total population of more than 30% in 35 to 50 years due to global warming (8).

**ØYSTEIN WIIG**

Natural History Museum, University of Oslo, Oslo N-0318, Norway.

### References

1. N. J. Lunn *et al.*, paper presented at the 14th Working Meeting of the IUCN/SSC Polar Bear Specialist Group, Seattle, WA, 20 to 24 June 2005.
2. I. Stirling, N. J. Lunn, J. Iacozza, *Arctic* 52, 294 (1999).
3. E. Richardson *et al.*, paper presented at the 14th Working Meeting of the IUCN/SSC Polar Bear Specialist Group, Seattle, WA, 20 to 24 June 2005.
4. Resolution no. 3 from the 14th Working Meeting of the IUCN/SSC Polar Bear Specialist Group, Seattle, WA, 20 to 24 June 2005 (available at pbsg.npolar.no).

5. M. K. Taylor *et al.*, *Arctic* **58**, 203 (2005).
6. E. W. Born, C. Sonne, paper presented at the 14th Working Meeting of the IUCN/SSC Polar Bear Specialist Group, Seattle, WA, 20 to 24 June 2005.
7. Resolution no. 1 from the 14th Working Meeting of the IUCN/SSC Polar Bear Specialist Group, Seattle, WA, 20 to 24 June 2005 (available at pbsg.npolar.no).
8. Press release from the 14th Working Meeting of the IUCN/SSC Polar Bear Specialist Group, Seattle, WA, 20 to 24 June 2005 (available at pbsg.npolar.no).

## Using Words Carefully

**SCIENTIFIC LANGUAGE SHOULD CONVEY AN** exact meaning, which both follows and furthers scientific understanding. Unfortunately, when scientific terms are used in public debates, they sometimes mislead rather than clarify.

Alberts *et al.* have pointed out the problems with the term “therapeutic cloning” (1). Nonscientists tend to think of a “clone” as a living copy of another person—it takes a focused effort to explain to the average citizen that therapeutic cloning does not entail making a copy of another person and that what many find abhorrent (including ourselves) is reproductive cloning. The term “therapeutic cloning” should be replaced with “somatic cell nuclear transfer” or simply “nuclear transfer” in all scientific literature and discussions.

“Embryo” leads to even more confusion, largely because few speakers or writers use the precise scientific definition, “the developing human individual from the time of implantation to the end of the eighth week after conception” (2). Many scientific publications and most legislation refer to the embryo as beginning at conception, not as the stage of human development that begins after implantation in the uterus. As a result, people easily overlook the distinctions between pre-implantation and post-implantation stages of development. As Clifford Grobstein noted, the exposure to the microenvironment of the uterine endometrium alters the developmental fate of the cells of the inner cell mass of the blastocyst. Before implantation, those cells can become any type of cell. If separated into two parts, they can yield two embryos; if cells from two different blastocysts are merged, they can result in a single embryo (3). He wrote, “It is only when the later-stage blastocyst has penetrated and implanted in the uterine wall that the properties of the inner cell mass change and it becomes committed to the production of a single individual” [(4), p. 27]. Not distinguishing between these two stages leads to confusing the concept of genetic individu-

ality, established at fertilization, with developmental individuality, established at the primitive streak stage of embryogenesis.

The problems caused by this inexact language are clear. As Irving Weissman has pointed out, the word “embryo” evokes an image very different from that of a pre-implantation blastocyst. “Whenever we asked people, even scientists, to draw an embryo, they’d usually draw a fetus with legs, head, and so on. Nobody drew a ball of 150 cells.” [(5), p. 83].

We recommend that *Science* and other publications use the term “preembryo,” earlier advocated by Grobstein, to cover the period between fertilization and implantation. When appropriate, one can use the more specific terms “zygote,” “morula,” or “blastocyst.” We further recommend using the term “early stem cells” instead of the term “embryonic stem cells.”

We have no illusions that more exact terminology will quiet disputes about when life begins and what research is permissible. We do believe that accurate language will result in clearer debates and will not so routinely mislead the uninformed.

**WILLIAM H. DANFORTH<sup>1</sup> AND WILLIAM B. NEAVES<sup>2</sup>**

<sup>1</sup>Washington University in St. Louis, 7425 Forsyth Boulevard, St. Louis, MO 63105, USA. <sup>2</sup>Stowers

Institute for Medical Research, 1000 East 50th Street, Kansas City, MO 64110, USA.

#### References

1. B. Vogelstein *et al.*, *Science* **295**, 1237 (2002).
2. MedLinePlus Medical Dictionary (accessed 14 June 2005 at [www.nlm.nih.gov/medlineplus/medlineplusdictionary.html](http://www.nlm.nih.gov/medlineplus/medlineplusdictionary.html)).
3. C. Grobstein, *Ann. N.Y. Acad. Sci.* **541**, 346 (1988).
4. C. Grobstein, *Science and the Unborn* (Basic Books, New York, 1988).
5. S. Lehrman, *Sci. Am.*, July 2003, p. 82.

## The Slide of Education

I RECENTLY STARTED GRADUATE STUDIES AT the University of California, Berkeley and have discovered that PowerPoint lectures have become ubiquitous across college campuses. Proponents of PowerPoint will argue that writing on the chalkboard takes too long and less material can be covered. I agree, and that is precisely why I prefer the old-fashioned method. With slides, it is all too easy to flip through a complex diagram or table in a matter of seconds, whereas writing on the board slows the instructor down and allows the students time to digest the material. Following PowerPoint lectures is difficult because they lack continuity; once a slide is advanced, it is gone. I surveyed 172 undergraduate students in Berkeley's introductory biology course, and 48% indicated that following and grasping material is easier with the chalkboard, with 40% preferring PowerPoint, and 12% ambivalent.

Slides also facilitate copying and pasting from textbooks or other sources. Lectures should complement the reading, not duplicate it. Even for diagrams and figures, a simplified chalk drawing is often easier to grasp than a busy slide image. Not surprisingly, 60% of the surveyed students are more motivated to attend chalkboard lectures, compared with 10% who favor slides. And of the students who do attend, 60% find staying awake easier during a chalkboard lecture, while only 13% are more alert with PowerPoint.

Some will accuse me of being a technophobe, but I am a computational biologist with a profound admiration of technology. I often use PowerPoint myself, but rarely

### Letters to the Editor

Letters (~300 words) discuss material published in *Science* in the previous 6 months or issues of general interest. They can be submitted through the Web ([www.submit2science.org](http://www.submit2science.org)) or by regular mail (1200 New York Ave., NW, Washington, DC 20005, USA). Letters are not acknowledged upon receipt, nor are authors generally consulted before publication. Whether published in full or in part, letters are subject to editing for clarity and space.

when teaching. There are occasional instances when a slide may help to get a point across, but before making another one for your lecture, please ask yourself whether it is necessary and whether it will really help the students.

LEONID TEYTELMAN

Department of Molecular and Cell Biology, University of California, Berkeley, 516 Barker Hall, Berkeley, CA 94720, USA.

## An Archaeological Dilemma

THE HOTLY DEBATED ISSUE CONCERNING THE publication of unprovenanced tablets coming out of Iraq is indeed a vexing one ("Looted tablets pose scholar's dilemma," A. Lawler, *News Focus*, 5 Aug., p. 869), but the rigid and uncompromising position of the archaeological establishment only compounds the tragedy that the looting of archaeological sites in Iraq (and elsewhere) has presented. Not only have these precious records of the past been ripped from their original context, but now the archaeologists wish to suppress the very knowledge of their existence by banning their recording and publication. Their assertion that the publication of such texts enhances their value has no scientific basis and has not been substantiated in any way. From my perspective, any and all such written documentation must be rescued, recorded, preserved, and published. Only then will we be able to save even a small part of what has been destroyed by the looters. Scholars publish unprovenanced texts that have been confiscated by Iraqi officials. They publish objects that have been returned to Iraq by various foreign authorities. Our field is built upon the tens of thousands of unprovenanced tablets that make up the majority of collections in museums, universities, and private collections the world over. In addition, it is well known that the current body of texts now in private hands includes critically important historical, literary, religious, and economic information that is completely new. To close our eyes to the existence of these texts borders on absurdity. Looting is the uncontrolled destruction of sites; archaeology is the controlled destruction of sites. Without publication, the net result of either is the same—loss of knowledge. As scholars, our primary purpose is to preserve and disseminate knowledge, not to suppress and ignore it. I hope more rational minds will prevail.

DAVID I. OWEN

Department of Near Eastern Studies, Cornell University, 409 White Hall, Ithaca, NY 14853-7901, USA.

## CORRECTIONS AND CLARIFICATIONS

**Letters:** "Notes and double knocks from Arkansas" by R. A. Charif *et al.* (2 Sept., p. 1489). The URL for the Supporting Online Material was incorrect. It should be [www.sciencemag.org/cgi/content/full/309/5740/1489c/DC1](http://www.sciencemag.org/cgi/content/full/309/5740/1489c/DC1).

**Cover Caption:** (2 Sept., p. 1445). The caption contained incorrect information. Only the 16S ribosomal RNA is shown; the transfer RNA is not shown.

**Special Section on Mapping RNA Form and Function:** "In the forests of RNA dark matter" by G. Riddihough (2 Sept., p. 1507). The image credit was incorrect. It should be Albion Baucom.

**News Focus:** "Is the friendly atom poised for a comeback?" by E. Marshall (19 Aug., p. 1168). An incorrect description of an energy forecast was attributed to physicist Thomas Cochran of the Natural Resources Defense Council in the story. What Cochran discussed in fact were the possible consequences of adding 700 Gigawatts of nuclear electric capacity, not 700 reactors, to the current global capacity of 367 GWe. This calculation was not related to any expectation about the amount of global warming to be avoided.

**Perspectives:** "The paradox of mantle redox" by C. McCammon (6 May, p. 807). There were two reference errors in the figure legend. In line 6, reference (18) should be (7). In line 8, reference (15) should be (13).

**Reports:** "Centennial-scale Holocene climate variability revealed by a high-resolution speleothem  $\delta^{18}\text{O}$  record from SW Ireland" by F. McDermott *et al.* (9 Nov. 2001, p. 1328). As a result of a detailed reanalysis of a portion of stalagmite CC3 using micro-milling followed by conventional stable isotope analyses, ion-probe analyses, and reanalyses using the original laser technique, it is evident that the large (~8%) decrease in  $\delta^{18}\text{O}$  (correlated to the 8.2 ka cooling event in this Report) is an analytical artefact (I. J. Fairchild *et al.*, *Earth Sci. Rev.*, in press). Reanalysis of the original calcite blocks from stalagmite CC3 indicates that anomalously low oxygen isotope ratios were produced by previously undetected incipient cracking of the sample during the original analysis by laser ablation gas chromatography isotope ratio mass spectrometry (LA-GC-IRMS).  $\delta^{18}\text{O}$  and  $\delta^{13}\text{C}$  data acquired during 2005 by LA-GC-IRMS accurately reproduce the conventionally analyzed micro-milled results apart from a small number of analytical points (<5) adjacent to visible cracks in the calcite. The new results impact on three paragraphs of the Report in which the significance of the isotope anomaly was discussed. The discussion of the coherent fluctuations in  $\delta^{18}\text{O}$  between stalagmite CC3 and the GISP2 ice core in the early to mid-Holocene (Report, Fig. 2) highlighted in the Abstract of the Report is unaffected. These data remain robust, as similar fluctuations were recorded in a previously published lower-resolution conventional analysis of the speleothem [F. McDermott *et al.*, *Quat. Sci. Rev.* **18**, 1021 (1999)]. The absence of a clear oxygen isotope anomaly associated with the "8.2 ka" cooling event at this Atlantic margin site may imply that cooler conditions resulted in deposition of calcite with higher  $\delta^{18}\text{O}$ , partially compensating for any small shift to lower  $\delta^{18}\text{O}$  in rainfall associated with putative freshwater releases to the North Atlantic [D. C. Barber *et al.*, *Nature* **400**, 344 (1999)].



## ASTRONOMY

### People, Stars, and Scopes

Vera Rubin

**A** former postdoc of mine once quipped that “American astronomy became pre-eminent because of two discoveries: Hale discovered money and Pickering discovered women.” Hale, an independently wealthy astronomer, was the driving force in building four telescopes—the 40-inch refractor at Yerkes Observatory (1897), the 60-inch (1908) and the 100-inch (1917) reflectors at Mount Wilson Observatory, and the 200-inch (1948) reflector on Palomar Mountain. Several were the largest telescopes in the world when built. The ability to see farther and with better resolution than earlier telescopes, aided by the development of the photographic plate, increased enormously the data gathered by observational astronomers. Measuring stellar positions, brightnesses, and tabulating data required the “cooperation of a great number of assistants to perform manipulations involving much labor and time, requiring intelligence and great accuracy, but not necessitating original mental power,” wrote an eminent woman in 1893. Mary Putnam Jacoby, a physician, concluded, “This is a most useful and important field of work for women” (1, 2).

Edward C. Pickering, the director of the Harvard College Observatory from 1876 to 1919, satisfied his observatory’s labor needs by hiring female assistants (“Pickering’s Harem”) who were “capable of doing as much and as good routine work as astronomers who would receive much larger salaries.” He noted that “three or four times as many assistants can thus be employed, and the work done correspondingly increased for a given expenditure” (3). About 40 women worked at the Harvard College Observatory between 1885 and 1920. Among them was Henrietta Swan Leavitt (1868–1921). Leavitt volunteered her services to the observatory a few years after

graduating from Radcliffe College in 1892, and she was appointed to the permanent staff in 1902 at a salary of 30 cents per hour (4).

In *Miss Leavitt’s Stars: The Untold Story of the Woman Who Discovered How to Measure the Universe*, George Johnson reconstructs the course of this brilliant woman’s life from the few available sources, even including the census records. Johnson, a *New York Times* science reporter and author, tells her story with elegance and sensitivity.

By 1904, already skilled at determining stellar brightness from photographic plates, Leavitt noticed that numerous stars in the Small Magellanic Cloud had images that varied systematically in brightness on plates taken at different times. Her 1908 paper identifying 1777 variable stars in the Magellanic Clouds (5) contains the modest statement, “It is worthy of notice that...the brighter variables have the longer periods.” Four years later, Leavitt published her masterpiece, “Periods of 25 Variable Stars in the Small Magellanic Cloud” (6), which demonstrated the tight relation between period and brightness (see figure).

Such stars, which exhibit a steep rise to maximum light and a slow decay to minimum light, are now called Cepheid variables. The Large and Small Magellanic Clouds, small satellites of our Milky Way Galaxy, are so distant that all of their stars are essentially at the same distance from us. From the observed period of a Cepheid, astronomers can infer the brightness of the star

**The brighter the star, the slower the blink.** Leavitt’s plot, from (6), of the brightness-variation period versus brightness for 25 variable stars in the Small Magellanic Cloud (background photograph). The abscissa is the log of the period in days; the ordinate is the magnitude of the star, with brightness increasing upward. The upper line fits the magnitudes at maximum light; the lower, the magnitudes at minimum.

**Miss Leavitt’s Stars**  
The Untold Story  
of the Woman  
Who Discovered  
How to Measure  
the Universe  
by George Johnson

Norton, New York, 2005.  
176 pp. \$22.95, C\$34.  
ISBN 0-393-05128-5.  
Weidenfeld and Nicolson,  
London. £14.99. ISBN 0-  
297-84647-7. Great  
Discoveries.

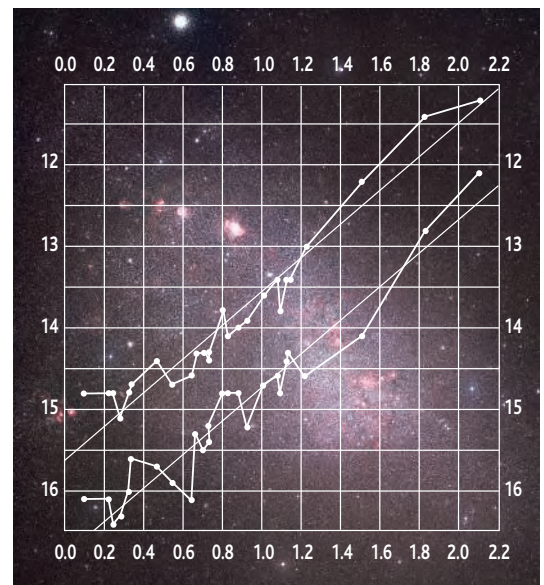
**Stargazer**  
The Life and Times  
of the Telescope  
by Fred Watson

Da Capo, Cambridge,  
MA, 2005. 352 pp.  
\$24.95, C\$32.95. ISBN  
0-306-81432-3. Allen  
and Unwin, St. Leonards,  
New South Wales,  
Australia, 2004. A\$35.  
ISBN 1-865-08658-4.

from Leavitt’s plot. Its distance, relative to the Magellanic Cloud’s distance, can then be determined from a comparison of its observed brightness to the brightness of the Magellanic Cepheids. Once the distance of a single Cepheid is known from other methods, absolute distances can be found for any observed Cepheid. By 1914, astronomers were attempting to calibrate Leavitt’s relation.

However, Leavitt’s job was to identify, catalog, and do other detailed work for Pickering. She was not given the time to pursue her discoveries. No record in the Harvard Observatory files indicates that Leavitt ever used a telescope professionally. According to Cecilia Payne-Gaposchkin, another of the eminent woman astronomers who came later to Harvard, this was “a harsh decision, which condemned a brilliant scientist to uncongenial work, and probably set back the study of variable stars for several decades” (7).

In his gentle account, Johnson does not enumerate the indignities that Leavitt accepted. Instead, midway through the book, he turns to the work of Harlow Shapley, Edwin Hubble, and other astronomers. He details their roles in using Cepheid variable stars to confirm that we live in the Milky Way Galaxy, and that the universe is filled with billions of distant galaxies. In his preface, Johnson explains that he had originally intended to use Leavitt “as nothing more than a device, a way to get into the story” of how people discovered the vastness of the universe. One of the orbiting Hubble telescope’s “key projects” was to identify Cepheid variables in more distant galaxies in order to evaluate the expansion rate of the universe at great distances from our galaxy.



Leavitt died at the young age of 53, four years before Gösta Mittag-Leffler of the Royal Swedish Academy of Sciences wrote her for information he wished to use to nominate her for the Nobel Prize in physics he thought she deserved. Mittag-Leffler's letter was answered by Shapley, by then director of the Harvard Observatory. Johnson sees the phrasing of Shapley's reply as indicating that he would deny Leavitt credit for her finding and was angling for the prize himself.

Despite the profound influence Leavitt's discovery had on the astronomy and cosmology that followed it, her name is little known. When the Smithsonian Institution's Air and Space Museum opened in 1976, its first planetarium show concerned the universe—and credited Hubble with discovering the period-luminosity law for Cepheids. My letters to the directors of the museum and the Harvard College Observatory elicited some activity, but the conclusion was that the program, taped by a famous movie star, could not be corrected. I have forgotten that star's name. Johnson's book will help ensure that Henrietta Leavitt's is remembered.

Hubble and his use of Cepheid variables also appear in *Stargazer: The Life and Times of the Telescope*. Despite its title, Fred Watson's book is more about people than telescopes. Its subjects are the opticians and scientists whose imaginations and hard work transformed the primitive telescope of the early 17th century into the technological giants of today. Some of their names—such as Galileo Galilei, Isaac Newton, and Hubble—are familiar to all. Others—Laurent Cassegrain, James Gregory, and George Ritchey—being attached to telescope types, are at least known to astronomers. And some—including George Bass, Chester Moor Hall, and Niccolò Zucchi—will be recognized only by specialists in the history of telescopes. Watson (an astronomer at the Anglo-Australian Observatory in New South Wales) has written a reader-friendly book, one full of stories about the laboratory skills, the science, and the personal intrigues that have accompanied the development of the telescope through the last four-plus centuries.

Galileo and Newton were the early giants whose foundational work made telescopes important. They understood the geometry of the lenses that were required, and they had the impressive technical skills necessary to fabricate them. But important contributions were made by many others, such as the barrister Hall. In 1729, Hall attempted to produce a telescope lens that did not suffer from chromatic aberration, one constructed so that light of all colors would be focused at a single point. He hoped that by cementing together two types of glass with different optical properties, the resulting compound lens would be achromatic. But fearful that two lenses of the same

diameter would arouse suspicion if ordered from the same optical company, he ordered the two different lenses from two different companies. He could not know that each company, busy with other work, would hire the same “jobbing craftsman” to grind and polish the lenses. His telescope worked, but was ultimately involved in what Watson describes as “one of the bitterest episodes in the entire history of the telescope.”

*Stargazer* is full of such stories, which make the book fun to read and distinguish it from more encyclopedic histories. Watson's tales often range from the past to the present. In 1509, Leonardo da Vinci was confident that the planets orbited Earth, not the Sun, and he illustrated this in his *Codex Leicester* (a notebook now owned by Bill and Melinda Gates). Leonardo's conviction “is revealed by the bold hole made by the point of his compass, preserved for all time in the original manuscript.”

Watson's book contains no footnotes or references in the text. Instead, 22 pages of “notes and sources” in fine print are packed after the epilogue. (Links back to the relevant main text are provided through page numbers and the first words of sentences.) The interesting stories that reside there should not be missed. For example, as background material for the tale about da Vinci mentioned above, Watson offers: “Leonardo's diagram appears in the *Codex Leicester*, folio 7r (reproduced in Desmond and Pedretti 2000, p. 75). The hole was noted while the *Codex* was on exhibition in Sydney, 6 September–5 November 2000.”

Women are not completely absent from *Stargazer*. However, the most notable—the unnamed beauty whose face adorns the chapter headings—is Andromeda as she appears in Johann Bayer's landmark celestial atlas, *Uranometria* (8).

It is amusing that Johnson and Watson each provide their book with a whimsical chapter: Johnson's prologue envisions distance estimates made by an ancient civilization; Watson's epilogue imagines the discoveries that follow the launch of the hypertelescope in 2055. *Miss Leavitt's Stars* and *Stargazer* draw welcome attention to the contributions of often-overlooked individuals. Both books will reward readers interested in people who have helped advance our understanding of the universe.

#### References and Notes

1. M. P. Jacoby, in *The World's Congress of Representative Women*, M. W. Sewall, Ed. (Rand McNally, Chicago, 1894), p. 157; quoted in (2).
2. D. J. Warner, *Conspectus Hist.* 1(7), 12 (1981).
3. E. C. Pickering, *Harvard Coll. Obs. Annu. Rep.* 53, 4 (1898).
4. Using, as Johnson does, “The Inflation Calculator” at [www.westegg.com](http://www.westegg.com), one finds that this rate, adjusted for inflation, corresponds to \$6.65 in 2005.
5. H. S. Leavitt, *Ann. Astron. Obs. Harvard Coll.* 60, 87 (1908).
6. [H. S. Leavitt], E. C. Pickering, *Harvard Coll. Obs. Circ.*

173 (1912). Although the paper is signed Edward C. Pickering, its first line reads, “The following statement regarding the periods of the 25 variable stars in the Small Magellanic Cloud has been prepared by Miss Leavitt.” History and Web-site referencing services are more fair and attribute the circular to Leavitt.

7. C. H. P. Gaposchkin, *Cecilia Payne-Gaposchkin: An Autobiography and Other Recollections*, K. Haramundanis, Ed. (Cambridge Univ. Press, Cambridge, 1984).
8. J. Bayer, *Uranometria* (Augsburg, Germany, 1603).

10.1126/science.1117658

## GEOLOGY

# The Grand Question

John C. Schmidt

For eight miles from the Milk Spring we continue to cross hills and valleys, then follow a low swale shaded by giant pines with trunks three to four feet in thickness. The banks are a parterre of flowers. On yonder hillside, beneath one of these kingly trees, is a spot which seems to glow with an unwonted wealth of floral beauty. It is scarcely a hundred yards distant; let us pluck a bouquet from it. We ride up the slope.

The earth suddenly sinks at our feet to illimitable depths. In an instant, in the twinkling of an eye, the awful scene is before us.

—Clarence E. Dutton

*Tertiary History of the Grand Canyon (1)*

No adults forget their first experience of walking from the relatively flat, forested plateaus of the Coconino or the Kaibab to the Grand Canyon's rim. Suddenly, they are confronted by a vast space of quiet wind and successions of gray, white, and red cliffs and benches that drop thousands of feet beneath them. Somewhere at the bottom of the canyon, an inner gorge holds a river they cannot see. The Grand Canyon is Earth's greatest celebration of geology. Whether tourist or earth scientist, at some point, we ask, “How did this happen?”

Depending on what guide book we read or what ranger talk we listen to, we might learn that the Colorado River is perhaps 30 million years old, having established its course through the Intermountain West prior to regional uplift. And that it then cut its canyons by maintaining its grade as the surrounding landscape rose, by processes known as antecedence (1, 2) or superposition (3). We might learn that complicated changes in stream course took place in the western Grand Canyon about 18 million years ago, but that the river's course was

The reviewer is in the Department of Aquatic, Watershed, and Earth Resources, Utah State University, Logan, UT 84322-5210, USA. E-mail: [jack.schmidt@usu.edu](mailto:jack.schmidt@usu.edu)



"The awful scene is before us." Part ("Looking East") of William Henry Holmes's meticulously detailed *Panorama from Point Sublime*, from the elephant folio-size *Atlas* that accompanied Dutton's *Tertiary History*.

well established by that time further upstream (4). We might learn that the Colorado River once flowed up the modern canyon of the Little Colorado River and perhaps toward the Gulf of Mexico (5). We might learn that the Grand Canyon is less than 5 million years old (6).

In *Grand Canyon: Solving Earth's Grandest Puzzle*, James Lawrence Powell attempts to guide us through more than a century of "geologizing," eventually leading us to the modern interpretation of the Colorado River's age and how the river formed its Grand Canyon. In doing so, Powell (a geologist now directing the National Physical Science Consortium) sketches for the lay reader episodes in the evolution of the science of geology, its methods, and its paradigms.

It is difficult to tell the story of the geological investigation of the Grand Canyon without also telling stories about the geologists themselves. The author does so extensively in describing the work of John Wesley Powell and his associates. This early part of the book is, unfortunately, less comprehensive and less elegant than other accounts focused solely on the topic (7–9). Some of the writing is trite, "the Mississippi can just keep rollin' along"; oversimplified, such as remarks about the three men who left the first Powell expedition; or inexact, "Kanab Canyon...reveals itself...as a nearly vertical, mile-high, but relatively thin, canyon." Kanab Canyon is narrow, but it is not "thin." Nonetheless, the introductory chapters with their descriptions

of the late-19th-century expeditions to the Grand Canyon region offer readers with varied backgrounds a common footing.

James Powell describes the thought and work of the early geologists, who made profound deductions from simple observations of rock strata and topography. He also provides a feeling for the intellectual context of their times. While Darwin was developing his explanation of evolution, geologists were debunking the notion that a Great Flood formed Earth's topography a few thousand years ago.

The author moves on to describe the observations of later generations of geologists, including the observations and reasoning that completely revised the early explanations of how the Grand Canyon

formed. To do so, researchers have had to look away from the Canyon itself to the oldest deposits of the Colorado River downstream from the Grand Canyon and the evidence of the most recent time when the Colorado River did not exist at key localities. They have had to examine igneous rocks, weigh

the significance of radiometric dates, and consider the timing and spatial implications of plate tectonics. The evidence is scattered and incompletely preserved, and geologists today are still unclear about details of the Colorado River's development. But these gaps are relatively minor—a few million years of missing evidence here or there, the absence of unambiguous evidence of the fate of the Colorado River prior to the establishment of the river's course in west-

ernmost Grand Canyon. Powell reviews the evidence for concluding that different parts of the Colorado River system are of different ages, that the Grand Canyon is about 5 million years old, and that its establishment is ultimately tied to the opening of the Gulf of California and the movement of Earth's tectonic plates. He also offers readers a taste of modern speculation and the uncertainties surrounding these generally accepted notions.

*Grand Canyon* will be enjoyed by anyone who is curious about how geologists think, piece together disparate information, and assemble explanations. Until a time machine is invented, we will never know for sure how the Grand Canyon formed. Nonetheless, we do know that the

rocks forming the canyon walls are of immense age and that the cliffs and slopes exposing those rocks are features of the last instants of their history.

In telling the Canyon's story, Powell provides an honest and open description of geological detective work and the rethinking of ideas. At a time when the National Park Service sells a book describing a creationist explanation of the Grand Canyon's formation little different than the ideas from which modern geology emerged more than 150 years ago, the book reminds us of the timeless contrast between the methods of modern natural science and the power of myth.

#### References

1. C. E. Dutton, *U.S. Geol. Surv. Monogr. 2* (Washington, DC, 1882).
2. J. W. Powell, *Exploration of the Colorado River of the West and Its Tributaries* (U.S. Government Printing Office, Washington, DC, 1875).
3. S. F. Emmons, *Science* 6, 19 (1897).
4. C. B. Hunt, *U.S. Geol. Surv. Prof. Pap.* 669-C, 59–130 (1969).
5. E. D. McKee, R. F. Wilson, W. J. Breed, C. S. Breed, *Evolution of the Colorado River in Arizona: A Hypothesis Developed at the Symposium on Cenozoic Geology of the Colorado Plateau in Arizona, August 1964* (Museum of Northern Arizona, Flagstaff, AZ, 1967).
6. I. Lucchitta, in *Grand Canyon Geology*, S. S. Beus, M. Morales, Eds. (Oxford Univ. Press, New York, ed. 2, 2003), pp. 260–274.
7. W. E. Stegner, *Beyond the Hundredth Meridian: John Wesley Powell and the Second Opening of the West* (Houghton Mifflin, Boston, 1954).
8. S. J. Pyne, *Grove Karl Gilbert: A Great Engine of Research* (Univ. Texas Press, Austin, TX, 1980).
9. D. Worster, *A River Running West: The Life of John Wesley Powell* (Oxford Univ. Press, New York, 2000). [Reviewed by S. J. Pyne, *Science* 291, 441 (2000).]

**Grand Canyon  
Solving Earth's  
Grandest Puzzle**  
by James Lawrence Powell  
Pi Press, New York, 2005.  
317 pp. \$27.95, C\$38.95.  
ISBN 0-13-147989-X.

## A Madisonian Approach to Climate Policy

David G. Victor,<sup>1\*</sup> Joshua C. House,<sup>2</sup> Sarah Joy<sup>2</sup>

After years of gridlock and indecision, serious efforts to slow the greenhouse express are finally taking hold. Unlike the integrated global scheme envisioned under the Kyoto Protocol, progress is arriving via fragmented and multi-speed efforts. The decentralized system is akin to the messy federalism that James Madison embraced in the U.S. Constitution (1). Whereas Madison foresaw individual states becoming “laboratories” for political innovation, this global federalism of climate policy has emerged through innovation within nations, regions, and individual firms.

The most important efforts have involved trading emissions credits for carbon dioxide (CO<sub>2</sub>), the leading human cause of climate change. So far, six trading systems have emerged—each a laboratory with its own procedures, stringency, and prices (see figure, right). The European Union (EU) is leading the pack with a system that caps CO<sub>2</sub> emissions from about 12,000 industrial facilities. Meanwhile, a distinct trading system in the United Kingdom continues to operate. The Kyoto Protocol includes a provision called the Clean Development Mechanism (CDM) that awards tradable credits for investments that cut emissions in developing countries. And the World Bank has established its own CDM-like mechanism, the Prototype Carbon Fund (PCF), which invests in carbon-reducing projects mainly in developing countries. Even in the United States, where the federal government has notoriously rejected any

binding limit on greenhouse gases, 31 firms have imposed their own modest emission cuts and are trading credits on the private Chicago Climate Exchange (CCX). In addition, the lack of federal effort has compelled states to launch their own initiatives. Nine states in the northeast are far advanced in designing a scheme that would cap CO<sub>2</sub> emissions from power plants and would allow carbon trading.

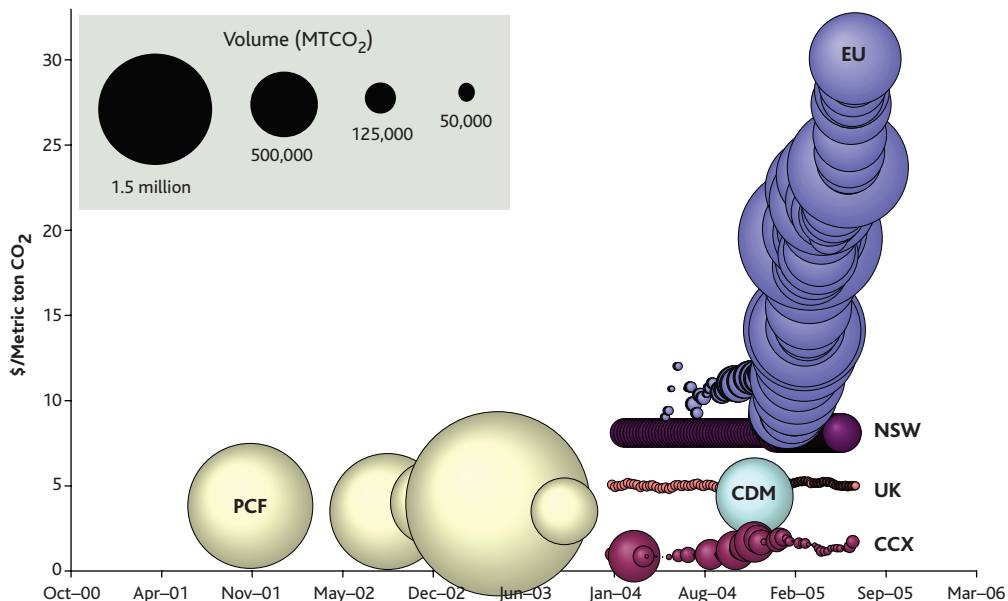
This fragmented “bottom-up” approach to carbon trading is not simply a stiff smile to be painted on the wreckage of grander

become inconvenient (such as when the United States abandoned the Kyoto process). A system that originates from the top takes the speed of its least ambitious nation (5, 6).

The strength of a bottom-up approach is its ability to tap stronger national and regional institutions for governance. Indeed, the most successful experiences with emission trading have all occurred within the boundaries of strong governing institutions (mainly in the United States) (7–9). The EU, although it now has 25 members, initially applied its carbon trading scheme to just the subset of 15 members that have the longest history of cooperation and were most capable of tolerating the intrusive procedures for allocating emission credits and enforcing compliance.

Still, progress is needed on three fronts. First, a suitable framework is needed to help stitch these fragmented efforts into a fuller global approach. For now, Madisonian laboratories allow flexibility that accommodates

Enhanced online at  
www.sciencemag.org/cgi/content/full/309/5742/1820



**Prices and volumes for six trading schemes.** Data for PCF and CDM observations represent individual projects; the EU’s Emission Trading System (ETS) values are daily, and the CCX values are weekly. We also show monthly values (derived from annual averages) for the U.K. trading system. NSW (Australia) trading values are monthly estimates based on trading averages for the 15 months preceding April 2005. Sources: Point Carbon, International Emissions Trading Association.

visions for global trading. Rather, it is pragmatic and effective (2–4). The architects of global trading were blinded by the theoretical benefits that could arise from trading among diverse economies; a universal system, they thought, would also prevent free riding. However, global institutions are too weak to monitor and enforce what is, in effect, a new monetary system. Global agreements are also vulnerable to exit when commitments

widely varied political preferences and institutions. For example, the trading scheme emerging in Canada will feature a “safety valve” to prevent pricing from exceeding 15 CAD (~U.S. \$12.5), which will assure industry that carbon trading won’t hurt competition with U.S. firms, which face no federal limits. By contrast, the EU system allows prices to vary more widely. Fault lines will arise between these different approaches,

<sup>1</sup>D.G.V. is adjunct senior fellow at the Council on Foreign Relations and director of the Program on Energy and Sustainable Development (PESD), Stanford, CA 94305–6055, USA. <sup>2</sup>J.C.H. and S.J. are Research Fellows at PESD.

\*Author for correspondence. E-mail: david.victor@stanford.edu

and governments will not allow trading between these different systems unless they have confidence in the integrity of each system and see a comparable level of effort. Formal coordination will be needed to create wider and deeper markets.

Today's conventional wisdom focuses on treaties, such as the Kyoto Protocol, as the instruments for international coordination. But treaties, because they are binding, focus drafters on legal compliance and are therefore inherently conservative. They are good at locking the least risky achievements into place but a poor way to chart an uncertain course.

A different approach would engage leaders to set ambitious, nonbinding goals that would steer the Madisonian effort. Heads of government would assemble cross-cutting deals into a package of climate policies. Peer review would promote learning and hold governments accountable. Canadian Prime Minister Paul Martin has advocated such a concept, what he calls the "L20," as a standing forum of about 20 leaders from North and South to address a wide array of global issues (10). On climate change, the L20's cross-cutting packages of commitments would address every major aspect of the problem, including support for scientific research, programs to develop better carbon-free energy technologies, commitments to control emissions, and policies that make societies more adaptive to a changing climate (11). The L20 could launch treaty negotiations for particular issues that require the force of binding law. It could oversee the technical and political work needed to interlace the different trading systems together into an increasingly global currency.

The L20 group would be small enough to make progress on such complex issues yet sufficiently broad to exert leverage on the global situation. (The top 20 emitters of greenhouse gases account for about three-fourths of the world total.) Such an approach—high-level engagement, concentration on a handful of important countries, the setting of aspirational goals, regular progress review, and subsequent codification into binding law—has been used effectively in controlling acid rain and water pollution in Europe, in arms control, and in breaking logjams in trade negotiations (12).

Second, and most importantly, the U.S. government must devise a serious response. Global efforts are difficult to inspire when the leader on most international matters is far back in the pack. Current U.S. policy relies on funding for climate science and low-carbon technologies, as well as voluntary emission controls, such as a pact announced with five Asian countries. But U.S. policy lacks a strong signal that will

induce firms to reduce carbon. Gridlock in the United States stems partly from unrealistic goals set in Kyoto, as well as political polarization. Recently signed comprehensive energy legislation does not include any limit on carbon.

The absence of serious action by the U.S. federal government has catalyzed individual states and even cities to pursue their own policies. But such efforts are too atomized to exert much leverage on the country's emissions, because federal institutions mostly govern the U.S. economy. For example, 10 states have set their own emissions targets, but none has a viable plan to achieve its goals. These 10 are among the least carbon-intensive in the nation. Their per capita emissions are about half the country average, and although they produce about one-third of the nation's income, they generate just 14% of its electricity (13). [Electric power plants are the largest single sector for CO<sub>2</sub> (14).] In California, the same week that Arnold Schwarzenegger's government announced a target to reduce greenhouse gas emissions to 2000 levels by 2010 (with deeper cuts later), it also pushed for a stronger power grid that will make it possible to import more coal-fired (and carbon-intensive) electricity from Nevada, Utah, and Wyoming. As Madison himself argued, effective governance requires assigning the functions of government to the institutions that have leverage and accountability.

Third, a new strategy is needed to engage developing countries, which already account for nearly half the world's total emissions. Thus far, these nations have steadfastly refused to limit their effluent because they rightly put a higher priority on development. Most visions for overcoming this challenge have imagined a Kyoto-like trading system; developing countries would receive extra credits needed to cover the higher emissions that would accompany their industrial growth (15). But this approach is doomed, because governments that have imposed strict caps and strong institutions for trading will object to the printing of extra credits that will cause capital and effort to flow into the developing countries. Indeed, the managers of the EU's trading system are likely to impose controls on trading outside the EU's zone precisely to avoid such a flood of foreign permits.

A Madisonian approach would engage developing countries on their own terms rather than through carbon caps and prices (16). For example, more programs to build natural gas infrastructures would help the governments of China and India to manage their local air pollution problems while cutting emissions of CO<sub>2</sub>. (Compared with coal, gas typically emits less than half the

CO<sub>2</sub> for every unit of useful energy, such as electricity.) Most of the capital and effort needed to build these gas infrastructures must come from the Chinese and Indian governments and private investors. The L20, however, can provide a framework for other governments to help. India's shift to gas is being hampered by the United States-led effort to isolate Iran, which is slowing plans to build an important pipeline from Iran's vast gas deposits to markets in Pakistan and India. External pressure and assistance to normalize Russia's gas industry would help to unlock vast Siberian gas deposits for export to China. In China alone, faster implementation of gas could cut annual CO<sub>2</sub> emissions in 2020 by an amount larger than all the emissions from all the cars in California (17).

For those who fear the plague of global warming, this bottom-up process will appear painfully slow and sprawling. The narrow focus of each fragment will seem contrary to the global geophysics of carbon. But it is the only way to build credible institutions that are essential for markets.

#### References and Notes

- In particular, see Federalist papers nos. 37, 39, 45, and 46 in *The Debate on the Constitution*, B. Bailyn, Ed. (Library of America, New York, 1993).
- G. M. Morgan, *Science* **289**, 2285 (2000).
- D. G. Victor, *Climate Change: Debating America's Policy Options* (Council on Foreign Relations, New York, 2004).
- J. Browne, *Foreign Affairs* **83**(4), 20 (2004).
- A. Underdal, *J. Peace Res.* **24**(2), 167 (1987).
- J. L. Boldsmith, E. A. Posner, *The Limits of International Law* (Oxford Univ. Press, New York, 2005).
- R. N. Stavins, *J. Econ. Perspect.* **12**(3), 69 (1998).
- A. D. Ellerman, P. L. Joscow, D. Harrison, "Emissions trading in the US: Experiences, lessons, and considerations for greenhouse gases" (Pew Center on Global Climate Change, Arlington, VA, 2003).
- R. W. Hahn, G. L. Hester, *Yale J. Regul.* **6**, 109 (1989).
- P. Martin, *Foreign Affairs* **84**(3), 2 (2005).
- For research applied to particular topics that might be on the L20 agenda, see the L20 website ([www.globalcentres.org/L20/](http://www.globalcentres.org/L20/)).
- D. G. Victor, K. Raustiala, E. B. Skolnikoff, *The Implementation and Effectiveness of International Environmental Commitments: Theory and Practice* (MIT Press, Cambridge, MA, 1998), pp. 659–707.
- Calculations based on data from the Carbon Dioxide Information Analysis Center (<http://cdiac.esd.ornl.gov/>).
- Calculation based on data from the Energy Information Administration ([www.eia.doe.gov/](http://www.eia.doe.gov/)).
- R. Stewart, J. Wiener, *Reconstructing Climate Policy* (AEI Press, Washington, 2003).
- See T. C. Heller, P. R. Shukla in *Beyond Kyoto: Advancing the International Effort Against Climate Change*, J. E. Aldy et al., Eds. (Pew Center on Global Climate Change, Arlington, VA, 2003).
- The International Energy Agency (IEA) estimates that by 2020 China will have built 67 GW of gas-fired electric power-generating capacity. If China increased its commitment to gas, at the expense of coal, by another 100 GW—equal, roughly, to the amount of combined-cycle gas-fired capacity that the United States commissioned in just 3 years from 2001 to 2003—then annual emissions in 2020 would be 130 million metric tons of CO<sub>2</sub> lower. (18).
- World Energy Outlook 2004* (IEA, Paris, 2004).
- PESD is funded by the Electric Power Research Institute and BP, PLC, along with Stanford University.

## Adaptation of SARS Coronavirus to Humans

Kathryn V. Holmes

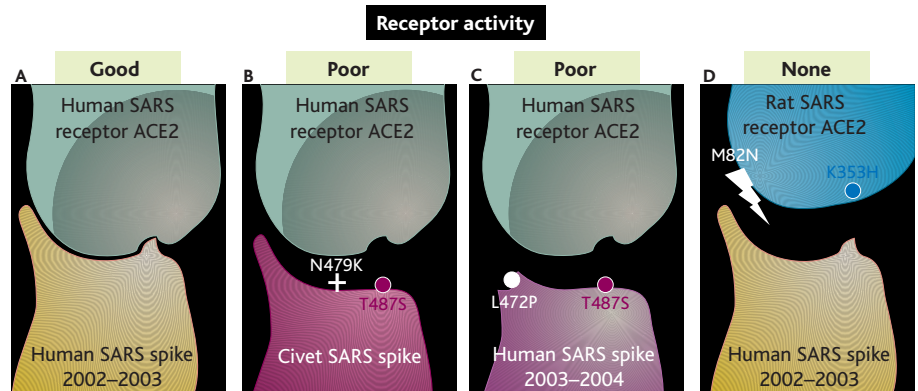
The 2002–2003 epidemic of SARS (severe acute respiratory syndrome) that killed nearly 10% of the more than 8000 infected people is probably the most thoroughly studied example of an animal virus “jumping” into humans. SARS coronavirus was caught in the act of adapting to humans, acquiring mutations in several genes that allowed it to be transmitted from person to person and cause lethal disease. Coronaviruses closely related to the human epidemic strains of SARS coronavirus were discovered in several wild animal species, including the Himalayan masked palm civet, in exotic meat markets in Southern China (1). By sequencing hundreds of SARS viral RNA genomes from humans and animals during and after the epidemic, mutations were identified that distinguish the species-specific strains (2). Which of these mutations account for the explosive and virulent SARS epidemic? Strong evidence implicates the viral spike glycoprotein as one major determinant of the species specificity of coronavirus infection (3). Infection is initiated by trimers of the ~200-kD spike glycoprotein on the coronavirus envelope. The trimers bind SARS virus particles to their specific receptor glycoprotein, angiotensin-converting enzyme 2 (ACE2), on the surface of host cells (4).

In the spike protein of SARS coronavirus, the ~220-amino acid receptor-binding domain was identified by mutational analysis and binding of neutralizing monoclonal antibodies (5, 6). Only four amino acids in the receptor-binding domain differ between the human epidemic and civet strains, but they cause more than a 1000-fold difference in binding affinity to human ACE2 (7). The landmark paper by Li *et al.* on page 1864 of this issue characterizes the structure of the receptor-binding domain of human SARS coronavirus spike protein bound to its receptor, human ACE2 (8). Together with previous elegant mutational analyses (7, 9), this structural study identifies critical molecular determinants that allow SARS coronavirus to

adapt to humans. The host cell receptor is bound by an extended loop in the spike protein that projects from a compact core within the receptor-binding domain. Of the 14 residues on the loop that contact 18 residues on human ACE2, only two differ between human and animal virus strains. The intimate interface between the loop of a spike protein

substitution for a leucine residue at position 472 that reduces the total binding surface to human ACE2. These amino acid substitutions may account for the reduced virulence and transmission of the virus in humans.

The ACE2 protein is highly conserved among mammals and surprisingly few amino acid substitutions at the virus-binding site can strongly affect its receptor activity for SARS coronavirus (7–9). Rat ACE2, which does not serve as a receptor for SARS coronavirus, contains a large N-linked glycan at an asparagine residue at position 82 in the binding interface that likely inhibits binding to the human SARS coronavirus spike protein. It also lacks the lysine-containing hydrophobic pocket critical for binding the key methyl group of threonine 487 [see the figure, panel D; (8)].



**Key amino acids in the SARS coronavirus spike protein and the receptor protein that determine the host range of the virus.** (A) There is a large binding interface between a loop structure in the spike protein of the human SARS coronavirus of 2002–2003 and its human receptor ACE2. (B) Two amino acid substitutions in the spike protein of a civet SARS virus reduce receptor activity of human ACE2 by adding a charge to the binding surface (N479K) and deleting a key methyl group (T487S) that fits into a hydrophobic pocket in the receptor. (C) In the spike protein from coronavirus of a mild SARS case from 2003–2004, the key methyl group is also missing and a proline residue (L472P) reduces the binding surface. (D) Rat ACE2 contains a large glycan at M82N and lacks the hydrophobic pocket (K353H).

from the 2002–2003 SARS coronavirus and its human receptor mediates efficient virus binding and infection (see the figure, panel A). In particular, a methyl group from a threonine residue at position 487 of the spike protein at the interface extends into a hydrophobic pocket in ACE2 that contains a lysine residue at position 353. The two amino acid residues that differ in the spike protein of a civet virus strain would strongly reduce binding to human ACE2 due to absence of the methyl group (a serine residue is present at position 487) and the introduction of a charged lysine residue at position 479 (see the figure, panel B). The spike protein from a coronavirus that caused a sporadic and mild SARS case in 2003–2004 (see the figure, panel C) resembles civet virus spike protein in that it has a serine residue at position 487 as well. This spike protein also has a proline sub-

stitution for a leucine residue at position 472 that reduces the total binding surface to human ACE2. These amino acid substitutions may account for the reduced virulence and transmission of the virus in humans. The ACE2 protein is highly conserved among mammals and surprisingly few amino acid substitutions at the virus-binding site can strongly affect its receptor activity for SARS coronavirus (7–9). Rat ACE2, which does not serve as a receptor for SARS coronavirus, contains a large N-linked glycan at an asparagine residue at position 82 in the binding interface that likely inhibits binding to the human SARS coronavirus spike protein. It also lacks the lysine-containing hydrophobic pocket critical for binding the key methyl group of threonine 487 [see the figure, panel D; (8)].

Many coronaviruses cause disease in mammals and birds, and specific receptor glycoproteins have been identified for coronaviruses of humans, cats, pigs, and mice (3). In addition to SARS coronavirus, only the newly discovered human coronavirus NL63 uses human ACE2 as its receptor (10). As shown by Li *et al.* (8), the extended loop on the SARS virus spike protein that binds human ACE2 has no homolog among spike proteins of other coronaviruses. Perhaps the large (~90 kD) amino-terminal domain of coronavirus spike proteins share a conserved structure from which virus-specific domains project that can bind to different host cell receptors. Will the NL63 spike protein, which lacks a tyrosine-rich receptor-binding loop like that on the SARS virus spike protein (11), bind to the same site on human ACE2 as does the SARS virus spike? How

The author is at the University of Colorado Health Sciences Center, Mail Stop 8333, Post Office Box 6211, Aurora, CO 80045, USA. E-mail: kathryn.holmes@uchsc.edu

could a unique receptor-binding domain be introduced into a spike protein? Coronavirus replication includes frequent RNA recombination events that can insert or delete long RNA sequences in the genome. Large deletions that occur spontaneously in the porcine transmissible gastroenteritis coronavirus eliminate binding to a carbohydrate moiety and change the tissue tropism and virulence of the virus (3). Coronaviruses can hijack foreign genes, such as the hemagglutinin esterase glycoprotein gene from influenza C virus (12). Genes of unknown origin that encode the virus-specific, nonstructural proteins are also acquired and inserted between the essential genes on the coronavirus genome (3). Thus, coronaviruses might change receptor specificity by mutation or by RNA recombination in the genes that encode their spike glycoproteins.

The rather alarming conclusion from the structural studies of the SARS virus spike-ACE2 interface (8) is that adaptation of a virus to a homologous receptor of a new host species may require very few amino acid substitutions at the large receptor-binding interface. This is true not only for SARS coronavirus, but also for other viruses including influenza A virus and parvoviruses (13, 14). Why, then, don't viruses constantly jump from one host species to another?

Probably because successful adaptation to a new host not only requires mutations to optimize receptor binding and entry, but also mutations in other viral genes that optimize virus replication and transmission in the new host. Only when a constellation of mutations allows a virus to replicate and transmit moderately well in the new host can infection in a new species become established.

Can we predict whether another human SARS epidemic will occur? So far, extensive epidemiological surveillance has not found the 2002–2003 epidemic strains of SARS coronavirus in humans or animals since the epidemic ended in July 2003 (2). However, SARS coronaviruses continue to circulate in civets and perhaps other animals and to cause sporadic, mild human cases (2, 15). Fortunately, if new mutants of SARS coronavirus from animals do initiate another SARS epidemic in humans, the disease could promptly be recognized with new diagnostic tests. The outbreak could be stopped by the stringent isolation procedures that controlled the first SARS epidemic of 2002–2003. This could perhaps be supplemented with promising new candidate vaccines and antiviral drugs that are currently being developed. The structure of the interface between the spike protein and receptor shown by Li *et al.* (8) suggests novel strategies for developing an improved SARS

vaccine and receptor-targeted drugs to block virus entry into host cells.

Can the next emerging virus epidemic, other than SARS, be predicted? Probably not. All viruses mutate, and an unfortunate combination of mutations could occur and be selected at any time. The inherent unpredictability of emerging viral diseases is the best reason for further characterization of viruses in wildlife that could jump to humans and for global surveillance for new epidemic diseases in humans and animals.

#### References and Notes

1. Y. Guan *et al.*, *Science* **302**, 276 (2003).
2. H. D. Song *et al.*, *Proc. Natl. Acad. Sci. U.S.A.* **102**, 2430 (2005).
3. M. M. C. Lai, K. V. Holmes, in *Fields' Virology*, D. M. Knipe, P. M. Howley, Eds. (Lippincott Williams and Wilkins, Philadelphia, ed. 3, 2001).
4. W. Li *et al.*, *Nature* **426**, 450 (2003).
5. G. J. Babcock *et al.*, *J. Virol.* **78**, 4552 (2004).
6. Y. He *et al.*, *J. Immunol.* **174**, 4908 (2005).
7. W. Li *et al.*, *EMBO J.* **24**, 1634 (2005).
8. F. Li *et al.*, *Science* **309**, 1864 (2005).
9. X. X. Qu *et al.*, *J. Biol. Chem.* **280**, 29588 (2005).
10. H. Hofmann *et al.*, *Proc. Natl. Acad. Sci. U.S.A.* **102**, 7988 (2005).
11. L. van der Hoek *et al.*, *Nat. Med.* **10**, 368 (2004).
12. S. L. Smits *et al.*, *J. Biol. Chem.* **280**, 6933 (2005).
13. L. Glaser *et al.*, *J. Virol.* **79**, 11533 (2005).
14. K. Hueffer *et al.*, *J. Virol.* **77**, 10099 (2003).
15. C. Tu *et al.*, *Emerg. Infect. Dis.* **10**, 2244 (2004).
16. This work was supported by NIH grant AI59578.

10.1126/science.1118817

## CHEMISTRY

# Bridging a Gap in Actinide Chemistry

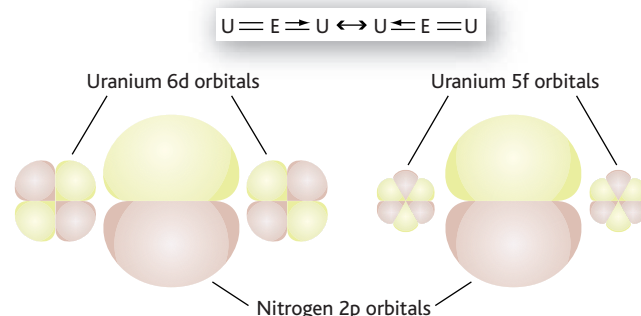
Carol J. Burns

Understanding the behavior of the actinide elements such as uranium and plutonium is central to predicting nuclear weapons performance, advanced nuclear fuel cycles, radioactive waste management, and environmental remediation. During much of the past century, knowledge of the chemical behavior of these elements was derived principally from investigations designed to develop processes for efficient large-scale separation and recovery. Although this has provided models to describe the coordination and redox behavior of the early actinides in acidic aqueous media, we still lack a comprehensive picture of the behavior of elements in this part of the periodic table. It has been particularly difficult to reconcile descriptions of the fascinating structural and electronic behavior of f-

series metals and compounds in condensed-matter systems [including those displaying f-electron itinerancy (1)] with the solution molecular behavior of these elements.

Recently, there have been suggestions in the literature that the behavior of solid-state actinide oxides has previously unappreciated similarities to that of molecular systems (2). The chemistry of individual metal sites tends to be dominated by strong (presumably relatively covalent) metal-oxygen multiple bonding; discrete terminal metal-oxo units with short metal-oxo bonds are common structural elements. One vital

aspect in understanding the electronic structure and thermodynamic stability of these systems is assessment of the type and strength of bonding found in the molecular metal-ligand bonds (particularly the stability of bridging versus terminal bonds; see the figure). Unfortunately, the molecular chemistry of AnE moieties (A, actinide; E, first-row element) has been largely restricted to date to metal-oxo complexes. Evans *et al.* report on page 1835 of this issue the first example of a molecular actinide complex containing a



**A bridge just right.** First-row elements (E) such as nitrogen have the capacity to bridge between two actinide metal centers. The nitrogen 2p orbitals are of the appropriate symmetry to overlap with both uranium (U) 6d and 5f orbitals. The bridging mode in the nitride complex reported by Evans *et al.* suggests delocalized metal-ligand multiple bonding, as illustrated schematically by the resonance structures (box at top).

metal-nitride unit (3). This species has been a key synthetic target; its preparation opens up a new era of comparative investigations of metal-ligand multiple bonds.

Recent years have witnessed a dramatic rise in interest within the chemistry community in investigating actinide complexes with the potential for metal-ligand multiple bonding. Most of these studies have involved organometallic systems. By conducting studies in nonaqueous media, it is possible to remove the complicating factors of solvent exchange and metal hydrolysis, and to provide more direct comparisons of chemical reactivity, optical properties, and structural chemistry as a function of metal, oxidation state, and ligand type. The nonaqueous chemistry of the actinides has revealed important differences in reaction chemistry among the early actinides, and has further highlighted the unique chemistry these elements display in comparison with metals in the d-transition series. Organometallic systems have proven useful in isolating a number of types of species with metal-ligand multiple bonds, including organoimido ( $An=NR$ , where R is an organic functional group) (4), phosphinidene ( $An=PR$ ) (5), and sulfido ( $An=S$ ) (6) groups. Studies of these systems have already begun to change our thinking about the role of metal valence orbitals in chemical bonding, and have highlighted new types of chemical reactions. Conspicuously absent, however, have been simple (unstabilized) complexes of the nitride group ( $M\equiv N$ , where M is a

metal element); these have come to be one of the holy grails for synthetic actinide chemists (7). It is also a particularly important member of the series, given current interest in the behavior of uranium nitrides as nuclear fuels.

The route employed by Evans and co-workers is an extension of recent chemistry carried out with trivalent uranium complexes supported by heavily substituted cyclopentadienyl ligands ( $C_5Me_4R$ ) as mild reductants. Reaction of uranium(III) complexes with sodium azide generates the nitride ligand by apparent loss of dinitrogen; this reactivity stands in contrast to the stability of other reported f-element azide complexes (8). The product consists of large rings with the overall pattern  $(UNUNN)_4$ . These large rings are flexible, and can adopt more than one conformation in the solid state. The origin of the bridging nitride ligand remains to be seen, and will undoubtedly be the subject of theoretical treatment; is nitrogen loss facilitated by the bridging geometry, or is a nucleophilic " $U\equiv N$ " group formed that is stabilized by coordination to another electrophilic uranium metal center? Whatever its origin, the structural chemistry associated with the nitride ligand is worth noting. The few known polymetallic species reported for actinides tend to display more asymmetric M-E-M bridges (9, 10); this has been associated with more electronically "localized" bonding. This may suggest that the nitride ligands in the work of Evans *et al.* are more capable of supporting delocalized bonding, or the type of metal-lig-

and orbital overlap that would be integral to f-electron itinerancy in more extended systems.

The ability of the  $[(C_5Me_4R)_2U]^+$  unit to reductively generate new types of metal-ligand multiple bonds is of note, and might be extended in the future to other ligand types, including the still-elusive carbon-based multiply bonded ligands (i.e., unstabilized alkylidene and alkylidyne groups). Certainly, the species described here hint that new classes of compounds will be prepared in which the overlap of metal valence and ligand orbitals facilitates electronic communication between metal centers. This will serve as another step in the bridge between the molecular chemistry of the actinides and the unique electronic character displayed by many f-element-containing condensed-matter systems.

#### References and Notes

1. N. J. Curro *et al.*, *Nature* **434**, 622 (2005).
2. S. D. Conradson *et al.*, *J. Am. Chem. Soc.* **126**, 13443 (2004).
3. W. J. Evans, S. A. Kozimor, J. W. Ziller, *Science* **309**, 1835 (2005).
4. J. G. Brennan, R. A. Andersen, *J. Am. Chem. Soc.* **107**, 514 (1985).
5. D. S. J. Arney, C. J. Burns, R. C. Schnabel, *J. Am. Chem. Soc.* **118**, 6780 (1996).
6. L. Ventelon *et al.*, *Chem. Commun.* 659 (1999).
7. One report has appeared of a bridging nitride ligand stabilized by coordination to an alkali metal cation (11).
8. I. Castro-Rodriguez *et al.*, *Science* **305**, 1757 (2004).
9. P. B. Duval *et al.*, *Angew. Chem. Int. Ed.* **40**, 3357 (2001).
10. M. P. Wilkerson *et al.*, *Inorg. Chem.* **39**, 5277 (2000).
11. I. Korobkov, S. Gambarotta, G. P. A. Yap, *Angew. Chem. Int. Ed.* **41**, 3433 (2002).

10.1126/science.1118701

## CHEMISTRY

# Palladium-Catalyzed Oxidation of Organic Chemicals with $O_2$

Shannon S. Stahl

**A**tmospheric oxygen maintains a tenuous existence on Earth, far from chemical equilibrium with its surroundings. This thermodynamic instability has destructive potential, manifested in accidental fires, explosions, and corrosion, for example, but it also can be harnessed for beneficial purposes. Aerobic organisms produce energy via respiration, which involves the complete oxidation of glucose and other organic molecules to carbon dioxide and water, and fossil fuel combustion supplies the majority of worldwide energy demands. The recent *Technology*

*Vision 2020* report published by the Council for Chemical Research highlights selective oxidation of organic chemicals as one of the most critical challenges facing the chemical industry (1), and molecular oxygen embodies the quintessential oxidant for chemical synthesis. This oxidant is available at virtually no cost and produces no environmentally hazardous by-products. But how can chemical reactions between organic molecules and oxygen gas be controlled to produce useful, selectively oxidized products without resulting in complete combustion of the starting materials?

The answer lies in the development of catalysts to guide the chemical reaction toward kinetically favored products. A number of industrial processes feature catalytic

methods for aerobic oxidation, but their scope is limited, and chemical reagents such as transition metal oxides and chlorine-based oxidants remain in common use. However, recent developments in homogeneous palladium catalysis point toward new opportunities for selective aerobic oxidation chemistry (2).

The importance of these results must be considered within the context of other homogeneous aerobic oxidation reactions. Among the most useful are autoxidations, radical-chain reactions that find application in the production of numerous large-volume commodity chemicals. Examples include terephthalic acid, a principal component of plastic soda bottles, and cyclohexanone, an important precursor to nylon fabrics and materials. Unfortunately, however, autoxidation reactions are only compatible with substrates that undergo selective radical chemistry. Enzymes and biomimetic catalysts that mediate aerobic oxidation have been classified as oxygenases or oxidases, depending on their catalytic mechanisms. Oxygenases mediate the transfer of one or both oxygen atoms from  $O_2$  to the organic molecule.

The author is in the Department of Chemistry, University of Wisconsin, 1101 University Avenue, Madison, WI 53706, USA. E-mail: stahl@chem.wisc.edu



Oxidases mediate substrate oxidation without oxygen-atom transfer and couple this process to the reduction of dioxygen to hydrogen peroxide or water. The energy transduction mechanism used by oxidases is reminiscent of fuel cells (see the figure), wherein the electrode-mediated redox reactions occur without a direct interaction between the substrates, molecular hydrogen and oxygen. Palladium-catalyzed aerobic oxidation reactions are similar to enzymatic oxidases and fuel cells in that the catalytic mechanism can be separated into two independent half-reactions: palladium(II)-mediated oxidation of the organic substrate ( $\text{SubH}_2$ ) and dioxygen-coupled oxidation of palladium(0). This mechanism has important implications for the development of new catalytic oxidation reactions. Autoxidation and oxygenase reactions are limited to oxygen-

oxidation of the reduced palladium catalyst. This process remains a landmark success in the use of homogeneous catalysis for commodity chemical synthesis.

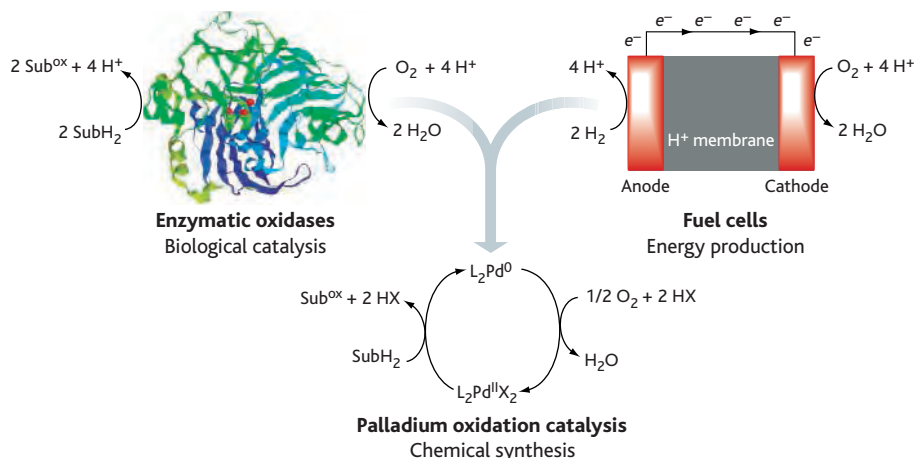
Despite this early achievement, subsequent advances in palladium catalysis were dominated by nonoxidative coupling reactions. Although palladium oxidation catalysis also progressed, certain features of the Wacker process proved to be quite restrictive. For example, many organic molecules are only sparingly soluble in water, the industrial reaction medium, and the copper cocatalysts that mediate dioxygen-coupled turnover are generally less effective in organic solvents. Consequently, many of the new applications of palladium-catalyzed oxidation required alternative oxidants such as benzoquinone or stoichiometric copper(II) salts. These modified condi-

palladium acetate–dimethyl sulfoxide [ $\text{Pd}(\text{OAc})_2/\text{DMSO}$ ] catalyst system in the mid-1990s by Larock and Hightower (4) and by Hiemstra and colleagues (5). This extremely simple catalyst system has been used in a variety of oxidative transformations, including alcohol oxidation, intramolecular hetero- and carbocyclization of alkenes, and dehydrosilylation of silyl enol ethers (2, 6). The metal-coordinating properties of DMSO serve to stabilize the catalyst and promote aerobic oxidation of the reduced catalyst, but mechanistic studies reveal that inefficient capture of reduced palladium by molecular oxygen results in competitive catalyst decomposition via metal aggregation (2). These observations account for the relatively low catalyst lifetime and turnover rates.

The field of homogeneous catalysis owes much of its success to the role of organic ligands that bind to the metal and modulate catalyst stability, reactivity, and selectivity. Palladium oxidation chemistry, however, has been dominated by ligand-free reaction conditions, perhaps because many common ligands for late transition metals, such as phosphines and related soft donors, are susceptible to oxidative decomposition. In the late 1990s, several research groups independently discovered that nitrogen-donor ligands, including aromatic imines and tertiary alkyl amines, confer benefits on catalytic reactivity (7–12). These reactions take place in diverse conditions, ranging from aqueous to nonpolar organic solvents, and exhibit catalytic turnover rates as much as two to three orders of magnitude higher than that of the  $\text{Pd}(\text{OAc})_2/\text{DMSO}$  system.

The nitrogen-ligated catalyst systems have been applied to traditional palladium-catalyzed reactions and in the discovery of novel oxidative transformations. Sheldon *et al.* used a water-soluble phenanthroline ligand with  $\text{Pd}(\text{OAc})_2$  to achieve aqueous, cocatalyst-free conditions for alcohol oxidation and Wacker-type oxidation of terminal alkenes (7). A group at Enichem S.p.A. (Novara, Italy) has used a related organic-soluble ligand, bathocuproine, to investigate direct routes for hydrogen peroxide synthesis from molecular oxygen (8). Sacrificial substrates, alcohols or carbon monoxide, reduce the ligated palladium(II) catalyst, and hydrogen peroxide forms via reaction of dioxygen and two proton equivalents with palladium(0). A palladium-dioxygen adduct, directly relevant to the latter reaction, has been crystallographically characterized, and studies of its reactivity provide key insights into the mechanism for aerobic oxidation of palladium(0) (2).

The impact of new aerobic oxidation methods will probably be experienced first



**Catalysis revival.** Palladium-catalyzed aerobic oxidation processes, which have recently been the subject of renewed interest, display mechanistic similarities to reactions in fuel cells and oxidase enzyme catalysis. ( $\text{SubH}_2$  is the organic substrate,  $\text{Sub}^{\text{ox}}$  is the oxidized organic substrate, L is the neutral donor ligand for palladium, and X is the anionic ligand for palladium.)

atom-transfer methods; however, an oxidase-style mechanism is formally compatible with any oxidative transformation. This feature is particularly important because numerous oxidation reactions do not involve the incorporation of oxygen into the substrate, for example, the oxidative amination of alkenes and the dehydrogenation of alcohols or alkanes. The diversity of palladium-mediated organometallic transformations substantially broadens the scope of possible reactivity.

Palladium-mediated oxidation reactions are not new, of course. Stoichiometric examples were first identified in the 1800s, but the explosive growth in the study of palladium catalysis originated with development of the Wacker process in the late 1950s (3). In this industrial method for the production of acetaldehyde ( $\text{C}_2\text{H}_4 + 1/2 \text{O}_2 \rightarrow \text{CH}_3\text{CHO}$ ), palladium(II) salts promote the oxidative coupling of ethylene and water, and copper(II) cocatalysts mediate aerobic

conditions generally limited the applications to laboratory-scale reactions because of their added cost, increased reaction waste, and more complicated product isolation.

The recent revival in palladium oxidation chemistry coincides with the growing recognition that efficient dioxygen-coupled catalysis can be achieved in the absence of copper cocatalysts or related redox mediators (2). In these reactions, catalyst regeneration occurs by direct reaction of molecular oxygen with the reduced palladium species. A prominent feature of the more recent discoveries is the use of oxidatively robust ligands to stabilize the palladium catalyst, promote catalytic turnover, and foster unprecedented reaction selectivity, including asymmetric transformations.

Early reports of direct dioxygen-coupled catalysis appeared in the late 1960s, but the recent surge of research activity in this area originated with codiscovery of the

in small-scale chemical synthesis—for example, in pharmaceutical discovery and academic research labs. In this context, the Pd(OAc)<sub>2</sub>/pyridine catalyst reported by Nishimura and Uemura (9) represents one of the most convenient and synthetically versatile catalyst systems to date. It has been used by several groups to perform a variety of reactions, including alcohol oxidation, oxidative C–C cleavage reactions with tertiary alcohols, and oxidative C–O, C–N, and C–C coupling reactions with alkenes (2, 9). Inspiration from this catalyst system also led to the discovery of asymmetric catalytic reactions. The groups of Stoltz and Sigman independently reported that the use of (–)-sparteine, a chiral naturally occurring diamine, in the oxidation of secondary alcohols enables preferential reaction of a single enantiomer of the substrate (10–11).

Practical applications of palladium-catalyzed aerobic oxidation for commercial use will require the development of even better catalysts and the discovery of new

chemical transformations. Recently, catalysts have been discovered that are active at room temperature and that operate effectively with ambient air rather than pure oxygen or elevated gas pressures (12–15). These results, made possible by the identification of new ligands for palladium, bode well for future catalyst development efforts. Prospects for new reaction development also appear promising. The oxidative coupling of simple alkenes and amine derivatives appears to be a straightforward analog of the Wacker process, but this reaction has eluded researchers for decades. A recent solution to this problem derives its success from the identification of palladium-catalyzed conditions compatible with direct dioxygen-coupled turnover (16). Aerobic oxidation chemistry is a subject of critical importance, and new opportunities afforded by the advances outlined above suggest that the field of palladium oxidation catalysis is poised for a comeback.

## References

1. *Vision 2020 Catalysis Report* ([www.ccrhq.org/vision/index/roadmaps/catrep.html](http://www.ccrhq.org/vision/index/roadmaps/catrep.html)).
2. S. S. Stahl, *Angew. Chem. Int. Ed.* **43**, 3400 (2004).
3. J. Smidt *et al.*, *Angew. Chem.* **71**, 176 (1959).
4. R. C. Larock, T. R. Hightower, *J. Org. Chem.* **58**, 5298 (1993).
5. R. A. T. M. van Benthem *et al.*, *J. Chem. Soc. Chem. Commun.*, 357 (1994).
6. M. Toyota, M. Ihara, *Synlett*, 1211 (2002).
7. G.-J. ten Brink, I. W. C. E. Arends, R. A. Sheldon, *Science* **287**, 1636 (2000).
8. D. Bianchi, R. Bortolo, R. D'Aloisio, M. Ricci, *Angew. Chem. Int. Ed.* **38**, 706 (1999).
9. T. Nishimura, S. Uemura, *Synlett*, 201 (2004).
10. E. M. Ferreira, B. M. Stoltz, *J. Am. Chem. Soc.* **123**, 7725 (2001).
11. D. R. Jensen, J. S. Pugsley, M. S. Sigman, *J. Am. Chem. Soc.* **123**, 7475 (2001).
12. M. J. Schultz, C. C. Park, M. S. Sigman, *Chem. Commun.*, 3034 (2002).
13. D. R. Jensen, M. J. Schultz, J. A. Mueller, M. S. Sigman, *Angew. Chem. Int. Ed.* **42**, 3810 (2003).
14. T. Iwasawa *et al.*, *J. Am. Chem. Soc.* **126**, 6554 (2004).
15. S. Paavola, K. Zetterberg, T. Privalov, I. Csöreghe, C. Moberg, *Adv. Synth. Catal.* **346**, 237 (2004).
16. J. L. Brice *et al.*, *J. Am. Chem. Soc.* **127**, 2868 (2005).

10.1126/science.1114666

## IMMUNOLOGY

# Insects Diversify One Molecule to Serve Two Systems

Louis Du Pasquier

The elimination of viruses, bacteria, and parasites by the immune systems of metazoa requires a variety of recognition and effector molecules. Antibody diversity, in the broad sense of different types of pathogen recognition molecules, is used by many animal groups. Likewise, diversity in lymphocyte antigen receptors ensures a broad defense. Diversity is achieved in multiple ways (1)—it can be encoded in the DNA of germline cells or it can be generated in somatic cells (see the table). On page 1874 of this issue (2), Watson *et al.* follow up work on the nervous system (3) and hemocytes [presumed immune cells in the circulating fluid of invertebrates (4)] of *Drosophila melanogaster* and show that in the majority of insects, a member of the immunoglobulin superfamily (IgSF) is extensively diversified by alternate splicing (i.e., somatically). Isoforms are expressed in immune tissues as membrane and soluble proteins. The molecule, called Dscam, was originally identified as the homolog of the

Down syndrome cell adhesion molecule in vertebrates, and its potential roles as receptors and effectors of the insect immune system raises questions as to how Dscam is integrated with other insect innate immune responses and whether individual flies have unique pathogen-binding repertoires of Dscam molecules. Even more intriguing is the regulation of axon guidance by the vertebrate homolog of Dscam. The involvement of diverse receptors and effectors encoded by the same locus in immune and nervous systems is unprecedented. It revives discussions about parallels between neuronal plasticity and cellular immunity (5) and their regulation and evolution that are not easily answered.








The diversity generated in Dscam and in vertebrate antigen receptors is by convergence—alternative ways of reaching a similar goal. Even if the mechanisms are different (alternative splicing in Dscam; rearrangement, mutation, and conversion of genes encoding vertebrate antigen receptors), it seems clear that like antigen receptors, a vast repertoire of recognition elements is available in the *Drosophila* immune system. But this repertoire must be under control at several levels. For example, if all of the potential 18,000 Dscam

receptors were expressed in one cell type, each receptor would have a density far below the threshold of utility. Therefore, it is not a surprise that the number of Dscam splice forms per single hemocyte is in the range 14 to 50 (4). This still represents a large diversity relative to a single specific antigen receptor expressed by a lymphocyte. It could offer a hemocyte the advantage of combinatorial associations of Dscam receptor isoforms for pathogen recognition. But at the same time, such diversity could pose a risk of autoimmunity. Although some Dscam receptor isoforms bind to bacteria, they are prone to interact with each other (6), which could result in autoimmunity. Therefore, receptor selection and biasing is required.

Hemocytes and nervous system tissues express biased Dscam repertoires (2, 4). Because diversity is due to alternative splicing and not to DNA rearrangements seen in lymphocytes that result in clonal eliminations, selection likely occurs through the regulation of splicing. Hemocytes would not have to go through elimination of self-recognition receptors. Dscam genes may have purged most self-specific specificities during evolution. Is it possible that some selection occurs after Dscam expression on the cell surface? Once selected, how stable is the repertoire? How is expression regulated in the renewing population of hemocytes?

Perhaps we should not let our questions be too influenced by the similarities with vertebrates. We do not yet know how or even whether Dscam expression is induced during immune responses. Moreover, the

The author is at the Institute of Zoology and Evolutionary Biology, University of Basel, Vesalgasse 1, CH-4051 Basel, Switzerland. E-mail: dupasquier@diel.eunet.ch

Taxonomic group	Genetic variability (polymorphism+polylocism)	Somatic variability			
		Alternative splicing	Mutation, conversion	Rearrangement	Combinatorial association of peptides
 Nematodes	Lectins				
 Mollusks	Fibrinogen-related proteins (immunoglobulin SF), <b>lectins</b> (s)	Fibrinogen-related proteins (immunoglobulin SF)	Fibrinogen-related proteins (immunoglobulin SF)		
 Arthropods	Thioester-containing proteins, <b>peptidoglycan binding proteins</b> (s), Gram-negative binding protein, <b>lectins</b> (s), Toll-like receptor (leucine-rich repeat)	Dscam (immunoglobulin SF) (s), <b>peptidoglycan binding proteins</b> (s)			
 Echinoderms	<b>Scavenger receptor cysteine rich</b> (s), 185/333	Scavenger receptor cysteine rich (s), 185/333			
 Prochordates	Variable region-containing chitin binding protein (immunoglobulin SF), <b>lectins</b> (s), <b>Toll-like receptors</b> (leucine-rich repeat)				
 Agnathans	<b>Agnathan paired receptors resembling Ag receptors</b> (immunoglobulin SF), <b>variable lymphocyte receptor</b> (leucine-rich repeat)		Variable lymphocyte receptor?	Variable lymphocyte receptor	
 Gnathostomes	Many immunoglobulin SF multigene families (s), Toll-like receptor (leucine-rich repeat), <b>lectins</b> (s), <b>peptidoglycan binding proteins</b> (s), complement, major histocompatibility complex class I and II	Immunoglobulin SF families (s)	Immunoglobulin (s)	Immunoglobulin (s), T cell receptor	Immunoglobulin (s), T cell receptor, Toll-like receptors (leucine-rich repeat), major histocompatibility complex class I and II

**How diversity is generated in molecules of some metazoan immune systems.** The indicated variability type does not imply that all the organisms in the corresponding taxonomic group express that trait. Red, membrane-associated molecules; black, soluble molecules; s, soluble forms can be encountered (1, 10–14).

Dscam immunological specificities and structures have not been elucidated. Their domain organization is more like cell adhesion molecules than antibodies. Even though the diversity and presumably capacity to bind pathogens reside essentially in three of 10 Ig-like domains (2, 6), the binding sites of Dscam are likely different from those of antigen receptors. There is little evidence of diversity in the Dscam interstrand loops that form the complementarity-determining regions of antigen receptors. In fact, a region (the A strand) of the Ig3 domain is most variable, much like the prochordate amphioxus variable region-containing chitin binding protein (see the table), another likely molecule of innate immunity with remarkable diversity (7).

Multiple binding specificities result from the incorporation of exons through alternative splicing of the Dscam gene. Some isoforms bind bacteria but others cannot. However, all forms bind to other Dscam isoforms with preference for identical ones (6). The two types of ligands—one self, one non-self (to oversimplify)—may reveal how Dscam can function in both the immune and nervous systems. Whereas a circulating hemocyte may act more as a sensor of the environment, a neuron may need the expression of a “tag” to allow proper interisoform interactions to promote axon branching. In the latter case, the sequence of each isoform may not matter as long as homophilic interactions occur. Thus, the nervous system may simply take advantage

of the diversity selected in the immune system under pathogen pressure. The differences in Dscam repertoires among different insects (2) are consistent with the examples of rapid evolution of vertebrate immune gene families under pressure from rapidly changing pathogens.

In addition, characteristics of the DSCAM locus in vertebrates (where the molecule functions in axon guidance only) can be interpreted in the same way. Human DSCAM is neither diversified nor involved in immunity. The involvement of Dscam in immunity may have been an insect specialization with feedback on the nervous system. Such evolutionary variations in the relationship between the nervous and immune systems could be approached by comparative genomics. The two human DSCAM genes are located on chromosomes 11 and 21 and belong to a tetrad of paralogs that is reminiscent of the ancient origin of this region and of genome duplications characterizing the history of vertebrates. These syntenic regions are rich in relatively conserved genes (many are found in prochordates) that participate in lymphocyte and neural biology (8). A number of IgSF genes in *Drosophila* segregate together on chromosome 3R: Dscam, Amalgam, several Beat, and several DPRs (deficient proboscis extension response) of the nervous system, respectively homologous to human DSCAM, CD96/Tactile, CRTAM (class I restricted T cell-associated molecule), and LSAMP (limbic system-associated mem-

brane protein), all of the immune and/or nervous system and present in the above tetrad of paralogs.

Together, these genomic aspects and the work of Watson *et al.* (2) suggest new connections, interesting coevolutions, and/or swaps of commitments between genes participating in neuronal and immune functions and lead us to agree with Boulanger and Shatz (9) that “the brain and the immune system speak a common biochemical language.”

#### References

- G. W. Litman, J. P. Cannon, J. P. Rast, *Adv. Immunol.* **87**, 209 (2005).
- F. L. Watson *et al.*, *Science* **309**, 1874 (2005); published online 18 August 2005 (10.1126/science.1116887).
- D. Schmucker *et al.*, *Cell* **101**, 671 (2000).
- G. Neves, J. Zucker, M. Daly, A. Chess, *Nat. Genet.* **36**, 240 (2004).
- L. M. Boulanger, G. S. Huh, C. J. Shatz, *Curr. Opin. Neurobiol.* **11**, 568 (2001).
- W. M. Wojtowicz, J. J. Flanagan, S. S. Millard, S. L. Zipursky, J. C. Clemens, *Cell* **118**, 619 (2004).
- J. P. Cannon, R. N. Haire, N. Schnitker, M. G. Mueller, G. W. Litman, *Curr. Biol.* **14**, R465 (2004).
- L. Du Pasquier, I. Ivana Zucchetti, R. De Santis, *Immunol. Rev.* **198**, 233 (2004).
- L. M. Boulanger, C. J. Shatz, *Nat. Rev. Neurosci.* **5**, 521 (2004).
- S. V. Nair, H. Del Valle, P. S. Gross, D. P. Terwilliger, L. C. Smith, *Physiol. Genomics* **22**, 33 (2005).
- T. Suzuki, I. T. Shin, A. Fujiyama, Y. Kohara, M. Kasahara, *J. Immunol.* **174**, 2885 (2005).
- J. Hoffmann, Ed., *Primitive Immune Systems* (Blackwell, Philadelphia, 2004).
- L. Du Pasquier, *Scand. J. Immunol.* **62** (suppl. 1), 39 (2005).
- P. Schmid-Hempel, *Annu. Rev. Entomol.* **50**, 529 (2005).

10.1126/science.1118828

# Characterization of a *Phytophthora* Mating Hormone

Jianhua Qi, Tomoyo Asano, Masashi Jinno, Kouhei Matsui, Keisuke Atsumi, Youji Sakagami, Makoto Ojika\*

Members of the fungus-like genus *Phytophthora* (meaning “plant destroyer”) cause devastating plant diseases that threaten important crops worldwide. The most notorious member of the genus is *P. infestans*, which is responsible for the potato late blight and which caused the Irish potato famine in the mid-1840s (1). Recently, a new aggressive species, which causes sudden oak death, has rapidly infected forests across the United States and Europe (2).

Sexual reproduction is one of the most important biological events in *Phytophthora*. The genus includes heterothallic species that consist of two mating types, A1 and A2 (1, 3). Although each individual can produce both male (antheridia) and female (oogonia) organs, geographical proximity is essential for sexual reproduction. Fertilized oogonia develop into sexual spores known as oospores, which have a thick-walled survival structure. Although hormonal regulation of sexual reproduction in *Phytophthora* was first proposed in 1929 (4), its chemical basis has remained to be elucidated (5, 6). The factor secreted by the A1 mating type, hormone  $\alpha$ 1, induces oospores

in the A2 mating type, whereas hormone  $\alpha$ 2 is secreted by A2 to induce oospores in the A1. We describe here the isolation and chemical characterization of mating hormone  $\alpha$ 1 from a *Phytophthora* species and its generality in the genus *Phytophthora*.

We used *P. nicotianae* to isolate the hormone  $\alpha$ 1. The supernatant fluid (1830 L in total volume) from culture broths of the A1 mating type was extracted with ethyl acetate (7). The organic extracts were chromatographed on silica gel, followed by reversed-phase chromatography. Further purification by repeated high-performance liquid chromatography (HPLC) yielded a total of 1.2 mg of pure hormone  $\alpha$ 1. We evaluated the hormonal (oospore-inducing) activity with the A2 mating type for all the chromatographic fractions until purification was completed (7). The chemical structure of hormone  $\alpha$ 1 was examined by conventional spectroscopic analysis: mass, infrared,  $^1\text{H}$  and  $^{13}\text{C}$  nuclear magnetic resonance (NMR) (fig. S1 and table S1), and two-dimensional NMR spectroscopy, revealing a diterpene structure for hormone  $\alpha$ 1 (Fig. 1A) (supporting online text). Because the  $^1\text{H}$  NMR spectrum

suggested the presence of unknown trace components (fig. S1), we confirmed the structure by a sequence of chemical reactions: conversion to a di-4-bromobenzoate derivative, HPLC purification, and then basic hydrolysis back to the hormone (7). The regenerated hormone was identical to the natural hormone both in spectroscopic analysis and in a hormonal activity test.

Hormone  $\alpha$ 1 induced obvious oospore formation ( $23 \pm 3$  oospores) on mycelia of the A2 mating type at a dose of 3 ng, and the number of oospores increased dose-dependently (Fig. 1B). This mating hormone did not induce any oospores on the A1 mating type at a dose of 300 ng. Cross reaction to other *Phytophthora* species demonstrated that the hormone was capable of oospore formation on the A2 mating types of all three species tested (Fig. 1B) and did not induce any oospores on their A1 mating types at a dose of 300 ng. Figure 1C shows characteristic spherical double-walled oospores accompanied by smaller antheridia (Fig. 1C). Sporangia, asexual spores, were produced in the absence of hormone  $\alpha$ 1 and were suppressed in the presence of the hormone. These results strongly suggest that this substance is not only hormone  $\alpha$ 1 of *P. nicotianae* but also a universal mating hormone in the heterothallic species of *Phytophthora*.

## References and Notes

- W. E. Fry, S. B. Goodwin, *Bioscience* **47**, 363 (1997).
- C. R. Lane *et al.*, *Plant Pathol.* **52**, 414 (2003).
- E. J. Savage *et al.*, *Phytopathology* **58**, 1004 (1968).
- S. F. Ashby, *Trans. Br. Mycol. Soc.* **14**, 18 (1929).
- W. H. Ko, *J. Gen. Microbiol.* **107**, 15 (1978).
- H. J. Jee, C. S. Tang, W. H. Ko, *Bot. Bull. Acad. Sin. (Taipei)* **43**, 203 (2002).
- Materials and methods are available as supporting material on Science Online.
- We thank N. Doko of Nagoya University for providing *P. infestans*. Supported by the Research for the Future Program from the Japan Society for the Promotion of Science (JSPS), a Grant-in-Aid for Scientific Research on Priority Areas from Ministry of Education, Culture, Sports, Science, and Technology, the Daiko Foundation, JSPS Research Fellowships for Young Scientists (J. Q.), and in part by a Grant-in-Aid for Center of Excellence Research.

## Supporting Online Material

www.sciencemag.org/cgi/content/full/309/5742/1828/DC1

Materials and Methods

SOM Text

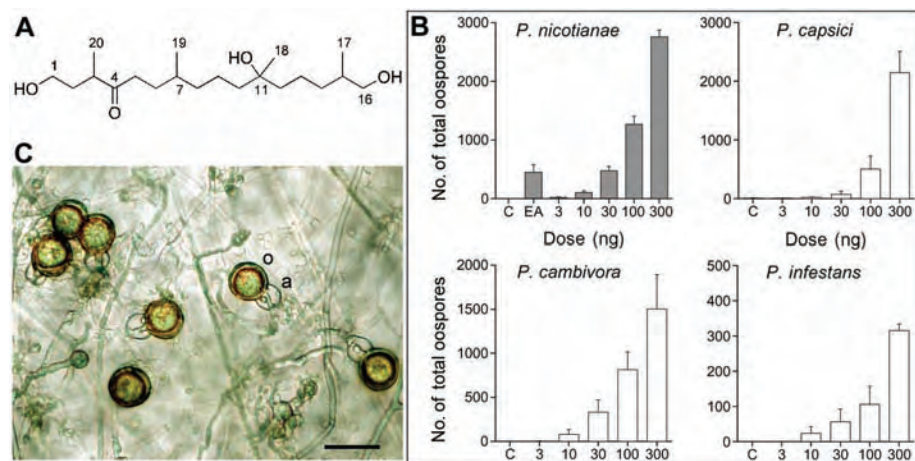
Fig. S1

Table S1

12 May 2005; accepted 11 August 2005  
10.1126/science.1114756

Graduate School of Bioagricultural Sciences, Nagoya University, Nagoya 464-8601, Japan.

\*To whom correspondence should be addressed.  
E-mail: ojika@agr.nagoya-u.ac.jp



**Fig. 1.** (A) The chemical structure of hormone  $\alpha$ 1 isolated from the A1 mating type of *P. nicotianae*. (B) The dose-dependent increase of sexual spore (oospore) formation in the A2 mating types of *P. nicotianae* and other species (*P. capsici*, *P. cambivora*, and *P. infestans*) on treatment with hormone  $\alpha$ 1. We counted the total number of oospores (vertical axis) that were produced around an  $\alpha$ 1-containing paper disk. EA represents an ethyl acetate extract corresponding to 8 ml of culture broth; C is the control. Values are means of four replicates  $\pm$  SE. (C) Photomicrograph of oospores induced on the *P. nicotianae* A2 mating type by hormone  $\alpha$ 1 at a dose of 100 ng. They are fertilized structures resulting from oogonia (female, o) and antheridia (male, a). Scale bar, 50  $\mu\text{m}$ .

## Suppression of Aging in Mice by the Hormone Klotho

Hiroshi Kurosu,<sup>1</sup> Masaya Yamamoto,<sup>1</sup> Jeremy D. Clark,<sup>1</sup> Johanne V. Pastor,<sup>1</sup> Animesh Nandi,<sup>1</sup> Prem Gurnani,<sup>1</sup> Owen P. McGuinness,<sup>3</sup> Hirotaka Chikuda,<sup>4</sup> Masayuki Yamaguchi,<sup>4</sup> Hiroshi Kawaguchi,<sup>4</sup> Ichihiro Shimomura,<sup>5</sup> Yoshiharu Takayama,<sup>2</sup> Joachim Herz,<sup>2</sup> C. Ronald Kahn,<sup>6</sup> Kevin P. Rosenblatt,<sup>1</sup> Makoto Kuro-o<sup>1\*</sup>

A defect in *Klotho* gene expression in mice accelerates the degeneration of multiple age-sensitive traits. Here, we show that overexpression of *Klotho* in mice extends life span. *Klotho* protein functions as a circulating hormone that binds to a cell-surface receptor and represses intracellular signals of insulin and insulin-like growth factor 1 (IGF1), an evolutionarily conserved mechanism for extending life span. Alleviation of aging-like phenotypes in *Klotho*-deficient mice was observed by perturbing insulin and IGF1 signaling, suggesting that *Klotho*-mediated inhibition of insulin and IGF1 signaling contributes to its anti-aging properties. *Klotho* protein may function as an anti-aging hormone in mammals.

*Klotho* was originally identified as a mutated gene in a mouse strain that accelerates age-dependent loss of function in multiple age-sensitive traits (*l*). An insertional mutation that

disrupts the 5' promoter region of the *Klotho* gene resulted in a strong hypomorphic allele. Mice homozygous for the mutated allele (*KL*<sup>-/-</sup> mice) appeared normal until 3 to 4 weeks old

but then began to manifest multiple age-related disorders observed in humans, including ectopic calcification, skin atrophy, muscle atrophy, osteoporosis, arteriosclerosis, and pulmonary emphysema. *KL*<sup>-/-</sup> mice suffered premature death around two months of age.

The *Klotho* gene encodes a single-pass transmembrane protein that is detectable in limited tissues, particularly the distal convoluted tubules in the kidney and the choroid plexus in the brain. Because a defect in the *Klotho* gene leads to systemic age-dependent

<sup>1</sup>Department of Pathology, <sup>2</sup>Department of Molecular Genetics, University of Texas (UT) Southwestern Medical Center at Dallas, 5323 Harry Hines Boulevard, Dallas, TX 75390-9072, USA. <sup>3</sup>Department of Molecular Physiology and Biophysics, Vanderbilt University School of Medicine, 702 Light Hall, Nashville, Tennessee 37232-0615, USA. <sup>4</sup>Department of Sensory and Motor System Medicine, University of Tokyo, 7-3-1 Hongo, Bunkyo, Tokyo 113-8655, Japan. <sup>5</sup>Department of Internal Medicine and Molecular Science, Graduate School of Medicine, Osaka University, 2-2 Yamadaoka, Suita, Osaka 565-0871, Japan. <sup>6</sup>Research Division, Joslin Diabetes Center, Department of Medicine, Harvard Medical School, One Joslin Place, Boston, MA 02215, USA.

\*To whom correspondence should be addressed. E-mail: makoto.kuro-o@utsouthwestern.edu

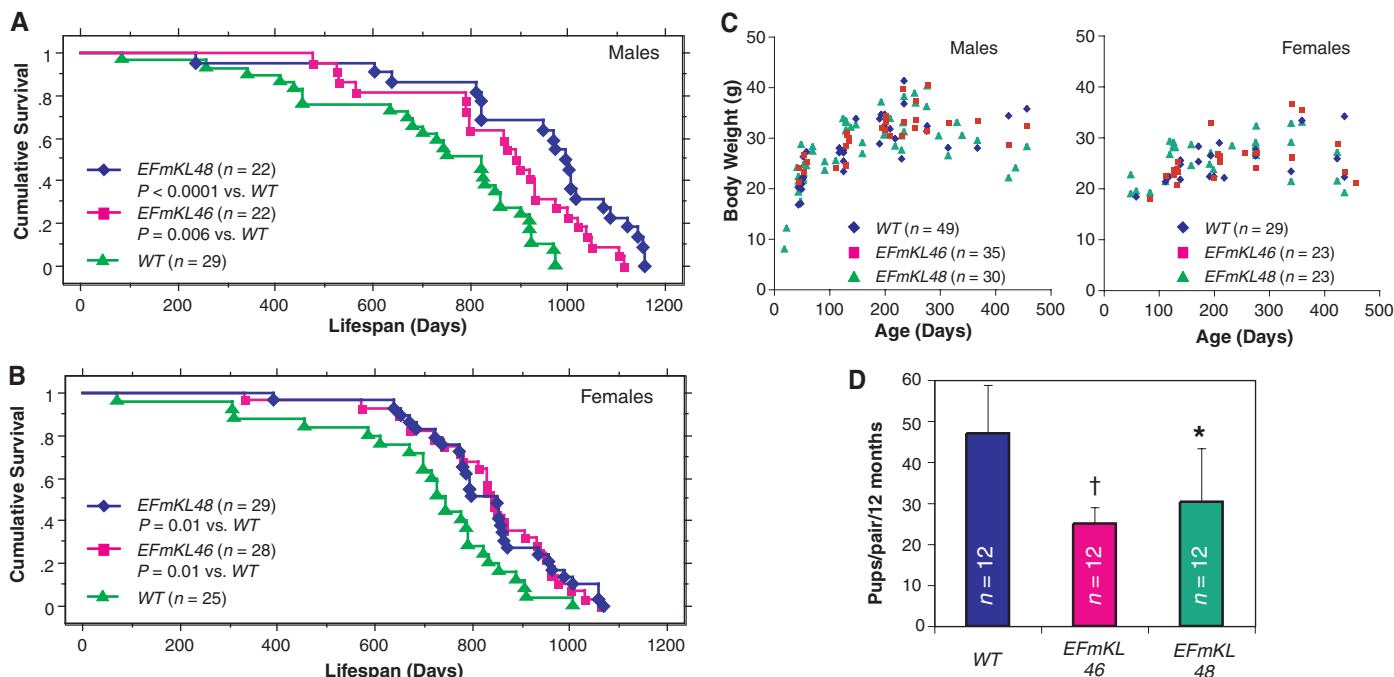


**Fig. 1.** *Klotho* overexpression extends life span in the mouse. Kaplan-Meier analysis of survival in (A) males [ $P = 0.006$  in *EFmKL46* versus wild-type (WT) mice, and  $P < 0.0001$  in *EFmKL48* versus wild type by log-rank test) and in (B) females ( $P = 0.01$  in *EFmKL46* versus wild type, and  $P = 0.01$  in *EFmKL48* versus wild type by log-rank test). The average life span of male wild-type, *EFmKL46*, and *EFmKL48* mice was  $715 \pm 44$  days,  $858 \pm 40$  days, and  $936 \pm 47$  days (means  $\pm$  SEM), respectively. The average life span of female wild-type, *EFmKL46*, and *EFmKL48* mice was  $697 \pm 45$  days,  $829 \pm 32$  days, and  $830 \pm 29$  days, respectively. (C) Body weight of wild-type, *EFmKL46*, and *EFmKL48* mice. No significant difference in growth was

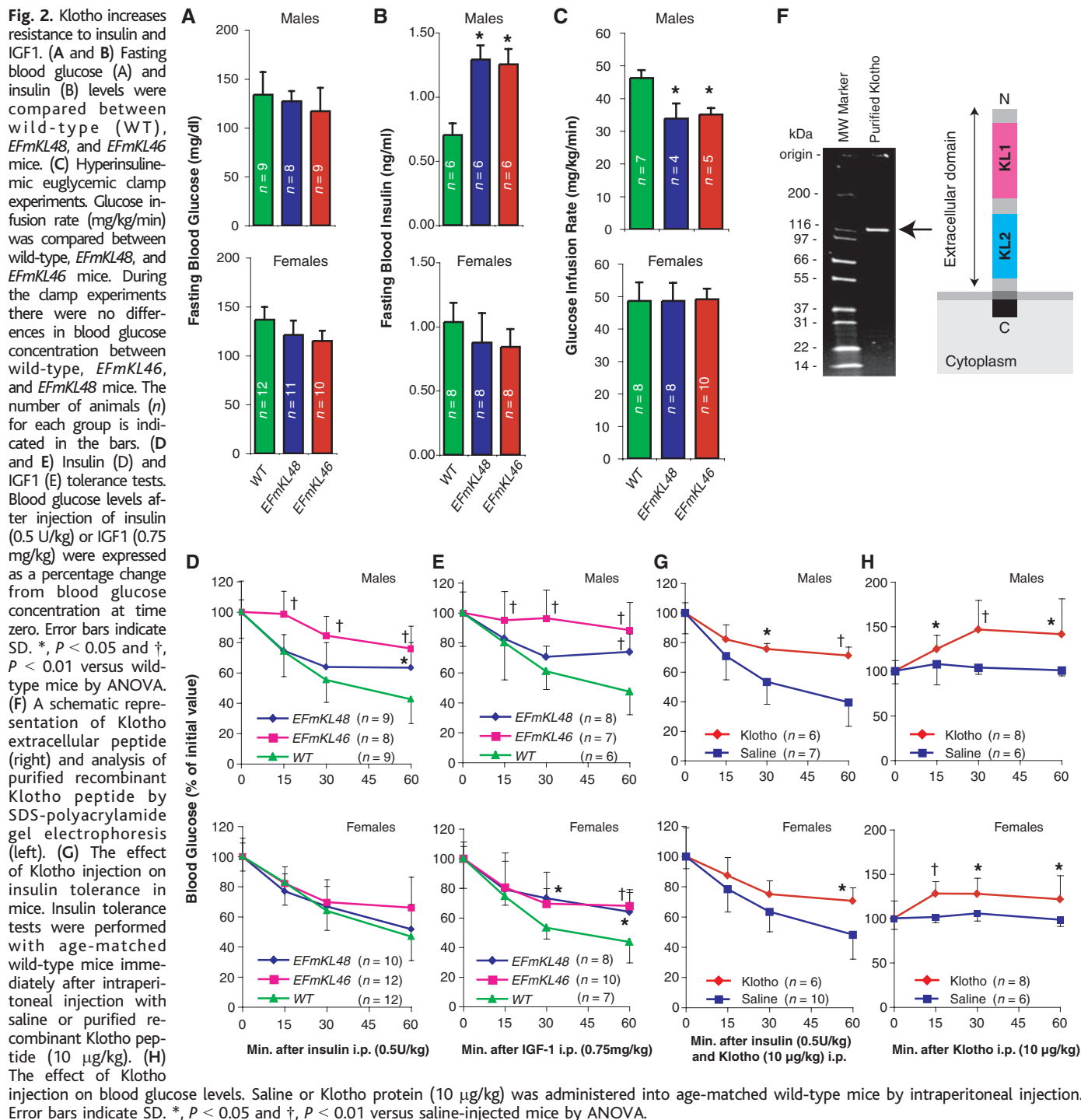
observed. (D) *Klotho* overexpression reduces fecundity. Twelve breeding pairs at 12 weeks of age were set up for each genotype. The number of offspring generated during 12 months was recorded for each breeding pair. Although average litter size (pups per birth) of wild-type, *EFmKL46*, and *EFmKL48* pairs was not significantly different ( $6.6 \pm 1.0$ ,  $6.1 \pm 1.3$ , and  $7.0 \pm 1.2$ , respectively), the number of births (births per pair per 12 months) was fewer in transgenic mice pairs ( $7.2 \pm 1.6$ ,  $4.2 \pm 0.8$ , and  $4.5 \pm 2.2$ , respectively), resulting in significantly fewer offspring in transgenic pairs. Data are means  $\pm$  SD. \*,  $P < 0.05$ ; †,  $P < 0.01$  versus wild-type mice by analysis of variance (ANOVA).

degeneration, the Klotho protein may function through a circulating humoral factor that regulates the development of age-related disorders or natural aging processes (2). Notably, some single-nucleotide polymorphisms in the human *KLOTHO* gene are associated with altered life span (3) and altered risk for coronary artery disease (4), osteoporosis (5–7), and stroke (8).

Little is known about Klotho protein function and the molecular mechanism by which it suppresses the development of aging-like phenotypes. The extracellular domain of Klotho protein

is composed of two internal repeats, KL1 and KL2, that share amino acid sequence homology to  $\beta$ -glucosidases of bacteria and plants (20 to 40% identity) (1). However, glucosidase activity is not present in recombinant Klotho protein (9), and the essential glutamate residue at the  $\beta$ -glucosidase active center is replaced with asparagine and alanine in KL1 and KL2, respectively (10). Here, we demonstrate that *Klotho* is an aging suppressor gene whose product functions as a hormone that inhibits intracellular insulin and IGF1 signaling.

**Klotho overexpression extends life span in mice.** We previously generated independent transgenic lines of mice that overexpress *Klotho* under the control of the human elongation factor 1 $\alpha$  promoter (1) (*EFmKL46* and *EFmKL48*) (fig. S1). Here, we compared the life span of the transgenic mice with that of wild-type controls that are near-coisogenic by virtue of backcrossing onto the C3H background four times. Each line was previously confirmed to express functional Klotho protein from the transgene (1). Mice carrying the



*EFmKL46* or *EFmKL48* transgenic alleles, fed *ad libitum*, outlived wild-type controls by 20.0 and 30.8%, respectively, in males (Fig. 1A) and by 18.8 and 19.0%, respectively, in females (Fig. 1B).

Caloric restriction is associated with increased longevity in various species (11). To assess whether mice overexpressing *Klotho* were restricting their own diets, we monitored

food intake and oxygen consumption in transgenic and wild-type mice for 24 hours at 32 to 36 weeks of age. No significant differences in these parameters were observed (table S1). Small body size is also associated with extended longevity in diet-restricted mice and in mice that are mutant for pituitary or growth hormone receptor function (12, 13). However, we did not observe any substantial difference

in growth between *EFmKL46*, *EFmKL48*, and wild-type mice (Fig. 1C). Both *EFmKL46* and *EFmKL48* breeding pairs generated fewer offspring than wild-type breeding pairs (Fig. 1D). As expected from the evolutionary theory of longevity, maximum fitness of the organism is a trade-off between life span and fertility (14). These data indicate that *Klotho* systemically modulates aging through mechanisms independent of food intake and growth, but potentially in association with reproduction.

***Klotho* increases resistance to insulin and IGF1.** Many genetic data demonstrate that inhibited insulin and IGF1 signaling extends life span in animals from *C. elegans*, to *Drosophila*, to mice (15–21). Because *Klotho* must mediate aging through effects of a systemic hormone, we investigated whether the *Klotho* gene is involved in the inhibition of insulin or IGF1 signaling. Mice defective in *Klotho* gene expression have reduced blood glucose and insulin levels coupled with enhanced sensitivity to insulin (22).

We compared glucose metabolism in the *Klotho*-overexpressing transgenic mice with wild-type animals. Blood glucose levels were normal in each transgenic line (Fig. 2A). However, male *EFmKL46* and *EFmKL48* mice had higher blood insulin levels than did wild-type males (Fig. 2B), suggesting that the male transgenic mice are somewhat insulin resistant. We directly assessed sensitivity to insulin with a hyperinsulinemic euglycemic clamp (23). As expected, male *EFmKL46* and *EFmKL48* mice required lower glucose infusion rates than did wild-type males to maintain normal blood glucose levels (Fig. 2C). Furthermore, insulin and IGF1 tolerance tests revealed significant attenuation in hypoglycemic response to injected insulin and IGF1 in male transgenic mice (Fig. 2, D and E). Although we were unable to detect insulin resistance in female transgenic mice (Fig. 2, C and D), they were significantly resistant to IGF1 (Fig. 2E). These studies demonstrate that *Klotho* overexpression induces resistance to insulin and IGF1.

***Klotho* functions as a hormone.** The extracellular domain of *Klotho* is shed on the cell surface and detected in the blood and cerebrospinal fluid in mice and humans (24). Immunoblot analysis of plasma with the use of rabbit anti-*Klotho* antiserum demonstrated that the extracellular *Klotho* peptide can be detected in wild-type, *EFmKL48*, and *EFmKL46* mice but not in *KL<sup>-/-</sup>* mice (fig. S2). Radioimmunoassay further demonstrated that *Klotho* peptide is ~100 pM in wild-type mice and about two times as high in the transgenic overexpression strains (fig. S3). The extracellular domain of *Klotho* may function as a hormone-like substance (2).

To assess the function of the *Klotho* extracellular peptide, we generated a soluble form of recombinant *Klotho* protein comprising the 952-amino acid extracellular domain, and de-

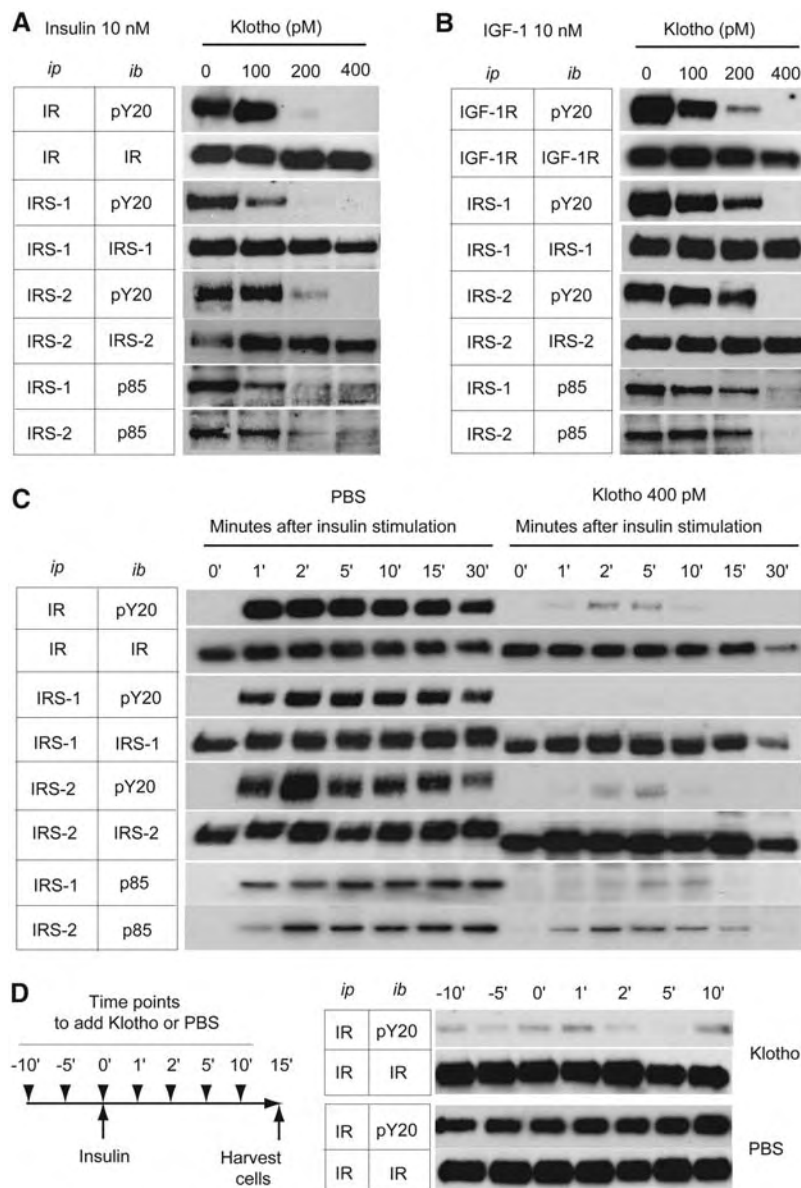


**Fig. 3.** *Klotho* protein inhibits intracellular insulin and IGF1 signaling. (A and B) Effect of *Klotho* on tyrosine phosphorylation of insulin and IGF1 receptors as well as IRS-1 and IRS-2, association of IRS-1 and IRS-2 with the PI3-kinase regulatory subunit (p85), and phosphorylation of Akt in L6 cells stimulated with 10 nM of insulin (A) or 10 nM of IGF1 (B). Antibodies used for immunoprecipitation (ip) and immunoblotting (ib) were indicated. IR, antibody to insulin receptor  $\beta$  chain; pY20, antibody to phosphotyrosine; IRS-1, antibody to IRS-1; IRS-2, antibody to IRS-2; p85, antibody to PI3-kinase regulatory subunit; IGF-1R, antibody to IGF1 receptor  $\beta$  chain. (C) A time course of the inhibitory effect of *Klotho* protein (400 pM) on insulin signaling in H4IIE cells. The cells were harvested before (0') and at the indicated time points after insulin stimulation (10 nM). (D) Inactivation of activated insulin receptor by *Klotho* protein. H4IIE cells were stimulated with insulin (10 nM) at time 0' and harvested 15 min later. *Klotho* (400 pM) or phosphate-buffered saline (PBS) was added at the indicated time points indicated (left panel). The cell lysates were immunoprecipitated with IR and immunoblotted with pY20 or IR (right panel).

terminated whether this promoted insulin resistance when injected into mice. Intraperitoneal injection of insulin (0.5 U/kg) and purified Klotho extracellular peptide (10  $\mu$ g/kg, Fig. 2F) in wild-type male and female mice attenuated the hypoglycemic response expected from insulin alone (Fig. 2G). Klotho peptide alone rapidly increased blood glucose levels in male wild-type mice and to a smaller extent in females (Fig. 2H). However, Klotho peptide injection did not induce significant changes in blood insulin and glucagon levels (fig. S4), suggesting that Klotho peptide inhibits insulin action directly in peripheral tissues.

To test whether Klotho antagonizes insulin at receptive cells, we determined whether re-

combinant Klotho peptide would reduce glucose uptake by blocking insulin binding to the insulin receptor. We measured cellular glucose uptake in cultured myoblastic cells (L6) incubated with or without insulin in the presence or absence of 100 pM of Klotho extracellular peptide. Klotho peptide suppressed insulin-induced glucose uptake by 55% without reducing the binding of [ $^{125}$ I] insulin to the cells (fig. S5). Thus, Klotho does not appear to inhibit ligand-binding to the insulin receptor, suggesting that Klotho may block insulin action by disrupting one or more alternative insulin-dependent intracellular signaling pathways. Accordingly, we measured the potential for [ $^{125}$ I]-labeled Klotho to bind directly to the cell surface. Hepatoma cells

bound [ $^{125}$ I] Klotho in a dose-dependent manner and saturated when the total Klotho concentration exceeded 600 pM, and unlabeled Klotho peptide inhibited the binding of [ $^{125}$ I] Klotho (fig. S6). Together, these observations suggest that cells present a receptor at their surface other than the insulin receptor that binds to the Klotho peptide.

**Klotho inhibits intracellular insulin and IGF1 signaling.** Because membrane-bound Klotho peptide must inhibit ligand activation of the insulin receptor within the cells, we investigated the influence of Klotho on insulin receptor signal transduction (25, 26). We incubated L6 cells or rat hepatoma cells (H4IIE) with recombinant Klotho peptide and insulin (10 nM) or IGF1 (10 nM). Klotho peptide did not inhibit the binding of [ $^{125}$ I] insulin or [ $^{125}$ I] IGF1 (fig. S5) but suppressed ligand-stimulated autophosphorylation of insulin and IGF1 receptors in a dose-dependent manner (Fig. 3, A and B). Additionally, Klotho reduced activation of signaling events downstream of receptor activation, including tyrosine-phosphorylated insulin receptor substrate (IRS) 1 and 2, the association of the subunit of phosphoinositide 3-kinase p85 with IRS proteins (Fig. 3, A and B). Because the inhibitory effect of Klotho on insulin signaling was observed as early as 1 min after insulin stimulation (Fig. 3C), the decline in tyrosine-phosphorylated insulin and IGF1 receptors is unlikely due simply to the loss of receptors. Notably, Klotho peptide can inactivate active insulin receptors that were previously tyrosine phosphorylated by insulin stimulation. In H4IIE cells that were exposed to 10 nM insulin before adding Klotho peptide, Klotho suppressed tyrosine phosphorylation of the insulin receptor (Fig. 3D). We observed a similar effect on IGF1 receptor autophosphorylation in L6 cells with IGF1 before adding Klotho peptide (9). Importantly, the inhibitory effect of Klotho on autophosphorylation of receptor tyrosine kinases is specific. We observed no inhibitory effect of Klotho on the epidermal growth factor receptor and the platelet-derived growth factor receptor (fig. S7). Overall, Klotho appears to inhibit activation of the insulin and IGF1 receptor and to repress activated insulin and IGF1 receptors. Whether Klotho peptide functions by accelerating removal of tyrosine phosphorylation from the activated insulin receptor remains to be determined.

**Inhibition of insulin and IGF1 signaling rescues  $KL^{-/-}$  phenotypes.** If the ability of Klotho to inhibit insulin and IGF1 signaling extends survival by retarding senescence, independent manipulations to inhibit insulin and IGF1 signaling may ameliorate some of the aging-like phenotypes in  $KL^{-/-}$  mice. Accordingly, we crossed a loss-of-function mutation of IRS-1 into the  $KL^{-/-}$  mice (27). Survival was improved in  $KL^{-/-}$  mice heterozygous for an IRS-1 null allele ( $KL^{-/-}$   $IRS-1^{+/-}$ ) relative to  $KL^{-/-}$  control mice

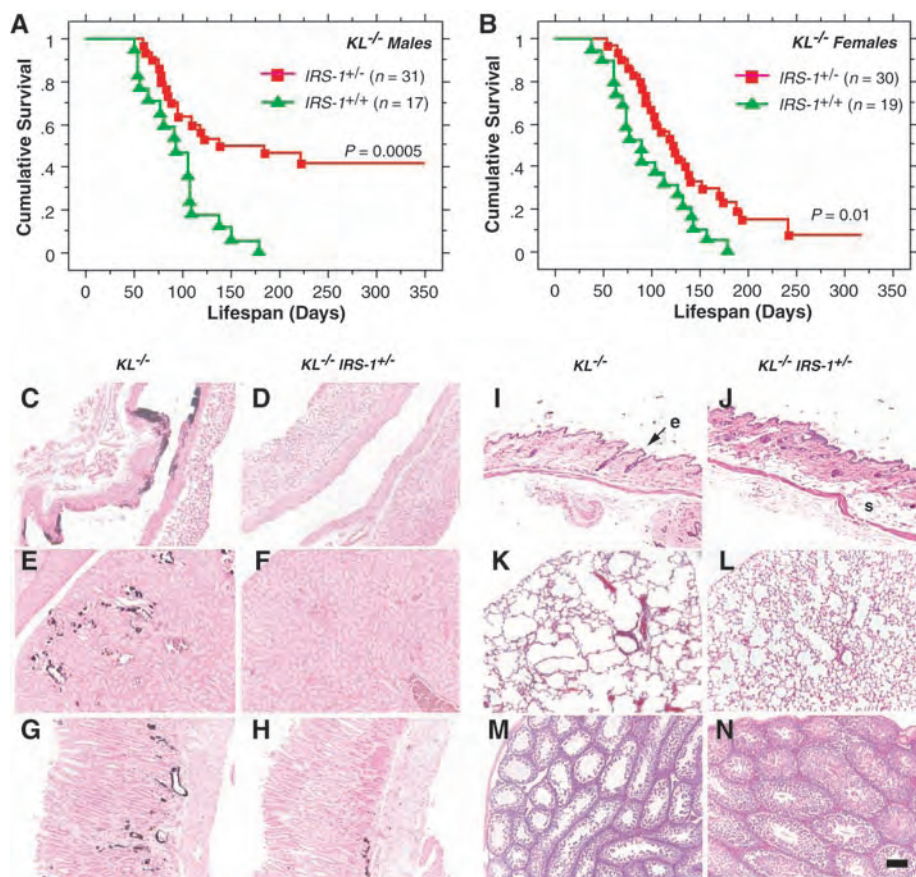


**Fig. 4.** Rescue of aging-like phenotypes in  $KL^{-/-}$  mice by genetic intervention in insulin and IGF1 signaling. (A and B) Life-span extension in  $KL^{-/-}$  mice by reducing IRS-1 expression.  $KL^{-/-}$  mice heterozygous for an IRS-1 null allele ( $IRS-1^{+/-}$ ) lived longer than those without the mutation ( $IRS-1^{+/+}$ ) both in males ( $P = 0.0005$  by log-rank test) and females ( $P = 0.01$  by log-rank test). [(C) to (N)] Rescue of aging-like phenotypes in  $KL^{-/-}$   $IRS-1^{+/-}$  mice at the histological level. Typical findings from four 8-week-old males of each genotype are shown. (C and D) Aorta (von Kossa staining). Calcification of arterial walls [black deposits in (C)] was decreased in  $KL^{-/-}$   $IRS-1^{+/-}$  mice (D). (E and F) Kidney (von Kossa staining). Calcification of small arteries and renal tubules [black deposits in (E)] was decreased in  $KL^{-/-}$   $IRS-1^{+/-}$  mice (F). (G and H) Stomach (von Kossa staining). Ectopic calcification in gastric mucosa and small arteries [black deposits in (G)] was alleviated in  $KL^{-/-}$   $IRS-1^{+/-}$  mice (H). (I and J) Cross-sections of the skin. Hematoxylin-eosin (HE) staining. Reduction in epidermal layer (e) thickness observed in  $KL^{-/-}$  mice (I) was improved and subcutaneous fat (s) was restored in  $KL^{-/-}$   $IRS-1^{+/-}$  mice (J). (K and L) Lung (HE staining). Emphysematous changes, including enlargement of air spaces and destruction of the normal alveolar architecture were observed in  $KL^{-/-}$  mice (K), but were alleviated in  $KL^{-/-}$   $IRS-1^{+/-}$  mice (L). (M and N) Testis (HE staining). Seminiferous tubules were atrophic and no mature sperm was observed in  $KL^{-/-}$  mice (M). Spermatogenesis was restored in  $KL^{-/-}$   $IRS-1^{+/-}$  mice (N). All panels were shown in the identical magnification ( $\times 200$ ). Scale bar, 200  $\mu$ m.



(Fig. 4, A and B). In addition,  $KL^{-/-}$   $IRS-1^{+/-}$  mice ameliorated many age-related pathologies typical of  $KL^{-/-}$  mice, including arteriosclerosis, ectopic calcification, skin atrophy, pulmonary emphysema, and hypogonadism (Fig. 4, C to N). Heterozygosity of  $IRS-1$  alone ( $KL^{+/+}$   $IRS-1^{+/-}$  littermates) appears to have no effect on survival and the age-progressive degeneration when compared with those factors in wild-type littermates during these experiments (9).

**Conclusion.** We previously reported that a defect in *Klotho* gene expression leads to a syndrome that may resemble premature aging (1). Here, we show that overexpression of *Klotho* can extend life span, and we suggest that *Klotho* functions as an aging suppressor gene in mammals. We found that the extracellular domain of *Klotho* protein circulates in the blood and binds to a putative cell-surface receptor. *Klotho* has marked effects on insulin physiology, apparently because it suppresses tyrosine phosphorylation of insulin and IGF1 receptors, which results in reduced activity of IRS proteins and their association with PI3-kinase, thereby inhibiting insulin and IGF1 signaling. Extended life span upon negative regulation of insulin and IGF1 signaling is an evolutionarily conserved mechanism to suppress aging (28). *Klotho* appears to be a peptide

hormone to modulate such signaling and thereby mediate insulin metabolism and aging.

#### References and Notes

1. M. Kuro-o et al., *Nature* **390**, 45 (1997).
2. Y. Takahashi, M. Kuro-o, F. Ishikawa, *Proc. Natl. Acad. Sci. U.S.A.* **97**, 12407 (2000).
3. D. E. Arking et al., *Proc. Natl. Acad. Sci. U.S.A.* **99**, 856 (2002).
4. D. E. Arking et al., *Am. J. Hum. Genet.* **72**, 1154 (2003).
5. N. Ogata et al., *Bone* **31**, 37 (2002).
6. K. Kawano et al., *J. Bone Miner. Res.* **17**, 1744 (2002).
7. Y. Yamada, F. Ando, N. Niino, H. Shimokata, *J. Mol. Med.* **83**, 50 (2005).
8. D. E. Arking, G. Atzmon, A. Arking, N. Barzilay, H. C. Dietz, *Circ. Res.* **96**, 412 (2005).
9. M. Kuro-o et al., data not shown.
10. F. Grabnitz, M. Seiss, K. P. Rucknagel, W. L. Staudenbauer, *Eur. J. Biochem.* **200**, 301 (1991).
11. R. Weindruch, R. L. Walford, S. Fligiel, D. Guthrie, *J. Nutr.* **116**, 641 (1986).
12. H. M. Brown-Borg, K. E. Borg, C. J. Meliska, A. Bartke, *Nature* **384**, 33 (1996).
13. R. A. Miller, *Sci. Aging Knowledge Environ.* **2001**, vp6 (2001).
14. G. C. Williams, *Evol. Int. J. Org. Evol.* **11**, 398 (1957).
15. C. Kenyon, J. Chang, E. Gensch, A. Rudner, R. Tabtiang, *Nature* **366**, 461 (1993).
16. J. Z. Morris, H. A. Tissenbaum, G. Ruvkun, *Nature* **382**, 536 (1996).
17. M. Tatar et al., *Science* **292**, 107 (2001).
18. D. J. Clancy et al., *Science* **292**, 104 (2001).
19. M. Holzenberger et al., *Nature* **421**, 182 (2003).
20. M. Blüher, B. B. Kahn, C. R. Kahn, *Science* **299**, 572 (2003).
21. C. Kenyon, *Cell* **120**, 449 (2005).
22. T. Utsugi et al., *Metabolism* **49**, 1118 (2000).
23. A. E. Halseth, D. P. Bracy, D. H. Wasserman, *Am. J. Physiol.* **276**, E70 (1999).

24. A. Imura et al., *FEBS Lett.* **565**, 143 (2004).
25. A. R. Saltiel, C. R. Kahn, *Nature* **414**, 799 (2001).
26. D. LeRoith, C. T. Roberts Jr., *Cancer Lett.* **195**, 127 (2003).
27. E. Araki et al., *Nature* **372**, 186 (1994).
28. M. Tatar, A. Bartke, A. Antebi, *Science* **299**, 1346 (2003).
29. We thank D. H. Wasserman and Vanderbilt Mouse Metabolic Phenotyping Center for physiological analysis of the mice; R. L. Dobbins for hyperinsulinemic euglycemic clamp experiments; J. A. Richardson and Molecular Pathology Core Facility at UT Southwestern for histological analysis; D. W. Russell at UT Southwestern for *Klotho* receptor identification; R. Komuro and H. Kuriyama at UT Southwestern for insulin and IGF1 signaling analysis; Genentech for providing IGF1; H. Masuda, T. Suga, R. Nagai, A. T. Dang, R. Shamlou, P. Bezerra, T. Reed, C. Lucu, W. Lai for earlier contributions and supports to this study; and E. C. Friedberg, M. S. Brown, and K. A. Wharton Jr. at UT Southwestern for critical reading of the manuscript. This work was supported in part by grants from Endowed Scholar Program at UT Southwestern (M.K.), Pew Scholars Program in Biomedical Science (M.K.), Eisai Research Fund (M.K.), High-Impact/High-Risk Research Program at UT Southwestern (M.K.), and NIH (R01AG19712 to M.K. and R01AG25326 to M.K. and K.P.R.). J.H. is supported by the NIH, the Perot Family Foundation, and the Humboldt Foundation.

#### Supporting Online Material

www.sciencemag.org/cgi/content/full/1112766/DC1  
Materials and Methods  
Figs. S1 to S7  
Table S1  
References

25 March 2005; accepted 4 August 2005

Published online 25 August 2005;

10.1126/science.1112766

Include this information when citing this paper.

## REPORTS

### Bright X-ray Flares in Gamma-Ray Burst Afterglows

D. N. Burrows,<sup>1\*</sup> P. Romano,<sup>2</sup> A. Falcone,<sup>1</sup> S. Kobayashi,<sup>1,3</sup>  
B. Zhang,<sup>4</sup> A. Moretti,<sup>2</sup> P. T. O'Brien,<sup>5</sup> M. R. Goad,<sup>5</sup> S. Campana,<sup>2</sup>  
K. L. Page,<sup>5</sup> L. Angelini,<sup>6,7</sup> S. Barthelmy,<sup>6</sup> A. P. Beardmore,<sup>5</sup>  
M. Capalbi,<sup>8</sup> G. Chincarini,<sup>2,9</sup> J. Cummings,<sup>6</sup> G. Cusumano,<sup>10</sup>  
D. Fox,<sup>11</sup> P. Giommi,<sup>8</sup> J. E. Hill,<sup>1</sup> J. A. Kennea,<sup>1</sup> H. Krimm,<sup>6</sup>  
V. Mangano,<sup>10</sup> F. Marshall,<sup>6</sup> P. Mészáros,<sup>1</sup> D. C. Morris,<sup>1</sup>  
J. A. Nousek,<sup>1</sup> J. P. Osborne,<sup>5</sup> C. Pagani,<sup>1,2</sup> M. Perri,<sup>8</sup> G. Tagliaferri,<sup>2</sup>  
A. A. Wells,<sup>5</sup> S. Woosley,<sup>12</sup> N. Gehrels<sup>6</sup>

Gamma-ray burst (GRB) afterglows have provided important clues to the nature of these massive explosive events, providing direct information on the nearby environment and indirect information on the central engine that powers the burst. We report the discovery of two bright x-ray flares in GRB afterglows, including a giant flare comparable in total energy to the burst itself, each peaking minutes after the burst. These strong, rapid x-ray flares imply that the central engines of the bursts have long periods of activity, with strong internal shocks continuing for hundreds of seconds after the gamma-ray emission has ended.

Gamma-ray bursts (GRBs) are the most powerful explosions since the Big Bang, with typical energies around  $10^{51}$  ergs. Long GRBs (duration  $> 2$  s) are thought to signal the creation

of black holes by the collapse of massive stars (1–4). The detected signals from the resulting highly relativistic fireballs consist of prompt gamma-ray emission (from internal shocks in

the fireball) lasting for several seconds to minutes, followed by afterglow emission (from external shocks as the fireball encounters surrounding material) covering a broad range of frequencies from radio through x-rays (5–7). Because of the time needed to accurately determine the GRB position, most afterglow

<sup>1</sup>Department of Astronomy and Astrophysics, 525 Davey Lab, Pennsylvania State University, University Park, PA 16802, USA. <sup>2</sup>Istituto Nazionale di Astrofisica (INAF)–Osservatorio Astronomico di Brera, Via Bianchi 46, 23807 Merate, Italy. <sup>3</sup>Center for Gravitational Wave Physics, 104 Davey Lab, Pennsylvania State University, University Park, PA 16802, USA. <sup>4</sup>Department of Physics, University of Nevada, Box 454002, Las Vegas, NV 89154–4002, USA. <sup>5</sup>Department of Physics and Astronomy, University of Leicester, University Road, Leicester LE1 7RH, UK. <sup>6</sup>NASA/Goddard Space Flight Center, Greenbelt, MD 20771, USA. <sup>7</sup>Department of Physics and Astronomy, Johns Hopkins University, 3400 North Charles Street, Baltimore, MD 21218, USA. <sup>8</sup>Agenzia Spaziale Italiana Science Data Center, Via Galileo Galilei, 00044 Frascati, Italy. <sup>9</sup>Dipartimento di Fisica, Università degli studi di Milano-Bicocca, Piazza delle Scienze 3, 20126 Milan, Italy. <sup>10</sup>INAF–Istituto di Astrofisica Spaziale e Fisica Cosmica Sezione di Palermo, Via Ugo La Malfa 153, 90146 Palermo, Italy. <sup>11</sup>Department of Astronomy, California Institute of Technology, MS 105-24, Pasadena, CA, 91125, USA. <sup>12</sup>Department of Astronomy and Astrophysics, University of California, Santa Cruz, CA 95064, USA.

\*To whom correspondence should be addressed.  
E-mail: burrows@astro.psu.edu

measurements have been made hours after the burst, and little is known about the characteristics of afterglows in the minutes following a burst, when the afterglow emission is actively responding to inhomogeneities in both the fireball and the circumburst environment.

The Swift (8) X-ray Telescope (XRT) (9) provides unique x-ray observations of young GRB and x-ray flash (XRF) afterglows, beginning in the first few minutes after the burst. (Here, we use the terms “burst” and “prompt emission” to refer to the burst seen in hard x-rays and gamma rays, and we use the term “afterglow” to refer to the soft x-ray, optical, and radio emission seen after the end of the detectable hard x-ray prompt emission.) Between 23 December 2004 and 5 May 2005, the XRT observed 13 afterglows within 200 s of the onset of GRBs discovered by the Swift Burst Alert Telescope (BAT) (10). In most cases, the

XRT found a bright, monotonically decaying afterglow (11–14). In contrast, the afterglows of both XRF 050406 and GRB 050502B (15) were a factor of 10 to 1000 times fainter than previous XRT-detected afterglows at  $T + 100$  s but brightened rapidly several minutes later before decaying back to their preflare fluxes (Fig. 1). The afterglow of XRF 050406 brightened by a factor of 6 between 150 and 213 s postburst and is similar to x-ray flares observed in a few previous cases (16). GRB 050502B is qualitatively different, with a giant flare that brightened by a factor of  $\sim 500$  to a peak at  $T + 740$  s. This flare contained roughly as much energy ( $\sim 9 \times 10^{-7}$  ergs  $\text{cm}^{-2}$ , 0.3 to 10 keV) as the prompt emission observed by the BAT ( $8 \times 10^{-7}$  ergs  $\text{cm}^{-2}$ , 15 to 350 keV), something never before seen and quite unexpected.

The rise and fall of the flare in XRF 050406 are both very steep. Following standard practice,

we characterized the x-ray afterglow decays as power-laws with the x-ray flux varying as  $F_x \propto t^\alpha$ , where  $t$  is the time since GRB onset. Using this same form to describe the x-ray flare, we found  $\alpha = +4.9 \pm 0.3$  during the rising portion and  $\alpha = -5.7 \pm 0.6$  during the decay, with  $\delta t/t_{\text{peak}} \sim 0.3$  and 0.6 for the rise and fall times, respectively. (The flare slopes are more symmetrical if the underlying power-law afterglow decay is subtracted.) Such large slopes cannot be explained by external forward shocks, in which the radiation physics implies a slower decay, with the decay time  $\delta t$  comparable to the postshock time  $t$  (17). The shape of the flare is reminiscent of that expected for an external reverse shock, created in the outflow when the forward shock is slowed substantially by interaction with an external medium. However, reverse shocks are expected to be far less steep and should be seen in the optical, not the x-ray, band. Synchrotron self-Compton (SSC) models may be able to produce x-ray emission from a reverse shock, but only for carefully balanced conditions (18). A far more natural explanation for this flare is continuation of strong internal shocks to a time of at least  $T + 213$  s.

The flare in GRB 050502B is slower, with  $\delta t_{\text{decay}}/t \sim 1$ , but the sharp spike at  $T + 740$  s (seen in the hard band in Fig. 2B) argues against an external shock mechanism (17). If produced by internal shocks, energy production by the central engine must continue for at least 740 s after the burst begins in this case.

Extended activity in the central engine can explain both of these flares. The central engine becomes active again around 150 and 300 s after the burst for XRF 050406 and GRB 050502B, respectively. The duration of the flare directly measures the duration of the central engine activity because the observed time sequence essentially follows the central engine time sequence (19).

With the exception of the flare at 213 s, the count rate of XRF 050406 was very low and detailed time-resolved spectroscopy is not possible. We can obtain some information on the spectral evolution of the flare, however, by dividing the data into two energy bands and examining light curves in those bands. Figure 2A shows the light curves in two bands (0.2 to 0.7 keV and 0.7 to 10 keV), together with the ratio of these bands. There is significant spectral evolution during the first 400 s of this afterglow. During the rising flare (about  $T + 180$  s to  $T + 200$  s), the hard band flux spikes up rapidly while the soft band flux remains constant, indicating that the flare is harder spectrally than the underlying afterglow. Indeed, the rising portion of the flare contributes no notable flux between 0.2 and 0.7 keV, although it increases the count rate in the hard band by a factor of 4. This provides strong constraints on the flare mechanism: It is difficult to quadruple the flux in the high-energy band while the low-energy band remains constant, unless the flare is

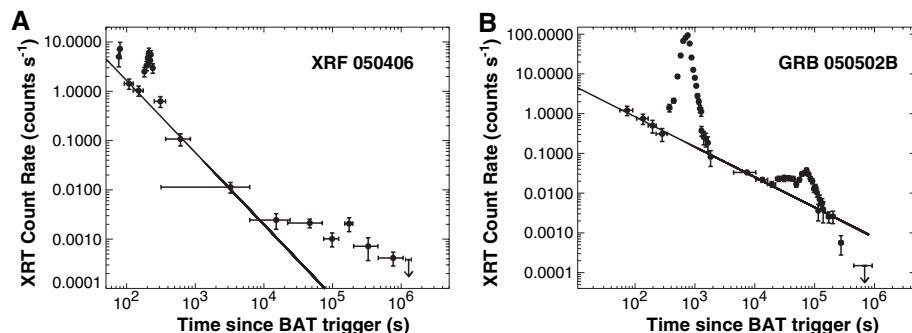


**Fig. 1.** Background-subtracted x-ray light curves of the afterglows of XRF 050406 (A) and GRB 050502B (B). Horizontal error bars show time bins; vertical error bars are means  $\pm$  SD. For XRF 050406 we obtained a total exposure time of 155 ks distributed over 17 days; for GRB 050502B the total exposure time was 176 ks over 11 days. The solid lines represent power-law fits to the underlying afterglow decays from about 100 to 10,000 s [power-law index ( $\pm$ SD) is  $-1.5 \pm 0.1$  and  $-0.8 \pm 0.2$  for XRF 050406 and GRB 050502B, respectively]. The bright x-ray flares are superposed on this underlying power-law decay. At later times the XRF 050406 light curve flattens, whereas the GRB 050502B has several bumps, both suggesting late-time energy injection into the external shock or continued internal shock activity. The rapid decline in count rate for GRB 050502B at  $T > 10^5$  s indicates a possible jet break at about 1 to 2 days postburst.

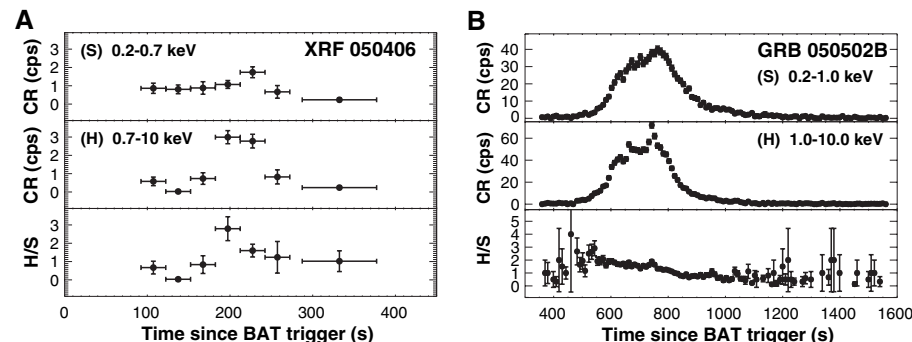


**Fig. 2.** Band ratio plots, showing spectral variations during the flares. In both cases, the top two panels show the count rates (CR) in counts per second (cps) in the soft (S) and hard (H) bands, whereas the bottom panel shows the band ratio (hard/soft). The boundaries between the hard and soft bands were chosen independently for each burst to provide comparable numbers of counts in the two bands. Horizontal error bars show time bins; vertical error bars are means  $\pm$  SD. (A) Light curves in 0.2-to-0.7-keV and 0.7-to-10-keV bands for XRF 050406. The rising part of the flare is substantially harder than the decaying part of the flare or the underlying afterglow, suggesting that the flare is not caused by the external shock responsible for the underlying afterglow. (B) Light curves in 0.2-to-1.0-keV and 1-to-10-keV bands for GRB 050502B. The band ratio shows strong spectral variations during the large flare, with the ratio of counts in these bands decreasing by a factor of 4. The sharp spike in the hard band at about 740 s supports the internal shock interpretation for this flare, because such sharp features cannot easily be produced by external shocks.

strongly absorbed by a column of neutral gas  $N_{\text{H}} \sim 10^{21} \text{ cm}^{-2}$  that does not affect the underlying afterglow. However, the soft band peaks during the time bin following the overall peak, indicating that the emission softens substantially as the flare decays. If absorption is invoked for the rising portion of the flare, then the absorption seems to decrease markedly during the flare decay, suggesting that the absorbing gas may be ionized by the flare (20, 21). After the flare, the band ratio returns to a value consistent with the preflare values. A band ratio plot of GRB 050502B also shows clear indications of spectral variations (Fig. 2B), with a trend similar to that in XRF 050406 (hardening at the beginning of the flare and gradually softening as the flare progresses), although in this case both bands increase during the rising portion of the flare.

We have referred to these events as x-ray flares because they were not detected by the higher energy BAT instrument on Swift. This is presumably due to the higher sensitivity of the XRT and to the steep spectral energy indices of the afterglows ( $\beta = -1.3$  for the flare in XRF 050406 and  $\beta = -1.4$  for the flare in GRB 050502B, where  $F_x \propto E^\beta$ ). In the case of XRF 050406, the prompt emission was classified as an XRF because of its relatively soft spectrum. The discovery of these large x-ray flares in the afterglows raises the possibility that these flares themselves would be classified as XRFs had they not been preceded by the higher energy bursts detected by the BAT. Indeed, GRB 050502B appears to be a remarkable combination of a normal GRB followed more than 10 min later by an XRF of comparable fluence. [There is indirect evidence for a similar sequence in GRB 031203 (22)]. If a normal, relatively hard burst such as GRB 050502B can produce such a bright x-ray flare through late-time internal shocks, this suggests that XRFs themselves may be related to the characteristics of the central engine rather than to geometrical effects (23, 24). However, the long durations and smooth temporal profile observed in these x-ray flares are quite different from those typically detected in XRFs (25).

Both of these afterglows appear to be dominated by long periods of energy production by the central engine, leading to a long period of x-ray emission from internal shocks extending long past the cessation of gamma-ray production. Such activity has previously been suggested as an explanation for extended GRB tails observed by the Burst and Transient Source Experiment (BATSE) instrument (26). In addition to the large flares several minutes after the burst, the plateaus or bumps beginning several hours later imply either that substantial energy is still being injected into the blast wave by refreshed shocks (27), that the external shocks are encountering dense clumps in the nearby interstellar medium (28), or that the internal shocks are still continuing up to several days after the burst in the

observer's frame. The last possibility would require that the central engine operated for a time scale of days, possibly due to fallback of material into the central black hole (29, 30).

If the central engine is still pumping substantial energy into the blast wave at such late times, how can one explain the short duration of the gamma-ray emission? The late internal shocks that produce the flares must produce lower energy photons than did the earlier internal shocks. This can be explained by higher bulk Lorentz factors, which result in lower magnetic fields at the larger radius reached by the internal shocks at these late times. For the internal shock model, the typical peak energy is  $E_p \propto L^{1/2} R^{-1} \propto L^{1/2} \Gamma^{-2} \delta t^{-1}$  (31), where  $L$  is the luminosity at the flare epoch,  $R$  is the internal shock radius,  $\Gamma$  is the Lorentz factor, and  $\delta t$  is the variability time scale. If the flare occurs when  $R$  is 3 to 10 times larger than the typical internal shock radius of the burst,  $E_p$  may be 10 times lower. This is consistent with the detection of these flares in the x-ray band rather than in gamma-rays and with the large  $\delta t$  observed in the x-ray flares. The higher bulk Lorentz factors may arise because these late-time internal shocks benefit from a low-density channel through the progenitor star, previously excavated by the jets that produce the original gamma-ray burst. These later outflows would then have lower amounts of entrained baryons and higher Lorentz factors, leading to lower photon energies at later times and pushing the late-time internal shock emission below the BAT energy band (15 to 150 keV).

#### References and Notes

1. S. E. Woosley, *Astrophys. J.* **405**, 273 (1993).
2. A. I. MacFadyen, S. E. Woosley, *Astrophys. J.* **524**, 262 (1999).
3. J. Hjorth *et al.*, *Nature* **423**, 847 (2003).

4. K. Z. Stanek *et al.*, *Astrophys. J.* **591**, L17 (2003).
5. P. Mészáros, M. J. Rees, *Astrophys. J.* **476**, 232 (1997).
6. J. van Paradijs, C. Kouveliotou, R. A. M. J. Wijers, *Annu. Rev. Astron. Astrophys.* **38**, 379 (2000).
7. B. Zhang, P. Mészáros, *Int. J. Mod. Phys.* **19**, 2385 (2004).
8. N. Gehrels *et al.*, *Astrophys. J.* **611**, 1005 (2004).
9. D. N. Burrows *et al.*, *Space Sci. Rev.*, in press.
10. S. Barthelmy *et al.*, *Space Sci. Rev.*, in press.
11. D. N. Burrows *et al.*, *Astrophys. J.* **622**, L85 (2005).
12. S. Campana *et al.*, *Astrophys. J.* **625**, L23 (2005).
13. G. Tagliaferri *et al.*, *Nature* **436**, 985 (2005).
14. G. Cusumano *et al.*, in preparation.
15. Details of the burst properties are available as a supplementary table on Science Online.
16. L. Piro *et al.*, *Astrophys. J.* **623**, 314 (2005).
17. K. Ioka, S. Kobayashi, B. Zhang, *Astrophys. J.*, in press.
18. S. Kobayashi *et al.*, *Astrophys. J.*, in press.
19. S. Kobayashi, T. Piran, R. Sari, *Astrophys. J.* **490**, 92 (1997).
20. D. Lazzati, R. Perna, G. Ghisellini, *Mon. Not. R. Astron. Soc.* **325**, L19 (2001).
21. R. Perna, D. Lazzati, *Astrophys. J.* **580**, 261 (2002).
22. D. Watson *et al.*, in preparation.
23. E. Woods, A. Loeb, *Astrophys. J.* **523**, 187 (1999).
24. B. Zhang, X. Dai, N. M. Lloyd-Ronning, P. Mészáros, *Astrophys. J.* **601**, L119 (2004).
25. J. Heise, J. in't Zand, R. M. Kippen, P. M. Woods, in *Gamma-Ray Bursts in the Afterglow Era*, E. Costa, F. Frontera, J. Hjorth, Eds. (Springer, Berlin Heidelberg, 2001), pp. 16–21.
26. K. Hurley *et al.*, *Nature* **372**, 652 (1994).
27. M. J. Rees, P. Mészáros, *Astrophys. J.* **496**, L1 (1998).
28. D. Lazzati, E. Rossi, S. Covino, G. Ghisellini, D. Malesani, *Astron. Astrophys.* **396**, L5 (2002).
29. A. I. MacFadyen, S. E. Woosley, A. Heger, *Astrophys. J.* **550**, 410 (2001).
30. A. King *et al.*, *Astrophys. J. Lett.*, in press.
31. B. Zhang, P. Mészáros, *Astrophys. J.* **581**, 1236 (2002).
32. This letter is based on observations with the NASA Swift gamma-ray burst Explorer. We thank the Swift operations team for their support. The authors acknowledge support from NASA in the United States, ASI in Italy, and Particle Physics and Astronomy Research Council in the UK.

#### Supporting Online Material

www.sciencemag.org/cgi/content/full/1116168/DC1 Table S1

15 June 2005; accepted 29 July 2005  
Published online 18 August 2005;  
10.1126/science.1116168

Include this information when citing this paper.

## Molecular Octa-Uranium Rings with Alternating Nitride and Azide Bridges

William J. Evans,\* Stosh A. Kozimor, Joseph W. Ziller

Uranium nitrides offer potential as future nuclear fuels and as probes of metal ligand multiple bonding involving the f-block actinide metals. However, few molecular examples are available for study owing to the difficulties in synthesis. Recent advances in organoactinide chemistry have provided a route to uranium nitride complexes that expands the options for developing UN chemistry. Several 24-membered uranium nitrogen rings,  $(\text{UNUN}_3)_4$ , have been synthesized by reduction of sodium azide with organometallic metallocene derivatives,  $[(\text{C}_5\text{Me}_4\text{R})_2\text{U}][(\mu\text{-Ph})_2\text{BPh}_2]$  ( $\text{R} = \text{Me, H}$ ;  $\text{Me} = \text{methyl, Ph} = \text{phenyl}$ ). The nanometer-sized rings contain unusual UNU nitride linkages that have short U-N distances within the double-bond range.

Uranium nitrides have potential applications as future fuels in nuclear reactors owing to their high melting point, density, and thermal

conductivity (1, 2). Attachment of nitride ions,  $\text{N}^{3-}$ , to uranium is also of interest with respect to the nature of multiple bonding when

5f valence orbital actinide metals are involved. However, in contrast to the common multiply bonded uranyl ion,  $(\text{O}=\text{U}=\text{O})^{2+}$ , few uranium nitrides are known. To develop a better understanding of actinide nitrides for their safe storage, usage, and subsequent waste reprocessing, theoretical studies have been carried out on the stability and properties of various binary and ternary compositions as simple as UN, NUN, NUO, etc. (3–5). Unfortunately, experimental data have been limited because the few isolable actinide nitrides are difficult to synthesize and solubilize.

Uranium nitrides are generally obtained by reduction of a nitrogen-containing substrate, such as  $\text{N}_2$  or  $\text{NH}_3$ , with uranium reducing agents at high temperatures and pressures (1, 6–8). Purity is a problem because the forcing reaction conditions can facilitate incorporation of contaminants. Until recently, low-temperature and solution-phase approaches to uranium nitrides from molecular precursors of high purity have not been considered, because appropriate starting materials were not clearly available. Perhaps the closest reported compound is a multi-component system,  $[\text{K}(\text{DME})_4][\{\text{K}(\text{DME})(\text{Et}_8\text{-calix}[4]\text{tetrapyrrole})\text{U}\}_2(\mu\text{-NK})_2]$  (DME = dimethoxyethane), obtained from reaction of potassium naphthalenide with a tetrapyrrole compound under  $\text{N}_2$  (9).

While studying actinide reduction chemistry, we developed a variety of hydrocarbon-soluble, molecular organometallic uranium complexes that can effect reductions under mild conditions (10–13). We report here that one class of reductants,  $[(\text{C}_5\text{Me}_4\text{R})_2\text{U}][(\mu\text{-Ph})_2\text{BPh}_2]$  [ $\text{R} = \text{Me}$ , **1** (13, 14),  $\text{H}$ , **2** (15)], reacts in solution at room temperature with sodium azide to form molecular, hydrocarbon-soluble uranium nitrides.

Specifically, 8 uranium and 16 nitrogen atoms combine to generate 24-atom rings with dimensions on the nanometer scale. Solubility is conferred by the supporting ligands, which, in this case, are methyl-substituted cyclopentadienyl groups,  $(\text{C}_5\text{Me}_4\text{R})^{1-}$  ( $\text{R} = \text{H}$ ,  $\text{Me}$ ). These results provide alternative opportunities to develop actinide nitride chemistry and expand the possibilities for f-block element supramolecular syntheses (16–19).

The loosely bound  $[\text{BPh}_4]^{1-}$  ligands in the f-block element metallocene borate salts,  $[(\text{C}_5\text{Me}_5)_2\text{M}][(\mu\text{-Ph})_2\text{BPh}_2]$  ( $\text{M} = \text{lanthanide}$ , uranium), are easily substituted with a variety of anionic groups (12, 14, 20–22). Treatment with carbon-based anions has led to highly reactive sterically oversaturated  $(\text{C}_5\text{Me}_5)_3\text{M}$  complexes (12, 14, 20) and sterically un-

saturated  $[(\text{C}_5\text{Me}_5)_2\text{MR}]_n$  alkyl complexes (21, 22) (Eq. 1). In contrast, the reaction of  $[(\text{C}_5\text{Me}_5)_2\text{U}][(\mu\text{-Ph})_2\text{BPh}_2]$ , **1** (14), with sodium azide,  $\text{NaN}_3$ , does not lead to the isolation of the expected substitution product, “ $[(\text{C}_5\text{Me}_5)_2\text{U}(\text{N}_3)]$ ,” but instead to a molecule with a  $(\text{UNUNNN})_4$  ring,  $[(\text{C}_5\text{Me}_5)_2\text{U}(\mu\text{-N})\text{U}(\mu\text{-N}_3)(\text{C}_5\text{Me}_5)_2]_4$  (Eq. 2), that was isolated in 54% yield (23). Two isomers of this complex were characterized by x-ray crystallography; one isomer, **3**, has the  $(\text{UNUNNN})_4$  ring in a pseudo-chair form (Fig. 1) and the other isomer, **4**, has a pseudo-boat ring geometry (Fig. 2) using the descriptors common for cyclohexane rings. The factors that lead to crystallization of one isomer rather than another appear to be subtle because both isomers could be obtained under similar conditions and were differentiated only by x-ray crystallography.

To determine if the formation of uranium nitride complexes of this type was specific only to  $(\text{C}_5\text{Me}_5)^{1-}$ -ligated metallocenes, we investigated the less sterically demanding  $(\text{C}_5\text{Me}_4\text{H})^{1-}$  analog of **1**,  $[(\text{C}_5\text{Me}_4\text{H})_2\text{U}][(\mu\text{-Ph})_2\text{BPh}_2]$ , **2** (15). Complex **2** also reacts with  $\text{NaN}_3$  to make the 24-membered uranium nitrogen ring structure.  $[(\text{C}_5\text{Me}_4\text{H})_2\text{U}(\mu\text{-N})\text{U}(\mu\text{-N}_3)(\text{C}_5\text{Me}_4\text{H})_2]_4$ , **5**, was isolated

as a chair isomer in 63% yield. Complexes **3**, **4**, and **5** are all air and moisture sensitive.

The dimensions of the  $\text{U}_8\text{N}_{16}$  rings of **3** and **5** are similar. The lengths between atoms that span the ring,  $\text{N}(5)\cdots\text{N}(5')$  and  $\text{N}(3)\cdots\text{N}(9)$  in **3** (Fig. 1), are  $\sim 0.9$  and  $\sim 1.2$  nm, respectively. When the cyclopentadienyl sheath is included, compounds **3** and **5** just fit inside a sphere of diameter 2.2 nm. The more compact isomer **4** has analogous ring dimensions of  $\sim 0.9 \times 1.0$  nm and can be contained within a 2.0-nm-diameter sphere. Previously reported uranium clusters of similar size,  $[(\text{C}_5\text{H}_2\text{Bu}_3)_4(\text{bipy})_2][\text{U}_6\text{O}_{13}]$  (bipy = bipyridene) (**18**),  $[\text{UO}_2\text{L}]_4^{8-}$  [ $\text{L} = (2\text{R},3\text{R},4\text{S},5\text{S})\text{-tetrahydrofuran-tetracarboxylic acid}$ ] (**19**), and the uranyl selenate nanotubes,  $[(\text{UO}_2)_{10}(\text{SeO}_4)_{17}(\text{H}_2\text{O})]^{14-}$  (**17**), all relied on the linear uranyl moiety,  $(\text{O}=\text{U}=\text{O})^{2+}$ , as a building block.

In **3**, **4**, and **5**, the eight  $[(\text{C}_5\text{Me}_4\text{R})_2\text{U}]^{2+}$  units are charge balanced by four  $(\text{N}_3)^{1-}$  azide ligands and four formally  $\text{N}^{3-}$  nitride ligands. The structural parameters for the metallocene components are typical for  $\text{U}^{4+}$  complexes (Table 1). The metrical data on the bridging nitrides are of greatest interest given the elusiveness of this ligand type in molecular actinide chemistry. The U-N(nitride) distances

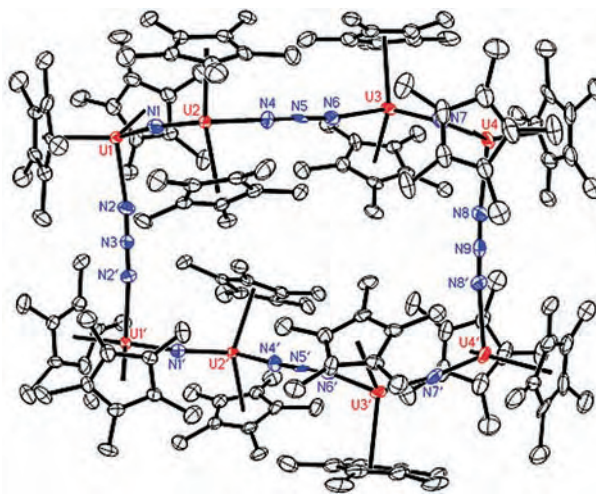
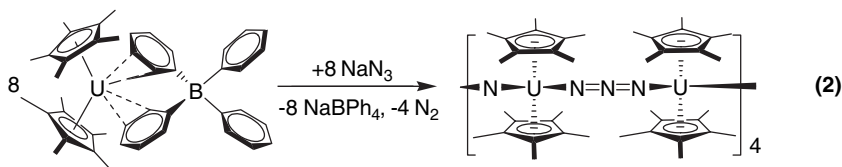
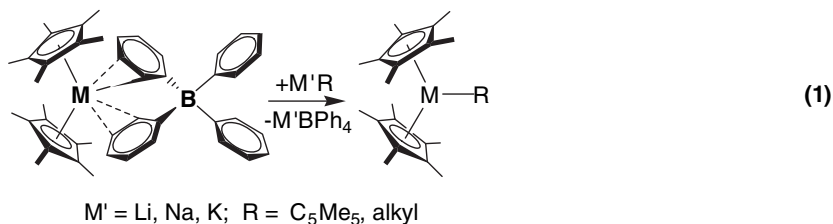


**Fig. 1.** A thermal ellipsoid plot of  $[(\text{C}_5\text{Me}_5)_2\text{U}(\mu\text{-N})\text{U}(\mu\text{-N}_3)(\text{C}_5\text{Me}_5)_2]_4$ , **3**, drawn at 50% probability.

Department of Chemistry, University of California, Irvine, CA 92697–2025, USA.

\*To whom correspondence should be addressed. E-mail: wevans@uci.edu

are similar in all three complexes and range from 2.047(6) to 2.090(8) Å with averages of 2.07(1), 2.07(1), and 2.05(3) Å in **3**, **4**, and **5**, respectively. These U-N(nitride) distances are shorter than U<sup>4+</sup>-N single bond distances and are in the double bond range. For comparison, U-N(imido) double bonds in tetra-valent (C<sub>5</sub>Me<sub>5</sub>)<sub>2</sub>U[=N(C<sub>6</sub>H<sub>5</sub>)](Cl)Li(TMEDA) (TMEDA = tetramethylethylenediamine) and (C<sub>5</sub>Me<sub>5</sub>)<sub>2</sub>U=N(C<sub>6</sub>H<sub>2</sub>^tBu<sub>3</sub>) (**24**) are 2.05(1) and 1.95(1) Å, respectively. The U-N(nitride) distances in **3**, **4**, and **5** are also shorter than the 2.444(9) Å U-N(nitride) distances determined by powder diffraction for the six-coordinate face-centered cubic uranium mononitride, UN (**6**).

These UN bond distances are consistent with a symmetrical bonding picture (Scheme 1a) rather than a localized short/long pattern (Scheme 1b). The existence of asymmetrical bonding patterns, when observed in transition metal chemistry, has been rationalized (25, 26) on the basis of special

electron configurations, which evidently do not include the 5f<sup>2</sup> electron configuration of U<sup>4+</sup>.

A U=N=U bonding picture would be simplistically expected to have a 180° U-N-U angle, but the U-N-U angles range from 169.4(4)° to 172.2(4)° in **3**, 166.6(4)° to 168.5(4)° in **4**, and 154.6(7)° to 158.9(6)° in **5**. U-E-U (E = S, O) angles can similarly deviate from linear geometries, e.g., the tetra-valent [(C<sub>5</sub>H<sub>4</sub>Me)<sub>3</sub>U]<sub>2</sub>(μ-S) (**27**) and trivalent [(C<sub>5</sub>Me<sub>5</sub>)<sub>2</sub>U]<sub>2</sub>(μ-O) (**28**) complexes have 164.9(4)° and 171.5(6)° angles, respectively. For comparison, the other reported molecular uranium nitride, [K(DME)<sub>4</sub>][{K(DME)(Et<sub>8</sub>-calix[4]tetrapyrrole)U}<sub>2</sub>(μ-NK)<sub>2</sub>] (**9**), has bent U-N-U bridges with 106.9(2)° angles. Although the nitrides in this complex are also bridged to potassium, the 2.076(6) and 2.099(5) Å U-N distances are surprisingly similar to those in **3**, **4**, and **5**. This result may be a consequence of the polydentate nature of the calix-tetrapyrrole ligand.

In contrast to the unusual uranium nitride linkages, the bridging azide ligands in **3**, **4**, and **5** have more precedent in lanthanide and actinide chemistry (29–31). They absorb at 2100, 2100, and 2111 cm<sup>-1</sup>, respectively, in the normal range in the infrared (29–31) and they are linear. The U-N(azide) distances in **3**, **4**, and **5** are all equivalent within experimental error, and they are longer than typical U<sup>4+</sup>-N single bonds (Table 1) (24). However, the azide metrical parameters are somewhat difficult to compare with literature values as both the M-N(azide) distances and the M-N-N angles vary considerably in lanthanide and actinide azide complexes (29–33).

The formation of **3**, **4**, and **5** is likely to involve the initial substitution of [BPh<sub>4</sub>]<sup>1-</sup> in **1** and **2** by azide to form “(C<sub>5</sub>Me<sub>4</sub>R)<sub>2</sub>U(N<sub>3</sub>)” moieties, a reaction well established for the starting materials (Eq. 1) (12, 14, 20–22). There is also ample precedent for the loss of dinitrogen from metal azides to form N<sup>3-</sup> nitride ions, although the necessary two-electron reductions are often photochemically or thermally induced (34, 35). In the formation of **3**, **4**, and **5**, eight U<sup>3+</sup> centers formally furnish the eight electrons needed to convert four azide ligands to nitrides. Only half of the azide ligands in the reaction are converted to nitrides, because two U<sup>3+</sup> centers are required per azide. This process could occur via bridged U<sup>3+</sup>-azide-U<sup>3+</sup> intermediates or via transient U<sup>5+</sup> nitrides such as “(C<sub>5</sub>Me<sub>4</sub>R)<sub>2</sub>UN” that would subsequently be reduced to U<sup>4+</sup> in the product by the remaining U<sup>3+</sup> ions (36). It is unclear with the data available on uranium azides why (N<sub>3</sub>)<sup>1-</sup> is reduced in this process, whereas several other uranium azide complexes are stable and isolable (31–33).

The reduction/oligomerization reaction in Eq. 2 is unusual in that it generates such a large molecular aggregate with an f-block bis(cyclopentadienyl) metallocene. More commonly, oligomerization of f-block metallocenes results in the formation of dimers and trimers. Hexametallic [(C<sub>5</sub>Me<sub>5</sub>)<sub>2</sub>Sm(CN)]<sub>6</sub>, which contains two atom linkers, is the most structurally similar (37).

The larger structures of **3**, **4**, and **5** arise in part because the repeat unit is bimetallic, i.e., it is composed of two different bis(cyclopentadienyl) components. The formally cationic [(C<sub>5</sub>Me<sub>4</sub>R)<sub>2</sub>U(μ-N<sub>3</sub>)]<sup>1+</sup> and anionic [(C<sub>5</sub>Me<sub>4</sub>R)<sub>2</sub>U(μ-N)]<sup>1-</sup> metallocenes would not be expected to self-condense to dimers or trimers for electrostatic reasons.

As noted previously (16, 19), the use of f-block elements in molecular assembly schemes is limited in part because the metals do not have dominant orbital requirements that generate fixed structures. The more flexible nature of their coordination chemistry makes them less controllable and predictable in supramolecular

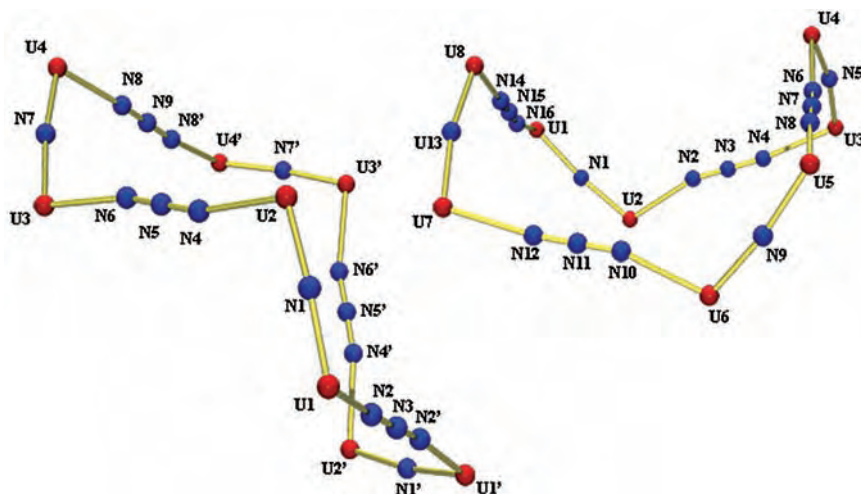
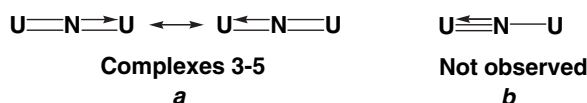


**Fig. 2.** Ball-and-stick representation of the (UNUNNN)<sub>4</sub> rings of isomers of [(C<sub>5</sub>Me<sub>5</sub>)<sub>2</sub>U(μ-N)U(μ-N<sub>3</sub>)(C<sub>5</sub>Me<sub>5</sub>)<sub>2</sub>]<sub>4</sub>, **3**; (C<sub>5</sub>Me<sub>5</sub>)<sub>2</sub>U(μ-N)U(μ-N<sub>3</sub>)(C<sub>5</sub>Me<sub>5</sub>)<sub>2</sub>]<sub>4</sub>, **4**, and [(C<sub>5</sub>Me<sub>4</sub>H)<sub>2</sub>U(μ-N)U(μ-N<sub>3</sub>)(C<sub>5</sub>Me<sub>4</sub>H)<sub>2</sub>]<sub>4</sub>, **5**.

**Table 1.** Selected bond distances (Å) and angles (degrees) for [(C<sub>5</sub>Me<sub>5</sub>)<sub>2</sub>U(μ-N)U(μ-N<sub>3</sub>)(C<sub>5</sub>Me<sub>5</sub>)<sub>2</sub>]<sub>4</sub>, **3**, [(C<sub>5</sub>Me<sub>5</sub>)<sub>2</sub>U(μ-N)U(μ-N<sub>3</sub>)(C<sub>5</sub>Me<sub>5</sub>)<sub>2</sub>]<sub>4</sub>, **4**, and [(C<sub>5</sub>Me<sub>4</sub>H)<sub>2</sub>U(μ-N)U(μ-N<sub>3</sub>)(C<sub>5</sub>Me<sub>4</sub>H)<sub>2</sub>]<sub>4</sub>, **5**.

Parameter	<b>3</b>	<b>4</b>	<b>5</b>
U-N(nitride) range	2.055(8)–2.090(8)	2.047(6)–2.078(6)	2.012(16)–2.089(16)
U-N(azide) range	2.467(8)–2.494(7)	2.476(7)–2.525(7)	2.449(14)–2.474(13)
U-C(Cp) range*	2.700(9)–2.876(11)	2.707(8)–2.860(9)	2.690(19)–2.827(17)
U-Cnt range†	2.490–2.527	2.488–2.528	2.474–2.504
U-N-U range	169.4(4)–172.2(4)	166.6(4)–168.5(4)	154.6(7)–158.9(6)
U-N-N range	164.8(6)–173.6(7)	160.8(6)–176.7(6)	160.3(12)–170.8(13)
N-U-N(azide) range	100.6(3)–107.3(3)	102.8(2)–110.2(2)	102.1(5)–104.4(5)
N-N-N range	178.1(8)–179.8(12)	178.2(9)–179.3(8)	178.8(18)–180(2)
Cnt-U-Cnt range†	126.2–128.4	127.4–129.0	121.6–128.2

\*Cp = (C<sub>5</sub>Me<sub>5</sub>)<sup>1-</sup> or (C<sub>5</sub>Me<sub>4</sub>H)<sup>1-</sup>. †Cnt = (C<sub>5</sub>Me<sub>4</sub>R)<sup>1-</sup> (R = Me, H) ring centroid.



**Scheme 1.**

syntheses. However, the present results show that by using the steric requirements of the bis(cyclopentadienyl) unit, the necessary structural rigidity is present to make nanometer-sized ring assemblies. It remains to be established why **3**, **4**, and **5** crystallize as closed oligomeric structures instead of open polymeric versions, but it is clear that this route to molecular supramolecular assemblies dense in uranium and nitrogen is viable.

#### References and Notes

1. L. Black *et al.*, *J. Alloys Compounds* **315**, 36 (2001).
2. F. G. Reshetnikov, *Atom. Energ.* **91**, 998 (2001).
3. G. P. Kushto, P. F. Souter, L. Andrews, M. Newrock, *J. Chem. Phys.* **14**, 5894 (1997).
4. N. Kaltsoyannis, *Inorg. Chem.* **39**, 6009 (2000).
5. L. Gagliardi, P. Pyykkö, *Angew. Chem. Int. Ed. Engl.* **43**, 1573 (2004).
6. C. P. Kempter, J. C. McGuire, M. R. Nadler, *Anal. Chem.* **31**, 156 (1959).
7. T. N. Le, N. Lorenzelli, L. Zuppiroli, *J. Nucl. Mater.* **184**, 230 (1991).
8. T. Urabe, K. Takahashi, M. Katsura, M. Miyake, *J. Alloys Compounds* **193**, 122 (1993).
9. I. Korobkov, S. Gambarotta, G. P. A. Yap, *Angew. Chem. Int. Ed. Engl.* **41**, 3433 (2002).
10. W. J. Evans, G. W. Nye, M. A. Johnston, J. W. Ziller, *J. Am. Chem. Soc.* **122**, 12019 (2000).
11. W. J. Evans, G. W. Nye, J. W. Ziller, *Angew. Chem. Int. Ed. Engl.* **39**, 240 (2000).
12. W. J. Evans, S. A. Kozimor, J. W. Ziller, N. Kaltsoyannis, *J. Am. Chem. Soc.* **126**, 14533 (2004).
13. W. J. Evans, S. A. Kozimor, J. W. Ziller, *Chem. Commun.*, in press.
14. W. J. Evans, G. W. Nye, K. J. Forrestal, J. W. Ziller, *Organometallics* **21**, 1050 (2002).
15. W. J. Evans, S. A. Kozimor, W. R. Hillman, J. W. Ziller, *Organometallics*, in press.
16. J.-C. Bünzli, C. Pigué, *Chem. Rev.* **102**, 1897 (2002).
17. S. Krivovichev *et al.*, *J. Am. Chem. Soc.* **127**, 1072 (2005).
18. P. B. Duval *et al.*, *Angew. Chem. Int. Ed. Engl.* **40**, 3357 (2001).
19. R. Thuéry, C. Villiers, J. Jaud, M. Ephritikhine, B. Masci, *J. Am. Chem. Soc.* **126**, 6838 (2004).
20. W. J. Evans, B. L. Davis, *Chem. Rev.* **102**, 2119 (2002).
21. W. J. Evans, J. M. Perotti, J. W. Ziller, *J. Am. Chem. Soc.* **127**, 1068 (2005).
22. W. J. Evans, J. M. Perotti, J. W. Ziller, *J. Am. Chem. Soc.* **127**, 3894 (2005).
23. Materials and Methods are available as supporting material on Science Online.
24. D. S. J. Arney, C. J. Burns, *J. Am. Chem. Soc.* **117**, 9448 (1995).
25. R. A. Wheeler, R. Hoffman, J. Strähle, *J. Am. Chem. Soc.* **108**, 5381 (1986).
26. R. A. Wheeler *et al.*, *J. Am. Chem. Soc.* **108**, 2222 (1986).
27. J. G. Brennan, R. A. Andersen, A. Zalkin, *Inorg. Chem.* **25**, 1761 (1986).
28. W. J. Evans, S. A. Kozimor, J. W. Ziller, *Polyhedron* **23**, 2689 (2004).
29. H. Schumann, C. Janiak, J. Pickardt, *J. Organomet. Chem.* **349**, 117 (1988).
30. U. P. Singh, S. Tyagi, C. L. Sharma, H. Görner, T. Weyhermüller, *J. Chem. Soc. Dalton Trans.* 4464 (2002).
31. J.-C. Berthet, M. Lance, M. Nierlich, J. Vigner, M. Ephritikhine, *J. Organomet. Chem.* **420**, C9 (1991).
32. I. Castro-Rodríguez, H. Nakai, L. N. Zakharov, A. L. Rheingold, K. Meyer, *Science* **305**, 1757 (2004).
33. I. Castro-Rodríguez, K. Olsen, P. Gantzel, K. Meyer, *J. Am. Chem. Soc.* **125**, 4565 (2003).
34. W. P. Griffith, *Coord. Chem. Rev.* **8**, 369 (1972).
35. K. Dehnicke, J. Strähle, *Angew. Chem. Int. Ed. Engl.* **31**, 955 (1992).
36. J. G. Brennan, R. A. Andersen, A. Zalkin, *J. Am. Chem. Soc.* **110**, 4554 (1988).
37. Y. Obora, T. Ohta, C. L. Stern, T. J. Marks, *J. Am. Chem. Soc.* **119**, 3745 (1997).
38. For support of this research, we thank the Chemical Sciences, Geosciences and Biosciences Division of the Office of Basic Energy Sciences of the U.S. Department of Energy. Experimental details, x-ray diffraction data, atomic coordinates, thermal parameters, and complete bond distances and angles for **3**, **4**, and **5** are provided as supporting material on Science Online. Crystallographic data were deposited in the Cambridge Crystallographic Database Centre (3: CCDC-275800, 4: CCDC-275801, 5: CCDC-275802).

#### Supporting Online Material

www.sciencemag.org/cgi/content/full/309/5742/1835/DC1

Materials and Methods

Figs. S1 to S3

Tables S1 to S3

References and Notes

22 June 2005; accepted 16 August 2005  
10.1126/science.1116452

## Ultrahigh Strength in Nanocrystalline Materials Under Shock Loading

Eduardo M. Bringa,<sup>1\*</sup> Alfredo Caro,<sup>1</sup> Yinmin Wang,<sup>1</sup> Maximo Victoria,<sup>1</sup> James M. McNaney,<sup>1</sup> Bruce A. Remington,<sup>1</sup> Raymond F. Smith,<sup>1</sup> Ben R. Torralva,<sup>1</sup> Helena Van Swygenhoven<sup>2</sup>

Molecular dynamics simulations of nanocrystalline copper under shock loading show an unexpected ultrahigh strength behind the shock front, with values up to twice those at low pressure. Partial and perfect dislocations, twinning, and debris from dislocation interactions are found behind the shock front. Results are interpreted in terms of the pressure dependence of both deformation mechanisms active at these grain sizes, namely dislocation-based plasticity and grain boundary sliding. These simulations, together with new shock experiments on nanocrystalline nickel, raise the possibility of achieving ultrahard materials during and after shock loading.

Dislocations are the carriers of plastic deformation in crystalline materials (1). The search for materials with ultrahigh hardness and strength is closely related to the search for the most effective obstacles to dislocation motion. Grain boundaries (GBs) are effective obstacles for dislocation motions (1–3); the strength or hardness of crystalline materials increases inversely with the square root of their grain size, a

relation known as the Hall-Petch effect (2, 3). As the dimensions of the grains approach nanometer sizes, this strengthening mechanism is limited by the onset of GB accommodation mechanisms, such as sliding (2–4). If these softening effects could be suppressed, harder materials could be created, with potential applications to such extreme environments as target capsules for the National Ignition Facility (5). From atomistic simulations, we show a substantial increase in strength during shock loading of nanocrystalline copper, with a complex dependence on shock pressure.

Experimental observations of increased strength have been reported in high-strain rate

deformation of nanocrystalline nickel and copper, up to strain rates of  $10^4 \text{ s}^{-1}$  (6–8). Dislocation plasticity in nanocrystalline materials is controlled by thermal and mechanical activation of sources at GBs, a mechanism that requires fluctuations, implying an intrinsic time scale that could explain the reported strain rate sensitivity. This suggests that an increase of the strain rate by several orders of magnitude, as in shock loading conditions (9, 10), may result in an even harder material. However, extrapolation of strength from a strain rate of  $10^4 \text{ s}^{-1}$  to greater than  $10^6 \text{ s}^{-1}$  becomes problematic, because strain rate cannot be increased by

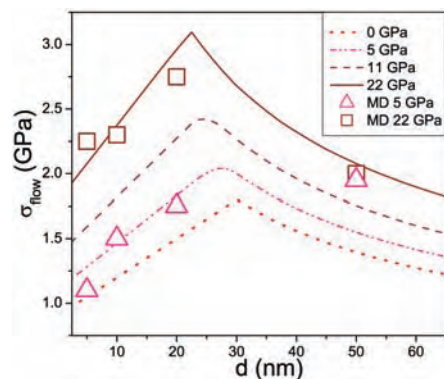


**Fig. 1.** Flow stress for different pressures, as a function of grain size, according to our qualitative model (16). MD results are also included. In this plot we use parameters from the literature or from our MD simulations (16):  $\sigma_0 = 0.9 \text{ GPa}$ ,  $\alpha = 0.04$ ,  $\beta = 1.0$ ;  $G_0 = 45 \text{ GPa}$ . We choose  $d_0 = d_1 = 30 \text{ nm}$  and  $\sigma_{\text{Disl}}(d_0) = \sigma_{\text{GBS}}(d_0)$  at  $P = 0 \text{ GPa}$ , to obtain the only free parameter,  $C = 0.04$ .

<sup>1</sup>Lawrence Livermore National Laboratory, Livermore, CA 94550, USA. <sup>2</sup>Paul Scherrer Institute, CH-5232 Villigen-PSI, Switzerland.

\*To whom correspondence should be addressed. E-mail: ebringa@llnl.gov

orders of magnitude without increasing the pressure. When uniaxial loading is due to a shock wave (i.e., a compression wave traveling faster than the sound speed), lateral relaxation does not have time to occur and pressure builds up. Under those conditions, a regime is entered where plasticity is controlled by both high strain rate and high pressure. We present atomistic simulations of shocked nanocrystalline samples, in which the extremely short compression time scales (or equivalently, very high volumetric strain rates) associated with shock loading are close to those observed in recent experiments (10–12). Such short time scales imply that dislocation creation and motion, and stress-driven GB accommodation, are the dominant plasticity mechanisms; thermally activated processes, such as diffusion, are observed to be negligible.

Both GB accommodation and dislocation activity have a pressure dependence, although for different reasons. GB accommodation has similarities to the plasticity of granular media, i.e., sliding of undeformable objects controlled by friction (13). In granular materials, the Mohr-Coulomb law of sliding friction predicts that the onset of plasticity occurs when the applied stress is larger than the value defined by the flow stress,  $\sigma_{\text{flow}} \propto (\sigma_{\text{coh}} + \alpha \sigma_{\text{normal}})$ , where  $\sigma_{\text{coh}}$  is related to the cohesion of the interface, and  $\alpha$  is related to the geometry of the grains. This criterion has been recently extended to nanocrystals (14, 15). Associating  $\sigma_{\text{normal}}$  with pressure, we conclude that the stress threshold for sliding plasticity increases linearly with pressure (15). Using molecular dynamics (MD) simulations, we verified that a nanocrystalline metal deforming plastically by

GB accommodation gets harder as hydrostatic pressure ( $P$ ) is increased (16) (fig. S1). With the scaling arguments presented by Van Swygenhoven and Caro (17) to express the dependence of deformation rate on grain size,  $d$ , the flow stress for GB sliding can tentatively be written as  $\sigma_{\text{GBS}} = (\sigma_0 + \alpha P)(1 + d/d_0)$ , where  $\sigma_0$  is the flow stress of a zero grain size material (an amorphous metal) at zero pressure, and  $d_0$  is a constant. Notably,  $\sigma_{\text{GBS}}$  increases as  $d$  increases in this regime. For shock-induced dislocation plasticity it is generally assumed that, as in the Steinberg-Guinan model (10), the dynamic strength and hardness of the material scales with the shear modulus,  $G$ , which in turn increases linearly with pressure,  $G(P) = G_0 + \beta P$  (10, 16). Adding the Hall-Petch relation, the flow stress for dislocation plasticity becomes  $\sigma_{\text{Disl}} = CG(P)(d/d_1)^{-0.5}$ , where  $\beta$ ,  $C$ , and  $d_1$  are constants. The effective flow stress for a nanocrystal can be taken as the minimum of  $\sigma_{\text{Disl}}$  and  $\sigma_{\text{GBS}}$ , although a more realistic model would include a mixture of both when  $\sigma_{\text{Disl}} \sim \sigma_{\text{GBS}}$ . At any pressure, as grain size decreases, the material hardens according to the Hall-Petch effect, down to the point where  $\sigma_{\text{Disl}} = \sigma_{\text{GBS}}$ . For smaller grain sizes, the material softens according to the law of GB sliding. As pressure increases, both mechanisms predict an increase in hardness, creating the possibility for pressure-induced ultrahard nanocrystalline materials. Figure 1 shows the qualitative hardness map that emerges from this model. These ultrahard hardness conditions can be achieved by shock loading (10–12).

In shock loading, one surface of the system, the piston, is driven inward along the  $z$  axis at a constant velocity  $U_p$ , leading to a shock wave

with velocity  $U_s$ . The first major difference between homogeneous deformation (4, 17–21) and shock loading (9) is that the total volumetric strain behind the shock front,  $\epsilon$ , is constant and determined by  $\epsilon = U_p/U_s$  ( $d\epsilon/dt = 0$ ) (19). The stress along the shock direction behind the shock front, i.e., the shock “pressure,” is also constant behind the shock front and given by  $\sigma_{zz} = \rho_0 U_p U_s$ , where  $\rho_0$  is the density of the preshocked material. With  $U_p$  in the range 0.1 to 3.0 km s<sup>-1</sup>, the shock pressure for copper is in the range ~5 to 230 GPa. We identified hardness and flow stress with the von Mises stress,  $\sigma_{\text{VM}}$ , well behind the shock front, where  $\sigma_{\text{VM}}^2 = 0.5[(\sigma_{xx} - \sigma_{yy})^2 + (\sigma_{yy} - \sigma_{zz})^2 + (\sigma_{zz} - \sigma_{xx})^2]$ . Figure 2A shows a typical shock profile. By increasing pressure,  $\sigma_{\text{VM}}$  increases until the onset of plasticity occurs (peak in Fig. 2A); then it decreases and evolves in a complex way depending on factors such as strain rate, pressure, microstructure, and dislocation properties in the materials. A satisfactory quantitative theory does not yet exist. The strain rate with which the material is deformed at the shock front is roughly given by  $\epsilon$  divided by the shock front rise time,  $d\epsilon/dt \approx \epsilon U_s/\Delta_z$ , where  $\Delta_z$  is the shock front width. This width depends on a number of factors, including grain size. Portions of the sample reached by the shock wave undergo a fast deformation,  $d\epsilon/dt \sim 10^9$  to  $10^{11}$  s<sup>-1</sup>, during the short shock rise time (several picoseconds) and then remain at constant strain, eventually relaxing the shear stress. Shock loading can irreversibly freeze-in some of the microstructural changes induced during the loading, producing a residual material still harder at zero pressure after the shock. Indeed, research

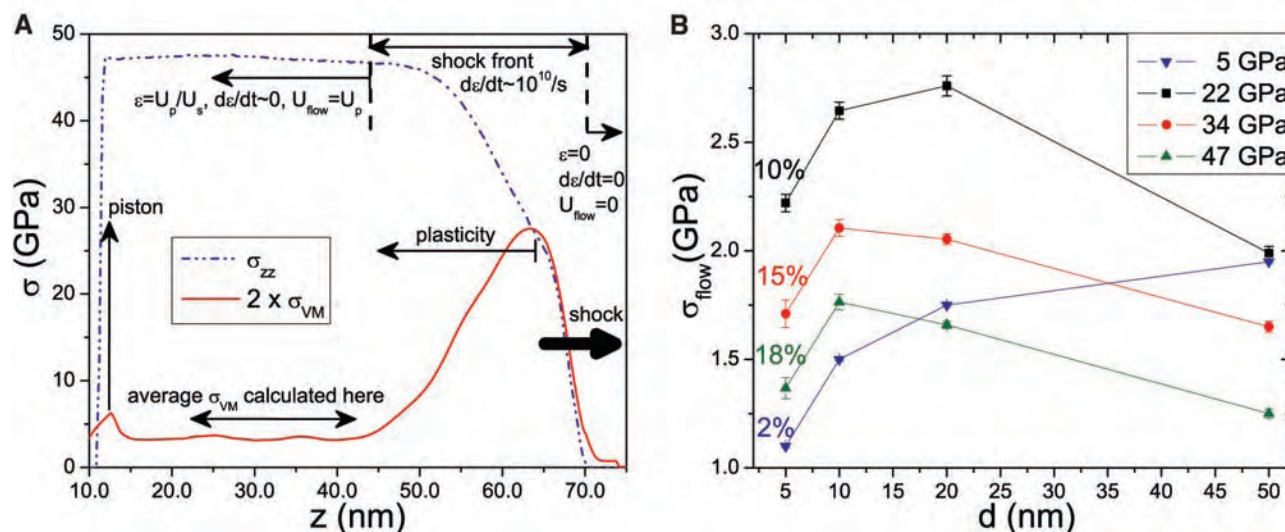


**Fig. 2.** (A) Typical stress profiles under uniaxial shock loading:  $\sigma_{zz}$  (shock pressure) and twice the von Mises stress. Values obtained from an image from our MD simulation ( $d \sim 20$  nm),  $\sim 10$  ps after the piston started to move with velocity  $U_p$ , advancing from left to right. The material has a flow velocity,  $U_{\text{flow}} = U_p = 1$  km/s, giving  $U_s = 5.5$  km/s, and  $\epsilon = 18\%$  behind the shock front. The shock front spreads more than in single-crystal simulations (9), with

a width close to the grain size. (B) Flow stress under shock loading at different shock wave pressures ( $\sigma_{zz}$ ). The flow stress is largest in the pressure range of 20 to 30 GPa. Total volumetric strains behind the shock front are also indicated. The flow stress was calculated as  $\sigma_{\text{VM}}$  averaged over  $\sim 20$  nm, in a region in front of the piston, when the shock front had already traveled  $\sim 100$  nm, as shown in (A). Error bars show means  $\pm$  SE.

over the last several decades shows clear indications of massive modification of the material after unloading and recovering of shocked materials (10–12, 22).

We report large-scale MD shock simulations in copper nanocrystalline samples with up to  $\sim 4 \times 10^8$  atoms (16). Shock loading conditions are ideally modeled by large-scale MD simulations (9, 23–26), which cover time and length scales similar to laser-shock experiments. Our simulations show that the large increase in pressure substantially reduces GB sliding, limiting the softening mechanism and doubling the flow stress. As a measure of  $\sigma_{\text{normal}}$ , we used the shockwave pressure,  $\sigma_{zz}$ . The main result of this work, the flow stress as a function of grain size and pressure, is shown in Fig. 2B (fig. S2). At low stress (5 GPa), comparable to the stress of quasi-static experiments, the hardness is relatively low; there is only GB sliding (4, 18), and samples with small grains are softer than those with large grains. At intermediate stress (5 to 25 GPa), the hardness at all grain sizes increases with increasing shock strength. This is the manifestation of the reduction of GB sliding and harder dislocation plasticity. MD results in this pressure range are also shown in Fig. 1, in qualitative agreement with our model. Figure 2B confirms the predicted trends, including the

shift in the position of the maximum hardness toward lower grain sizes as pressure increases. At large stress ( $>25$  GPa), a new phenomenon appears, reflected in the drop in strength ( $\sigma_{\text{flow}}$ ) shown in Fig. 2B (fig. S2): Increased nucleation and motion of dislocations, together with a large increase in temperature, allow the sample to deform more easily. At even higher pressures (150 to 220 GPa, depending on grain size) shock-induced melting occurs, with  $\sigma_{\text{flow}} \sim 0$ . A maximum in hardness, therefore, exists at some intermediate pressure. We found the maximum hardness, about twice the value at “low” pressure, at  $\sim 25$  GPa.

To provide insight into the atomistic processes involved in the deformation, Fig. 3 shows a 47-GPa shock wave traveling through 20-nm grains, for which only defective atoms are shown (movie S1). We observed the traces of numerous stacking faults indicating the passage of partial dislocations. Our simulations also show nanotwins, represented by mirror planes. This is similar to atomistic simulations of homogeneous deformation (4, 16–21) and shocks (9, 4–26) at similar grain sizes. However, the most salient feature of this figure is the presence of perfect dislocations represented by narrow ribbons of stacking faults bounded by partial dislocations inside the grains (fig. S3). The shock-induced nanotwin volume is less than 1% of the total volume at the end of our simulation. Twin growth is expected for longer pressure pulses, but experimental detection of this amount of twinning is difficult, given that a low density of twins already exists in the preshocked samples. We also found a number of defect clusters, about 1 nm in diameter, likely created by dislocation-dislocation interactions. These might act as dislocation obstacles when further deformation is carried out, contributing to increased hardness.

Shock-induced dislocation nucleation has been observed in numerous studies, but a detailed understanding has begun to emerge only recently. The barriers for dislocation nucleation do not increase strongly with pressure (27) above an initial threshold, at least in the shock regimes studied here for copper. Studies of shock waves in single-crystal copper with and without defects (9, 24–26) show increased dislocation production with shock pressure; that is, pressure does not inhibit the nucleation process. We found the same behavior for nanocrystalline copper at all grain sizes, with a threshold of  $\sim 6$  GPa, even for 5-nm grains (fig. S4). As pressure increases, dislocations nucleate initially at GB junctions (movie S2), and then from different locations along the GB. The stress is high enough to induce dislocation creation at such a small grain size, which is due to the reduction of GB sliding, a mechanism that, if dominant, would release the shear stress. This behavior can further be understood in terms of the differences in the pressure dependence of both GB sliding and dislocation-based plasticity. As the pressure increases, the grain size at which the maximum hardness occurs decreases (Figs. 1 and 2B).

In addition to the simulations shown above, we have performed experiments to understand the behavior of nanocrystalline metals under extreme conditions. Because of experimental constraints, it is very difficult to directly measure the dynamic deformation process during high-strain rate loading at the nanoscale. Figure 4 shows a plan-view transmission electron microscopy (TEM) picture of nanocrystalline nickel after shock loading at 40 GPa (16). Nickel and copper are both fcc materials with very similar shock impedances, but nickel has larger stacking-fault energy. There is clear evidence of dislocation activity occurring inside

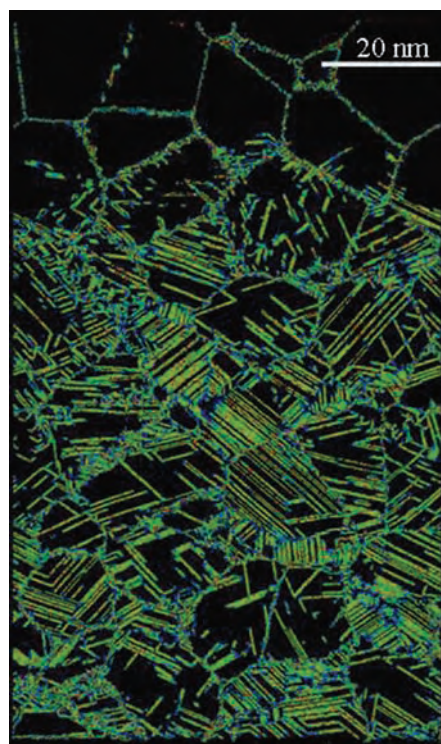


**Fig. 3.** An image taken from our simulation for  $d = 20$  nm and  $\sigma_{zz} = 47$  GPa. Only a thin slab (0.7 nm wide) is shown. The shock has traveled for 30 ps, from bottom to top, producing a high density of partial dislocations (attached to GBs) together with perfect dislocations (“isolated” inside grains, fig. S3) and nanotwins.

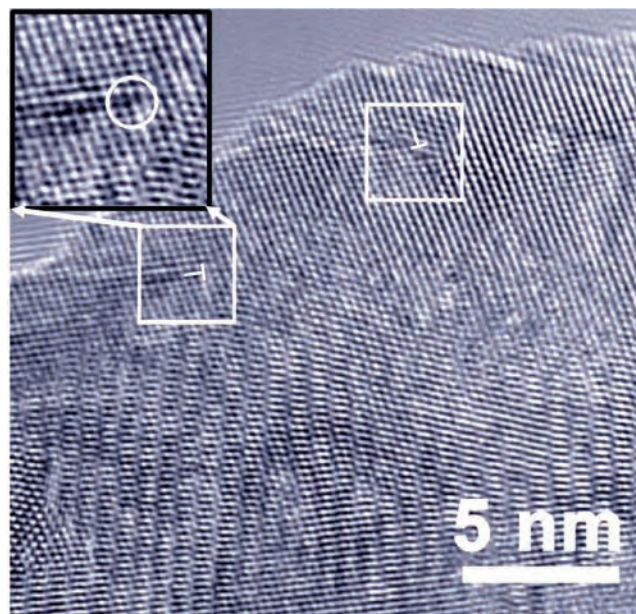


**Fig. 4.** A plan-view TEM image of nanocrystalline nickel after shock loading at 40 GPa. Dislocation activity is visible inside grains (white boxes); the inset shows a filtered image of the dislocation. The grain sizes before the shock loading are 30 to 50 nm. The final grain sizes are in the range 5 to 100 nm as a result of the residual shock heating in the recovered sample.



grains (boxes in Fig. 4) in agreement with our atomistic simulations. During loading at  $\sim 40$  GPa, our MD simulations predict a dislocation density of  $\sim 10^{13}$  cm $^{-2}$ , which is expected to decrease during recovery. Although the exact dislocation density in recovered samples is difficult to estimate, our high-resolution TEM images do show residual dislocations inside some nanograins (Fig. 4). This is quite unusual in nanocrystalline materials and not easily achievable under normal deformation conditions (28). Our experiments also indicate an increase in hardness in the samples recovered after shock loading, as expected from the measured residual dislocation densities.

Computer simulations of shocks in nanocrystalline copper show that the flow stress reaches ultrahigh values at high pressures produced by shock loading. This hardness increase of up to a factor of two compared with unshocked samples arises because the barriers for GB sliding increase with pressure (13–15), whereas dislocation nucleation is not as sensitive to pressure above a threshold of several gigapascals. Although the simulations we have carried out are for nanocrystalline copper, GB sliding reduction under pressure should be a general feature of shock-loaded materials, including alloy and nonmetallic nanocrystals. Harder nanocrystal-

line materials could offer novel applications, including improved armor materials and National Ignition Facility targets (5).

#### References and Notes

- R. Madec, B. Devincere, L. Kubin, T. Hoc, D. Rodney, *Science* **301**, 1879 (2003).
- M. A. Meyers, K. K. Chawla, *Mechanical Behavior of Materials* (Prentice-Hall, Upper Saddle River, NJ, 1999).
- J. R. Weertman, in *Nanostructured Materials: Processing, Properties and Potential Applications*, C. C. Koch, Ed. (William Andrew, Norwich, NY, 2002), pp. 397–421.
- J. Schiøtz, K. W. Jacobsen, *Science* **301**, 1357 (2003).
- T. R. Dittrich *et al.*, *Laser Part. Beams* **17**, 217 (1999).
- D. Jia, K. T. Ramesh, E. Ma, L. Lu, K. Lu, *Scripta Mater.* **45**, 613 (2001).
- L. Lu, S. X. Li, K. Lu, *Scripta Mater.* **45**, 1163 (2001).
- F. Dalla Torre *et al.*, *Acta Mater.* **50**, 3957 (2002).
- B. L. Holian, P. S. Lomdahl, *Science* **280**, 2085 (1998).
- B. A. Remington *et al.*, *Metall. Mater. Trans. A* **35**, 2587 (2004).
- M. A. Meyers *et al.*, *Acta Mater.* **51**, 1211 (2003).
- J. M. McNaney, J. Edwards, R. Becker, T. Lorenz, B. A. Remington, *Metall. Trans. A* **35**, 2625 (2004).
- C. A. Schuh, A. C. Lund, *Nat. Mater.* **2**, 449 (2003).
- A. C. Lund, C. A. Schuh, *Acta Mater.* **53**, 3193 (2005).
- B. Jiang, G. J. Weng, *J. Mech. Phys. Solids* **52**, 1125 (2004).
- Materials and methods are available as supporting material on Science Online.
- H. Van Swygenhoven, A. Caro, *Phys. Rev. B* **58**, 11246 (1998).
- H. Van Swygenhoven, M. Spaczer, A. Caro, D. Farkas, *Phys. Rev. B* **60**, 22 (1999).
- J. Schiøtz, F. D. Di Tolla, K. W. Jacobsen, *Nature* **391**, 561 (1998).

- V. Yamakov *et al.*, *Nat. Mater.* **1**, 45 (2002).
- H. Van Swygenhoven, P. M. Derlet, A. G. Frøseth, *Nat. Mater.* **3**, 399 (2004).
- M. W. Chen, J. W. McCauley, K. J. Hemker, *Science* **299**, 1563 (2003).
- K. Kadau, T. C. Germann, P. S. Lomdahl, B. L. Holian, *Science* **296**, 1681 (2002).
- E. Bringa *et al.*, *J. App. Phys.* **96**, 3793 (2004).
- F. A. Sapozhnikov, V. V. Dremov, M. S. Smirnova, *J. Phys. IV France* **110**, 323 (2003).
- L. Davila *et al.*, *Appl. Phys. Lett.* **86**, 161902 (2005).
- S. Cheng, J. A. Spencer, W. W. Milligan, *Act. Mater.* **51**, 4505 (2003).
- Z. Budrovic, H. Van Swygenhoven, P. M. Derlet, S. Van Petegem, B. Schmitt, *Science* **304**, 273 (2004).
- We thank A. M. Hodge and C. A. Schuh for help with the experiments; P. Erhart for calculating elastic constants; D. Farkas, T. Diaz de la Rubia, R. Lebensohn, M. A. Meyers, V. Bulatov, N. Park, and V. Dremov for useful discussions; M. Duchaineau for plotting the results; and Livermore Computing for MCR and Thunder time. This work was performed under the auspices of the U.S. Department of Energy at Lawrence Livermore National Laboratory under contract no. W-7405-Eng-48, with support from the Laboratory Directed Research and Development program.

#### Supporting Online Material

www.sciencemag.org/cgi/content/full/309/5742/1838/DC1

Materials and Methods

Figs. S1 to S4

Movies S1 and S2

References

29 June 2005; accepted 18 August 2005  
10.1126/science.1116723

## Influence of the Atlantic Subpolar Gyre on the Thermohaline Circulation

Hjálmar Hátún,<sup>1,2\*</sup> Anne Britt Sandø,<sup>3,4</sup> Helge Drange,<sup>3,4,5,6</sup> Bogi Hansen,<sup>1</sup> Heðinn Valdimarsson<sup>7</sup>

During the past decade, record-high salinities have been observed in the Atlantic Inflow to the Nordic Seas and the Arctic Ocean, which feeds the North Atlantic thermohaline circulation (THC). This may counteract the observed long-term increase in freshwater supply to the area and tend to stabilize the North Atlantic THC. Here we show that the salinity of the Atlantic Inflow is tightly linked to the dynamics of the North Atlantic subpolar gyre circulation. Therefore, when assessing the future of the North Atlantic THC, it is essential that the dynamics of the subpolar gyre and its influence on the salinity are taken into account.

Formation of the densest, deepest waters of the North Atlantic THC occurs following the northward flow of warm, saline waters (the At-

lantic Inflow) (Fig. 1) across the Greenland-Scotland Ridge. Through air-sea exchange, these waters subsequently lose much of their heat, but not their salt. Added freshwater from precipitation and river runoff reduces the salinity somewhat but still allows them to become the densest waters in the region. This makes the Arctic Mediterranean—the Arctic Ocean and the Nordic Seas—the dominant source area for the North Atlantic THC (1, 2). Because the density close to the freezing point is mainly determined by the salinity, changes in the upper-layer salinities of this region may have large impacts on the future development of this circulation.

Climate models featuring increasing greenhouse-gas scenarios predict an intensified freshwater supply to the Arctic Mediterranean during the 21st century (3). Observations indicate that this is already occurring (4, 5) and that large areas are freshening (5–7). This freshwater increase may partly explain why many climate models indicate a weakening of the North Atlantic THC starting from the end

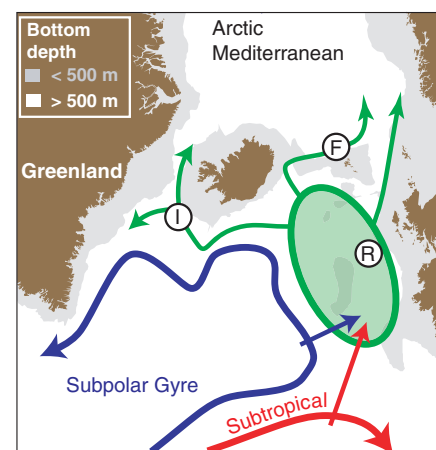


**Fig. 1.** Schematic of the main features of the surface circulation in the northeastern North Atlantic. The green shaded region shows where the subpolar and the subtropical waters meet, mix, and feed into the Arctic Mediterranean. The hydrographic observations used in the study are obtained in the Rockall Trough (R), Faroe Current (F), and Irminger Current (I).

<sup>1</sup>Faroese Fisheries Laboratory, Box 3051, FO-110, Tórshavn, Faroe Islands. <sup>2</sup>University of Washington, Box 357940, Seattle, WA 98195, USA. <sup>3</sup>Nansen Environmental and Remote Sensing Center, Thormøhlensgt. 47, N-5006 Bergen, Norway. <sup>4</sup>Bjerknes Center for Climate Research, Allégaten 55, 5007 Bergen, Norway. <sup>5</sup>Geophysical Institute University of Bergen, Allégaten 70, 5007 Bergen, Norway. <sup>6</sup>Nansen-Zhu International Research Centre, Institute of Atmospheric Physics, Chinese Academy of Sciences, Beijing 100029, China. <sup>7</sup>Marine Research Institute, Skúlagata 4, 121 Reykjavík, Iceland.

\*To whom correspondence should be addressed. E-mail: hjalmarh@ocean.washington.edu

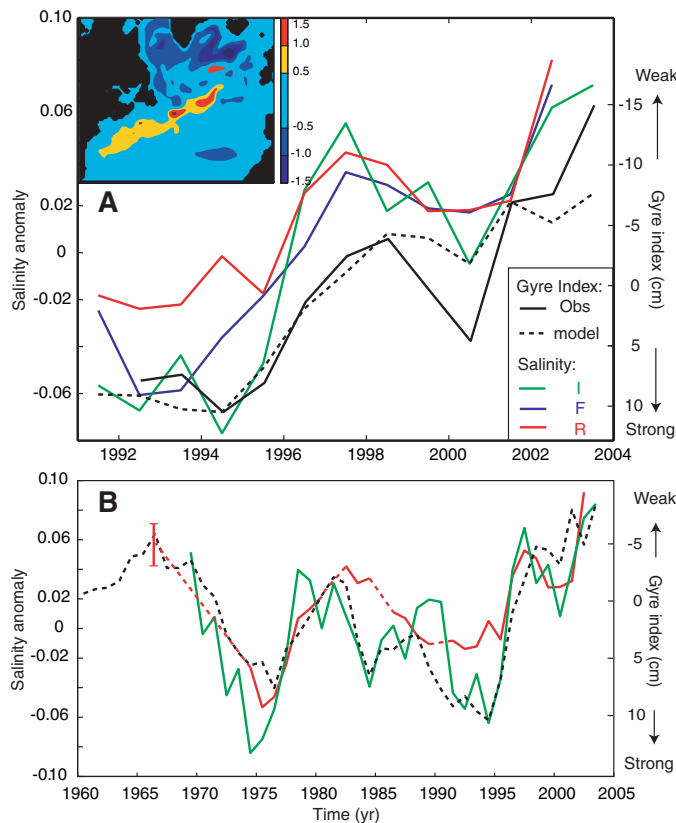
of the 20th century (3). Other models (8) predict a stable North Atlantic THC due to increasing salinities of the waters flowing toward the ventilation areas. This underscores the potential importance of recent observations that all three branches of the Atlantic Inflow to the Arctic Mediterranean (9) have shown increasing salinities during the last decade, with record-high values in 2003 (Fig. 2). This salinity anomaly has already been seen to influence the Arctic Mediterranean, and at Ocean Weather Station Mike in the Norwegian Sea (66°N, 2°E), the poleward-flowing Atlantic Water reached salinity values (and temperatures) in 2004 that were higher than ever since the observations started in 1948 (10, 11). These changes may be expected to have large impacts on the high-latitude climate system and its populations and ecosystems, although the detailed responses are difficult to predict.

The climate system is, however, strongly influenced by internal variability modes, which have to be distinguished from the fingerprints of the more gradual global warming. The Atlantic Inflow into the Arctic Mediterranean is drawn from both the North Atlantic subtropical gyre (SPG) and subtropical gyre (STG) (Fig. 1). Four possible mechanisms may explain the observed record-high salinity of the Atlantic Inflow: (i) changes in the (local) air-sea flux of freshwater [evaporation minus precipitation ( $E - P$ )]; (ii) increasing salinities of the STG water; (iii) increasing salinities of the SPG water; and (iv) dynamic changes in the relative contributions from the two gyres. Here, we discuss these four alternatives by combining observations and results from a numerical Ocean General Circulation Model (OGCM). This is the Nansen Center version (12–14) of the MICOM (Miami Isopycnal Coordinate Ocean Model) (15), forced with daily mean National Centers for Environmental Prediction/National Center for Atmospheric Research (NCEP/NCAR) (16) reanalyses of fresh water, heat, and momentum fluxes for the period 1948 to 2003. Simulated fields from this model system compare favorably with observations in the northeastern Atlantic and Nordic Seas (13, 17, 18) and simulate the salinity variations of the three Atlantic Inflow branches accurately (fig. S1).

To test the explanatory power of mechanism (i), the ( $E - P$ ) field, obtained from the NCEP/NCAR reanalyses, has been integrated over a box centered on the eastern SPG region, giving an index of the atmospheric freshwater flux (fig. S2). Comparing the temporal variation of this index to the observed upper-layer (14) salinity variations in the northeastern Atlantic, it is clear that the air-sea flux [mechanism (i)] cannot explain the observed record-high Atlantic Inflow salinities. This finding is consistent with other studies (19, 20).

As for mechanism (ii), the STG salinity has been observed to increase (5, 21). However, the

**Fig. 2.** Temporal evolution of key parameters. (A) Colored lines show annual averages of the observed salinity anomalies (74) in inflow areas R, F, and I in Fig. 1. The time series R and F are shifted 1 year backward, and the time series I is shifted 2 years backward to account for advective delays. The solid black line shows the principal component, the gyre index (inverted), associated with the leading North Atlantic sea-surface height mode, as obtained from altimetry observations. The dashed line represents the gyre index (inverted) obtained from MICOM. The inset shows the principal spatial mode of variability (EOF) of simulated sea-surface height (see also fig. S4B). (B) As in (A), but for a longer time period. The red vertical line in (B) indicates the approximate salinity range in the mid-1960s as deduced from surface salinity data (26).



salinity variations in the Atlantic Inflow (Figs. 1 and 2) do not correspond to the salinity variations in the STG (22) (fig. S3). Furthermore, the simulated salinity in the upper layers of the central SPG, mechanism (iii), shows no relation to the Atlantic Inflow salinity (fig. S3). For interannual to interdecadal time scales, neither mechanism (ii) nor (iii) seems able to explain the Atlantic Inflow salinity variations, which leaves only dynamical variations [e.g., mechanism (iv)] as a possible explanation.

Häkkinen and Rhines (23) described dynamical variations in the SPG during the decade 1992 to 2002 using altimeter data. A decline of the gyre circulation, as represented by the principal component (the “gyre index”) from an empirical orthogonal function (EOF) analysis, is seen to parallel the increasing salinities in the northeastern Atlantic (Fig. 2A).

The altimetry observations used by Häkkinen and Rhines extend back only to 1992, but the analysis can be extended backward, using results from MICOM. During the 1992 to 2003 period, MICOM reproduces the Häkkinen and Rhines mode (the “gyre mode”) both in terms of its spatial form (Fig. 2A, inset, and fig. S4) and its temporal variation (the gyre index) through the principal component (Fig. 2A). It is therefore reasonable to apply MICOM to put the changes into a longer time perspective and to explore causal relations. To do this, Fig. 2B compares the simulated gyre index with the

salinities of the two Atlantic Inflow branches (I and R) for which long-term observations are available. It is seen that the correspondence between the Atlantic Inflow salinity and the gyre index is not limited to the period after 1992 but extends back at least to the mid 1960s.

The variability of the Atlantic Inflow salinities is part of a larger picture, which may be illustrated by the changes from a high-index year (1993) to a low-index year (1998) (Fig. 3). The main features are a southward shift of the frontal zone between the two gyres in the Newfoundland Basin and a substantial salinity increase along the eastern margin of the North Atlantic, including the Iceland Basin. Density changes in the northeastern Atlantic are governed mainly by changes in temperature, which have been very similar to the salinity changes (fig. S4, C and D). Replacement of the cold and dense water in the Iceland and Irminger Basins with warmer and lighter waters implies an increase in the sea-surface height, whereas colder water replacing warmer water in the Newfoundland Basin likewise implies a decrease in the sea-surface height. This is the pattern detected by the gyre mode, explaining a >15-cm increase in the Iceland and Irminger Basins and a decrease of similar magnitude in the Newfoundland Basin (inset in Fig. 2A). The gyre index is therefore related not only to the strength of the gyre circulation but also to the

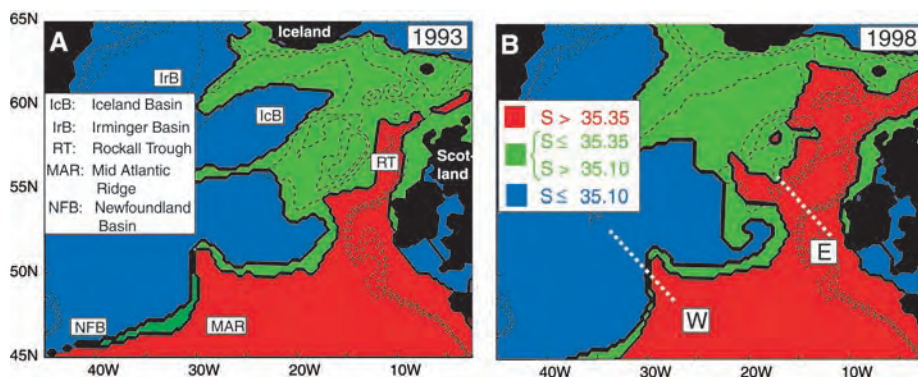


**Fig. 3.** The simulated upper-layer (14) spatial distribution of typical SPG water (blue), STG water (red), and a mixture, influenced by both gyres (green), averaged for the low-salinity year 1993 (A) and the high-salinity year 1998 (B). The 500-m, 1000-m, and 2000-m depth contours are outlined with dashed black lines, and two sections, one crossing the North Atlantic Current (W) and one covering the entrance to the Rockall Trough (E), are shown with dashed white lines.

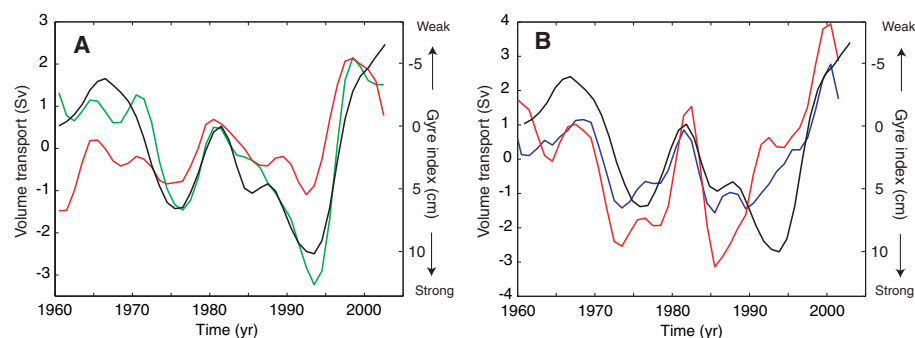


**Fig. 4.** Simulated anomalies of upper-layer (14) volume transport of different water masses through the two sections shown in Fig. 3B compared with the simulated gyre index (black; note inverse scales). (A) The transport anomaly of water with salinity below (green) and above (red) the 35.35 isohaline along section E (Fig. 3) into the Rockall Trough. (B) The transport anomaly of water with salinity below (blue) and above (red) 34.95 through section W (Fig. 3), crossing the North Atlantic Current (NAC). Annual averages, smoothed with a 3-year running mean, are shown. Positive values of transport anomalies for the red lines on (A) and (B) indicate anomalous transport toward the northeast. For the green line on (A) and the blue line on (B), positive values indicate anomalous transport toward the southwest.

shape of the gyre. During the high-index period in the early 1990s, the gyre had an east-west shape with strong protrusions into the eastern basins (Fig. 3A), whereas in the low-index years in the late 1990s, it had a more north-south shape, largely confined to the west of the Mid-Atlantic Ridge (Fig. 3B).

A more detailed understanding may be obtained by focusing on the Rockall Trough, which is a main passageway for the Atlantic Inflow. The upper layers of the trough are fed from two sources (24, 25): water from the North Atlantic Current (NAC), which follows the boundary between the two gyres (green areas in Fig. 3), and water of more southern origin from areas west of and over the continental slope (eastern part of the red areas in Fig. 3). On a section across the trough (section E in Fig. 3B), the waters from the two sources are generally found to be separated by a front, which straddles the 35.35 isohaline (fig. S5). By extracting the volume transports on both sides of this front from MICOM, we obtain

estimates of the influence of each of the two sources on the inflow through the trough. The result (Fig. 4A) clearly shows that the effect of the gyre circulation is to modulate the influence of the relatively fresh NAC on the inflow through the trough.

This influence may be traced upstream to section W across the NAC over the Mid Atlantic Ridge (Fig. 3B). In the model, this section consistently includes the entire frontal zone associated with the current, and the 34.95 isohaline encompasses the sectional area from which the transport of SPG water has been extracted (fig. S6). The transport of STG water through section W has been extracted from the region south of the front defined by the 34.95 isohaline. The resulting time series (Fig. 4B) do not follow the gyre index quite as well as for Fig. 4A, but they still strongly support that the SPG circulation is linked to the relative contributions from the two gyres to the NAC at this location: When the gyre index is high, the volume transport of SPG water through the

section is also high and the volume transport of STG water is low, and vice versa for a low gyre index.

We conclude that on interannual to interdecadal time scales, the salinity of the Atlantic Inflow to the Arctic Mediterranean is controlled mainly by the dynamics of the SPG circulation and its effects on the location, intensity, and composition of the NAC in the northeastern Atlantic. This conclusion does not exclude the possibility that intensified evaporation in the tropical Atlantic and export of freshwater to the Pacific may affect the Atlantic Inflow salinity on longer time scales. According to some climate models (3, 8), this may have a stabilizing effect on the THC. Our results demonstrate, however, that the recently observed record-high Atlantic Inflow salinities are not primarily a consequence of this mechanism and that the coupling between the tropical Atlantic and the Atlantic Inflow to the Arctic Mediterranean is highly dependent on the dynamics of the SPG. In periods with intensive SPG circulation, the stabilizing effect of increasing tropical salinities on the thermohaline ventilation in the Arctic Mediterranean will be reduced. The mechanisms that induce SPG variations were discussed by Häkkinen and Rhines (23), and these mechanisms and their response to human-induced global warming clearly merit more detailed investigations. That has not been the focus of this paper, but our results demonstrate that realistic description of these mechanisms in climate models is a precondition for reliable assessment of the future North Atlantic THC. Our results also show the key importance of long and continued observational time series for this purpose.

#### References and Notes

- R. R. Dickson, J. Brown, *J. Geophys. Res.* **99**, 12319 (1994).
- B. Hansen, S. Østerhus, D. Quadfasel, W. R. Turrell, *Science* **305**, 953 (2004).
- U. Cubasch, G. Meehl, in *Climate Change 2001: The Scientific Basis*, J. T. Houghton et al., Eds. (Cambridge Univ. Press, Cambridge, 2001), pp. 525–582.
- B. J. Peterson et al., *Science* **298**, 2171 (2002).
- R. Curry, B. Dickson, I. Yashayaev, *Nature* **426**, 826 (2003).
- J. Blindheim et al., *Deep-Sea Res.* **47**, 655 (2000).
- R. Curry, C. Mauritzen, *Science* **308**, 1772 (2005).
- M. Latif, E. Roeckner, U. Mikolajewicz, R. Voss, *J. Clim.* **13**, 1809 (2000).
- B. Hansen, S. Østerhus, *Prog. Oceanogr.* **45**, 109 (2000).
- S. Østerhus, personal communication.
- H. Drange et al., in *The Nordic Seas: An Integrated Perspective*, AGU Monograph 158, H. Drange, T. Dokken, T. Furevik, R. Gerdes, W. Berger, Eds. (American Geophysical Union, Washington, DC, 2005), pp. 1–10.
- M. Bentsen, H. Drange, T. Furevik, T. Zhou, *Clim. Dyn.* **22**, 701 (2004).
- H. Drange et al., in *The Nordic Seas: An Integrated Perspective*, AGU Monograph 158, H. Drange, T. Dokken, T. Furevik, R. Gerdes, W. Berger, Eds. (American Geophysical Union, Washington, DC, 2005), pp. 199–220.
- Materials and methods are available as supporting material on Science Online.
- R. Bleck, C. Rooth, C. Hu, L. T. Smith, *J. Phys. Oceanogr.* **22**, 1486 (1992).

16. E. Kalnay *et al.*, *Bull. Am. Meteorol. Soc.* **77**, 437 (1996).
17. J. E. Nilsen, Y. Gao, H. Drange, T. Furevik, M. Bentsen, *Geophys. Res. Lett.* **30**, 10.1029/2002GL016597 (2003).
18. H. Hátún, A. Sandø, H. Drange, M. Bentsen, in *The Nordic Seas: An Integrated Perspective*, AGU Monograph 158, H. Drange, T. Dokken, T. Furevik, R. Gerdes, W. Berger, Eds. (American Geophysical Union, Washington, DC, 2005), pp. 239–250.
19. M. Bersch, *J. Geophys. Res.* **107**, 10.1029/2001JC000901 (2002).
20. N. P. Holliday, *J. Geophys. Res.* **108**, 10.1029/2002JC001344 (2003).
21. T. P. Boyer, S. Levitus, J. I. Antonov, R. A. Locarnini, H. E. Garcia, *Geophys. Res. Lett.* **32**, 10.1029/2004GL021791 (2005).
22. T. M. Joyce, P. Robbins, *J. Clim.* **9**, 3121 (1996).
23. S. Häkkinen, P. B. Rhines, *Science* **304**, 555 (2004).
24. N. P. Holliday, R. T. Pollard, J. F. Read, H. Leach, *Deep-Sea Res.* **47**, 1303 (2000).
25. D. J. Ellett, J. H. A. Martin, *Deep-Sea Res.* **20**, 585 (1973).
26. D. J. Ellett, S. R. Jones, "Surface temperature and salinity time-series from the Rockall Channel, 1948–1992" (Fisheries research data report number 36, Ministry of Agriculture, Fisheries, and Food, Directorate of Fisheries Research, Lowestoft, 1994; www.cefas.co.uk/publications/files/datarep36.pdf).
27. We thank M. Bentsen for model development, P. Rhines for commenting on the paper; M. Miles for language editing, and S. Häkkinen for the extended gyre index in Fig. 2A, based on altimetry. The work is

supported by the Nordic Council of Ministers program Vestnordisk Oeanklima; the Ocean Surface Topography Science Team of NASA; the Research Council of Norway through RegClim, NOClm, and the Program of Supercomputing; and the European Union DG-XII Climate and Environment Program through DYNAMITE (GOCE-0093903) and NOCES (EVK2-2001-00115).

**Supporting Online Material**  
[www.sciencemag.org/cgi/content/full/309/5742/1841/DC1](http://www.sciencemag.org/cgi/content/full/309/5742/1841/DC1)  
 Materials and Methods  
 Figs. S1 to S6

12 May 2005; accepted 4 August 2005  
 10.1126/science.1114777

# Changes in Tropical Cyclone Number, Duration, and Intensity in a Warming Environment

P. J. Webster,<sup>1</sup> G. J. Holland,<sup>2</sup> J. A. Curry,<sup>1</sup> H.-R. Chang<sup>1</sup>

We examined the number of tropical cyclones and cyclone days as well as tropical cyclone intensity over the past 35 years, in an environment of increasing sea surface temperature. A large increase was seen in the number and proportion of hurricanes reaching categories 4 and 5. The largest increase occurred in the North Pacific, Indian, and Southwest Pacific Oceans, and the smallest percentage increase occurred in the North Atlantic Ocean. These increases have taken place while the number of cyclones and cyclone days has decreased in all basins except the North Atlantic during the past decade.

During the hurricane season of 2004, there were 14 named storms in the North Atlantic, of which 9 achieved hurricane intensity. Four of these hurricanes struck the southeast United States in rapid succession, causing considerable damage and disruption. Analysis of hurricane characteristics in the North Atlantic (1, 2) has shown an increase in hurricane frequency and intensity since 1995. Recently, a causal relationship between increasing hurricane frequency and intensity and increasing sea surface temperature (SST) has been posited (3), assuming an acceleration of the hydrological cycle arising from the nonlinear relation between saturation vapor pressure and temperature (4). The issue of attribution of increased hurricane frequency to increasing SST has resulted in a vigorous debate in the press and in academic circles (5).

Numerous studies have addressed the issue of changes in the global frequency and intensity of hurricanes in the warming world. Our basic conceptual understanding of hurricanes suggests that there could be a relationship between hurricane activity and SST. It is well established that SST > 26°C is a requirement for tropical cyclone formation in the current climate (6, 7). There is also a hypothesized relationship between SST and the

maximum potential hurricane intensity (8, 9). However, strong interannual variability in hurricane statistics (10–14) and the possible influence of interannual variability associated with El Niño and the North Atlantic Oscillation (11, 12) make it difficult to discern any trend relative to background SST increases with statistical veracity (8). Factors other than SST have been cited for their role in regulating

hurricane characteristics, including vertical shear and mid-tropospheric moisture (15). Global modeling results for doubled CO<sub>2</sub> scenarios are contradictory (15–20), with simulations showing a lack of consistency in projecting an increase or decrease in the total number of hurricanes, although most simulations project an increase in hurricane intensity.

Tropical ocean SSTs increased by approximately 0.5°C between 1970 and 2004 (21). Figure 1 shows the SST trends for the tropical cyclone season in each ocean basin. If the Kendall trend analysis is used, trends in each of the ocean basins are significantly different from zero at the 95% confidence level or higher, except for the southwest Pacific Ocean. Here we examine the variations in hurricane characteristics for each ocean basin in the context of the basin SST variations. To this end, we conducted a comprehensive analysis of global tropical cyclone statistics for the satellite era (1970–2004). In each tropical ocean basin, we examined the numbers of tropical storms and hurricanes, the number of storm days, and the hurricane intensity distribution. The tropical cyclone data are derived from the best track archives

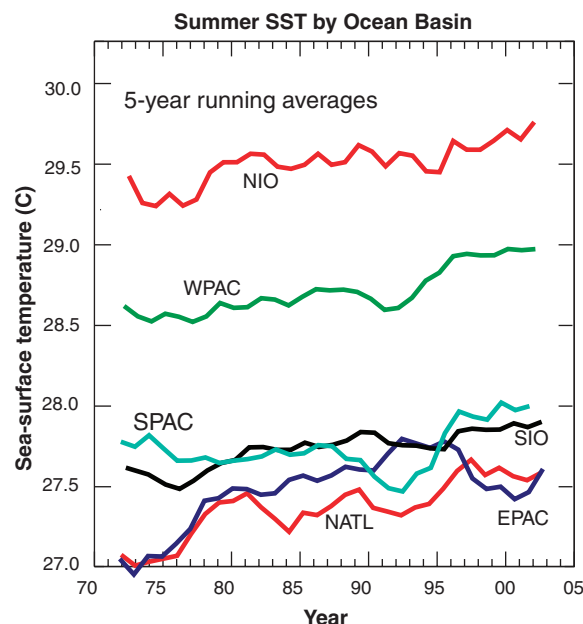


**Fig. 1.** Running 5-year mean of SST during the respective hurricane seasons for the principal ocean basins in which hurricanes occur: the North Atlantic Ocean (NATL: 90° to 20°E, 5° to 25°N, June–October), the Western Pacific Ocean (WPAC: 120° to 180°E, 5° to 20°N, May–December), the East Pacific Ocean (EPAC: 90° to 120°W, 5° to 20°N, June–October), the Southwest Pacific Ocean (SPAC: 155° to 180°E, 5° to 20°S, December–April), the North Indian Ocean (NIO: 55° to 90°E, 5° to 20°N, April–May and September–November), and the South Indian Ocean (SIO: 50° to 115°E, 5° to 20°S, November–April).

<sup>1</sup>School of Earth and Atmospheric Sciences, Georgia Institute of Technology, Atlanta, GA 30332, USA. <sup>2</sup>National Center for Atmospheric Research, Boulder, CO, USA.

of the Joint Typhoon Warning Center and of international warning centers, including special compilations and quality control (22).

Tropical cyclonic systems attaining surface wind speeds between 18 and 33 m s<sup>-1</sup> are referred to as tropical storms. Although storms of intensity >33 m s<sup>-1</sup> have different regional names, we will refer to these storms as hurricanes for simplicity. Hurricanes in categories 1 to 5, according to the Saffir-Simpson scale (23), are defined as storms with wind speeds of 33 to 43 m s<sup>-1</sup>, 43 to 50 m s<sup>-1</sup>, 50 to 56 m s<sup>-1</sup>, 56 to 67 m s<sup>-1</sup>, and >67 m s<sup>-1</sup>, respectively. We define the ocean basins that support tropical cyclone development as follows: North Atlantic (90° to 20°W, 5° to

25°N), western North Pacific (120° to 180°E, 5° to 20°N), eastern North Pacific (90° to 120°W, 5° to 20°N), South Indian (50° to 115°E, 5°-20°S), North Indian (55° to 90°E, 5°-20°N), and Southwest Pacific (155° to 180°E, 5° to 20°S). Within these basins, total tropical storm days are defined as the total number of days of systems that only reached tropical storm intensity. Total hurricane days refer to systems that attained hurricane status, including the period when a system was at tropical storm intensity. Total tropical cyclone number or days refers to the sum of the statistics for both tropical storms and hurricanes.

Figure 2 shows the time series for the global number of tropical cyclones and the number

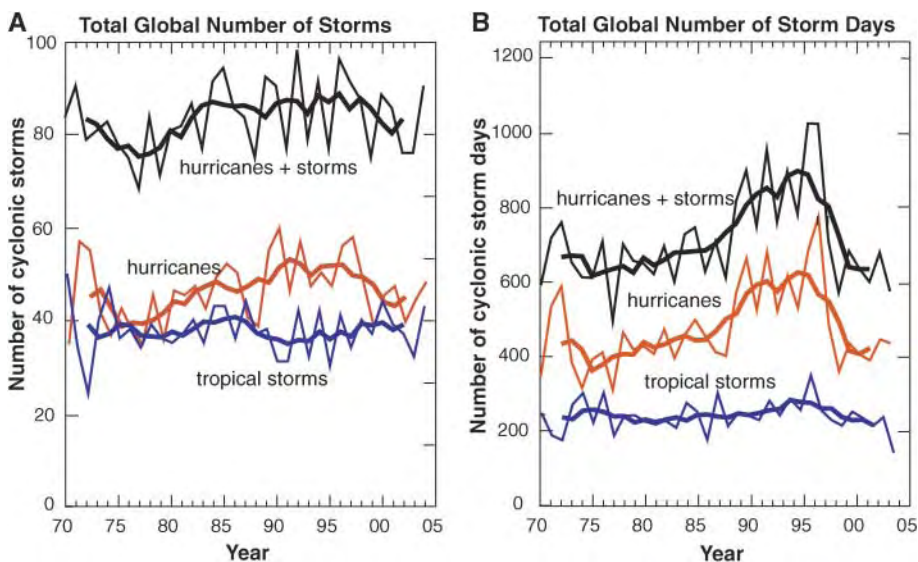
of cyclone days for the period 1970–2004, for hurricanes, tropical storms, and all cyclonic storms. None of these time series shows a trend that is statistically different from zero over the period (24). However, there is a substantial decadal-scale oscillation that is especially evident in the number of tropical cyclone days. For example, globally, the annual number of tropical cyclone days reached a peak of 870 days around 1995, decreasing by 25% to 600 days by 2003.

Figure 3 shows that in each ocean basin time series, the annual frequency and duration of hurricanes exhibit the same temporal characteristics as the global time series (Fig. 2), with overall trends for the 35-year period that are not statistically different from zero. The exception is the North Atlantic Ocean, which possesses an increasing trend in frequency and duration that is significant at the 99% confidence level. The observation that increases in North Atlantic hurricane characteristics have occurred simultaneously with a statistically significant positive trend in SST has led to the speculation that the changes in both fields are the result of global warming (3).

It is instructive to analyze the relationship between the covariability of SST and hurricane characteristics in two other ocean basins, specifically the eastern and western North Pacific. Decadal variability is particularly evident in the eastern Pacific, where a maximum in the number of storms and the number of storm days in the mid-1980s (19 storms and 150 storm days) has been followed by a general decrease up to the present (15 storms and 100 storm days). This decrease accompanied a rising SST until the 1990–1994 pentad, followed by an SST decrease until the present. In the western North Pacific, where SSTs have risen steadily through the observation period, the number of storms and the number of storm days reach maxima in the mid-1990s before decreasing dramatically over the subsequent 15 years. The greatest change occurs in the number of cyclone days, decreasing by 40% from 1995 to 2003.

In summary, careful analysis of global hurricane data shows that, against a background of increasing SST, no global trend has yet emerged in the number of tropical storms and hurricanes. Only one region, the North Atlantic, shows a statistically significant increase, which commenced in 1995. However, a simple attribution of the increase in numbers of storms to a warming SST environment is not supported, because of the lack of a comparable correlation in other ocean basins where SST is also increasing. The observation that increases in North Atlantic hurricane characteristics have occurred simultaneously with a statistically significant positive trend in SST has led to the speculation that the changes in both fields are the result of global warming (3).

Examination of hurricane intensity (Fig. 4) shows a substantial change in the intensity distribution of hurricanes globally. The number of category 1 hurricanes has remained approxi-



**Fig. 2.** Global time series for 1970–2004 of (A) number of storms and (B) number of storm days for tropical cyclones (hurricanes plus tropical storms; black curves), hurricanes (red curves), and tropical storms (blue curves). Contours indicate the year-by-year variability, and the bold curves show the 5-year running average.

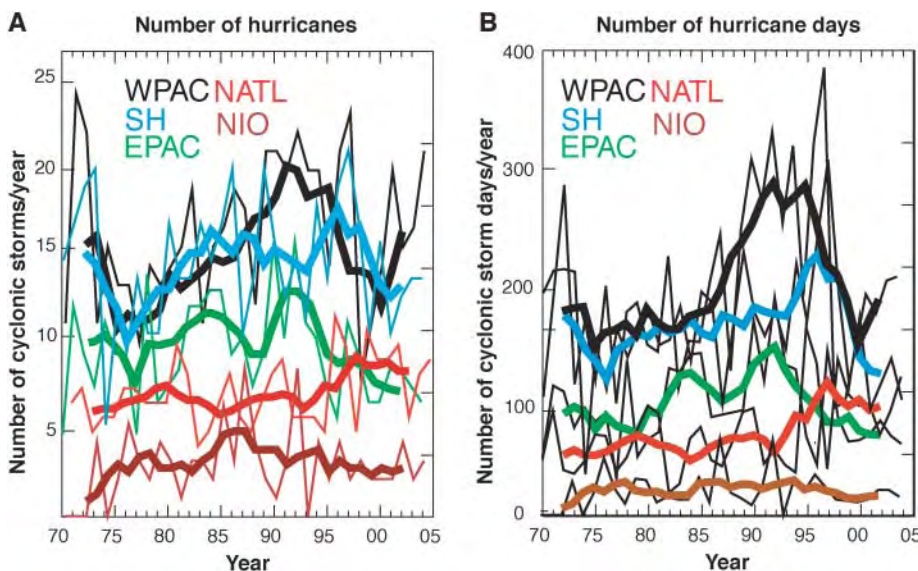


**Fig. 3.** Regional time series for 1970–2004 for the NATL, WPAC, EPAC, NIO, and Southern Hemisphere (SH plus SPAC) for (A) total number of hurricanes and (B) total number of hurricane days. Thin lines indicate the year-by-year statistics. Heavy lines show the 5-year running averages.

mately constant (Fig. 4A) but has decreased monotonically as a percentage of the total number of hurricanes throughout the 35-year period (Fig. 4B). The trend of the sum of hurricane categories 2 and 3 is small also both in number and percentage. In contrast, hurricanes in the strongest categories (4 + 5) have almost doubled in number (50 per pentad in the 1970s to near 90 per pentad during the past decade) and in proportion (from around 20% to around 35% during the same period). These changes occur in all of the ocean basins. A summary of the number and percent of storms by category is given in Table 1, binned for the years 1975–1989 and 1990–2004. This increase in category 4 and 5 hurricanes has not been accompanied by an increase in the actual intensity of the most intense hurricanes: The maximum intensity has remained remarkably static over the past 35 years (solid black curve, Fig. 4A).

Cyclone intensities around the world are estimated by pattern recognition of satellite features based on the Dvorak scheme (25). The exceptions are the North Atlantic, where there has been continuous aircraft reconnaissance; the eastern North Pacific, which has occasional aircraft reconnaissance; and the western North

Pacific, which had aircraft reconnaissance up to the mid-1980s. There have been substantial changes in the manner in which the Dvorak technique has been applied (26). These changes may lead to a trend toward more intense cyclones, but in terms of central pressure (27) and not in terms of maximum winds that are used here. Furthermore, the consistent trends in the North Atlantic and eastern North Pacific, where the Dvorak scheme has been calibrated against aircraft penetrations, give credence to the trends noted here as being independent of the observational and analysis techniques used. In addition, in the Southern Hemisphere and the North Indian Ocean basins, where only satellite data have been used to determine intensity throughout the data period, the same trends are apparent as in the Northern Hemisphere regions.

We deliberately limited this study to the satellite era because of the known biases before this period (28), which means that a comprehensive analysis of longer-period oscillations and trends has not been attempted. There is evidence of a minimum of intense cyclones occurring in the 1970s (11), which could indicate that our observed trend toward more intense cyclones is a reflection of a long-period oscillation. How-

ever, the sustained increase over a period of 30 years in the proportion of category 4 and 5 hurricanes indicates that the related oscillation would have to be on a period substantially longer than that observed in previous studies.

We conclude that global data indicate a 30-year trend toward more frequent and intense hurricanes, corroborated by the results of the recent regional assessment (29). This trend is not inconsistent with recent climate model simulations that a doubling of CO<sub>2</sub> may increase the frequency of the most intense cyclones (18, 30), although attribution of the 30-year trends to global warming would require a longer global data record and, especially, a deeper understanding of the role of hurricanes in the general circulation of the atmosphere and ocean, even in the present climate state.

References and Notes

1. S. B. Goldenberg, C. W. Landsea, A. M. Maestas-Nunez, W. M. Gray, *Science* **293**, 474 (2001).
2. J. B. Elsner, B. Kocher, *Geophys. Res. Lett.* **27**, 129 (2000).
3. K. E. Trenberth, *Science* **308**, 1753 (2005).
4. K. E. Trenberth et al., *Bull. Am. Meteorol. Soc.* **84**, 1205 (2003).
5. R. A. Pielke Jr. et al., *Bull. Am. Meteorol. Soc.*, in press (available at [http://sciencepolicy.colorado.edu/admin/publication\\_files/resource-1762-hurricanes%20and\\_global\\_warming.pdf](http://sciencepolicy.colorado.edu/admin/publication_files/resource-1762-hurricanes%20and_global_warming.pdf)).
6. J. Lighthill et al., *Bull. Am. Meteorol. Soc.* **75**, 2147 (1994).
7. W. M. Gray, *Mon. Weather Rev.* **96**, 669 (1968).
8. K. A. Emanuel, *Nature* **326**, 483 (1987).
9. G. J. Holland, *J. Atmos. Sci.* **54**, 2519 (1997).
10. M. A. Lander, C. P. Guard, *Mon. Weather Rev.* **126**, 1163 (1998).
11. C. W. Landsea, R. A. Pielke Jr., A. M. Maestas-Nunez, J. A. Knaff, *Clim. Change* **42**, 89 (1999).
12. J. C. L. Chan, K. S. Liu, *J. Clim.* **17**, 4590 (2004).
13. W. M. Gray, *Mon. Weather Rev.* **112**, 1649 (1984).
14. C. K. Folland, D. E. Parker, A. Colman, R. Washington, in *Beyond El Nino: Decadal and Interdecadal Climate Variability*, A. Navarra, Ed. (Springer-Verlag, Berlin, 1999), pp. 73–102.
15. L. J. Shapiro, S. B. Goldenberg, *J. Clim.* **11**, 578 (1998).
16. H. G. Houghton et al., *Climate Change—2001: The Scientific Basis* (Cambridge Univ. Press, Cambridge, 2001).
17. A. Henderson-Sellers et al., *Bull. Am. Meteorol. Soc.* **79**, 19 (1998).
18. T. R. Knutson, R. E. Tuleya, *J. Clim.* **17**, 3477 (2004).
19. J. F. Royer, F. Chauvin, B. Timbal, P. Araspin, D. Grimal, *Clim. Dyn.* **38**, 307 (1998).
20. M. Sugi, A. Noda, N. Sato, *J. Meteorol. Soc. Jpn.* **80**, 249 (2002).
21. P. Agudelo, J. A. Curry, *Geophys. Res. Lett.* **31**, Art. No. L22207 (2004).
22. C. J. Neumann, in *Global Guide to Tropical Cyclone Forecasting*, G. J. Holland, Ed. (WMO/TD-560, World Meteorological Organization, Geneva, Switzerland, 1993), chap. 1.
23. See [www.aoml.noaa.gov/general/lib/laescae.html](http://www.aoml.noaa.gov/general/lib/laescae.html) for a description of the Saffir-Simpson scale.
24. R. M. Hirsche, J. R. Slack, R. Smith, *Water Resource Res.* **18**, 107 (1982).
25. V. F. Dvorak, *Mon. Weather Rev.* **103**, 420 (1975).
26. C. S. Velden, T. L. Olander, R. M. Zehr, *Weather and Forecasting* **13**, 172 (1998).
27. J. P. Kossin, C. S. Velden, *Mon. Weather Rev.* **132**, 165 (2004).
28. G. J. Holland, *Aust. Meteorol. Mag.* **29**, 169 (1981).
29. K. Emanuel, *Nature* **436**, 686 (2005).
30. See [www.prime-intl.co.jp/kyosei-2nd/PDF/24/11\\_murakami.pdf](http://www.prime-intl.co.jp/kyosei-2nd/PDF/24/11_murakami.pdf).
31. This research was supported by the Climate Dynamics Division of NSF under award NSF-ATM 0328842 and by the National Center for Atmospheric Research, which is funded by NSF.

22 June 2005; accepted 18 August 2005  
10.1126/science.1116448

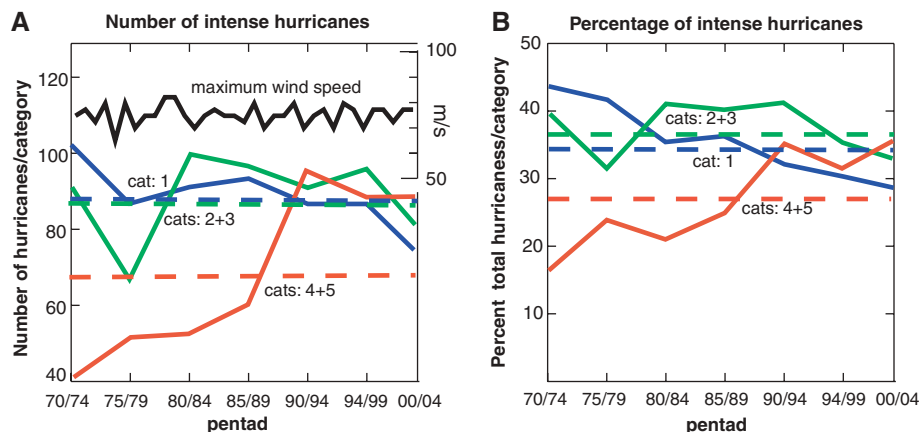


**Fig. 4.** Intensity of hurricanes according to the Saffir-Simpson scale (categories 1 to 5). (A) The total number of category 1 storms (blue curve), the sum of categories 2 and 3 (green), and the sum of categories 4 and 5 (red) in 5-year periods. The bold curve is the maximum hurricane wind speed observed globally (measured in meters per second). The horizontal dashed lines show the 1970–2004 average numbers in each category. (B) Same as (A), except for the percent of the total number of hurricanes in each category class. Dashed lines show average percentages in each category over the 1970–2004 period.

**Table 1.** Change in the number and percentage of hurricanes in categories 4 and 5 for the 15-year periods 1975–1989 and 1990–2004 for the different ocean basins.

Basin	Period			
	1975–1989		1990–2004	
	Number	Percentage	Number	Percentage
East Pacific Ocean	36	25	49	35
West Pacific Ocean	85	25	116	41
North Atlantic	16	20	25	25
Southwestern Pacific	10	12	22	28
North Indian	1	8	7	25
South Indian	23	18	50	34

# The Origin of Planetary Impactors in the Inner Solar System

Robert G. Strom,<sup>1</sup> Renu Malhotra,<sup>1\*</sup> Takashi Ito,<sup>2</sup>  
Fumi Yoshida,<sup>2</sup> David A. Kring<sup>1</sup>

Insights into the history of the inner solar system can be derived from the impact cratering record of the Moon, Mars, Venus, and Mercury and from the size distributions of asteroid populations. Old craters from a unique period of heavy bombardment that ended  $\sim 3.8$  billion years ago were made by asteroids that were dynamically ejected from the main asteroid belt, possibly due to the orbital migration of the giant planets. The impactors of the past  $\sim 3.8$  billion years have a size distribution quite different from that of the main belt asteroids but very similar to that of near-Earth asteroids.

The Moon and all the terrestrial planets were resurfaced during a period of intense impact cratering that occurred between the time of their accretion,  $\sim 4.5$  billion years ago (Ga), and  $\sim 3.85$  Ga. The lunar cratering record and the radiometrically dated Apollo samples have shown that the intense bombardment of the Moon ended at  $\sim 3.85$  Ga; the impact flux since that time has been at least an order of magnitude smaller. The 3.85-Ga epoch might represent the final end of an era of steadily declining large impacts (the tail end of the accretion of the planets). However, it has also been argued that only a sudden injection of impacting objects into the terrestrial planet zone could account for the abrupt end of the intense bombardment; thus, this event has been named the Late Heavy Bombardment (LHB), or sometimes the Lunar Cataclysm, to distinguish it from the prior final accretion of the planets at 4.5 Ga. Specifically, the lunar cataclysm hypothesis (1–3) postulates that the intense bombardment of the Moon lasted only a very short period of time, 20 to 200 million years (My) (2–6). Recent results on the impact ages of lunar meteorites (which represent a much broader region of the lunar surface than the Apollo samples) support this hypothesis (7–9). Furthermore, the impact-reset ages of meteoritic samples of asteroids (10, 11) and the metamorphosing by impact shock effects at 3.92 Ga of the only known sample of the heavily cratered highlands of Mars, meteorite Allan Hills 84001 (12), indicate that the LHB affected the entire inner solar system, not just the Moon.

Identifying the sources of planetary impactors has proven elusive. Dynamical models invoking both geocentric and heliocentric debris and both asteroidal and cometary

reservoirs have been proposed (13), but chemical analyses of Apollo samples of impact melts point to a dominantly asteroid reservoir for the lunar cataclysm (11). Here we provide evidence that the source of the LHB impactors was the main asteroid belt and that the dynamical mechanism that caused the LHB was unique in the history of the solar system and distinct from the processes that produce the flux of objects currently hitting planetary surfaces.

We examined the crater size distributions (14) of surfaces of various ages on the Moon, Mars, and Mercury, using published data

(15, 16) supplemented by new crater counts (table S1). Of the terrestrial planets, only the Moon, Mercury, and Mars have heavily cratered surfaces. These surfaces all have complex crater size distributions (Fig. 1A). The curves for Mercury and Mars are steeper than the lunar curve at diameters less than  $\sim 40$  km, because plains formation has obliterated a fraction of the smaller craters (fig. S1). Therefore, the lunar highlands curve best represents the shape of what we shall call the Population 1 crater size distribution.

The crater curves for martian old plains east of the Tharsis region, old plains within the Hellas basin on Mars, and plains within and surrounding the Caloris basin on Mercury have the same shape as the lunar highland curve over the same diameter range but with a lower crater density (17). The lower crater densities imply that these older plains probably formed near the tail end of the LHB,  $\sim 3.8$  Ga. For the younger surfaces, the crater size distribution curves are flat and distinctly different (Fig. 1B). These include the lightly cratered (and hence younger) plains on Mars and the Moon, as well as fresh craters with well-defined ejecta blankets (Class 1 craters) on the Moon. This crater population we call Population 2.

The crater density on Venus (Fig. 2) is about an order of magnitude less than on Mars. Only young craters are present, evi-

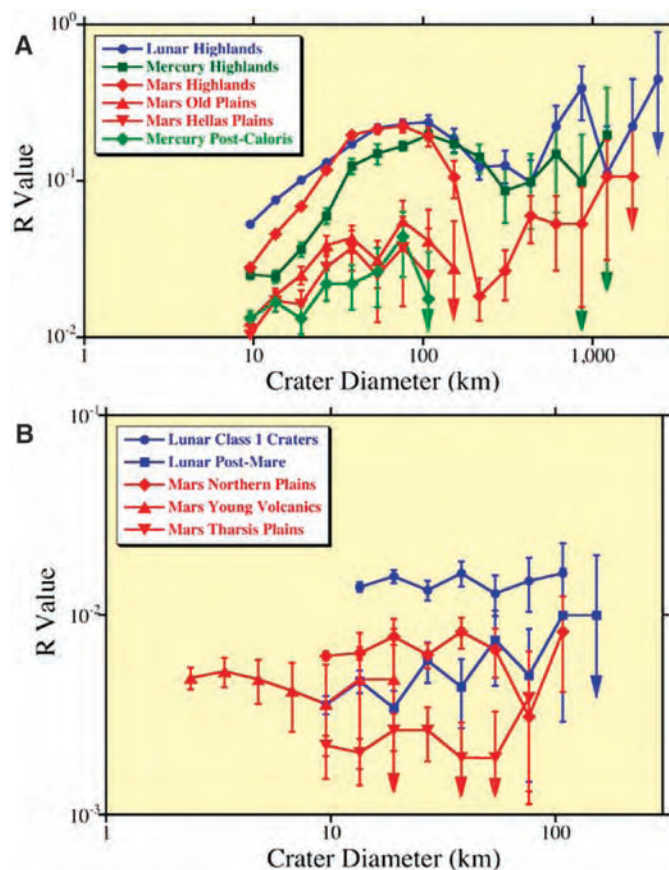


**Fig. 1.** The crater size distributions on the Moon, Mars, and Mercury, shown as R plots (14). (A) The curves for heavily cratered surfaces on the Moon (blue), Mars (red), and Mercury (green). (B) The curves for younger surfaces on the Moon (blue) and Mars (red). The size distributions on younger surfaces (Population 2) are different from those for the old surfaces that represent the LHB (Population 1). The arrowheads represent lower limits of errors that are below the abscissa.

<sup>1</sup>Lunar and Planetary Laboratory, University of Arizona, Tucson, AZ 85721, USA. <sup>2</sup>National Astronomical Observatory, Osawa, Mitaka, Tokyo 181-8588, Japan.

\*To whom correspondence should be addressed. E-mail: renu@lpl.arizona.edu

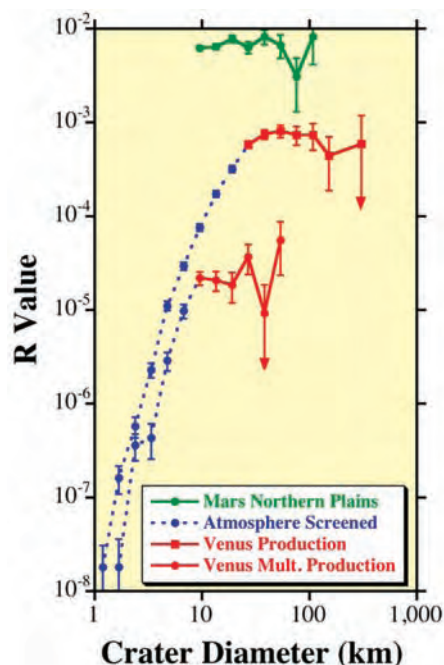


**Fig. 2.** Size distributions of all Venus craters and, separately, multiple craters, compared to craters on the Mars Northern Plains (green). The downturn in the Venus curves (dotted blue lines) is due to atmospheric screening of projectiles. The unscreened portions (red) are the same as Population 2 on Mars.

ently because older craters have been erased by multiple global resurfacing events (18). Furthermore, small craters are scarce on Venus because its thick atmosphere screens out small impactors (19). Part of the Venus crater population consists of clusters of craters (multiples) that result from fragmentation of the impacting object in the dense atmosphere. These comprise 16% of all Venus craters (table S1). The size distribution of these multiples is also shown in Fig. 2, where the diameter is derived from the sum of the crater areas in the cluster. The turnover of the curve for multiple craters does not occur until diameters less than 9 km; at larger diameters, the curve is flat. This, together with the much lower crater density, strongly suggests that the impacting population on Venus was the same as Population 2 on the Moon and Mars. It is also evidence that the turnover of the crater curve is indeed due to atmospheric screening.

The two characteristic shapes of the crater curves in the inner solar system are summarized in Fig. 3. We conclude that the terrestrial planets have been impacted by two populations of objects that are distinguishable by their size distributions. Population 1 is responsible for the LHB, and Population 2 is responsible for impacts since the LHB period.

A number of studies on the physics of impact cratering on solid bodies have derived projectile-crater scaling laws. We used

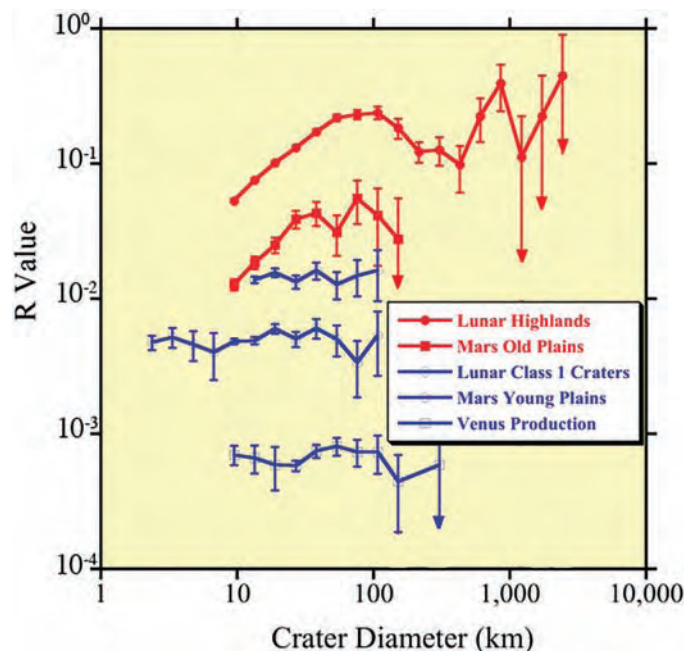


**Fig. 3.** These crater curves summarize the inner solar system cratering record, with two distinctly different size distributions. The red curves are Population 1 craters that represent the LHB period. The lower density blue curves (Population 2) represent the post-LHB era on the Moon, Mars, and Venus. The Mars young plains curve is a combination of the Mars Northern Plains and Mars young volcanics. The Venus curve is a composite of the production population for all craters greater than 9 km, including multiples in the range of 9- to 25-km diameter.

the Pi scaling law (20–22) to derive the projectile size distribution for Population 1 and Population 2 impactors. We used the lunar highland crater curves as representative of Population 1 and the martian young plains as representative of Population 2, as these provide the best statistics. (We did not include crater diameters greater than 500 km, because of scaling uncertainties.) We assumed projectile parameters appropriate for asteroidal impacts: a density of  $3 \text{ g cm}^{-3}$  (similar to basaltic rock), an impact angle of  $45^\circ$ , and impact velocities of  $17 \text{ km s}^{-1}$  and  $12 \text{ km s}^{-1}$  on the Moon and on Mars, respectively (23). We compared these distributions (Fig. 4) to recent determinations of the size distributions of the main belt asteroids (MBAs) (24–27) and near-Earth asteroids (NEAs) (28). The size distribution of the current MBAs is virtually identical to the Population 1 projectile size distribution, as pointed out by Neukum *et al.* (29). This result indicates that the objects responsible for the LHB originated from MBAs. Unless comets or Kuiper belt objects have the same size distribution, these objects could not have been major contributors to the LHB.

The close match between the current MBA size distribution and that of the LHB projectiles implies that the main asteroid belt has remained unchanged in its size distribution over the past 3.8 Gy. There are two possible interpretations of this result: Either collisional processes produced a steady-state size distribution in the main asteroid belt at least as early as 3.8 Ga, or the collision frequency in the main asteroid belt was drastically reduced around 3.8 Ga.

The mechanism responsible for ejecting asteroids from the main asteroid belt and into

terrestrial planet-crossing orbits during the LHB had to be unique to the early solar system, because there is no evidence for any event of similar magnitude in the inner planets' cratering history since then. Furthermore, that mechanism had to be one that ejected asteroids from the main belt in a size-independent manner, preserving the MBA size distribution in the inner planet impactor population. This precludes size-dependent nongravitational transport processes, such as the Yarkovsky effect, and instead implicates a dynamical process, such as sweeping gravitational resonances, that is largely insensitive to asteroid mass.

A dynamical mechanism involving the orbital migration of the giant planets is consistent with the above constraints and explains the congruence of the size distributions of the MBAs and the Population 1 projectiles. Such migration of the outer planets is thought to have occurred on a time scale of about  $10^7$  to  $10^8$  years early in solar system history (30–33), and it would have caused severe depletion of asteroids because of orbital instabilities that ensued as strong gravitational resonances swept across the asteroid belt (34). This phenomenon would have caused the Moon and terrestrial planets to be cataclysmically bombarded by asteroids and icy planetesimals (comets) for a period of 10 to 100 My (35). A recently proposed variation on the giant planet migration theory invokes the change in the eccentricities of Jupiter and Saturn, if and when these planets passed through a 1:2 orbital resonance during their orbital migration (36). Such a resonance passage would have destabilized the planetesimal disk beyond the orbits of the planets, causing a sudden massive delivery of comets to the inner solar system. In



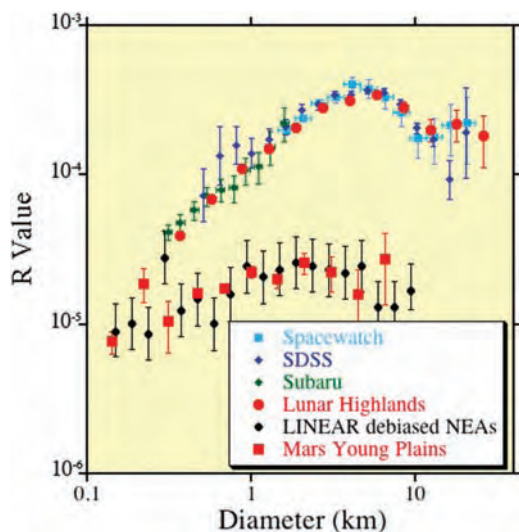


**Fig. 4.** The size distributions of the projectiles (derived from the crater size distributions), compared with those of the MBAs and NEAs. The red dots (upper curve) are for the lunar highlands (Population 1), and the red squares (lower curve) are for the Mars young plains (Population 2). The other colors and point styles are for the asteroids derived by various authors: In the upper curves, the light blue, the dark blue, and the green symbols are from Spacewatch (24), the Sloan Digital Sky Survey (25), and the Subaru asteroid surveys (26), respectively; the black dots in the lower curves are the debiased LINEAR NEAs (28). An arbitrary normalization factor was applied to obtain the R values for the asteroids. The MBA size distribution is virtually identical with Population 1 projectiles responsible for the LHB crater record. The NEA size distribution is the same as Population 2 projectiles responsible for the post-LHB crater record.

this scenario, the asteroid belt is also destabilized because of sweeping gravitational resonances; together, these cause a major spike in the intensity of cometary as well as asteroid impacts on the inner planets (37).

In either scenario, the relative intensity of comets versus asteroids in the projectile population of the LHB is not well determined by the published dynamical simulations. Because the impact signature in the crater record in the inner solar system is asteroidal, we conclude that either comets played a minor role or their impact record was erased by later-impacting asteroids.

Both of these mechanisms predict a LHB lasting between  $\sim 10$  My and  $\sim 150$  My. Therefore, the LHB was a catastrophic event that occurred from  $\sim 3.9$  Ga to 3.8 Ga. Because of this, it is not possible to use the crater record to date surfaces older than  $\sim 3.9$  Gy; the previous crater record has been obliterated by this event. The heavily cratered highlands of the Moon, Mars, and Mercury that register Population 1 impacts were resurfaced 3.9 Ga, although older rock relics may have survived.

The size distribution of Population 2 projectiles (Fig. 4) is the same as that of the NEAs and quite different from that of the LHB projectiles. Thus, NEAs are largely responsible for the cratering record after 3.8 Ga. This result is contrary to previous findings (38) that may have been based on data uncorrected for observational biases (cf. 28) and analysis, based on cumulative (rather than differential) size distributions, that was not sufficiently sensitive to the differences in the distributions.

A plausible reason that the MBAs and the NEAs have such different size distributions is the Yarkovsky effect, which causes secular changes in the orbital energy of an asteroid because of the asymmetric way a spinning asteroid absorbs and reradiates solar energy

(39). Over a few tens of millions of years, the effect is large enough to transport a substantial number of asteroids smaller than 20 km in diameter into strong Jovian resonances (40) that deliver them into terrestrial planet-crossing orbits. The magnitude of the effect depends on the size of the asteroid: For diameters greater than about 10 m, the smaller the asteroid, the larger the effect. This explains why the NEAs (Population 2 projectiles) have relatively more small objects compared to the MBAs. Because the younger post-LHB surfaces have been impacted primarily by NEAs, the ages of these surfaces can be derived from the crater production rate of NEAs. However, the ages derived from the NEA impacts will be an upper limit, because we do not know the comet crater production rate with any certainty.

Our results further imply that dating surfaces of solid bodies in the outer solar system using the inner planet cratering record is not valid. Attempts have been made to date outer planet surfaces on an absolute time scale by assuming that the crater population found in the inner solar system is the same throughout the entire solar system and has the same origin. In light of our results, this assumption is false. Additional evidence to support this conclusion is found in the cratering record of the Jovian satellites. Indeed, Callisto has a crater size distribution different from both Population 1 and Population 2 craters (41, 42).

#### References and Notes

- G. Turner, P. H. Cadogan, C. J. Yonge, *Proc. Lunar Sci. Conf.* **4**, 1889 (1973).
- F. Tera, D. A. Papanastassiou, G. J. Wasserburg, *Abstr. Lunar Planet. Sci. Conf.* **4**, 723 (1973).
- F. Tera, D. A. Papanastassiou, G. J. Wasserburg, *Earth Planet. Sci. Lett.* **22**, 1 (1974).
- G. Ryder, *Eos* **71**, 313 (1990).
- G. B. Dalrymple, G. Ryder, *J. Geophys. Res.* **98**, 13085 (1993).
- G. B. Dalrymple, G. Ryder, *J. Geophys. Res.* **101**, 26069 (1996).

- B. A. Cohen, T. D. Swindle, D. A. Kring, *Science* **290**, 1754 (2000).
- B. A. Cohen, T. D. Swindle, D. A. Kring, *Meteoritics Planet. Sci.*, in press.
- I. J. Daubar, D. A. Kring, T. D. Swindle, A. J. T. Jull, *Meteoritics Planet. Sci.* **37**, 1797 (2002).
- D. D. Bogard, *Meteoritics* **30**, 244 (1995).
- D. A. Kring, B. A. Cohen, *J. Geophys. Res.* **107**, 4-1, 2002.
- G. Turner, S. F. Knott, R. D. Ash, J. D. Gilmour, *Geochim. Cosmochim. Acta* **61**, 3835 (1997).
- W. K. Hartmann, G. Ryder, L. Dones, D. Grinspoon, in *Origin of the Earth and Moon*, R. M. Canup, K. Righter, Eds. (Univ. of Arizona Press, Tucson, AZ, 2000), pp. 493-512.
- Throughout this paper, we display the crater and projectile size distributions using the "Relative" (R) plot method (43), which was devised to better show the size distribution of craters and crater number densities for determining relative ages. The R plot provides a more sensitive and discriminating comparison tool than cumulative distribution plots, which tend to mask important details of the crater size distribution curves and can lead to erroneous interpretations. For an R plot, the size distribution is normalized to a power law differential size distribution function,  $dN(D) \sim D^p dD$ , where  $D$  is diameter and  $p = -3$ , because most crater size distributions are observed to be within  $\pm 1$  of a  $p = -3$  power law distribution. The discretized equation for R is  $R = D^3 N / A(b_2 - b_1)$ , where  $D$  is the geometric mean diameter of the size bin ( $\sqrt{b_1 b_2}$ ),  $N$  is the number of craters in the size bin,  $A$  is the area over which the counts were made, and  $b_1$  and  $b_2$  are the lower and upper limit of the size bin, respectively. The size bins are usually defined in  $\sqrt{2}$  because there are many more small craters than large craters. In an R plot,  $\log R$  is plotted on the y axis and  $\log D$  is plotted on the x axis. A  $p = -3$  distribution plots as a horizontal straight line; a  $p = -2$  distribution slopes down to the left at an angle of  $45^\circ$ , and a  $p = -4$  distribution slopes down to the right at  $45^\circ$ . The vertical position of the line is a measure of crater density; the higher the vertical position, the higher the crater density.
- R. G. Strom, G. Neukum, in *Mercury*, F. Vilas, C. R. Chapman, M. S. Matthews, Eds. (Univ. of Arizona Press, Tucson, AZ, 1988), pp. 363-373.
- R. G. Strom, S. K. Croft, N. G. Barlow, in *Mars*, H. H. Kieffer et al., Eds. (Univ. of Arizona Press, Tucson, AZ, 1992), pp. 383-423.
- This also demonstrates that the shape of the lunar highlands curve has not been affected by crater saturation. The curves for the old plains of Mars and Mercury show the same size distribution as the lunar highlands, but their crater densities are well below saturation density. This confirms a theoretical result that a surface impacted by a population with the same size distribution as the one observed for the highlands would maintain the same shape at saturation (44).
- R. G. Strom, G. G. Schaber, D. D. Dawson, *J. Geophys. Res.* **99**, 10899 (1994).
- K. J. Zahnle, *J. Geophys. Res.* **97**, 10243 (1992).
- R. M. Schmidt, K. R. Housen, *Int. J. Impact Eng.* **5**, 543 (1987).
- S. K. Croft, *J. Geophys. Res.* **90**, 828 (1985).
- H. J. Melosh, *Impact Cratering: A Geologic Process* (Oxford Univ. Press, New York, 1989).
- Asteroid impact velocities on the Moon have a root-mean-square value of  $\sim 16$  km  $s^{-1}$  (45); this does not include the Moon's orbital velocity around Earth. We adopted 17 km  $s^{-1}$  as the lunar impact velocity and a lower value, 12 km  $s^{-1}$ , for Mars (in proportion to the lower heliocentric velocity of that planet).
- R. Jedicke, T. S. Metcalfe, *Icarus* **131**, 245 (1998).
- Z. Ivezić et al., *Astron. J.* **122**, 2749 (2001).
- F. Yoshida et al., *Publ. Astron. Soc. Jpn.* **55**, 701 (2003).
- F. Yoshida et al., in preparation.
- J. S. Stuart, R. P. Binzel, *Icarus* **170**, 295 (2004).
- G. Neukum, B. A. Ivanov, W. K. Hartmann, *Space Sci. Rev.* **96**, 55 (2001).
- R. Malhotra, *Nature* **365**, 819 (1993).
- R. Malhotra, *Astron. J.* **110**, 420 (1995).
- J. A. Fernandez, W. H. Ip, *Icarus* **58**, 109 (1984).

33. J. M. Hahn, R. Malhotra, *Astron. J.* **117**, 3041 (1999).  
 34. J. Liou, R. Malhotra, *Science* **275**, 374 (1997).  
 35. H. F. Levison et al., *Icarus* **151**, 286 (2001).  
 36. K. Tsiganis, R. Gomes, A. Morbidelli, H. G. Levison, *Nature* **435**, 459 (2005).  
 37. R. Gomes, H. F. Levison, K. Tsiganis, A. Morbidelli, *Nature* **435**, 466 (2005).  
 38. S. C. Werner, A. W. Harris, G. Neukum, B. A. Ivanov, *Icarus* **156**, 287 (2002).  
 39. A. Morbidelli, D. Vokrouhlický, *Icarus* **163**, 120 (2003).  
 40. P. Farinella, D. Vokrouhlický, *Science* **283**, 1507 (1999).  
 41. R. G. Strom, A. Woronow, M. Gurnis, *J. Geophys. Res.* **86**, 8659 (1981).  
 42. P. M. Schenk, C. R. Chapman, K. Zahnle, J. M. Moore, in *Jupiter: The Planet, Satellites and Magnetosphere*, F. Bagenal, T. E. Dowling, W. B. McKinnon, Eds. (Cambridge Univ. Press, Cambridge, 2004), pp. 427–456.  
 43. Crater Analysis Techniques Working Group, *Icarus* **37**, 467 (1979).  
 44. A. Woronow, *J. Geophys. Res.* **82**, 2447 (1977).  
 45. C. F. Chyba, *Icarus* **92**, 217 (1991).  
 46. We acknowledge research support from NASA, Nation-

al Astronomical Observatory of Japan, and the Japan Society for the Promotion of Science.

#### Supporting Online Material

www.sciencemag.org/cgi/content/full/309/5742/1847/DC1

Fig. S1  
Tables S1 to S4

13 April 2005; accepted 17 August 2005  
10.1126/science.1113544

# Parallel Patterns of Evolution in the Genomes and Transcriptomes of Humans and Chimpanzees

Philipp Khaitovich,<sup>1\*</sup> Ines Hellmann,<sup>1\*</sup> Wolfgang Enard,<sup>1\*</sup>  
 Katja Nowick,<sup>1</sup> Marcus Leinweber,<sup>1</sup> Henriette Franz,<sup>1</sup>  
 Gunter Weiss,<sup>2</sup> Michael Lachmann,<sup>1</sup> Svante Pääbo<sup>1†</sup>

The determination of the chimpanzee genome sequence provides a means to study both structural and functional aspects of the evolution of the human genome. Here we compare humans and chimpanzees with respect to differences in expression levels and protein-coding sequences for genes active in brain, heart, liver, kidney, and testis. We find that the patterns of differences in gene expression and gene sequences are markedly similar. In particular, there is a gradation of selective constraints among the tissues so that the brain shows the least differences between the species whereas liver shows the most. Furthermore, expression levels as well as amino acid sequences of genes active in more tissues have diverged less between the species than have genes active in fewer tissues. In general, these patterns are consistent with a model of neutral evolution with negative selection. However, for X-chromosomal genes expressed in testis, patterns suggestive of positive selection on sequence changes as well as expression changes are seen. Furthermore, although genes expressed in the brain have changed less than have genes expressed in other tissues, in agreement with previous work we find that genes active in brain have accumulated more changes on the human than on the chimpanzee lineage.

In some behavioral and cognitive traits, humans have changed dramatically since their evolutionary divergence from a common ancestor shared with chimpanzees (1, 2). It seems reasonable to assume that a number of these changes were driven by positive Darwinian selection. However, although positive selection has been demonstrated for several human genes (3–5), the overall patterns of evolution of chimpanzee and human genes are consistent with selective neutrality (6). It has long been argued that changes in gene expression may provide an additional and crucial perspective on the evolutionary differences between humans and chimpanzees (7), but relevant data to address this issue have only recently started to become available (8). On a more general level, data from yeast, fruit flies,

humans, and mice have been used to argue that regulatory evolution and protein evolution act independently of each other and thus that they are “decoupled” (9, 10). However, other results seem to contradict this assertion (11–14). The chimpanzee and human genome sequences now provide the opportunity to address these questions by studying the evolution of gene expression, as well as of the DNA sequences of the genes expressed in various tissues in two closely related mammals. To this end, we have measured gene expression in five different tissues in six humans and five chimpanzees. We find that gene sequences and gene expression evolve in qualitatively similar manners, suggesting that the evolutionary forces that act on them are similar in effect and nature. Through analyses of evolutionary patterns at both levels, it is possible to identify groups of genes that violate neutral expectations and may have been positively selected.

Using probes on Affymetrix *UI33plus2* arrays that target sequences that are identical between the human and the chimpanzee ge-

nomes (15), we analyzed the expression for 51,460 probe sets (~21,000 genes) in heart, kidney, liver, testis, and prefrontal cortex of the brain from six humans and five chimpanzees (table S1). In each tissue, we measured the extent of differences in gene expression between and within species as an average squared difference in normalized expression across all probe sets with detectable gene expression (table S2). Figure 1 schematically illustrates the results. Two major findings stand out. First, gene expression patterns differ less between humans and chimpanzees in the brain than in the other tissues (bootstrap test,  $P < 0.0001$ ). Second, the ratio of expression divergence between species to diversity within species is higher in testis than in any other tissue (5.6 versus 1.8 to 2.5,  $P < 0.0001$ ). Consequently, 32% of the probe sets detected in testis show significant expression differences between humans and chimpanzees, whereas ~8% do so in brain, heart, kidney, and liver (fig. S1). It is conceivable that the patterns of transcriptome divergence and diversity observed among the five tissues are mainly due to differences between tissue-specific genes, i.e., those expressed in one single tissue. Alternatively, the patterns could be due to differences also in genes that are expressed in several tissues. To distinguish between these two alternatives, we analyzed probe sets detected in all five tissues, and probe sets specific to one tissue, separately. We find that both groups of genes show similar patterns of evolution (fig. S2). In particular, brain shows fewer differences than other tissues and testis shows an excess of divergence relative to diversity (table S3). Thus, the different expression patterns observed among tissues are due to effects that a tissue exerts not only on genes expressed in that tissue but also on genes expressed in that as well as in many other tissues. A further noteworthy finding is that ubiquitously expressed genes differ less among individuals within a species as well as between species than do genes expressed in single tissues (table S3; fig. S2).

Next, we analyzed the evolution of protein-coding DNA sequences of genes for which expression was detected in at least one tissue (15). As an estimate of the protein divergence of each gene, we used the number of non-synonymous nucleotide substitutions per non-synonymous site ( $K_a$ ), normalized to the number of substitutions per site in inter-

<sup>1</sup>Max Planck Institute for Evolutionary Anthropology, Deutscher Platz 6, D-04103 Leipzig, Germany. <sup>2</sup>WE Informatik, Bioinformatik, University of Düsseldorf, Universitätsstrasse 1, D-40225 Düsseldorf, Germany.

\*These authors contributed equally to this work.

†To whom correspondence should be addressed.  
E-mail: paabo@eva.mpg.de

scattered repeats in a 250-kbp window around the center of each gene (Ki) (6, 15). In general, low Ka/Ki ratios indicate stronger purifying selection acting on amino acid substitutions, whereas higher ratios indicate fewer constraints or possibly an enrichment of amino acid substitutions by positive selection [for a review, see (16)]. In agreement with previous work (17–20), we find that brain-specific genes show Ka/Ki ratios that are significantly lower than those of other tissue-specific genes (Mann-Whitney U-test,  $P < 10^{-6}$ ) (Fig. 2A) and that ubiquitously expressed genes show lower Ka/Ki ratios than genes expressed in single tissues (Mann-Whitney U-test,  $P < 10^{-6}$ ) (table S4).

When the divergence of gene expression is similarly analyzed with respect to tissues (Fig. 2B), the results show that for both sequence and expression divergence, brain shows the least differences and liver the most, with testis, heart, and kidney at intermediate levels. Consequently, the higher the expression divergence in a tissue, the higher the protein divergence (Pearson's  $r = 0.94$ ,  $P < 0.05$ ) (Fig. 2C). Parallel patterns can also be seen with respect to the breadth of expression, i.e., the number of tissues in which a gene is expressed. Genes expressed in only one tissue show the highest expression and sequence divergence, and genes expressed in all five tissues the lowest divergence. This parallelism between expression divergence and protein divergence is also seen when analyzed on a gene-by-gene basis ( $R^2 = 0.0011$ ,  $P < 10^{-6}$ ), implying that similar factors influence protein and expression divergence. Two such factors are the tissues in which a gene is expressed and its expression breadth. Both factors influence expression divergence (multiway analysis of variance  $R^2 = 0.075$ ,  $P < 10^{-6}$ ) and protein divergence ( $R^2 = 0.071$ ,  $P <$

$10^{-6}$ ). If we correct for the influence of these factors, the relation between expression and protein divergence becomes much weaker but remains significant ( $R^2 = 0.00019$ ,  $P < 0.05$ ). This is not surprising, given that we do not consider other factors that may affect both expression and sequence divergence, such as protein-protein interactions (21, 22). The weak relation between expression and sequence divergence is likely due to the inherently large measurement errors of expression data. In addition, it may indicate that some evolutionary forces affect gene expression and protein divergence differentially.

We also analyzed the relation between expression divergence and sequence divergence in putative core promoters (Kp), defined as a 1500-bp region upstream and  $\leq 500$ -bp region downstream of the transcriptional start (15). Kp as well as the ratio Kp/Ki are significantly correlated with expression divergence ( $R^2 = 0.001$ ,  $P < 10^{-6}$  and  $R^2 = 0.0004$ ,  $P < 10^{-3}$ , respectively) (table S4). Given that genetic differences in promoters are more likely to directly cause differences in expression levels than differences in coding regions, these correlations may seem surprisingly weak. However, many or most sites in these promoter regions are likely not relevant for transcriptional activity (median Kp/Ki = 0.82 versus 0.15 for Ka/Ki) and the relevant transcription start sites might not be identified for all tissues. Much more work is necessary to elucidate the relation between the evolution of promoter sequences and expression levels.

Our analyses show that each tissue is associated with a certain level of evolutionary constraints acting on the genes expressed in it—for instance, brain imposes more constraints than liver. These constraints add up across tissues so that genes expressed in many

tissues are subject to more constraints than are genes expressed in few tissues. The signatures of these constraints are seen both at the level of DNA sequence differences and at the level of expression differences. We have recently suggested that the evolution of gene expression patterns largely conforms to the predictions of a neutral model of evolution (23), i.e., that most expression differences observed within and between species are selectively neutral or nearly neutral. Because most evolutionary

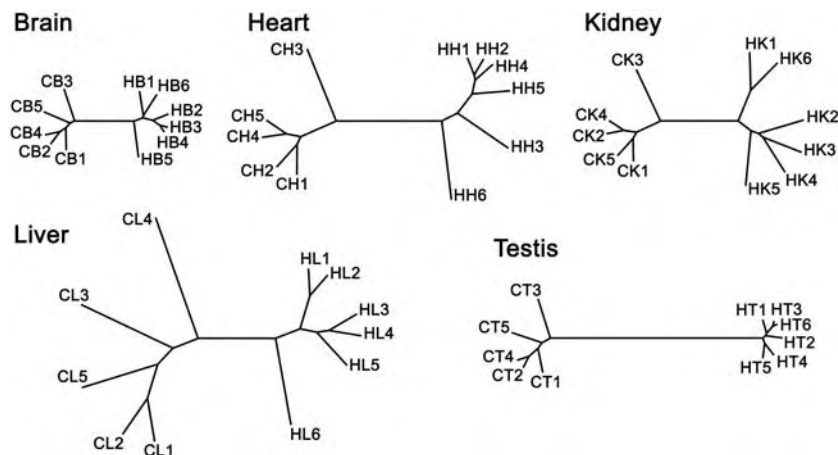


**Fig. 1.** Schematic illustration of gene expression variation among and between humans and chimpanzees in five tissues. The trees are inferred from the mean of the squared difference of expression intensities of all detected probe sets (15). Brain shows the smallest divergence and diversity. The ratio of divergence to diversity in testis is 5.6, which is significantly different from the ratio in all other tissues (table S2).

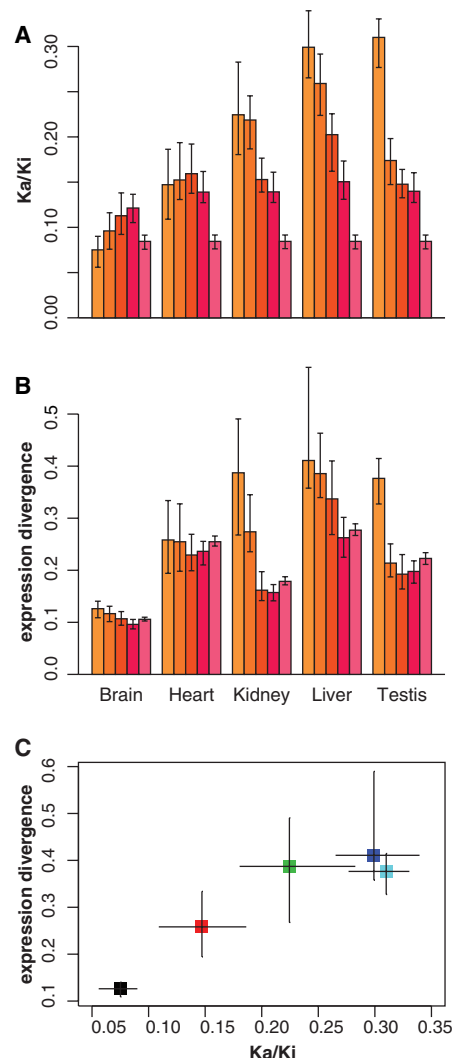


**Fig. 2.** Protein sequence and gene expression divergences between humans and chimpanzees and their correlation. (A) Median protein sequence divergence (Ka/Ki), of genes expressed in one tissue (lightest color, left) to five tissues (darkest color, right). (B) Median expression divergence of genes expressed in one tissue (lightest color, left) to five tissues (darkest color, right). (C) Correlation of expression and protein sequence divergences. Tissues [(brain (black), heart (red), kidney (green), liver (dark blue), testis (cyan))] with a high amino acid sequence divergence tend to have a high expression divergence (Pearson's  $r = 0.94$ ,  $P < 0.05$ ). All error bars in the figure represent 95% confidence intervals of the median values as calculated from 10,000 bootstrap replicates.

changes in nucleotide sequences conform to a neutral theory (24), the parallelism between sequence evolution and expression evolution observed here supports the notion that most evolutionary changes in gene expression are similarly selectively neutral or nearly neutral (23). A consequence of the neutral hypothesis is that the extent of expression differences found between species is largely determined by the time since they shared a common ancestor and the extent of negative selection in a particular tissue [see also (14)]. Our observation that brain, heart, kidney, and liver have similar ratios of expression divergence between species to diversity within species (Fig. 1, table S2) is compatible with a model in which gene expression changes are a function of time. The divergence to diversity ratios are smaller than would be expected if time were the sole factor influencing gene expression. A probable explanation for this is that experimental and environmental variation contributes proportionally more to interindividual differences than to divergence. Because deviations from neutral expectations can indicate the action of positive selection, we next attempted to identify such deviations in gene expression patterns, and—in a subsequent step—to corroborate such indications with observations at the DNA sequence level whenever suitable DNA sequence data were available.

It was recently proposed that a high ratio of gene expression divergence between species to gene expression diversity within species may indicate the action of positive selection (23, 25, 26). This is analogous to tests proposed for quantitative traits (27) and akin to tests that compare between- and within-species differences at functional sites to infer positive selection (28). However, because realistic evolutionary models for neutral expression changes are not yet available and because environmental factors have a considerable influence on gene expression diversity, a high ratio of divergence to diversity represents an indication rather than proof of positive selection. As seen above, testis differs from other organs studied in that the ratio of expression divergence to diversity is higher (Fig. 1). If the cellular composition of testicles differed between humans and chimpanzees more than it does for other tissues, this observation could be explained by only a few genetic differences between the species. However, although human and chimpanzee testicles differ in size, there is no evidence that the cellular composition of this organ differs between the species (29). Another possibility is that the genetic component of the expression diversity in testis is not lower than expected from the expression divergence, but that gene expression patterns in testis have a smaller environmental (i.e., non-genetic) component. In that case, we

would expect genes expressed in testis to be subject to as much constraint as genes expressed in tissues such as liver or heart that have a comparable expression divergence. The property of being expressed in testis should then have a similar effect on diversity levels in other tissues as the property of being expressed in, for example, liver. However, we find that among the five tissues, expression in testis is associated with the highest number of significant reductions in diversity in tissues other than testis, whereas expression in liver is associated with the highest number of significant increases of diversity in tissues other than liver (fig. S3) (15). This suggests that strong selective constraints on genes, rather than low environmental influence, account for the low extent of expression diversity in testis. Thus, the higher ratio of gene expression divergence to diversity in testis as compared with the other tissues is indeed indicative of positive selection. Unfortunately, this pattern cannot be corroborated at the DNA sequence level because human DNA sequence diversity data collected in an unbiased way are not yet available. However, we can test predictions about

the chromosomal distribution of instances of positive selection in genes active in testis. If a substantial fraction of such positively selected variants are genetically recessive, we would expect differently expressed genes to be enriched on the X chromosome, where they could exert their full effect in males (30). Therefore, we investigated if genes with expression differences between humans and chimpanzees are unevenly distributed among chromosomes. In testis, genes on the X chromosome show a significant excess of expression differences when compared to the other chromosomes (binomial test corrected for multiple testing,  $P < 10^{-5}$ ), whereas in the other tissues we find no significant differences among chromosomes (Fig. 3). To test if this pattern also exists at the DNA sequence level, we investigated the DNA sequence divergence of genes expressed in different tissues with respect to chromosomal location (fig. S4). For genes expressed in brain, heart, kidney, and liver, neither the autosomes nor the X differ from each other with respect to  $K_a/K_i$ . In contrast, among genes expressed in testis, those located on the X have significantly higher  $K_a/K_i$  ratios than those located

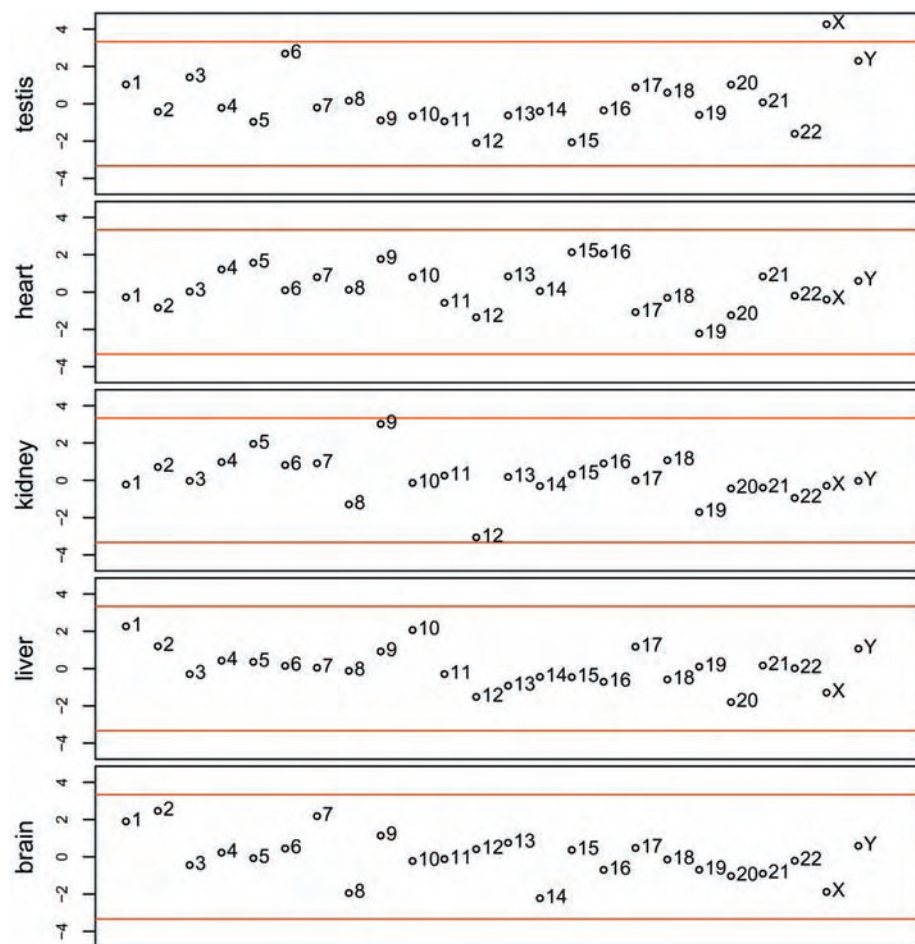


**Fig. 3.** The number of expression changes between humans and chimpanzees across chromosomes. Red lines indicate the normalized deviation that would be significant at  $P = 0.05$ , corrected for 24 tests in five tissues.

on the autosomes (Mann-Whitney U-test,  $P < 0.0005$ ) (table S5). Thus, genes expressed in testis—especially those located on the X—tend to accumulate expression changes as well as sequence changes that may have been positively selected. This is compatible with the observation that genes involved in reproduction tend to evolve under positive selection [examples in apes include (31) and (32)]. At the organismal level, this may correlate with mating strategies in different ape species (33).

Next, we examined whether differences in gene expression are equally distributed along the human and chimpanzee lineages. Because suitable data from outgroup species are lacking for most tissues, we estimated the amount of expression changes along the human and chimpanzee lineages using the observation that up-regulations of gene expression are of bigger amplitude but less numerous than are down-regulations (34). Consequently, if more gene expression changes happened on one of the two lineages, the result would be a skewed distribution of gene expression differences observed between the species [fig. S5 and (15)]. The distributions are positively and significantly skewed for brain, heart, liver, and testis (table S6), suggesting that more gene expression changes occurred on the human evolutionary lineage than on the chimpanzee lineage. In magnitude, this acceleration of gene expression change is largest in brain, and significantly larger than in any of the other tissues ( $P < 0.05$ ) except heart ( $P = 0.10$ ). This is in agreement with previous work that found a larger acceleration of gene expression changes on the human relative to the chimpanzee lineage in brain than in liver when using an orangutan as an outgroup (35–37). Thus, although gene expression is more constrained in brain than in other tissues, it has changed relatively more on the human lineage.

To investigate if such a pattern is seen also at the amino acid sequence level, we inferred how many amino acid changes occurred on the human and chimpanzee lineage, respectively, using alignments of orthologous genes from human, chimpanzee, mouse, and rat (6). For genes expressed specifically in

heart, kidney, liver, and testis, the ratios of the numbers of changes on the human and chimpanzee lineages vary between 0.79 and 1.04, whereas for all genes the ratio is 1.12 (Table 1). By contrast, for genes expressed in brain, the ratio of human-specific to chimpanzee-specific amino acid changes is 1.40, higher, though not significantly ( $P = 0.08$ ), than for genes not expressed in brain and higher than for genes expressed in any other single tissue ( $P < 0.05$ ). This finding is in agreement with recent work showing a faster evolution on the human lineage for a set of genes involved in brain function and development (38). Thus, the acceleration seen for gene expression is corroborated on the sequence level for brain but not for other tissues. Such an acceleration on the human lineage could be caused by a relaxation of selective constraints on both the structure and expression of brain proteins during human evolution. A more compelling alternative is that the acceleration is caused by positive selection that changed the functions of genes expressed in the brains of humans more than in the brains of chimpanzees. However, further work elucidating the phenotypic effect of genetic changes on the human lineage is necessary to establish this.

In summary, we find that the patterns of evolutionary change in gene expression are largely compatible with a neutral model, in which different levels of constraints acting in different tissues add up for single genes. These evolutionary constraints act in a similar manner on the coding regions of DNA sequences and thus lead to parallel patterns in expression and sequence evolution. In contrast to the overall picture of selective neutrality, two examples of putative positive selection stand out. First, testis shows an excess of expression differences between species and an enrichment of both expression and amino acid sequence differences on the X chromosome. Second, the brain, although under more constraints than the other tissues, has an excess of gene expression and amino acid changes on the human lineage compared to other tissues. This suggests that evolutionary changes at both the level of gene regulation and the level of protein sequence

have played crucial roles in the evolution of certain organ systems, such as those involved in cognition or male reproduction. Consequently, the modest number of sequence differences in genes between humans and chimpanzees cannot be taken as evidence that regulatory changes would necessarily be more important than structural protein changes during human evolution (7). Rather, both types of changes are likely to have acted in concert.

References and Notes

1. R. G. Klein, *The Human Career* (Univ. Chicago Press, Chicago, ed. 2, 1999).
2. M. Tomasello, J. Call, *Primate Cognition* (Oxford Univ. Press, Oxford, 1997).
3. E. J. Vallender, B. T. Lahn, *Hum. Mol. Genet.* **13** (Suppl. 2), R245 (2004).
4. A. G. Clark et al., *Science* **302**, 1960 (2003).
5. W. Enard, S. Paabo, *Annu. Rev. Genomics Hum. Genet.* **5**, 351 (2004).
6. The Chimpanzee Sequencing and Analysis Consortium, *Nature* **437**, 69 (2005).
7. M. C. King, A. C. Wilson, *Science* **188**, 107 (1975).
8. T. M. Preuss, M. Caceres, M. C. Oldham, D. H. Geschwind, *Nat. Rev. Genet.* **5**, 850 (2004).
9. I. K. Jordan, L. Marino-Ramirez, Y. I. Wolf, E. V. Koonin, *Mol. Biol. Evol.* **21**, 2058 (2004).
10. A. Wagner, *Proc. Natl. Acad. Sci. U.S.A.* **97**, 6579 (2000).
11. Z. Gu, D. Nicolae, H. H. Lu, W. H. Li, *Trends Genet.* **18**, 609 (2002).
12. K. D. Makova, W. H. Li, *Genome Res.* **13**, 1638 (2003).
13. S. V. Nuzhdin, M. L. Wayne, K. L. Harmon, L. M. McIntyre, *Mol. Biol. Evol.* **21**, 1308 (2004).
14. B. Lemos, B. R. Bettencourt, C. D. Meiklejohn, D. L. Hartl, *Mol. Biol. Evol.* **22**, 1345 (2005).
15. Materials and methods are available as supporting material on Science Online.
16. J. C. Fay, C. I. Wu, *Annu. Rev. Genomics Hum. Genet.* **4**, 213 (2003).
17. L. Duret, D. Mouchiroud, *Mol. Biol. Evol.* **17**, 68 (2000).
18. E. E. Winter, L. Goodstadt, C. P. Ponting, *Genome Res.* **14**, 54 (2004).
19. L. Zhang, W. H. Li, *Mol. Biol. Evol.* **21**, 236 (2004).
20. K. Kuma, N. Iwabe, T. Miyata, *Mol. Biol. Evol.* **12**, 123 (1995).
21. H. B. Fraser, A. E. Hirsh, L. M. Steinmetz, C. Schafhe, M. W. Feldman, *Science* **296**, 750 (2002).
22. B. Lemos, C. D. Meiklejohn, D. L. Hartl, *Nat. Genet.* **36**, 1059 (2004).
23. P. Khaitovich et al., *PLoS Biol.* **2**, 682 (2004).
24. M. Kimura, *The Neutral Theory of Molecular Evolution* (Cambridge Univ. Press, Cambridge, New York, 1983).
25. W. P. Hsieh, T. M. Chu, R. D. Wolfinger, G. Gibson, *Genetics* **165**, 747 (2003).
26. S. A. Rifkin, J. Kim, K. P. White, *Nat. Genet.* **33**, 138 (2003).
27. M. Turelli, J. H. Gillespie, R. Lande, *Evolution Int. J. Org. Evol.* **42**, 1085 (1988).
28. J. H. McDonald, M. Kreitman, *Nature* **351**, 652 (1991).
29. J. Wistuba et al., *Biol. Reprod.* **69**, 582 (2003).
30. B. Charlesworth, J. A. Coyne, N. H. Barton, *Am. Nat.* **130**, 113 (1987).
31. G. J. Wyckoff, W. Wang, C. I. Wu, *Nature* **403**, 304 (2000).
32. W. J. Swanson, V. D. Vacquier, *Nat. Rev. Genet.* **3**, 137 (2002).
33. A. F. Dixon, *Primate Sexuality* (Oxford Univ. Press, Oxford, 1998).
34. P. Khaitovich, S. Paabo, G. Weiss, *Genetics* **170**, 929.
35. W. Enard et al., *Science* **296**, 340 (2002).
36. J. Gu, X. Gu, *Trends Genet.* **19**, 63 (2003).
37. M. Caceres et al., *Proc. Natl. Acad. Sci. U.S.A.* **100**, 13030 (2003).
38. S. Dorus et al., *Cell* **119**, 1027 (2004).
39. We thank T. Mikkelsen of the Broad Institute and all other members of the Chimpanzee Sequencing Con-

**Table 1.** Protein evolution in tissues along lineages. From alignments for human, chimpanzee, mouse, and rat genes (6), we calculated the amino acid changes on the human and the chimpanzee lineages for tissue-specific genes. For each tissue, we used a  $\chi^2$ -test to determine if the ratio of human- to chimpanzee-specific changes is significantly different from the ratio observed for genes not expressed in that tissue but in one or more of the other tissues.

Tissue	Genes	Amino acids	Human	Chimpanzee	Ratio	P-value
Brain	201	81,316	113	81	1.40	0.077
Heart	69	25,604	37	47	0.79	0.173
Kidney	110	37,772	92	96	0.96	0.549
Liver	115	42,155	91	94	0.97	0.524
Testis	504	199,147	487	470	1.04	0.297
All genes	5268	2,120,869	3417	3051	1.12	—

sortium for sharing analysis results; C. Allen and H. McClure of the Yerkes Primate Center, Atlanta, and W. Collignon and R. Bontrop of the Biomedical Primate Research Centre, Rijswijk, for tissue samples; T. Arendt of the Paul Flechsig Institute, Leipzig, for dissections; H. B. Fraser, H. Kaessmann, L. Vigilant, and all members of our laboratory for discussion; and

the Max Planck Society and the Bundesministerium für Bildung und Forschung for financial support.

**Supporting Online Material**  
www.sciencemag.org/cgi/content/full/1108296/DC1  
Materials and Methods  
Figs. S1 to S6

Tables S1 to S8  
References and Notes

6 December 2004; accepted 6 April 2005  
Published online 1 September 2005;  
10.1126/science.1108296  
Include this information when citing this paper.

# Achieving Stability of Lipopolysaccharide-Induced NF- $\kappa$ B Activation

Markus W. Covert,\* Thomas H. Leung,\* Jahlionais E. Gaston, David Baltimore†

The activation dynamics of the transcription factor NF- $\kappa$ B exhibit damped oscillatory behavior when cells are stimulated by tumor necrosis factor- $\alpha$  (TNF $\alpha$ ) but stable behavior when stimulated by lipopolysaccharide (LPS). LPS binding to Toll-like receptor 4 (TLR4) causes activation of NF- $\kappa$ B that requires two downstream pathways, each of which when isolated exhibits damped oscillatory behavior. Computational modeling of the two TLR4-dependent signaling pathways suggests that one pathway requires a time delay to establish early anti-phase activation of NF- $\kappa$ B by the two pathways. The MyD88-independent pathway required Infeon regulatory factor 3-dependent expression of TNF $\alpha$  to activate NF- $\kappa$ B, and the time required for TNF $\alpha$  synthesis established the delay.

The transcription factor NF- $\kappa$ B regulates numerous genes that function in diverse processes, including inflammatory responses, immune system development, apoptosis, learning in the brain, and bone development (1). Aberrant NF- $\kappa$ B activity has been linked to oncogenesis, tumor progression, and resistance to chemotherapy (2). NF- $\kappa$ B has also been identified as a tumor promoter in inflammation-associated cancer (3). Understanding the specificity and temporal mechanisms that govern NF- $\kappa$ B activation may therefore be important in understanding cancer progression, and systems-based and computational approaches are being developed to address this issue (4, 5).

The activity of NF- $\kappa$ B shows damped oscillatory behavior in cells stimulated with TNF $\alpha$ . Using a computational model coordinated to molecular and biochemical techniques, we have demonstrated that the oscillations in NF- $\kappa$ B activity are largely due to negative feedback by the NF- $\kappa$ B inhibitor protein I $\kappa$ B $\alpha$  (6). Another study performed in single cells has provided further evidence for these conclusions (7).

NF- $\kappa$ B mediates cellular responses to a wide variety of stimuli other than TNF $\alpha$  (8), and we wanted to determine whether NF- $\kappa$ B activation dynamics exhibited oscillations under other stimulation conditions. We observed non-oscillatory dynamics of active NF- $\kappa$ B when cells were

stimulated with LPS (Fig. 1A). This difference in NF- $\kappa$ B activation could be linked to differences in the TNF $\alpha$  and LPS signaling pathways. Upon TNF $\alpha$  binding to the TNF receptor, the receptors aggregate and bind adaptor proteins, leading to activation of the I $\kappa$ B kinase (IKK) complex. Phosphorylation of I $\kappa$ B by IKK leads to ubiquitination and

degradation of I $\kappa$ B and allows free NF- $\kappa$ B to bind target genes. One such target is I $\kappa$ B $\alpha$ , and its production results in a negative feedback loop (9–11).

In contrast, LPS signals through TLR4. TLR4 activates two downstream pathways, each of which is thought to directly activate NF- $\kappa$ B (12–14). The MyD88-dependent pathway recruits the kinases interleukin-1 receptor-associated kinase 1 (IRAK1) and IRAK4, which phosphorylate TNF receptor-associated factor 6 (TRAF6), leading to the activation of the IKK complex. The MyD88-independent pathway leading to NF- $\kappa$ B activation is not fully understood. The pathway is dependent on the TIR domain-containing adaptor inducing interferon- $\beta$  (Trif) adaptor molecule, and Trif-related adaptor molecule (Tram), receptor-interactor protein 1 (RIP1), and RIP3 have been identified as important factors in the pathway (15–17). However, the end result of these pathways is the same as the end result of the TNF $\alpha$ -activated pathway: degradation of I $\kappa$ B, which is followed by activation of I $\kappa$ B $\alpha$  gene transcription. We monitored I $\kappa$ B $\alpha$  mRNA transcript and protein levels over a 180-min time course in LPS-stimulated wild-type cells and found that I $\kappa$ B $\alpha$  protein expression decreased and

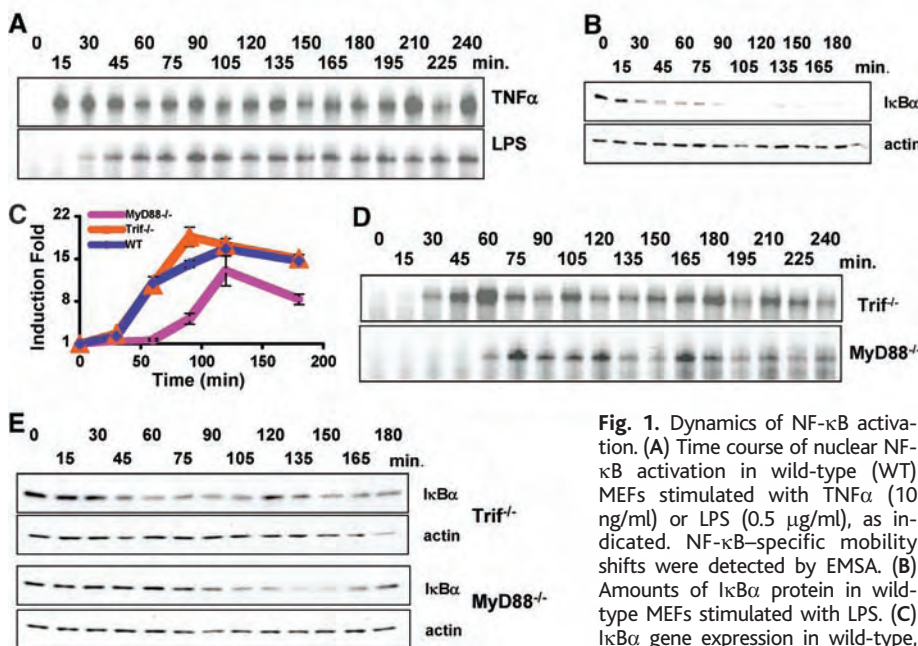


**Fig. 1.** Dynamics of NF- $\kappa$ B activation. (A) Time course of nuclear NF- $\kappa$ B activation in wild-type (WT) MEFs stimulated with TNF $\alpha$  (10 ng/ml) or LPS (0.5  $\mu$ g/ml), as indicated. NF- $\kappa$ B-specific mobility shifts were detected by EMSA. (B) Amounts of I $\kappa$ B $\alpha$  protein in wild-type MEFs stimulated with LPS. (C) I $\kappa$ B $\alpha$  gene expression in wild-type, Trif-deficient, and MyD88-deficient MEFs stimulated with LPS, determined by quantitative PCR (qPCR). Error bars show means  $\pm$  SD. (D) Time course of nuclear NF- $\kappa$ B activation in Trif-deficient and MyD88-deficient MEFs stimulated with LPS. (E) I $\kappa$ B $\alpha$  protein in Trif-deficient and MyD88-deficient MEFs stimulated with LPS. All experiments described here were repeated two or three times with a high degree of reproducibility.

Division of Biology, California Institute of Technology, Pasadena, CA 91125, USA.

\*These authors contributed equally to this work.  
†To whom correspondence should be addressed.  
E-mail: baltimo@caltech.edu

remained low, whereas mRNA expression increased and remained high (Fig. 1, B and C). Therefore, it remains puzzling that there are oscillations in NF- $\kappa$ B activity and I $\kappa$ B $\alpha$  protein expression after activation by TNF but not in cells stimulated with LPS.

NF- $\kappa$ B activation through the MyD88-dependent pathway occurs earlier than activa-

tion by the MyD88-independent pathway (16). This suggested that the non-oscillatory behavior of NF- $\kappa$ B activation through TLR4 could be due to the interaction of the two pathways. We monitored nuclear NF- $\kappa$ B activity over a 240-min time course in LPS-stimulated MyD88-deficient, Trif-deficient, and MyD88-Trif doubly deficient mouse embryo fibroblasts

(MEFs) (Fig. 1D). LPS stimulation of MEFs that contained only one TLR4 pathway resulted in an oscillatory NF- $\kappa$ B activation response. LPS-stimulated cells deficient in both MyD88 and Trif showed no NF- $\kappa$ B activation. Moreover, in comparison with wild-type and Trif-deficient cells, LPS-stimulated MyD88-deficient cells were substantially slower to reach initial peak NF- $\kappa$ B activation. Over a 180-min time course, the amount of I $\kappa$ B $\alpha$  protein decreased in LPS-stimulated Trif- and MyD88-deficient cells, and the protein was then resynthesized, further confirming the underlying oscillatory NF- $\kappa$ B activation response. The period of oscillation for NF- $\kappa$ B activation ( $\sim$ 45 min) was shorter than the period of the oscillation in I $\kappa$ B $\alpha$  abundance ( $\sim$ 90 min) (Fig. 1E).

A lag in NF- $\kappa$ B activation could occur in two ways: (i) The kinetics of the MyD88-independent pathway could simply be much slower than the kinetics of the MyD88-dependent pathway, or (ii) the MyD88-dependent and MyD88-independent pathways could display similar kinetics, in which case the initiation of the MyD88-independent pathway signaling must be delayed. We built a computational model to simulate NF- $\kappa$ B activation by TLR4 stimulation (Fig. 2A). The feedback loop between NF- $\kappa$ B and I $\kappa$ B $\alpha$  is a slightly modified version of our earlier model (6, 18). Because the kinetic details of the MyD88-dependent and MyD88-independent pathways are not known, we described both pathways simply as first-order processes whose parameters were determined from our quantitated time course data (Fig. 2B). The model indicated that both the MyD88-independent and MyD88-dependent pathways are likely to have similar activation kinetics but that the MyD88-independent pathway requires a roughly 30-min time delay before it is activated (Fig. 2C).

This delay in pathway activation may occur at the level of IKK (Fig. 2E). We therefore monitored IKK activity in LPS-stimulated MyD88-deficient, Trif-deficient, and wild-type MEFs (Fig. 2F). IKK activation in wild-type and Trif-deficient MEFs began as early as 15 min after stimulation of cells with LPS and was sustained until 90 min. At that point, IKK activity in wild-type MEFs continued to increase, whereas IKK activity in Trif-deficient cells decreased. Furthermore, IKK activity in MyD88-deficient MEFs began to increase at 45 min. In contrast, TNF $\alpha$ -dependent activation of IKK reaches peak activity between 5 and 10 min and is inactive by 30 min (19, 20). This difference in the length of IKK activity may help explain the difference in period length between nuclear NF- $\kappa$ B activity and I $\kappa$ B $\alpha$  protein levels for TLR4 stimulation. In Trif-deficient cells, IKK activity remains high through two complete oscillations of nuclear

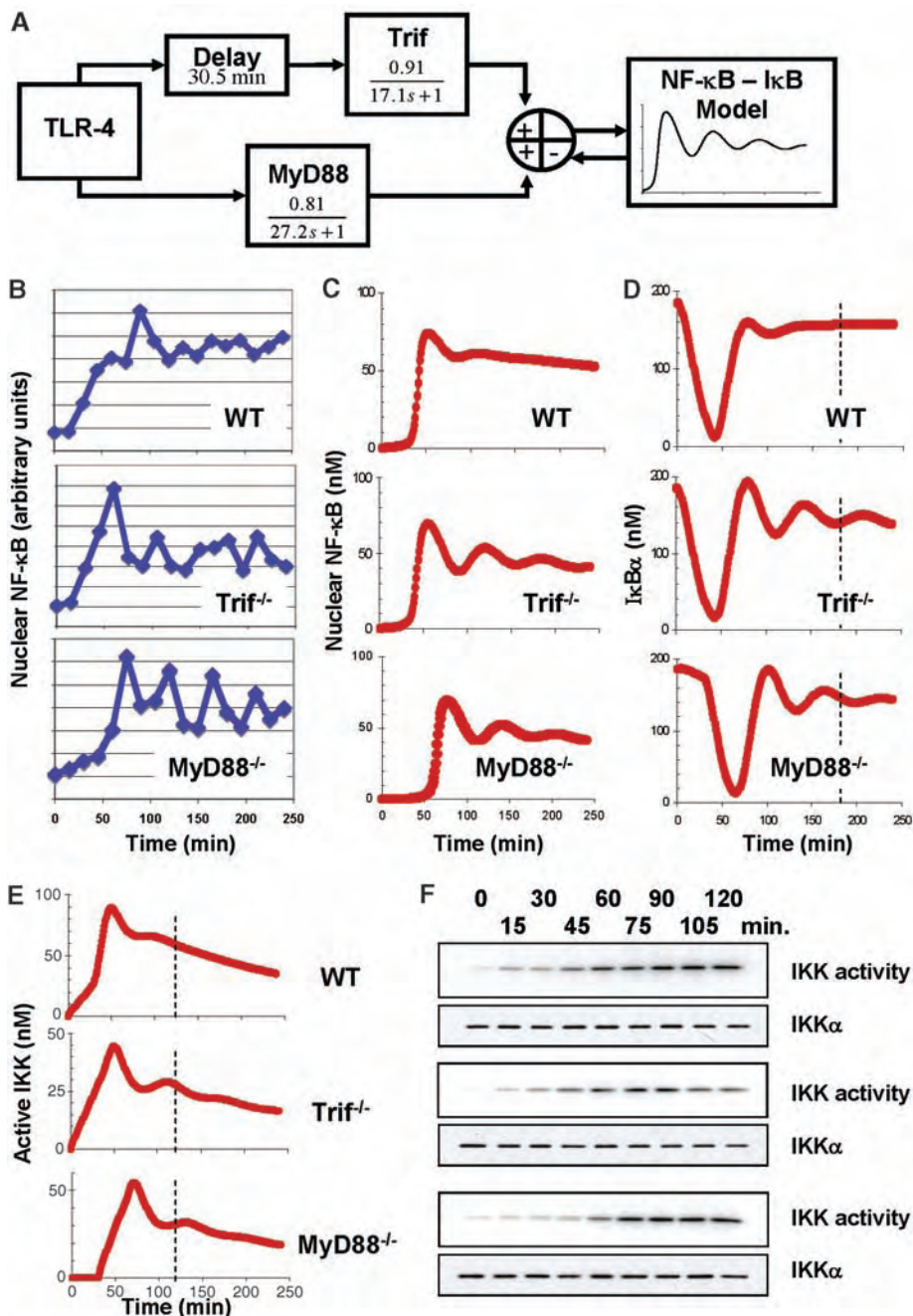


**Fig. 2.** Modeling the activation of NF- $\kappa$ B. (A) Schematic of a computational model of TLR4-dependent activation of NF- $\kappa$ B, partially represented as a block diagram (27). The blocks in the model contain first-order transfer functions of the form  $K/(\tau s + 1)$ , where  $K$  is called the steady state gain of the function and  $\tau$  describes the time behavior. The parameter values were determined by (B) phosphoimager quantitation of NF- $\kappa$ B activation time courses (Fig. 1, A and D). "Trif" is used to denote the MyD88-independent pathway. (C to E) The predicted time courses of nuclear NF- $\kappa$ B activity (C), I $\kappa$ B $\alpha$  protein levels (D), and IKK activity (E). (F) IKK activity in wild-type, Trif-deficient, and MyD88-deficient cells. Dashed lines in (D) and (E) facilitate comparison of model predictions with data in Fig. 1E and (F).

NF- $\kappa$ B activity. This suggests that the oscillations in nuclear NF- $\kappa$ B activity are not due solely to I $\kappa$ B $\alpha$  protein abundance.

The computational model is necessarily minimal with respect to parameters and was derived primarily from the quantitative electromobility shift assay (EMSA) data. As such, the model fails to predict the discrepancy in period for I $\kappa$ B $\alpha$  protein synthesis and NF- $\kappa$ B activation, as well as the extended activation of IKK. However, the I $\kappa$ B $\alpha$  protein synthesis data qualitatively agrees with our model's prediction that I $\kappa$ B $\alpha$  protein levels would oscillate in the knockout cells but not in the wild-type cells (Figs. 1E and 2D) and the IKK activation data supports the prediction that the MyD88-independent pathway requires a time delay for activation (Fig. 2, E and F).

This delay might occur if NF- $\kappa$ B activation by the MyD88-independent pathway required protein synthesis. Thus, we pretreated wild-type, MyD88-deficient, Trif-deficient, and MyD88-Trif doubly deficient cells with cycloheximide before LPS stimulation, and monitored NF- $\kappa$ B activation over a 135-min time course (Fig. 3A). In LPS-stimulated wild-type or Trif-deficient cells, cycloheximide pretreatment triggered activation of NF- $\kappa$ B greater than that in wild-type cells, and MyD88-Trif doubly deficient cells demonstrated no inducible NF- $\kappa$ B activation. However in LPS-stimulated MyD88-deficient cells, NF- $\kappa$ B activation was abolished. Thus, the MyD88-independent pathway appears to require protein synthesis to activate NF- $\kappa$ B.

We used microarray technology to compare gene expression levels in LPS-stimulated

MyD88-deficient cells at 0 and 45 min. Increased transcription of seven genes—T cell costimulatory receptor 4-1BB, glycoprotein CD83, chemokine interferon-inducible protein 10 (IP-10), macrophage inflammatory protein (MIP)-1 $\alpha$ , MIP-1 $\beta$ , and MIP-2, and TNF $\alpha$ —was detected and confirmed by quantitative polymerase chain reaction (qPCR) ( $P$  value < 0.001, fold change > 2) (table S2). The majority of the identified genes (4-1BB, IP-10, the MIPs, and TNF $\alpha$ ) encode extracellular messengers. We therefore treated MyD88-deficient cells with neutralizing antibodies or soluble receptors specific to certain candidate genes, stimulated the cells with LPS, and monitored activation of NF- $\kappa$ B (Fig. 3B). In MyD88-deficient cells, only pretreatment with soluble TNF receptor blocked LPS-stimulated activation of NF- $\kappa$ B. We detected small concentrations of TNF $\alpha$  (<30 pg/ml) by enzyme-linked immunosorbent assay in the supernatant of LPS-stimulated MyD88-deficient cells. In addition, expression of TNF $\alpha$  transcript in LPS-stimulated MyD88-deficient cells was up-regulated between 13- and 58-fold before NF- $\kappa$ B was active (Fig. 3C). Thus, the Trif-dependent pathway activates TNF $\alpha$  production and secretion in an NF- $\kappa$ B-independent manner. The secreted TNF $\alpha$  binds its receptors on the cell leading to NF- $\kappa$ B activation.

Interferon-regulatory factor 3 (IRF3) is a MyD88-independent pathway-specific transcription factor that directly regulates early response genes (for example, those encoding interferon- $\beta$  and IP-10) and is active within 30 min of LPS stimulation (21). Furthermore, the TNF $\alpha$  promoter has several potential IRF binding sites. We used a retrovirus expressing an RNA interference cassette to silence endogenous IRF3 protein expression (22) in MyD88-deficient MEFs. Protein immunoblotting showed that the virus decreased the amount of IRF3 to one-eighth that in control cells (Fig. 3D). Depletion of IRF3 impaired the activation of NF- $\kappa$ B. Thus, IRF3 appears to mediate the activation of TNF $\alpha$  in the MyD88-independent pathway.

Previous studies by two different groups suggested that Trif directly activates NF- $\kappa$ B by interacting with adaptor molecules TRAF6 and Tank-binding kinase 1 (TBK1) (23, 24). However, LPS-stimulated TRAF6-deficient macrophages were still capable of NF- $\kappa$ B activation with similar kinetics to the MyD88-independent pathway, and TLR3 signaling, which is dependent on Trif, was also not affected (25). We suggest that the activation of NF- $\kappa$ B by the Trif-dependent pathway results by means of a secondary response through TNF $\alpha$  and IRF3, establishing an autocrine pathway for delayed NF- $\kappa$ B activation (Fig. 3E). The combination of two out-of-phase oscillatory-based responses appears to allow for the stable and consistent early NF- $\kappa$ B response to LPS.

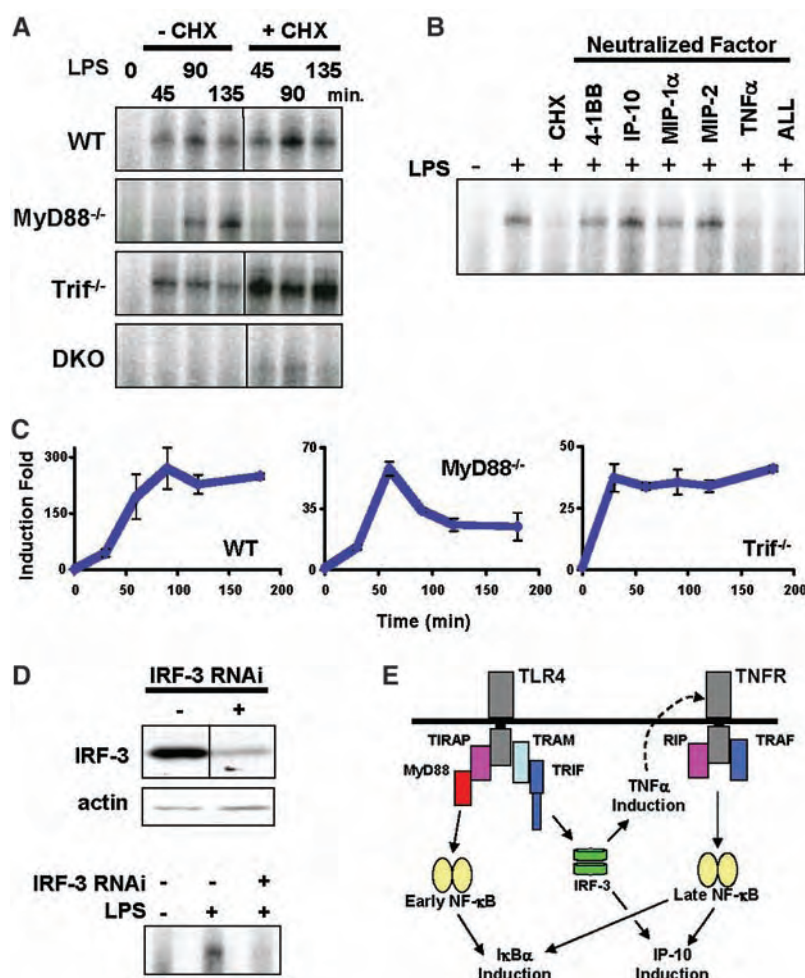


**Fig. 3.** MyD88-independent pathway activation of NF- $\kappa$ B requires IRF3-mediated expression of TNF $\alpha$ . Determination of LPS-induced nuclear NF- $\kappa$ B activity in MyD88-deficient MEFs by EMSA, where cells were (A) treated with cycloheximide (CHX) (25  $\mu$ g/ml) for 60 min; (B) cotreated with one or all of the following: cycloheximide, soluble 4-1BB receptor (8  $\mu$ g/ml), antibody to IP-10 (16.5  $\mu$ g/ml), antibody to MIP-1 $\alpha$  (2  $\mu$ g/ml), antibody to MIP-2 (0.75  $\mu$ g/ml), soluble TNF $\alpha$  receptor II (8.3  $\mu$ g/ml); (C) infected with a lentiviral small interfering RNA construct to knock down IRF3 expression. (D) TNF $\alpha$  gene expression in wild-type, Trif-deficient, and MyD88-deficient MEFs stimulated with LPS, determined by qPCR. (E) Schematic of the proposed pathway for activation of NF- $\kappa$ B by means of Trif. Trif activates IRF3 through TBK1 and I $\kappa$ B kinase  $i$ , after which TNF $\alpha$  is expressed and secreted, activating NF- $\kappa$ B through the TNF pathway. TIRAP, Toll-interleukin 1 receptor domain-containing adaptor protein.



Nature often builds on a single mechanism to increase specificity and complexity. For transcription, increasingly complex genomes often contain a greater number of transcription factor family members than separate transcription factor families (26). This suggests that diversity within a gene family may provide specificity and versatility. Here the canonical pathway of NF- $\kappa$ B activation, which is activated once in cells treated with TNF $\alpha$ , is activated twice in response to TLR4 stimulation to create a distinct NF- $\kappa$ B activation profile.

#### References and Notes

1. S. Ghosh, M. J. May, E. B. Kopp, *Annu. Rev. Immunol.* **16**, 225 (1998).
2. A. S. Baldwin, *J. Clin. Invest.* **107**, 241 (2001).
3. E. Pikarsky et al., *Nature* **431**, 461 (2004).
4. T. Bouwmeester et al., *Nat. Cell Biol.* **6**, 97 (2004).
5. K. H. Cho, S. Y. Shin, H. W. Lee, O. Wolkenhauer, *Genome Res.* **13**, 2413 (2003).
6. A. Hoffmann, A. Levchenko, M. L. Scott, D. Baltimore, *Science* **298**, 1241 (2002).
7. D. E. Nelson et al., *Science* **306**, 704 (2004).
8. M. S. Hayden, S. Ghosh, *Genes Dev.* **18**, 2195 (2004).
9. K. Brown, S. Park, T. Kanno, G. Franzoso, U. Siebenlist, *Proc. Natl. Acad. Sci. U.S.A.* **90**, 2532 (1993).
10. M. L. Scott, T. Fujita, H. C. Liou, G. P. Nolan, D. Baltimore, *Genes Dev.* **7**, 1266 (1993).
11. S. C. Sun, P. A. Ganchi, D. W. Ballard, W. C. Greene, *Science* **259**, 1912 (1993).
12. K. Kawasaki, H. Nogawa, M. Nishijima, *J. Immunol.* **170**, 413 (2003).
13. G. M. Barton, R. Medzhitov, *Science* **300**, 1524 (2003).
14. S. Akira, K. Takeda, T. Kaisho, *Nat. Immunol.* **2**, 675 (2001).
15. E. Meylan et al., *Nat. Immunol.* **5**, 503 (2004).
16. M. Yamamoto et al., *Science* **301**, 640 (2003).
17. M. Yamamoto et al., *Nat. Immunol.* **4**, 1144 (2003).
18. Materials and methods are available as supporting material on Science Online.
19. J. A. DiDonato, M. Hayakawa, D. M. Rothwarf, E. Zandi, M. Karin, *Nature* **388**, 548 (1997).
20. F. Mercurio et al., *Science* **278**, 860 (1997).
21. S. Doyle et al., *Immunity* **17**, 251 (2002).
22. T. H. Leung, A. Hoffmann, D. Baltimore, *Cell* **118**, 453 (2004).
23. Z. Jiang, T. W. Mak, G. Sen, X. Li, *Proc. Natl. Acad. Sci. U.S.A.* **101**, 3533 (2004).
24. S. Sato et al., *J. Immunol.* **171**, 4304 (2003).
25. J. Gohda, T. Matsumura, J. Inoue, *J. Immunol.* **173**, 2913 (2004).
26. E. S. Lander et al., *Nature* **409**, 860 (2001).
27. D. E. Seborg, T. F. Edgar, D. A. Mellichamp, *Process Dynamics and Control*, Wiley Series in Chemical Engineering (John Wiley & Sons, New York, 1989), pp. 7–130.
28. We thank M. Yamamoto and S. Akira for generously providing the MEFs; M. Boldin, M. Meffert, and A. Hoffmann for valuable discussions; and the Millard and Muriel Jacobs Genetics and Genomics Laboratory at the California Institute of Technology for assistance with the gene expression study. This work was funded by the NIH (GM039458-21). M.W.C. is a Robert Black Fellow supported by the Damon Runyon Cancer Research Foundation (DRG-#1835-04). T.H.L. is a student in the UCLA-California Institute of Technology Medical Scientist Training Program and supported by the Achievement Rewards for College Scientists foundation.

#### Supporting Online Material

www.sciencemag.org/cgi/content/full/309/5742/1854/DC1

Materials and Methods

Fig. S1

Tables S1 and S2

References

15 March 2005; accepted 28 July 2005

10.1126/science.1112304

# Stimulus Specificity of Gene Expression Programs Determined by Temporal Control of IKK Activity

Shannon L. Werner,\* Derren Barken,\* Alexander Hoffmann†

A small number of mammalian signaling pathways mediate a myriad of distinct physiological responses to diverse cellular stimuli. Temporal control of the signaling module that contains I $\kappa$ B kinase (IKK), its substrate inhibitor of NF- $\kappa$ B (I $\kappa$ B), and the key inflammatory transcription factor NF- $\kappa$ B can allow for selective gene activation. We have demonstrated that different inflammatory stimuli induce distinct IKK profiles, and we examined the underlying molecular mechanisms. Although tumor necrosis factor- $\alpha$  (TNF $\alpha$ )-induced IKK activity was rapidly attenuated by negative feedback, lipopolysaccharide (LPS) signaling and LPS-specific gene expression programs were dependent on a cytokine-mediated positive feedback mechanism. Thus, the distinct biological responses to LPS and TNF $\alpha$  depend on signaling pathway-specific mechanisms that regulate the temporal profile of IKK activity.

The evolutionarily conserved, signal-responsive transcription factor NF- $\kappa$ B plays a role in a myriad of physiological functions. These include lymphoid tissue development, immune, inflammatory, and environmental stress responses, and neuronal signaling (1, 2). A number of human pathologies are caused by the impairment of signal-responsive NF- $\kappa$ B regulation, including chronic inflammatory diseases (3) and cancers (4). Thus, mechanisms that regulate NF- $\kappa$ B activity and allow it to control stimulus-specific physiological re-

sponses are of pressing clinical relevance (5, 6) and are also of interest as a model system for studies of complex mammalian signaling systems.

NF- $\kappa$ B is held in an inactive state by association with one of three I $\kappa$ B proteins. In response to stimulation, the I $\kappa$ B kinase (IKK) phosphorylates NF- $\kappa$ B-bound I $\kappa$ B proteins, targeting them for proteolysis through the ubiquitin-proteasome pathway (7). A mathematical model based on ordinary differential equations recapitulated signaling of the IKK-I $\kappa$ B-NF- $\kappa$ B signaling module in response to the inflammatory cytokine tumor necrosis factor- $\alpha$  (TNF $\alpha$ ) in murine embryonic fibroblasts (MEFs) (8). This model predicted dynamic signaling behavior resulting from I $\kappa$ B resynthesis, as observed biochemically (8) or in single-cell real-time imaging studies (9).

Further refinements of the model have led to correct predictions of cross-regulation between I $\kappa$ B family members (10) and have uncovered important negative feedback mediated by the I $\kappa$ B $\epsilon$  isoform (11).

The functional pleiotropism of NF- $\kappa$ B is based on the responsiveness of IKK to diverse signals transduced by plasma membrane-bound receptors or subcellular organelles (Fig. 1A) (12). Although different stimuli activate the same IKK-I $\kappa$ B-NF- $\kappa$ B signaling module, they elicit different gene expression programs. Because temporal control of NF- $\kappa$ B activity can lead to selective gene expression (8), we reasoned that stimulus-specific temporal control of IKK activity might allow for distinct biological responses if signal processing within the IKK-I $\kappa$ B-NF- $\kappa$ B signaling module resulted in distinct NF- $\kappa$ B activity profiles. To examine the signal processing characteristics of the signaling module, we generated a collection of potential IKK profiles with a simple algorithm (Fig. 1B). The algorithm allows for variable rises in IKK activity (over a time period of  $a = 0, 60, 120, \text{ or } 240 \text{ min}$ ), a first plateau of various amplitudes ( $x = 4, 12, 34, \text{ or } 101 \text{ nM}$ ) and durations ( $b = 0, 5, 15, 30, 60, \text{ or } 120 \text{ min}$ ), variable decays (over a time period of  $c = 0, 60, 120, \text{ or } 240 \text{ min}$ ), and a second, equal or lower, plateau of activity at or above baseline ( $y = 1, 4, 12, 34, \text{ or } 101 \text{ nM}$ ).

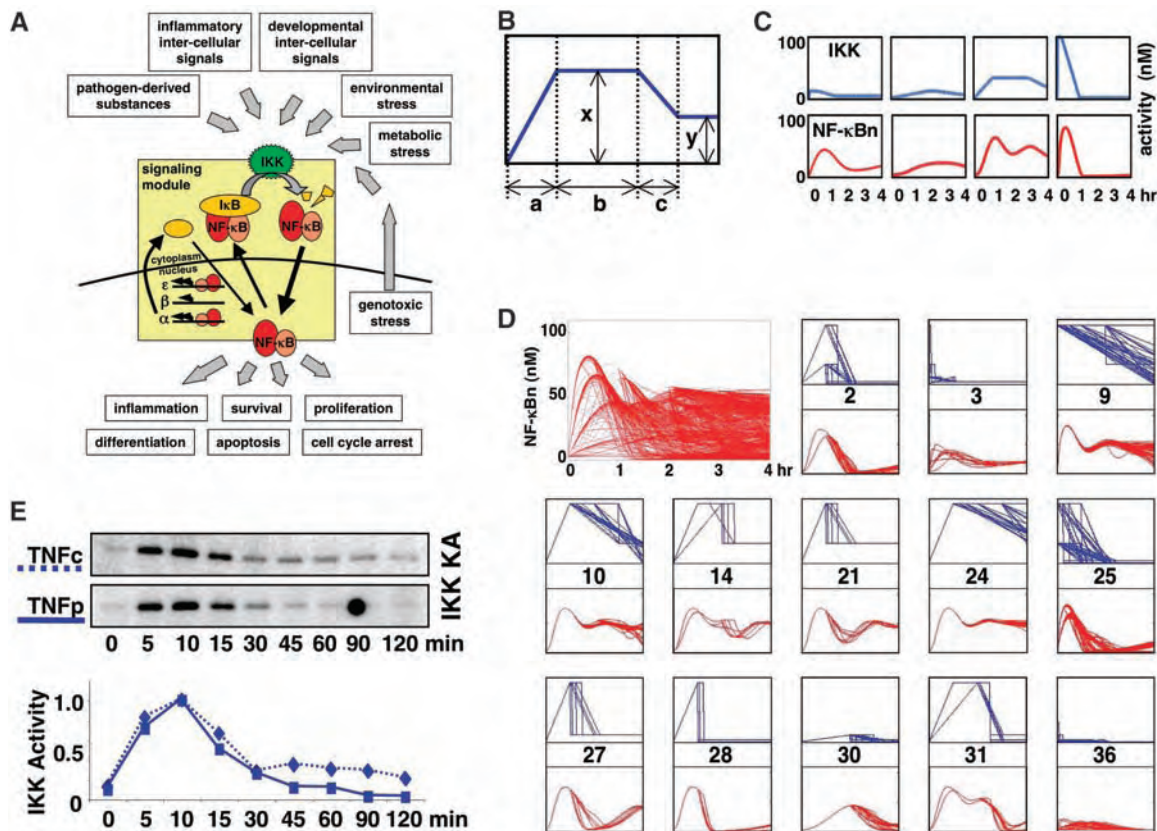
The resulting comprehensive library of 687 distinct IKK activity profiles (fig. S1) served as inputs for computational simulations with our newly refined mathematical model (13). Each IKK input-NF- $\kappa$ B output pair (examples in Fig. 1C) reflects signal processing within the IKK-I $\kappa$ B-NF- $\kappa$ B signaling module. By grouping similar NF- $\kappa$ B activity profiles using standard K-means clustering, we investigated which IKK activity profiles are distinguished

Signaling Systems Laboratory, Department of Chemistry and Biochemistry, 9500 Gilman Drive, Mailcode 0375, La Jolla, CA 92093-0375, USA.

\*These authors contributed equally to this work.

†To whom correspondence should be addressed. E-mail: ahoffmann@ucsd.edu

**Fig. 1.** Exploring the temporal control of IKK activity in regulating NF- $\kappa$ B signaling. (A) The schematic illustrates that many physiological signals impinge on the IKK-I $\kappa$ B-NF- $\kappa$ B signaling module to produce different physiological responses. (B) A set of diverse IKK profiles was computationally generated by the following algorithm: Each input had a rising phase (parameter *a*), a first plateau (parameter *b*), a falling phase (parameter *c*), and a second plateau, each with varying time values of 0, 60, 120, or 240 min (parameter *a*), or 0, 5, 15, 30, 60, or 120 min (parameter *b*), or 0, 60, 120, or 240 min (parameter *c*). The heights of the first (parameter *x*) and second (parameter *y*) plateaus were also varied to 4, 12, 34, or 101 nM IKK (parameter *x*), or 1, 4, 12, 34, or 101 nM IKK (parameter *y*) ( $y \leq x$ ). (C) Four examples from a library of 687 distinct IKK activity profiles (blue) that were generated as described in (B). The resulting NF- $\kappa$ B activity profile (red) was computed using the mathematical model of the IKK-I $\kappa$ B-NF- $\kappa$ B signaling module, version 2.0 (13). (D) NF- $\kappa$ B activity profiles (red, top left) produced by 687 IKK profiles were clustered by K-means clustering (MatLab 7.0 Statistical Toolbox). Shown here is a selection of 13 out of



36 clusters (for all, see fig. S2). The corresponding IKK profiles (blue) were grouped accordingly. (E) IKK activity was measured in mouse embryonic fibroblasts (MEFs) after chronic (TNFc) or 45-min pulse (TNFp) TNF stimulation (1 ng/ml) by IKK IP-kinase assay (IKK KA). GST-I $\kappa$ B $\alpha$ (1-54) served as a substrate in the assay, and its phosphorylation by IKK was quantitated, normalized, and graphed.

by the signaling module and which profiles, although seemingly different, are likely to have similar biological effects. Examination of the clusters (Fig. 1D and fig. S2) revealed, for example, that the amplitude of the first peak of IKK activity was not a major determinant of the NF- $\kappa$ B activity profile (for example, clusters 2 and 25). However, different rates of IKK activation (contrast clusters 9 and 10) and the duration of the first peak of activity (contrast clusters 14 and 21, or 28 and 31) did result in different NF- $\kappa$ B activity profiles. The signaling module does not distinguish very much between different decay rates of IKK activity at late times (for example, clusters 9 and 24). However, the level of IKK activity in the second phase (secondary plateau) was very important (compare clusters 21, 27, and 28). Although transient aberrations in IKK activity do not result in much NF- $\kappa$ B activity (cluster 36), large but very transient IKK activities have similar signaling effects as sustained smaller increases (cluster 3): Both result in an NF- $\kappa$ B activity profile that persists much longer than the duration of the transient pulse of IKK activity. The signaling module appears to be particularly sensitive to sus-

tained low IKK activity (cluster 30) but robust to transient perturbations.

One prediction of this computational exploration was that long-lasting NF- $\kappa$ B activity may be mediated by unexpectedly low amplitudes of IKK activity, whereas transient NF- $\kappa$ B activity requires a much higher increase in IKK activity. Examining the actual kinase activity profiles in cells exposed to either brief (45 min) or prolonged stimulation with TNFa revealed that IKK was highly active at early time points but that activity dropped to low levels after about 30 min (Fig. 1E). Consistent with the computational investigation, IKK activity profiles were similar, with only a slightly increased late plateau of activity elicited by persistent stimulation. However, these stimulation conditions have distinct biological effects mediated by a late phase of NF- $\kappa$ B activity (8). The importance of small changes in late or prolonged IKK activity suggests that mechanisms may have evolved to modulate it with remarkable precision.

Actual cellular IKK activity profiles are determined by signaling pathways emanating from receptors that allow for stimulus-specific signal processing (fig. S3). We therefore mea-

sured the IKK activity profiles in response to the inflammatory stimuli TNF and bacterial lipopolysaccharide (LPS), which engage TNF receptor TNFR and toll-like receptor 4 (TLR4), respectively. Transient administration of these stimuli (45 min) resulted in different IKK activity profiles (Fig. 2A and fig. S4). LPS elicited a small increase in IKK activity within the first 30 min, a larger increase between 45 and 90 min, and a slowly attenuating late phase. In contrast, TNF elicited a sharp peak of IKK activity within the first 15 min, with a return to baseline within 60 min. Computational simulations with those experimentally determined IKK activity profiles predicted temporally distinct NF- $\kappa$ B activity profiles (Fig. 2B). Experimental analysis revealed temporal NF- $\kappa$ B activity profiles (Fig. 2C) and I $\kappa$ B protein levels (fig. S5) similar to those predicted. Thus, our computational model recapitulates NF- $\kappa$ B activation events in response to multiple inflammatory stimuli. The successful in silico reconstitution of LPS and TNF signaling may mean that no further biochemical factors and mechanisms need be invoked to explain the regulation of nuclear NF- $\kappa$ B translocation by IKK.

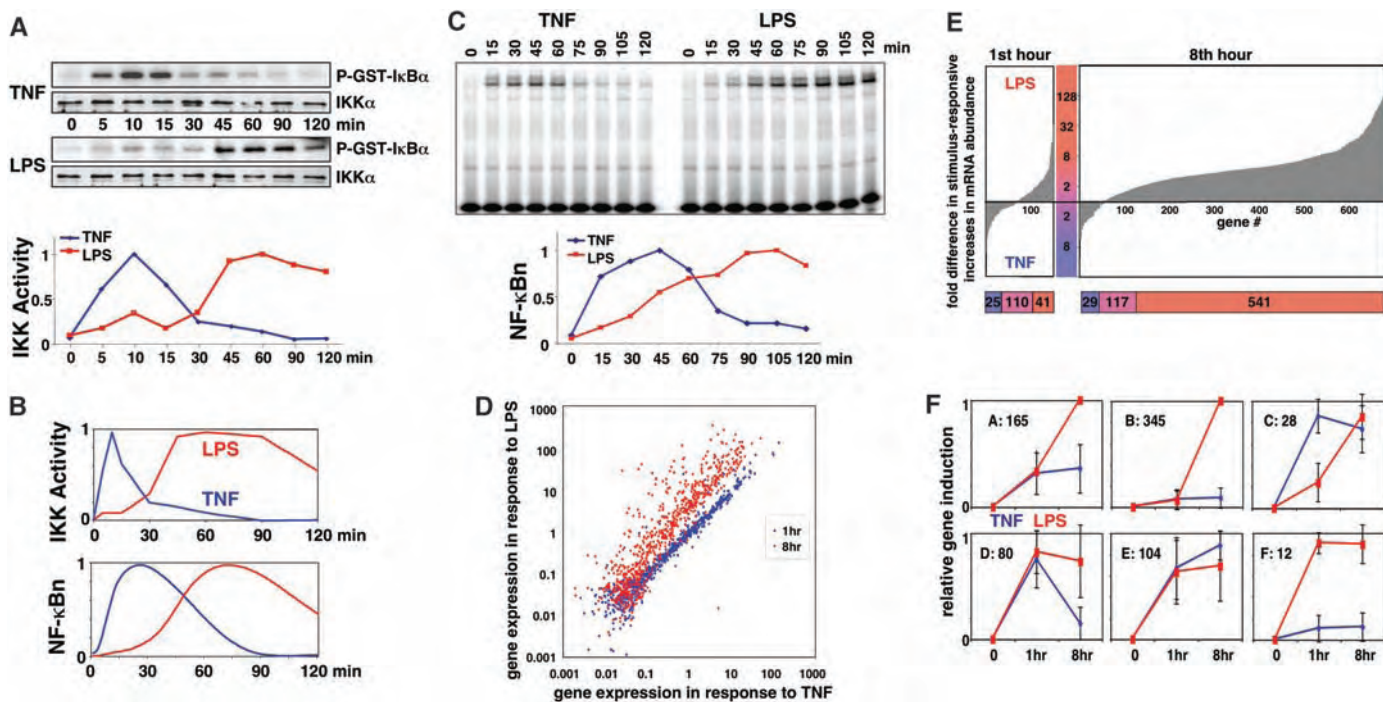


**Fig. 2.** Stimulus-specific signaling by the IKK-NF- $\kappa$ B signaling module. (A) IKK profiles were measured by IKK IP-kinase assay in MEFs stimulated with a 45-min pulse of either TNF (1 ng/ml) or LPS (0.1  $\mu$ g/ml). Equal protein loading was confirmed with an immunoblot against IKK $\alpha$ . Quantitated and normalized results were graphed. (B) IKK profiles measured in (A) were graphed on a linear time scale (top) and used as inputs in computational simulations to predict normalized NF- $\kappa$ B activity profiles (bottom) in response to TNF (blue) or LPS (red). (C) NF- $\kappa$ B activity profiles were measured by electrophoretic mobility shift assay (EMSA) in response to a 45-min pulse TNF (1 ng/ml) and LPS (0.1  $\mu$ g/ml). Results from the EMSA were normalized and graphed. (D) Microarray gene expression profiling revealed 734 genes whose expression was increased by a factor of  $>3$  in response to either LPS or TNF stimulation at the 1- or 8-hour time point. mRNA transcript levels of each gene (in arbitrary units)

are shown for the 1-hour (blue) and 8-hour (red) time points after TNF stimulation (x axis) and LPS-stimulation (y axis). (E) Of the genes shown in (D), 176 showed increased expression by a factor  $>3$  in response to either LPS or TNF in hour 1 and 687 genes in hour 8. For each gene, the relative difference in the induction fold in response to TNF and LPS was calculated and graphed after ordering the genes from high TNF specificity (left) to high LPS specificity (right). The Venn diagram (bottom) details the number of genes whose expression is preferentially increased (by a factor of  $>2$ ) in response to TNF (blue) or LPS (red) stimulation. Genes that do not show stimulus specificity are represented by the violet box. (F) Genes whose expression is increased by a factor of  $>3$  in response to either TNF or LPS (734 total) were grouped by clustering of their normalized induction folds at time points 1 and 8 hours. The mean, standard deviation, and number of genes present in a selected number of clusters are indicated.

We used gene expression microarrays to compare gene expression programs in response to transient stimulation of MEFs with LPS and TNF. Although there was substantial overlap between LPS- and TNF-induced gene expression programs at early time points, many genes showed higher transcript levels at late times in response to LPS than to TNF (Fig. 2D). Indeed, of the genes whose expression was induced by a factor of  $>3$  by either TNF or LPS at 1 hour, only a minority were stimulus specific (66/176 = 37.5%), whereas a majority were more highly induced by LPS at the 8-hour time point (541/687 = 78.7%) (Fig. 2E). Temporal clustering of the normalized fold-induction data of responding genes (Fig. 2F) confirmed that small numbers of genes are either coregulated by TNF and LPS (cluster E, 104 members) or are stimulus specific at the early time point (clusters C and F, 40 members). Interestingly, a very large number of genes are expressed in a LPS-specific manner at the late time point (clusters A, B, and D, 590 members). LPS-specific late gene activation correlates with the LPS-specific secondary plateau of IKK activity.

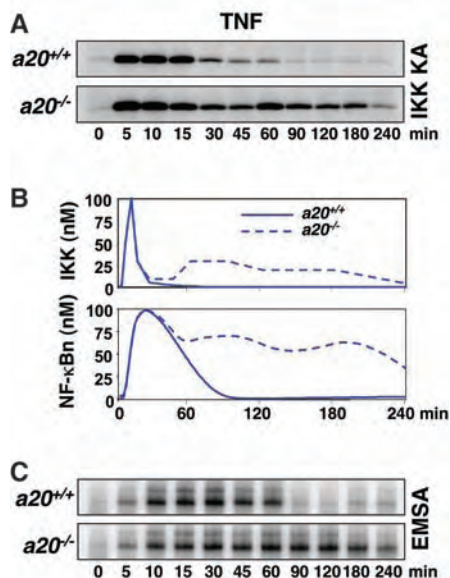


**Fig. 3.** Temporal control of TNF signaling through A20-mediated negative feedback. (A) IKK activity profiles were measured by IKK IP-kinase assays from  $a20^{+/+}$  and  $a20^{-/-}$  cells in response to 45-min pulse TNF stimulation over a 4-hour time course. (B) Quantitated experimental IKK data (top) was used as an input for computational simulations that predicted NF- $\kappa$ B activity profiles in  $a20^{+/+}$  and  $a20^{-/-}$  cells (bottom). (C) NF- $\kappa$ B activity profiles were measured by EMSA in response to 45-min pulse TNF in  $a20^{+/+}$  and  $a20^{-/-}$  cells over a 4-hour time course.

These observations emphasize the potential importance of late IKK activity, whose regulation may be subject to stimulus-responsive protein synthesis.

In the TNFR signaling pathway, the NF- $\kappa$ B response gene *A20* has been proposed to function in postinduction attenuation of NF- $\kappa$ B activity by modulating the signaling

mechanisms that regulate IKK activation (14, 15). Using our computational model, we examined whether misregulation of IKK in A20-deficient cells was sufficient to explain the increased activation of NF- $\kappa$ B and the consequent inflammatory phenotype seen in A20-deficient mice. Quantitative measurements of the TNF-induced IKK activity profile in wild-type and *a20*<sup>-/-</sup> cells (Fig. 3A) were used as inputs of our computational model to predict NF- $\kappa$ B activation profiles (Fig. 3B). Biochemical analyses of nuclear

NF- $\kappa$ B activity (Fig. 3C) and cytoplasmic I $\kappa$ B protein levels (fig. S6) match the computational predictions. Thus, A20 appears to function in fibroblasts in attenuating NF- $\kappa$ B signaling by modulating the temporal profile of IKK activity in the TNF signaling pathway but less so in the LPS signaling pathway (fig. S7).

For the TLR4 signaling pathway, the molecular mechanisms that regulate IKK are less well understood (16). LPS-induced IKK activity has a biphasic profile (Fig. 2B and fig. S3). By using the ribosome inhibitor cyclo-

heximide, we found that the LPS-specific second phase of IKK activity was dependent on new protein synthesis (Fig. 4A) and varied with the density of the primary cells in culture (Fig. 4B). Consequently, we hypothesized that LPS-specific primary response genes may function to potentiate late IKK activity through an autocrine mechanism. LPS rapidly increased expression of genes encoding 10 secreted cytokines and chemokines, many of which were also expressed in response to TNF stimulation (Fig. 4C). However, the interleukin-10 (IL-10),

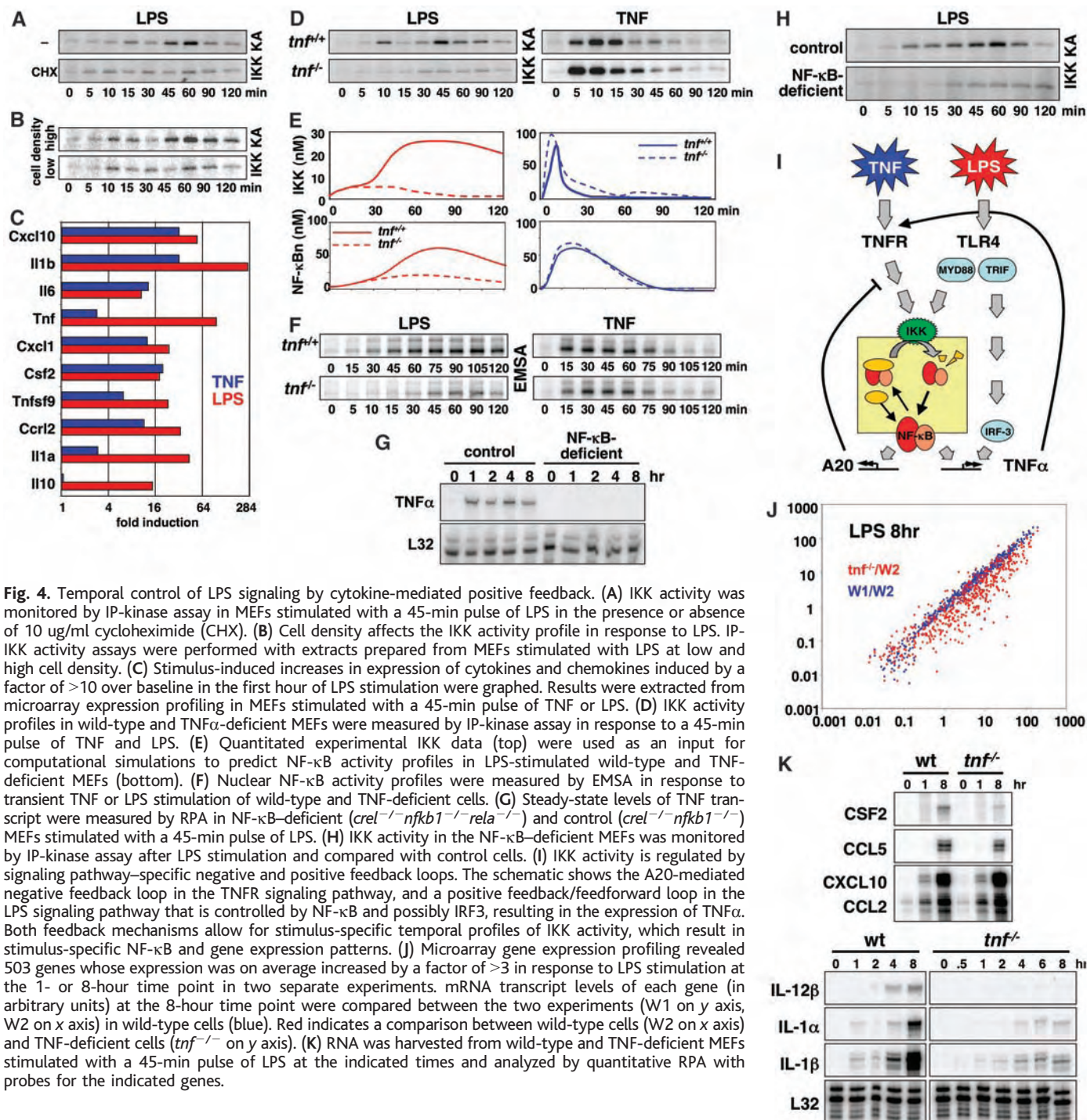


**Fig. 4.** Temporal control of LPS signaling by cytokine-mediated positive feedback. (A) IKK activity was monitored by IP-kinase assay in MEFs stimulated with a 45-min pulse of LPS in the presence or absence of 10  $\mu$ g/ml cycloheximide (CHX). (B) Cell density affects the IKK activity profile in response to LPS. IP-kinase activity assays were performed with extracts prepared from MEFs stimulated with LPS at low and high cell density. (C) Stimulus-induced increases in expression of cytokines and chemokines induced by a factor of  $>10$  over baseline in the first hour of LPS stimulation were graphed. Results were extracted from microarray expression profiling in MEFs stimulated with a 45-min pulse of TNF or LPS. (D) IKK activity profiles in wild-type and TNF $\alpha$ -deficient MEFs were measured by IP-kinase assay in response to a 45-min pulse of TNF and LPS. (E) Quantitated experimental IKK data (top) were used as an input for computational simulations to predict NF- $\kappa$ B activity profiles in LPS-stimulated wild-type and TNF-deficient MEFs (bottom). (F) Nuclear NF- $\kappa$ B activity profiles were measured by EMSA in response to transient TNF or LPS stimulation of wild-type and TNF-deficient cells. (G) Steady-state levels of TNF transcript were measured by RPA in NF- $\kappa$ B-deficient (*crel*<sup>-/-</sup>*nfkb1*<sup>-/-</sup>*rela*<sup>-/-</sup>) and control (*crel*<sup>-/-</sup>*nfkb1*<sup>-/-</sup>) MEFs stimulated with a 45-min pulse of LPS. (H) IKK activity in the NF- $\kappa$ B-deficient MEFs was monitored by IP-kinase assay after LPS stimulation and compared with control cells. (I) IKK activity is regulated by signaling pathway-specific negative and positive feedback loops. The schematic shows the A20-mediated negative feedback loop in the TNFR signaling pathway, and a positive feedback/feedforward loop in the LPS signaling pathway that is controlled by NF- $\kappa$ B and possibly IRF3, resulting in the expression of TNF $\alpha$ . Both feedback mechanisms allow for stimulus-specific temporal profiles of IKK activity, which result in stimulus-specific NF- $\kappa$ B and gene expression patterns. (J) Microarray gene expression profiling revealed 503 genes whose expression was on average increased by a factor of  $>3$  in response to LPS stimulation at the 1- or 8-hour time point in two separate experiments. mRNA transcript levels of each gene (in arbitrary units) at the 8-hour time point were compared between the two experiments (W1 on x axis, W2 on y axis) in wild-type cells (blue). Red indicates a comparison between wild-type cells (W2 on x axis) and TNF-deficient cells (*tnf*<sup>-/-</sup> on y axis). (K) RNA was harvested from wild-type and TNF-deficient MEFs stimulated with a 45-min pulse of LPS at the indicated times and analyzed by quantitative RPA with probes for the indicated genes.

IL-1 $\alpha$ , IL-1 $\beta$ , and TNF genes were specifically expressed in response to LPS. TNF functions in endotoxin toxicity by a proinflammatory paracrine mechanism (17, 18). When we stimulated TNF-deficient cells at high density with LPS, the late phase of IKK activity was lost, whereas TNFR-responsive IKK activation remained intact (Fig. 4D). With these measured IKK profiles, our computational model predicted a defect in NF- $\kappa$ B activation by LPS in TNF-deficient cells (Fig. 4E), which we confirmed experimentally (Fig. 4F).

By employing MEFs deficient in canonical NF- $\kappa$ B proteins, we revealed that LPS-induced expression of TNF requires NF- $\kappa$ B (Fig. 4G). Furthermore, LPS-induced IKK activity was lower in NF- $\kappa$ B-deficient cells than in controls (Fig. 4H), whereas TNF-induced IKK activity was largely unaffected by NF- $\kappa$ B deficiency (fig. S8). Together, these results indicate that TNF involvement in TLR4 signaling constitutes a positive feedback mechanism. TLR4 signaling to IKK was previously shown to be mediated by the adaptor protein MyD88 and, with delayed kinetics, by TRIF through an unknown signaling pathway (16, 19). Our data suggest that the proposed signaling pathway is mediated by de novo synthesis of TNF (Fig. 4I). Secondary IKK activation mediated by TNF autocrine feedback may thus depend not only on the first phase of NF- $\kappa$ B activity, as shown here, but also possibly on TRIF-dependent IRF-3 activity.

To address whether this LPS-specific IKK regulatory mechanism determines LPS-specific gene expression, we examined gene expression in TNF-deficient cells. At the 1-hour time point, gene expression profiles overlapped with controls (fig. S9), but at the 8-hour time point, a large group of genes showed lower expression in *tnf*<sup>-/-</sup> cells than in controls (Fig. 4J). Specifically, and as confirmed by RNase protection assays (RPA) (Fig. 4K and fig. S10), late expression of colony-stimulating factor 2 (CSF2), IL-12 $\beta$ , IL-1 $\alpha$ , and IL-1 $\beta$  was dependent on TNF, but late expression of chemokine (C-C motif) ligand 5 (CCL5), CCL2, and chemokine (C-X-C motif) ligand 10 (CXCL10) was not.

These findings indicate that TNF (and possibly other cytokines) mediate feedforward mechanisms in response to endotoxin challenges that produce positive feedback on IKK activity (and likely also regulate other signal transduction events) and are critical for the induction of a stimulus-specific gene expression program. The particular sensitivity of the biological response to the temporal profile of IKK activity suggests that the underlying molecular mechanisms [including negative and positive feedback mechanisms (Fig. 4I)] may provide sensitive signaling nodes that cells may use for signaling cross-talk.

#### References and Notes

1. S. Gerondakis, M. Grossmann, Y. Nakamura, T. Pohl, R. Grumont, *Oncogene* **18**, 6888 (1999).
2. S. Ghosh, M. Karin, *Cell* **109** (suppl), S81 (2002).

3. Y. Yamamoto, R. B. Gaynor, *J. Clin. Invest.* **107**, 135 (2001).
4. B. B. Aggarwal, *Cancer Cell* **6**, 203 (2004).
5. M. Karin, Y. Yamamoto, Q. M. Wang, *Nat. Rev. Drug Discov.* **3**, 17 (2004).
6. J. E. Darnell Jr., *Nat. Rev. Cancer* **2**, 740 (2002).
7. S. Ghosh, M. J. May, E. B. Kopp, *Annu. Rev. Immunol.* **16**, 225 (1998).
8. A. Hoffmann, A. Levchenko, M. L. Scott, D. Baltimore, *Science* **298**, 1241 (2002).
9. D. E. Nelson et al., *Science* **306**, 704 (2004).
10. R. Quiambao et al., in preparation.
11. J. D. Kearns, S. Basak, S. L. Werner, C. S. Huang, A. Hoffmann, in preparation.
12. H. L. Pahl, *Oncogene* **18**, 6853 (1999).
13. Materials and Methods are available as supporting material on Science Online.
14. E. G. Lee et al., *Science* **289**, 2350 (2000).
15. I. E. Wertz et al., *Nature* **430**, 694 (2004).
16. S. Akira, K. Takeda, T. Kaisho, *Nat. Immunol.* **2**, 675 (2001).
17. B. Beutler, V. Krays, *J. Cardiovasc. Pharmacol.* **25** (suppl 2), S1 (1995).
18. B. Beutler, I. W. Milsark, A. C. Cerami, *Science* **229**, 869 (1985).
19. G. M. Barton, R. Medzhitov, *Science* **300**, 1524 (2003).
20. We thank C. Huang for excellent technical assistance; A. Ma for A20-deficient 3T3 cells; T. Huxford for GST- $\kappa$ B $\alpha$ (1-54); Santa-Cruz Biotechnology for antibodies; and A. Levchenko, G. Ghosh, S. Subramaniam, and D. Baltimore for insightful discussions. This study was supported by NIH grants GM72024 and GM071573.

#### Supporting Online Material

www.sciencemag.org/cgi/content/full/309/5742/1857/DC1

Materials and Methods

Figs. S1 to S10

Tables S1 to S7

References

8 April 2005; accepted 28 July 2005

10.1126/science.1113319

## HST2 Mediates SIR2-Independent Life-Span Extension by Calorie Restriction

Dudley W. Lamming,<sup>1\*</sup> Magda Latorre-Esteves,<sup>1\*</sup>  
Oliver Medvedik,<sup>1\*</sup> Stacy N. Wong,<sup>2\*</sup> Felicia A. Tsang,<sup>2</sup>  
Chen Wang,<sup>2</sup> Su-Ju Lin,<sup>2†</sup> David A. Sinclair<sup>1†</sup>

Calorie restriction (CR) extends the life span of numerous species, from yeast to rodents. Yeast Sir2 is a nicotinamide adenine dinucleotide (NAD<sup>+</sup>)-dependent histone deacetylase that has been proposed to mediate the effects of CR. However, this hypothesis has been challenged by the observation that CR can extend yeast life span in the absence of Sir2. Here, we show that Sir2-independent life-span extension is mediated by Hst2, a Sir2 homolog that promotes the stability of repetitive ribosomal DNA, the same mechanism by which Sir2 extends life span. These findings demonstrate that the maintenance of DNA stability is critical for yeast life-span extension by CR and suggest that, in higher organisms, multiple members of the Sir2 family may regulate life span in response to diet.

A major cause of aging in the yeast *Saccharomyces cerevisiae* stems from homologous recombination between ribosomal DNA (rDNA) repeat sequences and the formation of extrachromosomal circles of rDNA known as ERCs, which accumulate exponentially and eventually lead to the death of the mother cell (1, 2). The

Fob1 protein promotes ERC formation by stalling rDNA replication forks, which are inherently unstable structures (3). Accordingly, deletion of *FOB1* reduces ERC formation and extends yeast life span (4).

In contrast, ERC formation is repressed by the activity of Sir2, an NAD<sup>+</sup>-dependent his-

tone deacetylase (HDAC) that catalyzes the formation of heterochromatin at the rDNA locus (5–8) and is the founding member of the sirtuin deacetylase family. Additional copies of the *SIR2* gene extend yeast life span by decreasing ERC formation, whereas deletion of *SIR2* increases ERC formation and shortens life span (9), a phenotype that can be suppressed by deleting *FOB1* (4).

The life span of most species including *S. cerevisiae* is extended by CR (10). Yeast and *Drosophila* lacking the *SIR2* gene do not live longer when subjected to CR, suggesting that Sir2 underlies this life-span extension (11–15). However, there is increasing evidence that the situation is not so simple (16–18). Although CR is blocked by a *sir2 $\Delta$  mutation, CR can extend the life span of yeast cells lacking both *SIR2* and *FOB1* (18, 19). CR can also extend the life span of *Caenorhabditis elegans* worms*

<sup>1</sup>Paul F. Glenn Laboratories for the Biological Mechanisms of Aging, Department of Pathology, Harvard Medical School, 77 Avenue Louis Pasteur, Boston, MA 02115, USA. <sup>2</sup>Center for Genetics and Development, and Section of Microbiology, University of California Davis, 351 Briggs Hall, Davis, CA 95616, USA.

\*These authors contributed equally to this work.

†To whom correspondence should be addressed. E-mail: slin@ucdavis.edu (S.-J.L.), david\_sinclair@hms.harvard.edu (D.A.S.)

**Fig. 1.** A screen for genes that stabilize the rDNA locus identifies *HST2* (A) rDNA locus (*RDN1*) silencing assays. W303AR cells carrying the gene candidates on a 2 $\mu$  plasmid were grown to log phase in YPD (2% glucose) and then spotted in 10-fold dilutions on SC media with and without adenine. Silencing of the *RDN1::ADE2* reporter results in growth retardation on plates lacking adenine. (B) Overexpression of *HST2* can suppress rDNA recombination even in the absence of Sir2. A plasmid carrying *HST2* (pSP400-Hst2) was integrated into the *URA3* locus of W303AR5 *sir2::TRP1* and W303AR *sir2::TRP1 fob1::hph<sup>r</sup>*. W303AR5 cells containing the gene candidates were grown to log phase in 2% YPD and then plated on YPD plates with low adenine. rDNA recombination rates were calculated by determining the frequency of loss of *ADE2* in the rDNA of strain W303AR5 at the first cell division after plating, as scored by the number of half red-sectored colonies per total number of colonies (30). At least 6000 colonies were examined for each data point. Results show average values and SD for at least three experiments. (C) Treatment with 5 mM nicotinamide (NAM) blocks life-span extension by CR (0.5% glucose or an *hxx2 $\Delta$*  deletion). Life-span analyses were performed as described (11). Average life spans: W303 *sir2 $\Delta$  fob1 $\Delta$*  2% glucose 24.7, 0.5% glucose 30.4, 2% glucose + 5mM NAM 14.8, 0.5% glucose + 5 mM NAM 15.9. (D) NAM blocks life-span extension by *hxx2 $\Delta$*  in BY4742 *sir2 $\Delta$  fob1 $\Delta$* . Average life spans: BY4742 *sir2 $\Delta$  fob1 $\Delta$*  25.7; *sir2 $\Delta$  fob1 $\Delta$  hxx2 $\Delta$*  37.9; *sir2 $\Delta$  fob1 $\Delta$*  + 5 mM NAM 25.9; *sir2 $\Delta$  fob1 $\Delta$  hxx2 $\Delta$*  + 5 mM NAM 26.5.

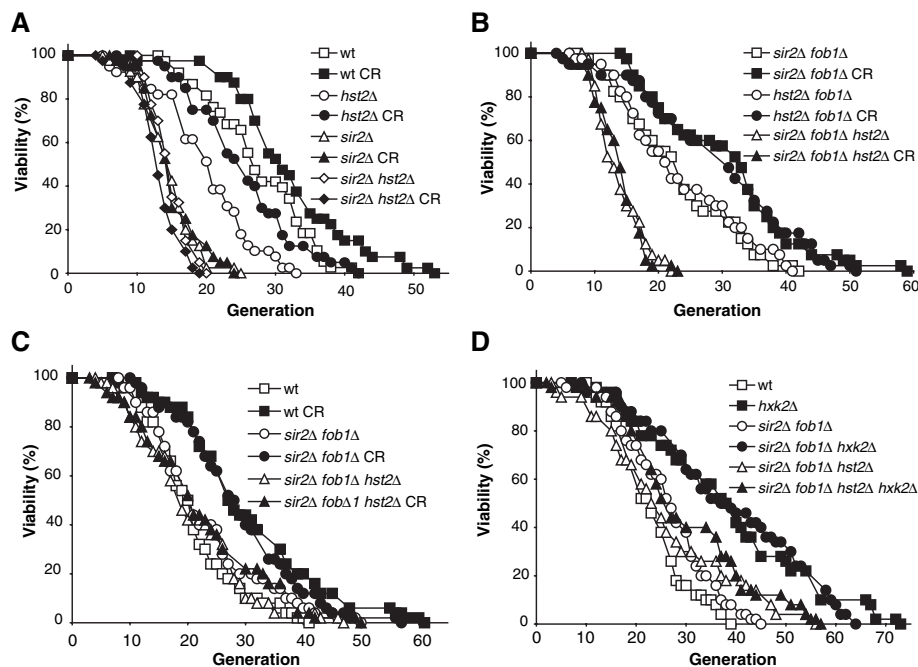
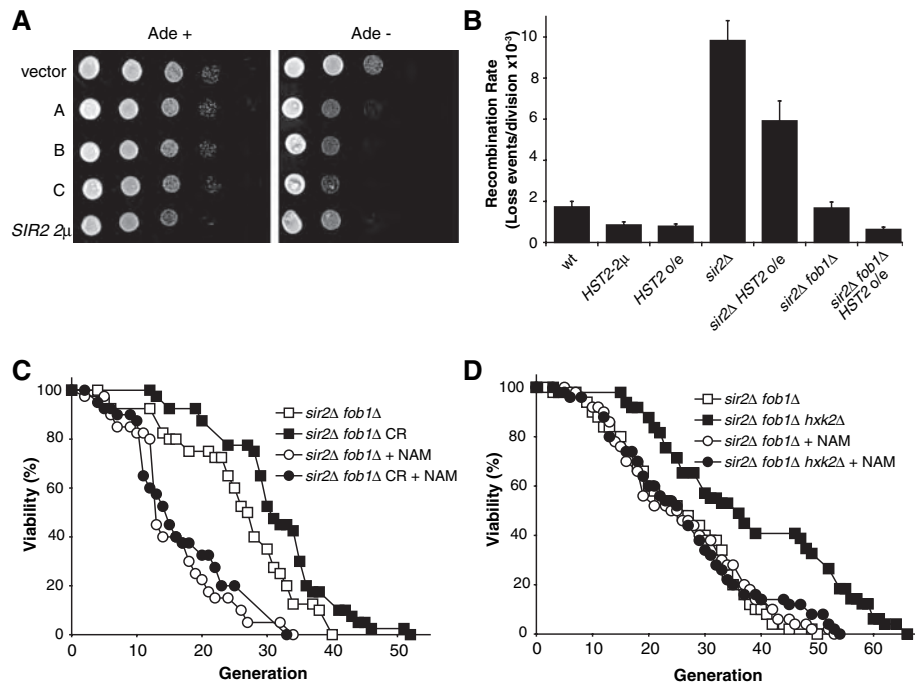


**Fig. 2.** Hst2 is required for Sir2-independent life-span extension by CR. (A) Average life spans: W303AR5 (wild type, wt) 2.0% glucose 26.7, 0.5% glucose 31.1; *hst2 $\Delta$*  2.0% glucose 18.9, 0.5% glucose 24.2; *sir2 $\Delta$*  2.0% glucose 13.7, 0.5% glucose 14.0; *sir2 $\Delta$  hst2 $\Delta$*  2.0% glucose 13.9, 0.5% glucose 12.2. (B) Average lifespans: W303AR5 *sir2 $\Delta$  fob1 $\Delta$*  2.0% glucose 21.9, 0.5% glucose 29.6; *hst2 $\Delta$  fob1 $\Delta$*  2% glucose 22.3, 0.5% glucose 28.3; *sir2 $\Delta$  fob1 $\Delta$  hst2 $\Delta$*  2.0% glucose 13.0, 0.5% glucose 12.9. (C) Average life spans: BY4742 (wild type, wt) 2.0% glucose 20.6, 0.5% glucose 30.4; *sir2 $\Delta$  fob1 $\Delta$*  2% glucose 23.0, 0.5% glucose 28.9; *sir2 $\Delta$  fob1 $\Delta$  hst2 $\Delta$*  2.0% glucose 20.6, 0.5% glucose 21.7. (D) Average life spans: BY4742 (wild type, wt) 23.2; *hxx2 $\Delta$*  38.4; *sir2 $\Delta$  fob1 $\Delta$*  26.6; *sir2 $\Delta$  fob1 $\Delta$  hst2 $\Delta$*  25.9; *sir2 $\Delta$  fob1 $\Delta$  hst2 $\Delta$  hxx2 $\Delta$*  30.1.

lacking the worm SIR2 gene, *sir-2.1* (20). Not surprisingly, there is much confusion and debate in the aging field regarding these findings,

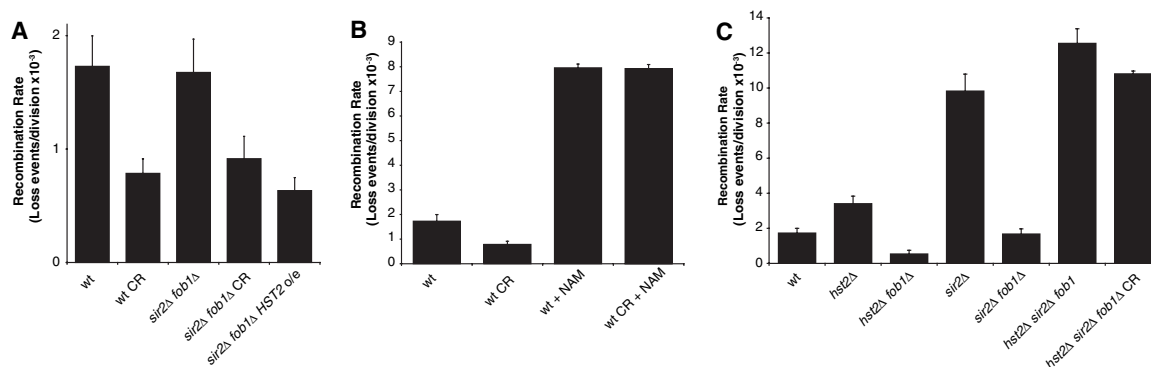
with some researchers postulating that Sir2 may not regulate life-span extension by CR and that yeast life-span extension is inde-

pendent of suppression of ERC formation (19, 21).

To help resolve this issue, we screened for genes that could increase yeast life span via the same mechanism as that by which *SIR2* increases life span by taking advantage of the positive correlation between rDNA silencing and longevity (2, 22). The marker genes *MET15* and *ADE2* were integrated into the rDNA locus such that increased rDNA silencing led to the accumulation of a brown pigment on Pb<sup>2+</sup>-containing media, or decreased growth on plates lacking adenine, respectively. A high-copy 2 $\mu$  yeast genomic library was introduced into the reporter strain and, from ~20,000 colonies, we isolated three genomic fragments that resulted in a robust increase in rDNA silencing (fragments A, B, and C) (Fig. 1A). The three candidates were then tested for rDNA recombination, which negatively correlates with life span. Candidates A and B, but not C, showed a marked decrease in rDNA recombination rate (fig. S1).

The gene responsible for the phenotype of fragment A was identified as *HST2* (homolog of *SIR2*) (fig. S2). *HST2* encodes a NAD<sup>+</sup>-dependent deacetylase whose closest human homolog is *SIRT2* (16, 23, 24). Although Hst2 is known as a cytoplasmic protein (16), it has recently been shown to also be present in the nucleus, where it interacts with chromatin and down-regulates the expression of subtelomeric genes in concert with Hst1 (16, 23). Unexpectedly, we found that overexpression of *HST2* suppressed rDNA recombination not only in wild-type cells, but also in the absence

**Fig. 3.** CR extends life span via *HST2* by suppressing rDNA recombination. (A) CR and overexpression of *HST2* can suppress recombination by an equivalent amount. The rDNA recombination assay was performed as described in the legend to Fig. 1B, but CR treated strains were grown to log phase in 0.5% YPD before plating. (B) Treatment with NAM (5 mM) prevents CR from suppressing recombination. (C) Deletion of either *HST2* or *SIR2* results in increased rDNA recombination. A *fob1* $\Delta$  deletion suppresses hyper-recombination in a *sir2* $\Delta$  strain but only if *HST2* is present. Recombination



of *SIR2* (Fig. 1B). This showed that *HST2* does not necessarily act via *SIR2* as previously hypothesized (16), and raised the possibility that Hst2 might be the factor responsible for mediating Sir2-independent life-span extension by CR.

To test this hypothesis, we first determined whether inhibiting Hst2 enzymatic activity affected the ability of CR to extend life span. We used nicotinamide (NAM), a vitamin B<sub>3</sub> precursor that has been shown to inhibit yeast sirtuins in vitro (25, 26) and in vivo (25, 27). As reported for other yeast strains (19), the life span of W303AR5 *sir2* $\Delta$  *fob1* $\Delta$  was extended by mild CR (Fig. 1C). However, in the presence of NAM, there was no significant effect of CR on life span. The same effect was observed for strain BY4742 carrying an *hvk2* $\Delta$  (hexokinase 2) mutation, which is a genetic mimic of intense CR (11, 19) (Fig. 1D). Together, these experiments were consistent with the hypothesis that Hst2 (or another sirtuin) is required for Sir2-independent life-span extension by CR.

To determine whether the effect was due to Hst2 specifically, we tested whether deleting the *HST2* gene affected the ability of CR to extend life span. Although CR could extend the life span of an *hst2* $\Delta$  strain, it was unable to extend the life span of either *sir2* $\Delta$  *hst2* $\Delta$  (Fig. 2A) or *sir2* $\Delta$  *fob1* $\Delta$  *hst2* $\Delta$  strains (Fig. 2B). Thus, *HST2* is necessary for *SIR2*-independent life-span extension by CR.

To ensure that our results were not strain-specific, we also performed our experiments in BY4742, in which the Sir2-independent CR pathway was originally identified (19). Again, deletion of *HST2* in the *sir2* $\Delta$  *fob1* $\Delta$  strain completely prevented life-span extension by CR (Fig. 2C). In the *hvk2* $\Delta$  CR mimetic, deletion of *HST2* strongly abrogated but did not completely prevent life-span extension in the *sir2* $\Delta$  *fob1* $\Delta$  background (Fig. 2D), suggesting the possible involvement of another factor in life-span extension.

It has been postulated that Sir2-independent life-span extension is unrelated to rDNA

assays were performed as described in the legend to Fig. 1B. *HST2* was disrupted in W303AR5 using the *kan*<sup>r</sup> marker, and *FOB1* was disrupted using the *hph*<sup>r</sup> marker (31, 32).

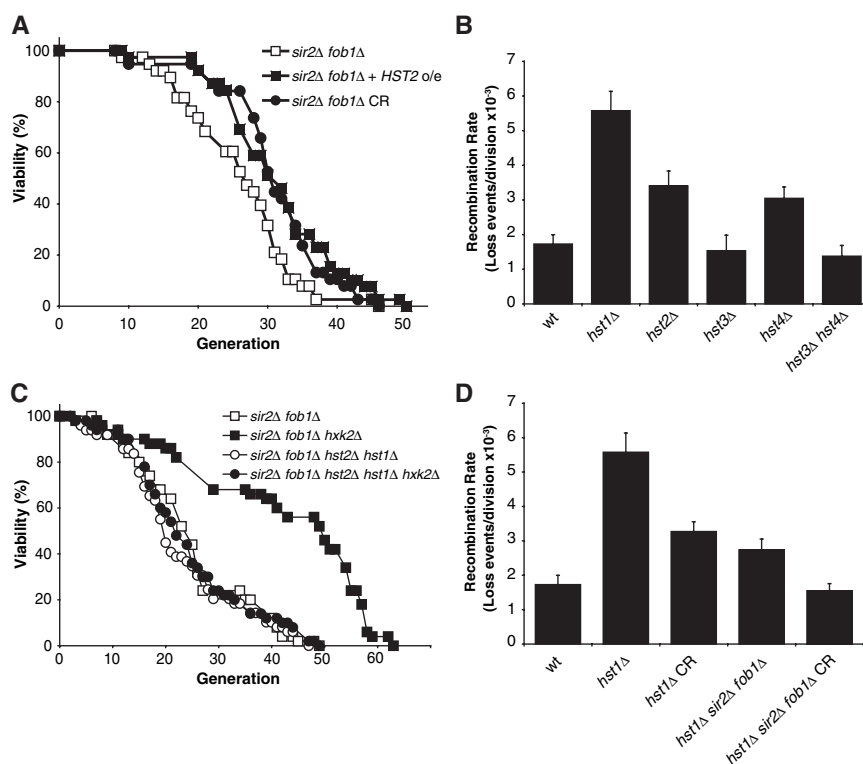


**Fig. 4.** Additional *HST2* promotes life span in the absence of Sir2 and Hst1 plays a supportive role. (A) The average and maximum life span of W303AR5 *sir2* $\Delta$  *fob1* $\Delta$  are increased by overexpression of *HST2* similar to growth on 0.5% glucose. Life spans were analyzed as described (11). Average life spans: W303AR5 *sir2* $\Delta$  *fob1* $\Delta$  2.0% glucose 25.1, 0.5% glucose 29.9; W303AR5 *sir2* $\Delta$  *fob1* $\Delta$  *HST2* overexpression (o/e) 30.5. (B) Deletion of *HST1*, *HST2*, or *HST4* increases rDNA recombination. (C) Deletion of *HST1* blocks the residual life-span extension by *hvk2* $\Delta$  in a *sir2* $\Delta$  *fob1* $\Delta$  *hst2* $\Delta$  strain. Average life spans: BY4742 *sir2* $\Delta$  *fob1* $\Delta$  24.8; *sir2* $\Delta$  *fob1* $\Delta$  *hvk2* $\Delta$  41.8; *sir2* $\Delta$  *fob1* $\Delta$  *hst2* $\Delta$  *hst1* $\Delta$  22.7; *sir2* $\Delta$  *fob1* $\Delta$  *hst2* $\Delta$  *hst1* $\Delta$  *hvk2* $\Delta$  24.8. (D) Deletion of *HST1* does not prevent CR from suppressing recombination in a wild-type or a *sir2* $\Delta$  *fob1* $\Delta$  strain.

recombination (19). However, our data provide strong evidence to the contrary. (i) Consistent with the life-span data, CR suppressed rDNA recombination to about 50% of the initial rate in the *sir2* $\Delta$  *fob1* $\Delta$  strain, the same reduction as seen for wild-type cells on CR or overexpressing *HST2* (Fig. 3A). (ii) The ability of CR to suppress recombination is completely blocked by NAM (Fig. 3B), again consistent with the life-span data above. (iii) Deletion of *HST2*

from a wild-type strain led to an approximate doubling in the rates of rDNA recombination, which could be suppressed by a *fob1* deletion (Fig. 3C), demonstrating that *HST2* is necessary for rDNA stability, even in a wild-type strain. (iv) Although single deletions of *HST2* or *SIR2* in a *fob1* $\Delta$  strain resulted in rDNA recombination rates similar to or lower than those of the wild type, deletion of both *HST2* and *SIR2* in this background resulted in a

fivefold increase in recombination (Fig. 3C). This elevated recombination was only slightly reduced by CR. Finally, we observed a highly significant negative correlation between life span and rDNA recombination rate (fig. S3). Although these data do not exclude the possibility that CR may mediate yeast life span independently of its effects on the rDNA, these data provide strong evidence that CR extends life span by suppressing rDNA recombination irrespective of whether *SIR2* is present or absent. They also demonstrate that in a *sir2Δ fob1Δ* strain, Hst2 is critical for maintaining rDNA stability.

Although the deletion of *HST2* blocked the ability of CR to extend life span in the *sir2Δ fob1Δ* strain, it was formally possible that this was caused by toxic levels of ERCs in the strain, precluding alternative CR pathways from taking effect. Therefore, we determined whether *HST2* could increase life span when overexpressed in order to test whether *HST2* is a bona fide longevity gene (9). Consistent with the ability of *HST2* to increase rDNA silencing and decrease rDNA recombination (Fig. 1 and fig. S1), overexpression of *HST2* in W303AR5 *sir2Δ fob1Δ* extended life span to the same extent as CR in this strain background (Fig. 4A), as well as in a wild-type strain (fig. S4). No additive effect of *HST2* overexpression and CR was observed, indicating that *HST2* and CR extend life span of *sir2Δ fob1Δ* mutants through the same pathway (28).

Next, we investigated whether the residual life-span extension seen for the *hxxk2Δ* mutant (a mimic of intense CR) lacking *SIR2* and *HST2* (Fig. 2C) was due to the activity of another sirtuin. As previously reported (16), deletion of *HST1* markedly increased rDNA recombination in a wild-type strain (Fig. 4B). Although deleting *HST3* and *HST4* together has been shown to decrease chromosomal stability and increase mitotic recombination (29), we did not observe increased rDNA recombination in a W303AR5 *hst3Δ hst4Δ* strain, although recombination in an *hst4Δ* single mutant is about twice as high as that in the wild type. Because deletion of *HST1* had the greatest effect on rDNA recombination, we suspected that Hst1 might be the factor responsible for the residual life-span extension. This hypothesis was consistent with our finding that the general sirtuin inhibitor NAM completely blocked the life-span extension of a *sir2Δ fob1Δ* strain by *hxxk2Δ* (Fig. 1D) and a recent report that Hst1 functions in the nucleus with Hst2 in gene silencing (23). Whereas deletion of either *HST3* or *HST4* in this strain did not affect the ability of *hxxk2Δ* to extend life span (fig. S5), deletion of *HST1* completely eliminated the residual life-span extension provided by *hxxk2Δ* in the BY4742 *sir2Δ fob1Δ hst2Δ* strain (Fig. 4C).

In a previous study, the life span of a *sir2Δ fob1Δ hst1Δ* strain was extended by CR (19), leading the authors to conclude that *HST1* plays

no role in CR. Indeed, in agreement with this finding, we find that CR is effective in suppressing recombination of such a mutant (Fig. 4D). However, this study implies that *HST2* underlies the CR-mediated life-span extension of this strain and that *HST1* plays a minor role that is observed only in the absence of *SIR2* and *HST2*.

Our results show that *HST2* is responsible for Sir2-independent life-span extension by CR and that it does so by suppressing rDNA recombination, the same mechanism by which *SIR2* extends life span. These findings highlight the importance of genomic stability as a determinant of yeast life span and raise the likelihood that multiple members of the sirtuin family in higher organisms also play critical roles in maintaining genomic stability and possibly in extending life span during times of adversity.

References and Notes

1. A. A. Falcon, J. P. Aris, *J. Biol. Chem.* **278**, 41607 (2003).
2. D. A. Sinclair, L. Guarente, *Cell* **91**, 1033 (1997).
3. T. Kobayashi, D. J. Heck, M. Nomura, T. Horiuchi, *Genes Dev.* **12**, 3821 (1998).
4. P. A. Defossez *et al.*, *Mol. Cell* **3**, 447 (1999).
5. J. S. Smith *et al.*, *Proc. Natl. Acad. Sci. U.S.A.* **97**, 6658 (2000).
6. S. Imai, C. M. Armstrong, M. Kaerberlein, L. Guarente, *Nature* **403**, 795 (2000).
7. K. G. Tanner, J. Landry, R. Sternglanz, J. M. Denu, *Proc. Natl. Acad. Sci. U.S.A.* **97**, 14178 (2000).
8. J. C. Tanny, D. Moazed, *Proc. Natl. Acad. Sci. U.S.A.* **98**, 415 (2001).
9. M. Kaerberlein, M. McVey, L. Guarente, *Genes Dev.* **13**, 2570 (1999).
10. E. J. Masoro, *Exp. Gerontol.* **35**, 299 (2000).
11. S. J. Lin, P. A. Defossez, L. Guarente, *Science* **289**, 2126 (2000).
12. R. M. Anderson, K. J. Bitterman, J. G. Wood, O. Medvedik, D. A. Sinclair, *Nature* **423**, 181 (2003).
13. S. J. Lin *et al.*, *Nature* **418**, 344 (2002).
14. B. Rogina, S. L. Helfand, *Proc. Natl. Acad. Sci. U.S.A.* **101**, 15998 (2004).

15. J. G. Wood *et al.*, *Nature* **430**, 686 (2004).
16. S. Perrod *et al.*, *EMBO J.* **20**, 197 (2001).
17. K. Houthoofd, B. P. Braeckman, T. E. Johnson, J. R. Vanfleteren, *Exp. Gerontol.* **38**, 947 (2003).
18. J. C. Jiang, J. Wawryn, H. M. Shantha Kumara, S. M. Jazwinski, *Exp. Gerontol.* **37**, 1023 (2002).
19. M. Kaerberlein, K. T. Kirkland, S. Fields, B. K. Kennedy, *PLoS Biol.* **2**, E296 (2004).
20. D. A. Sinclair, J. Wood, data not shown.
21. M. Kaerberlein, K. T. Kirkland, S. Fields, B. K. Kennedy, *Mech. Ageing Dev.* **126**, 491 (2005).
22. B. K. Kennedy, N. R. Austriaco Jr., J. Zhang, L. Guarente, *Cell* **80**, 485 (1995).
23. A. Halme, S. Bumgarner, C. Styles, G. R. Fink, *Cell* **116**, 405 (2004).
24. S. M. Gasser, M. M. Cockell, *Gene* **279**, 1 (2001).
25. K. J. Bitterman, R. M. Anderson, H. Y. Cohen, M. Latorre-Esteves, D. A. Sinclair, *J. Biol. Chem.* **277**, 45099 (2002).
26. J. Landry, J. T. Slama, R. Sternglanz, *Biochem. Biophys. Res. Commun.* **278**, 685 (2000).
27. C. M. Gallo, D. L. Smith Jr., J. S. Smith, *Mol. Cell. Biol.* **24**, 1301 (2004).
28. D. W. Lammung *et al.*, data not shown.
29. C. B. Brachmann *et al.*, *Genes Dev.* **9**, 2888 (1995).
30. K. T. Howitz *et al.*, *Nature* **425**, 191 (2003).
31. M. S. Longtine *et al.*, *Yeast* **14**, 953 (1998).
32. A. L. Goldstein, J. H. McCusker, *Yeast* **15**, 1541 (1999).
33. We thank members of the Lin and Sinclair labs for valuable insights and J. Wood for critical reading of the manuscript. This work was supported by the National Institute of General Medical Sciences, the National Institute on Aging, the Harvard-Armisen Foundation, and The Paul F. Glenn Laboratories for the Biological Mechanisms of Aging at Harvard. S.-J.L. and D.A.S. are Ellison Medical Research Foundation New Research Scholars. D.W.L. is supported by a National Eye Institute training grant. D.A.S. is a cofounder and board member of, and has equity in, Sirtris Pharmaceuticals, a company whose goal is to discover sirtuin-modulating drugs.

Supporting Online Material

www.sciencemag.org/cgi/content/full/1113611/DC1  
 Materials and Methods  
 Figs. S1 to S5  
 References and Notes

15 April 2005; accepted 8 July 2005  
 Published online 28 July 2005;  
 10.1126/science.1113611  
 Include this information when citing this paper.

# Structure of SARS Coronavirus Spike Receptor-Binding Domain Complexed with Receptor

Fang Li,<sup>1</sup> Wenhui Li,<sup>3</sup> Michael Farzan,<sup>3</sup> Stephen C. Harrison<sup>1,2\*</sup>

The spike protein (S) of SARS coronavirus (SARS-CoV) attaches the virus to its cellular receptor, angiotensin-converting enzyme 2 (ACE2). A defined receptor-binding domain (RBD) on S mediates this interaction. The crystal structure at 2.9 angstrom resolution of the RBD bound with the peptidase domain of human ACE2 shows that the RBD presents a gently concave surface, which cradles the N-terminal lobe of the peptidase. The atomic details at the interface between the two proteins clarify the importance of residue changes that facilitate efficient cross-species infection and human-to-human transmission. The structure of the RBD suggests ways to make truncated disulfide-stabilized RBD variants for use in the design of coronavirus vaccines.

The SARS coronavirus (SARS-CoV) is the agent of severe acute respiratory syndrome, which emerged as a serious epidemic in 2002 to 2003, with over 8,000 infected cases and a

fatality rate of ~10% (1–4). Coronaviruses, which are large, enveloped, positive-strand RNA viruses, infect a variety of mammalian and avian species and can cause upper res-



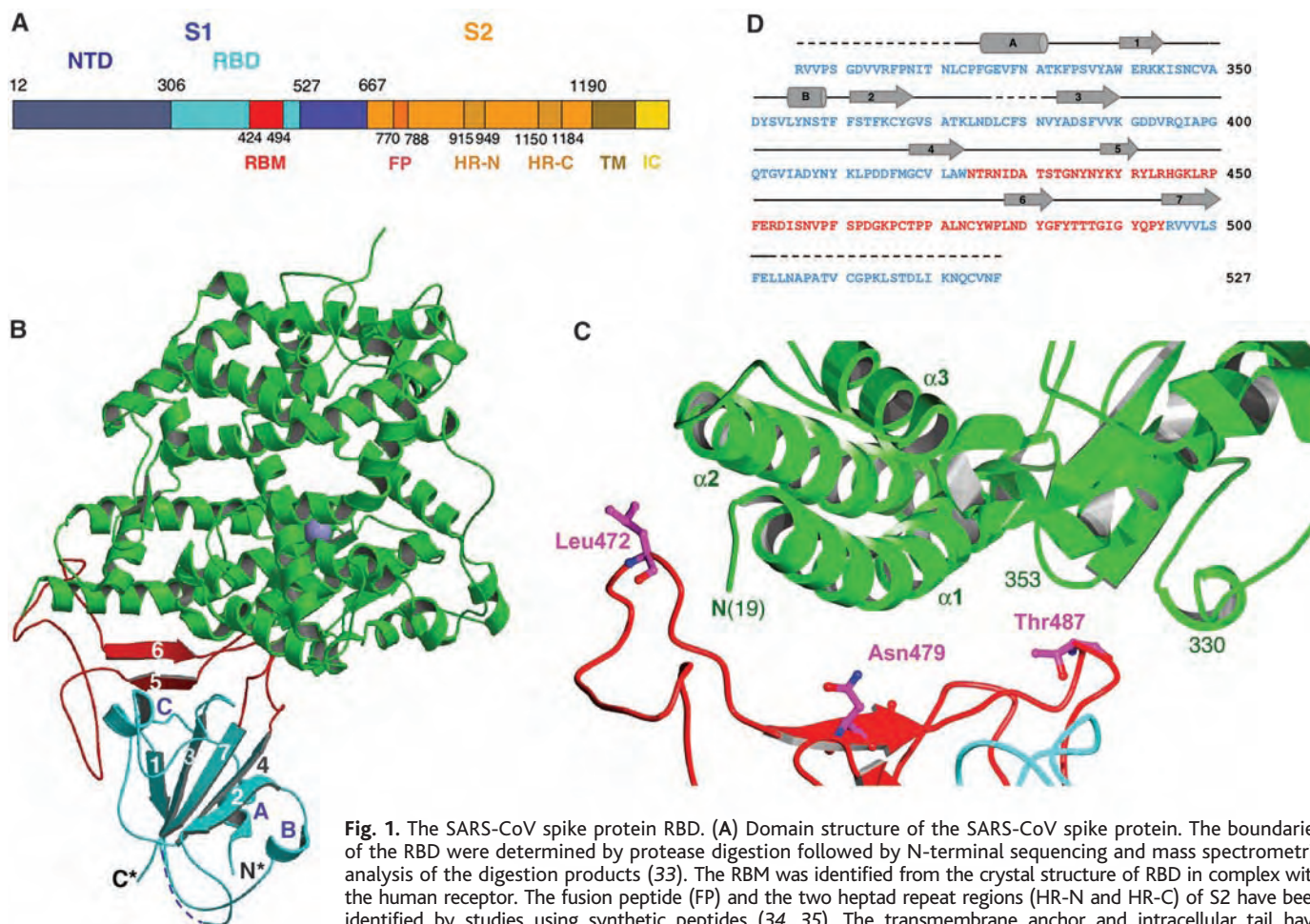


**Fig. 1.** The SARS-CoV spike protein RBD. (A) Domain structure of the SARS-CoV spike protein. The boundaries of the RBD were determined by protease digestion followed by N-terminal sequencing and mass spectrometric analysis of the digestion products (33). The RBM was identified from the crystal structure of RBD in complex with the human receptor. The fusion peptide (FP) and the two heptad repeat regions (HR-N and HR-C) of S2 have been identified by studies using synthetic peptides (34, 35). The transmembrane anchor and intracellular tail have assigned from sequence characteristics. (B) Crystal structure of the RBD (core structure in cyan and RBM in red) in complex of the human receptor ACE2 (green). (C) Detail of the binding interface, with side chains of three residues (Leu<sup>472</sup>, Asn<sup>479</sup>, and Thr<sup>487</sup> from left to right) critical for cross-species and human-to-human transmission of SARS-CoV. (D) Sequence and secondary structures of the RBD. Helices are drawn as cylinders, and strands are drawn as arrows. The RBM is in red; the remainder of the RBD is in cyan. Disordered regions are shown as dashed lines (36).

piratory, gastrointestinal, and central nervous system diseases (5). The large spike protein (S) on the virion surface mediates both cell attachment and membrane fusion (5). In the case of several avian and mammalian coronaviruses, S is cleaved by furin or a related protease into S1 and S2; the former bears the receptor attachment site; the latter, the fusion activity. The structures of refolded heptad-repeat fragments of S2 from the mouse hepatitis coronavirus (MHV) and from SARS-CoV (6–8) confirm earlier predictions (4) that the postfusion conformation has the trimer-of-hairpins organization characteristic of “class 1” fusion proteins, such as those of HIV, influen-

za virus, and Ebola virus (9). S on mature SARS-CoV virions does not appear to be cleaved, and the sequence that aligns with the MHV cleavage site lacks the essential residues for furin susceptibility (3, 4, 10, 11). We therefore refer to the S1 and S2 “regions” (12), which contain 666 and 583 amino acid residues, respectively (Fig. 1A).

Coronaviruses exploit a wide variety of cellular receptors (5). SARS-CoV and another human coronavirus, HCoV-NL63, both use as their receptor a cell-surface zinc peptidase, angiotensin-converting enzyme 2 (ACE2) (13, 14). The crystal structure of the ACE2 ectodomain (15) shows a claw-like N-terminal peptidase domain, with the active site at the base of a deep groove, and a C-terminal “collectrin” domain. A fragment of the S1 region, residues 318 to 510, is sufficient for tight binding to the peptidase domain of ACE2 (11, 16, 17). This fragment, the receptor-binding domain (RBD), is the critical determinant of virus-receptor interaction and thus of viral host range and tropism (18). SARS-CoV isolated from patients during the 2002–2003

epidemic, and also from milder sporadic cases in 2003 to 2004, appears to derive from a nearly identical virus circulating in palm civets and raccoon dogs (19, 20). Changes in just a few residues in the RBD can lead to efficient cross-species transmission (18, 20). The RBD also includes important viral-neutralizing epitopes (21–23), and it may be sufficient to raise a protective antibody response in inoculated animals.

We expressed the SARS-CoV spike protein RBD, residues 306 to 575, in Sf9 cells and purified the fragment (24). Brief treatment with chymotrypsin yielded a shorter fragment, residues 306 to 527. Soluble ACE2, residues 19 to 615, was expressed in Sf9 cells and purified as described in (24). The two components were mixed, and the complex was purified by size-exclusion chromatography on Superdex 200 (Amersham Biosciences, Piscataway, NJ). Crystals in space group *P*21, *a* = 82.3 Å, *b* = 119.4 Å, *c* = 113.2 Å,  $\beta$  = 91.2°, with two complexes per asymmetric unit, were grown at room temperature from a mother liquor containing 24% polyethylene glycol 6000,

<sup>1</sup>Department of Biological Chemistry and Molecular Pharmacology, Harvard Medical School and Laboratory of Molecular Medicine, and <sup>2</sup>Howard Hughes Medical Institute, Children’s Hospital, 320 Longwood Avenue, Boston, MA 02115, USA. <sup>3</sup>Department of Microbiology and Molecular Genetics, Harvard Medical School, New England Primate Research Center, Southborough, MA 01772, USA.

\*To whom correspondence should be addressed. E-mail: harrison@crystal.harvard.edu

150 mM NaCl, 100 mM Tris at pH 8.2, and 10% ethylene glycol. We determined the structure of the ACE2/SARS-CoV/RBD complex by molecular replacement with ACE2 as the search model, and we refined it at 2.9 Å resolution (24). The final model contains residues 19 to 615 of the N-terminal peptidase domain of human ACE2 and residues 323 to 502 (except for 376 to 381) of the RBD; as well as glycans N-linked to ACE2 residues 53, 90, 322, and 546 and to RBD residue 330; and 65 solvent molecules. The  $R_{\text{free}}$  is 27.5% and  $R_{\text{work}}$  is 22.1% (see table S1 for definitions).

The ACE2 peptidase domain has two lobes that close toward each other after substrate engagement (15). In one of the two complexes in the asymmetric unit of our crystals, ACE2 is fully open; in the other, it is slightly closed (fig. S1). The SARS-CoV S protein contacts the tip of one lobe of ACE2 (Fig. 1). It does not contact the other lobe, nor does it occlude the peptidase active site. Binding of the spike protein to ACE2 is not altered by the addition of a specific ACE2 inhibitor, which is expected to favor the closed state (18). Thus, both structural and biochemical data indicate that viral attachment is unaffected by the open-to-closed transition.

The RBD contains two subdomains (Fig. 1): a core and an extended loop. The core is a five-stranded anti-parallel  $\beta$  sheet ( $\beta 1$  to  $\beta 4$  and  $\beta 7$ ), with three short connecting  $\alpha$  helices ( $\alpha A$  to  $\alpha C$ ). There are nine cysteines in the chymotryptic fragment. Disulfide bonds connect cysteines 323 to 348, 366 to 419, and 467 to 474. The remaining cysteines are disordered but two (378 and 511) are in the same neighborhood and could form a disulfide in the recombinant fragment, even if they have other partners in the intact S protein. The extended loop subdomain lies at one edge of the core; it presents a gently concave outer surface formed by a two-stranded  $\beta$  sheet ( $\beta 5$  and  $\beta 6$ ). The base of this concavity cradles the N-terminal helix of ACE2; a ridge to one side of it, which is reinforced by the Cys<sup>467</sup>-Cys<sup>474</sup> disulfide bridge, contacts the loops between ACE2 helices  $\alpha 2$  and  $\alpha 3$ ; a ridge to the other side inserts between a short ACE2 helix (residues 329 to 333) and a  $\beta$  hairpin at ACE2 residue 353 (Fig. 1C). Residues 445 to 460 of the RBD anchor the entire receptor-binding loop to the core of the RBD. We refer to this loop (residues 424 to 494), which makes all the contacts with ACE2, as the receptor-binding motif (RBM).

The RBM surface is complementary to the receptor tip, with about 1700 Å<sup>2</sup> of buried surface at the interface (Fig. 2A and fig. S2), consistent with their high affinity (dissociation constant  $K_d \sim 10^{-8}$ ) (18, 21). A total of 18 residues of the receptor contact 14 residues of the viral spike protein (Table 1). Networks of hydrophilic interactions, which occur largely among amino acid side chains, predominate.

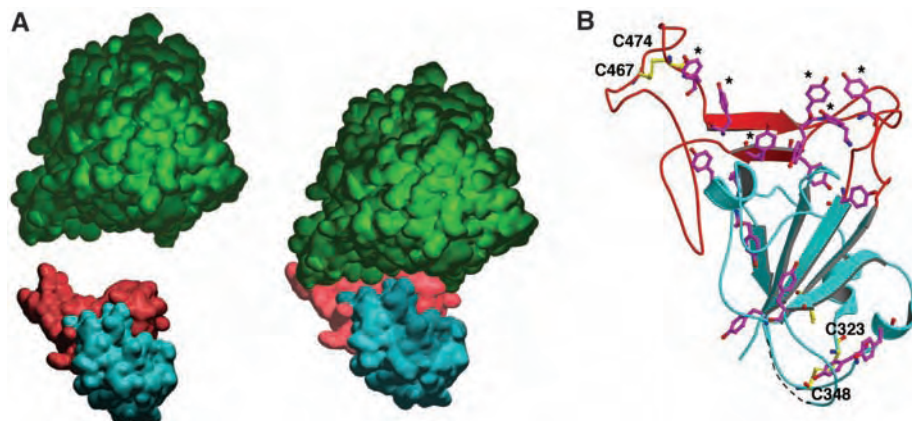


**Fig. 2.** Features contributing to specific recognition of ACE2 by the SARS-CoV RBD. (A) Surface complementarity, Space-filling representation of ACE2 (in green), RBD (core structure in cyan and RBM in red), and the complex of ACE2 and RBD are shown. The complex buries 1700 Å<sup>2</sup> at the binding interface. (B) Distribution of tyrosines (magenta) and cysteines (yellow) on the RBD. The RBM is particularly tyrosine-rich. The six tyrosines that contact ACE2 are accompanied by an asterisk. The three disulfide bonds link C323 to C348, C366 to C419, and C467 to C474; two are labeled, and the third is partly concealed by the lower corner of the  $\beta$  sheet.

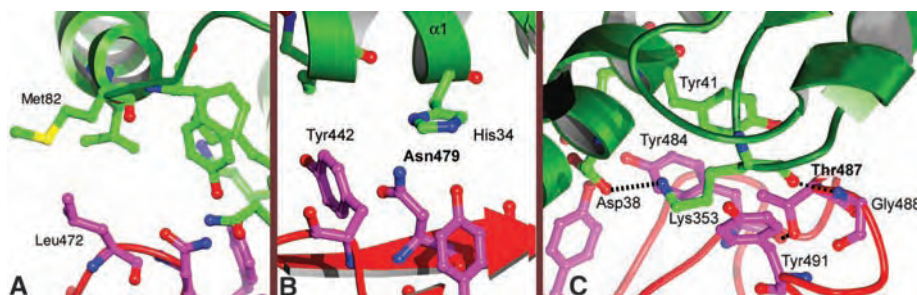


**Fig. 3.** Residues important for species specificities of SARS-CoV. (A) Met<sup>82</sup> of human ACE2 is asparagine in rat ACE2, introducing a glycan that appears to interfere with infection of rat cells. (B) Asn<sup>479</sup> (boldface) is present in most SARS-CoV sequences from human specimens. Lys<sup>479</sup>, which is found in most sequences from palm-civet specimens, would have steric and electrostatic interference from residues (e.g., His<sup>34</sup>) on the N-terminal helix of human ACE2. (C) Thr<sup>487</sup> (boldface) appears to enhance human-to-human transmission of SARS-CoV. The methyl group of Thr<sup>487</sup> lies in a hydrophobic pocket at the ACE2/RBD interface. On rat and mouse ACE2, residue 353 is histidine, disfavoring viral binding. The dashed black lines indicate hydrogen bonds.

Six RBM residues at this interface are tyrosines, which present both a polar hydroxyl group and a hydrophobic aromatic ring (Fig. 2B).

Coronaviruses are classified in three groups (5); SARS-CoV belongs to group 2 (fig. S3). Spike-protein sequences from several members of group 2 lead us to expect that all have rather similar structures, including the RBD core (fig. S3). The SARS-CoV RBM is substantially shorter than are the corresponding regions in several other group-2 viral spike proteins, however, and it has no evident sequence similarity to the others (fig. S3). Thus, this extended loop is probably a hypervariable decoration of an otherwise-conserved domain. In the case of MHV, the receptor (murine carcinoembryonic antigen cell adhesion molecule 1a, or CEACAM1a) (25, 26) makes contact not with the extended-loop subdomain (nor, indeed, with any part of the domain homologous to the SARS-CoV RBD), but rather with structures in the N-terminal region of the spike protein (27). Receptors and receptor-binding regions

of other group-2 coronaviruses have not been identified. The group-1 human coronavirus 229E receptor is aminopeptidase N; the corresponding RBD on its spike protein is known (28).

The SARS-CoV appears to derive from a cross-species infection with a coronavirus isolated from palm civets (19, 20). S-gene sequences from civet and human specimens obtained during the 2002-to-2003 epidemic show that their RBDs differ at only four positions, residues 344, 360, 479, and 487, but the human viral spike protein binds the human receptor 10<sup>3</sup> to 10<sup>4</sup> times more tightly than does its civet spike counterpart (18). Residues 344 and 360 are far from the binding interface in the complex described here, and mutation to the corresponding civet CoV residues does not affect affinity or infectivity (18). The critical changes are therefore at positions 479 and 487, both of which lie in the RBD-receptor contact (Figs. 1 and 3 and Table 1).

**Table 1.** Contacts between ACE2 and SARS-CoV RBD. Residues in ACE2 that contact the RBD are listed by their position (numbers across the top of each column) and by their single-letter identity (36) in the palm-civet, mouse, rat,

and human receptors. The residues they contact in the structure described here and their position numbers in the spike proteins from human isolates are shown at the bottom of each column.

24	27	31	34	37	38	41	42	45	79	82	83	90	325	329	330	353	354	
L	T	T	Y	Q	E	Y	Q	V	L	T	Y	D	Q	E	N	K	G	civet ACE2
N	T	N	Q	E	D	Y	Q	L	T	S	F	T	Q	A	N	H	G	mouse ACE2
K	S	K	Q	E	D	Y	Q	L	I	N	F	N	P	T	N	H	G	rat ACE2
Q	T	K	H	E	D	Y	Q	L	L	M	Y	N	Q	E	N	K	G	human ACE2
N473	Y475	Y475	Y440	Y491	Y436	Y484	Y436	Y484	L472	L472	N473	T402	R426	R426	T486	G488	Y491	human SARS
		Y442	N479			T486	Y484				Y475					T487	G488	
						T487										Y491		

The changes at these two positions are relatively subtle. In most viral sequences from palm-civet specimens, residue 479 is lysine and 487 is serine, whereas in SARS-CoV sequences from the 2002–2003 epidemic, these residues are asparagine and threonine, respectively. The presence of lysine at 479 reduces affinity for human but not for civet ACE2; serine at 487 reduces affinity for both receptors (18). Position 479 lies opposite the ACE2 N-terminal helix ( $\alpha 1$ ), on which several residues differ in identity between civet and human (Table 1). Some civet coronavirus sequences have asparagine at position 479, and the difference does not appear to be critical for binding to the civet receptor (18). At position 487 in the spike protein, replacing threonine (SARS-CoV) with serine (civet viral sequences) would remove the threonine methyl group, which lies in a hydrophobic pocket bounded by atoms in the side chains of Tyr<sup>41</sup> and Lys<sup>353</sup> on the receptor and Tyr<sup>484</sup> in the RBM (Fig. 3C). This pocket appears to be relatively inflexible. A main-chain hydrogen bond (carbonyl of ACE2 Lys<sup>353</sup> to amide of RBD Gly<sup>488</sup>) fixes the relative positions of receptor and spike protein quite precisely. Moreover, the Thr<sup>487</sup> rotamer is determined by a hydrogen bond from O $\gamma$  to the main-chain carbonyl of Tyr<sup>484</sup>; the aliphatic part of the Lys<sup>353</sup> side chain is sandwiched between the rings of ACE2 Tyr<sup>41</sup> and RBD Tyr<sup>491</sup>, and the  $\epsilon$ -NH<sup>+</sup> is neutralized by ACE2 Asp<sup>38</sup>. Mutation to serine would thus leave a hard-to-fill van der Waals hole; indeed, a mutation in which Thr<sup>487</sup> is replaced by Ser in the human RBD decreases affinity for human ACE2 by more than 20-fold (18). Civet ACE2 is essentially identical to human ACE2 at all the relevant positions in the vicinity of this interaction; like the human receptor, it appears to bind RBDs with threonine at 487 more tightly than those with serine (18). All of the more than 100 S-protein sequences obtained during the 2002–2003 SARS epidemic have threonine at this position, whereas all 14 such sequences from palm-civet and raccoon-dog isolates have serine (29, 30).

Viruses from sporadic SARS cases during 2003 to 2004, each of which was an independent cross-species event from which no human-to-human transmission occurred, all

had asparagine at 479 and serine at 487 (29, 30). It is therefore plausible that a key factor determining severity (and possibly human-to-human transmission) is the presence or absence of a  $\gamma$ -methyl group on the 487 side chain. The 2003–2004 sequences differed, however, at two other RBD positions from those sequences obtained during the epidemic of the previous winter: Leu<sup>472</sup> had changed to proline and Asp<sup>480</sup> to glycine. Inspection of the model suggests that the leucine-to-proline change might have contributed to attenuation, by reducing the spike-receptor contact surface (Fig. 3A). A similar rationale is harder to find for the aspartate-to-glycine substitution, because the aspartyl side chain projects into solution, and mutation of this residue to alanine has no effect on RBD binding to ACE2 (16).

Two other species differences are worth noting. Rat ACE2 does not support infection by SARS-CoV, and mouse ACE2 does so only inefficiently (30). At position 82, where the human receptor has a methionine, the rat protein has a glycosylated asparagine; the glycan would disrupt by steric interference a hydrophobic contact between Met<sup>82</sup> and Leu<sup>472</sup> in the RBM (Fig. 3A). At position 353, where the human receptor has a lysine critical for the contact with Thr<sup>487</sup> in the RBM (Fig. 3B), the rat receptor has histidine. Mouse ACE2 also has histidine at 353, but it does not have a glycosylation site at 82. It thus bears one but not both of the differences that render rat ACE2 inactive as a receptor, and mutation of His<sup>353</sup> to lysine in mouse ACE2 allows high-level infection of murine cells by SARS-CoV (30).

The residues singled out for description in the preceding paragraphs are not, of course, the only ones critical for the tight complementarity of the SARS-CoV RBD and human (or palm civet) ACE2. They are simply the positions at which there are differences among isolates and receptors important for binding and entry. Other species might in principle harbor variants of the same virus that would require changes at different positions to be able to infect human cells, and other changes in the civet virus might permit cross-species infection even in the absence of the serine-to-threonine mutation at position 487. The structure might

allow one to recognize such changes in future animal isolates. For example, the human receptor (but not the civet receptor) bears an N-linked glycan at position 90. Mutation of Asn<sup>90</sup> to eliminate the glycan enhances S-protein-mediated binding and infection of human cells by pseudotyped lentiviruses (18). The glycan faces a loop in the RBD containing residues 399 to 412. Changes in this loop that reduce likely interference with the glycan might have the same enhancing effects as does elimination of the glycan on the receptor or mutation of Ser<sup>487</sup> to threonine on the S protein.

Neutralizing antibodies against SARS-CoV recognize epitopes in the RBD (21–23). For example, a high-affinity recombinant human monoclonal antibody, 80R, which is sensitive to mutation within the RBM, inhibits viral entry by blocking association of virus and receptor (21, 31). The soluble SARS-CoV RBD is therefore of potential use as an immunogen (23, 32). In the structure described here, the interface of the RBD with the receptor is very well defined, but the opposite face of the RBD is more disordered. The latter surface would interact with the rest of the spike protein, and it indeed contains the N and C termini of the RBD fragment as well as the disordered loop, residues 376 and 381. Thus, this face of the protein could be modified in various ways in the molecular engineering of a candidate vaccine. The loop from 376 to 381 could probably be shortened and the disordered cysteines removed; other disulfides could be introduced to add stability; and the C-terminal segment could be used to link the RBD to an oligomeric core. Of the 23 glycosylation sites on S, three are in the RBD. Only one (Asn<sup>330</sup>) is sufficiently ordered in our structure to show even a single sugar, and all are well separated from the RBM. Glycosylation is therefore unlikely to interfere with potential neutralizing epitopes within the RBD; introduction of new glycosylation sites could in principle “focus” the antigenicity of a candidate immunogen.

**References and Notes**

1. T. G. Ksiazek et al., *N. Engl. J. Med.* **348**, 1953 (2003).
2. J. S. Peiris et al., *Lancet* **361**, 1319 (2003).
3. M. A. Marra et al., *Science* **300**, 1399 (2003).
4. P. A. Rota et al., *Science* **300**, 1394 (2003).

5. M. M. C. Lai, K. V. Holmes, in *Fields' Virology*, D. M. Knipe, P. M. Howley, Eds. (Lippincott, Williams, and Wilkins, Philadelphia, PA, 2001).
6. Y. Xu et al., *J. Biol. Chem.* **279**, 49414 (2004).
7. Y. Xu et al., *J. Biol. Chem.* **279**, 30514 (2004).
8. V. M. Supekar et al., *Proc. Natl. Acad. Sci. U.S.A.* **101**, 17958 (2004).
9. W. Weissenhorn et al., *Mol. Membr. Biol.* **16**, 3 (1999).
10. M. J. Moore et al., *J. Virol.* **78**, 10628 (2004).
11. X. Xiao, S. Chakraborti, A. S. Dimitrov, K. Gramatikoff, D. S. Dimitrov, *Biochem. Biophys. Res. Commun.* **312**, 1159 (2003).
12. T. M. Gallagher, M. J. Buchmeier, *Virology* **279**, 371 (2001).
13. W. Li et al., *Nature* **426**, 450 (2003).
14. H. Hofmann et al., *Proc. Natl. Acad. Sci. U.S.A.* **102**, 7988 (2005).
15. P. Towler et al., *J. Biol. Chem.* **279**, 17996 (2004).
16. S. K. Wong, W. Li, M. J. Moore, H. Choe, M. Farzan, *J. Biol. Chem.* **279**, 3197 (2004).
17. G. J. Babcock, D. J. Eshaki, W. D. Thomas Jr., D. M. Ambrosino, *J. Virol.* **78**, 4552 (2004).
18. W. Li et al., *EMBO J.* **24**, 1634 (2005).
19. Y. Guan et al., *Science* **302**, 276 (2003).
20. H. D. Song et al., *Proc. Natl. Acad. Sci. U.S.A.* **102**, 2430 (2005).
21. J. Sui et al., *Proc. Natl. Acad. Sci. U.S.A.* **101**, 2536 (2004).
22. E. N. van den Brink et al., *J. Virol.* **79**, 1635 (2005).
23. Y. He, H. Lu, P. Siddiqui, Y. Zhou, S. Jiang, *J. Immunol.* **174**, 4908 (2005).
24. Materials and methods are available as supporting materials on *Science* Online.
25. R. K. Williams, G. S. Jiang, K. V. Holmes, *Proc. Natl. Acad. Sci. U.S.A.* **88**, 5533 (1991).
26. G. S. Dveksler et al., *J. Virol.* **65**, 6881 (1991).
27. H. Kubo, Y. K. Yamada, F. Taguchi, *J. Virol.* **68**, 5403 (1994).
28. A. Bonavia, B. D. Zelus, D. E. Wentworth, P. J. Talbot, K. V. Holmes, *J. Virol.* **77**, 2530 (2003).
29. Chinese SARS Molecular Epidemiology Consortium, *Science* **303**, 1666 (2004).
30. W. Li et al., *J. Virol.* **78**, 11429 (2004).
31. J. Sui et al., *J. Virol.* **79**, 5900 (2005).
32. Y. He et al., *Biochem. Biophys. Res. Commun.* **324**, 773 (2004).
33. F. Li, W. Li, M. Farzan, S. C. Harrison, data not shown.
34. B. Sainz Jr., J. M. Raush, W. R. Gallaher, R. F. Garry, W. C. Wimley, *J. Virol.* **79**, 7195 (2005).
35. Y. Xu et al., *Biochemistry* **43**, 14064 (2004).
36. Single-letter abbreviations for the amino acid residues are as follows: A, Ala; C, Cys; D, Asp; E, Glu; F, Phe; G, Gly; H, His; I, Ile; K, Lys; L, Leu; M, Met; N, Asn; P, Pro; Q, Gln; R, Arg; S, Ser; T, Thr; V, Val; W, Trp; and Y, Tyr.
37. We thank staff at the Advanced Light Source beamlines 8.2.1 and 8.2.2 for assistance and M. Berardi and E. Settembre for discussions. This work was supported by NIH grants CA13202 (to S.C.H.) and AI061601 (to M.R.F.). S.C.H. is an Investigator in the Howard Hughes Medical Institute. Coordinates and structure factors have been submitted to the Protein Data Bank with accession number 2AJF.

## Supporting Online Material

www.sciencemag.org/cgi/content/full/309/5742/1864/DC1

## Materials and Methods

Figs. S1 to S4

Table S1

References

22 June 2005; accepted 11 August 2005

10.1126/science.1116480

## Toward High-Resolution de Novo Structure Prediction for Small Proteins

Philip Bradley, Kira M. S. Misura, David Baker\*

The prediction of protein structure from amino acid sequence is a grand challenge of computational molecular biology. By using a combination of improved low- and high-resolution conformational sampling methods, improved atomically detailed potential functions that capture the jigsaw puzzle-like packing of protein cores, and high-performance computing, high-resolution structure prediction (<1.5 angstroms) can be achieved for small protein domains (<85 residues). The primary bottleneck to consistent high-resolution prediction appears to be conformational sampling.

It has been known for more than 40 years that the three-dimensional structures of proteins are completely determined by their amino acid sequences (1), and the prediction of protein structure from amino acid sequence—the “de novo” structure prediction problem—is a long-standing challenge in computational biology and chemistry. Although there are notable exceptions, the majority of protein structures are likely to be at global free-energy minima for their amino acid sequences. The de novo protein structure prediction problem hence is to find the lowest free-energy structure for a specified amino acid sequence. The problem is challenging because the size of the conformational space to be searched is vast (2) and because the accurate calculation of the free energies of protein conformations in solvent is difficult.

Although there has been considerable progress in low-resolution de novo protein struc-

ture prediction (3), both the accuracy and the reliability of the structural models produced by these methods is fairly low:  $C_{\alpha}$ -RMSDs (root mean square deviation of alpha-carbon coordinates after optimal superposition) of ~4 Å with incorrect packing of the amino acid side chains. Achieving higher resolution requires both more physically realistic energy functions and better conformational searching; the problem is difficult because the more realistic the energy function, the more rugged the landscape, and thus the more difficult it is to search. Here, we show that high-resolution de novo structure prediction can be achieved by generating structurally diverse populations of low-resolution models and refining these structures in the context of a physically realistic all-atom energy function.

Critical to high-resolution structure prediction is a force field for which native structures are low in free energy compared with non-native structures and a refinement protocol that can efficiently navigate the corresponding free-energy landscape. We have developed an all-atom force field (4) that focuses on short-range interactions—primarily van der Waals packing,

hydrogen bonding, and desolvation—while neglecting long-range electrostatics. The high-resolution refinement protocol (5, 6) is designed to search in the local neighborhood of a starting model for low-energy structures. The protocol consists of multiple rounds of Metropolis Monte Carlo with minimization (7); each trial consists of a random perturbation of one or several backbone torsion angles, fast side-chain optimization using a rotamer representation (8, 9), and a gradient-based minimization of the energy function with respect to backbone and side-chain torsion angles. In this way, the continuous space of backbone conformations and the discrete set of side-chain packing arrangements are searched simultaneously. Details on the energy function and methods are provided in (10).

Figure 1 and fig. S1 illustrate the challenge of high-resolution de novo structure prediction. All-atom refinement trajectories begun at the native state produce models (refined natives) that sample a deep near-native free-energy basin. Although these structures typically have lower all-atom energies than do non-native structures, Rosetta de novo models—built from an extended-chain starting conformation—do not sample close enough to the native structure to fall into this narrow energy well during all-atom refinement. The narrow widths of the native basins reflect the fact that nativelylike side-chain packing can be disrupted by even relatively small backbone perturbations. Thus, the critical step in high-resolution structure prediction is generating low-resolution models that are within the “radius of convergence” of the native free-energy minimum using the all-atom refinement protocol. This is challenging, because the low-resolution search integrates out the side-chain degrees of freedom to smooth the energy landscape and hence lacks the detail necessary to reliably discriminate nativelylike models, leading to false minima. We attempt to overcome this problem by generating low-resolution models for a large number of se-

University of Washington, Department of Biochemistry, and Howard Hughes Medical Institute, Box 357350, Seattle, WA 98195, USA.

\*To whom correspondence should be addressed. E-mail: dabaker@u.washington.edu

**Table 1.** Benchmark proteins and results. Protein Data Bank (PDB) (18) or Structural Classification of Proteins (SCOP) (19) ID is given in column 1 (10). Protein length, fraction alpha helix, and fraction beta strand are given in columns 2 to 4.  $C_{\alpha}$ -RMSD values for the model with the lowest all-atom energy in rounds

ID	L	% $\alpha$	% $\beta$	Round 1	Round 2	Cluster	Protein name
1b72A	49	69	0	0.8 (0.8)	1.1 (0.9)	1.0	Hox-B1 homeobox protein
1shfA	59	5	40	11.1 (9.0)	10.8 (8.5)	10.9	Fyn tyrosine kinase
1tif_	59	22	37	5.3 (2.3)	4.1 (2.8)	3.8	IF3-N
2reb_2	60	61	20	1.2 (0.9)	2.1 (1.6)	1.3	RecA
1r69_	61	63	0	2.1 (2.4)	1.2 (1.5)	1.7	434 repressor
1csp_	67	4	53	5.1 (4.5)	4.7 (4.2)	5.1	Cold-shock protein
1di2A_	69	46	33	2.6 (2.3)	2.6 (2.2)	1.9	RNA binding protein A
1n0uA4	69	43	24	9.9 (8.3)	10.2 (8.1)	2.7	Elongation factor 2
1mla_2	70	34	37	8.4 (7.3)	8.7 (8.1)	7.2	Malonyl-CoA ACP transacylase
1af7_	72	72	0	10.1 (7.9)	10.4 (8.1)	1.7	Cher domain 1
1ogwA_	72	26	33	2.7 (2.3)	1.0 (1.0)	2.6	Ubiquitin
1dcjA_	73	31	27	3.2 (2.2)	2.5 (2.4)	2.0	Yhhp
1dtjA_	74	39	27	1.0 (0.8)	1.2 (0.9)	1.8	KH domain of Nova-2
1o2fb_	77	38	27	10.1 (8.7)	N/A	10.3	Glucose-permease IIBC
1mkyA3	81	32	24	3.2 (3.6)	6.3 (6.1)	3.7	Enga
1tig_	88	35	35	4.1 (4.2)	3.5 (3.4)	2.4	IF3-C

1 and 2 are given in columns 5 and 6, respectively (20). RMSD values calculated over all heavy atoms in the protein core (21) are given in parentheses. Column 7 reports the best  $C_{\alpha}$ -RMSD of the centers of the largest five clusters when the low-energy models from round 1 are clustered.

sequence homologs in addition to the target sequence. Each homolog has a slightly different landscape in the low-resolution potential and produces a characteristic set of models due to variable hydrophobic patterning, loop lengths, and local structural biases (fig. S2). Models for each of the homologs are then mapped back to the target sequence, producing a large and structurally diverse starting population for all-atom refinement.

This approach was first tested on prediction target T0281 from the Sixth Critical Assessment of Techniques for Protein Structure Prediction (3) (CASP) experiment. Target 281 is a 70-residue alpha-beta protein with predicted secondary structure consisting of an N-terminal alpha helix, two or three beta strands, and two additional alpha helices. Rosetta de novo simulations with the target sequence generated a family of topologies characterized by a two- or three-stranded antiparallel sheet with alpha helices packed on both sides. When sequence homologs of the target were folded, several new topologies were found in which the helices packed together on one side of a three-stranded beta sheet (11). We picked clusters of models from both the target and the homologs for all-atom refinement; models for homologs were mapped back to the target sequence using the Rosetta loop modeling protocol (12). The low-energy models after all-atom refinement were clustered, and the lowest energy member of the largest cluster (which originated in simulations of one of the sequence homologs) was submitted as our first prediction (Fig. 2). When the experimental structure was released, this model was found to have a  $C_{\alpha}$ -RMSD of 1.6 Å, making it perhaps the most accurate blind de novo structure prediction in the history of the CASP experiment.

To test this approach further, we constructed a benchmark of 16 small proteins with relatively deep multiple sequence alignments (Table 1)

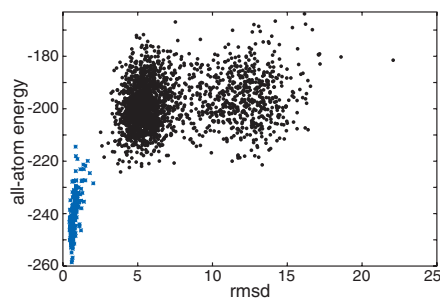


**Fig. 1.** Free-energy landscape for the small protein barstar (PDB code 1a19). Rosetta all-atom energy (y axis) is plotted against  $C_{\alpha}$ -RMSD (x axis) for models generated by simulations starting from the native structure (refined natives, blue points) or from an extended chain (de novo models, black points). The free-energy function includes the entropic contribution to the solvation free energy but not the configurational entropy.

(10). For each protein, 15 to 50 sequence homologs were selected for folding, and low-resolution models were built for each (10). The sequence of the target protein was threaded onto each model, and the structure was refined with the all-atom refinement protocol described above to generate 20,000 to 30,000 all-atom models (round 1). To introduce additional diversity into the high-resolution search, we built a second set of models (round 2) by refining low-energy models from the first round with sequences from close homologs and then mapping back to the target sequence (10). The all-atom energy and  $C_{\alpha}$ -RMSD to native are plotted for each population in figs. S4 and S5. As a stringent test of the all-atom energy function, the single lowest energy model from each round was identified and compared with the native structure (Table 1, columns 5 and 6).

For five of the proteins, the lowest energy model generated in either round 1 (three cases) or round 2 (four cases) had a  $C_{\alpha}$ -RMSD to the

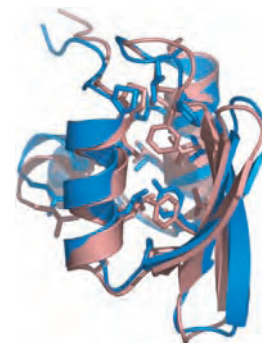


**Fig. 2.** 1.6 Å  $C_{\alpha}$ -RMSD blind structure prediction for CASP6 target T0281, hypothetical protein from *Thermus thermophilus* Hb8. Superposition of our first submitted model for this target in CASP6 (blue) with the crystal structure (red; PDB code 1whz) showing core side chains. This figure was generated in PyMOL (22).

native structure of less than 1.5 Å. The accuracy of the recapitulation of both the protein backbone and the core side chains is illustrated by structural superpositions of the lower RMSD of the round 1 low-energy model and the round 2 low-energy model onto the corresponding native structures (Fig. 3, A to E). Scatter plots of  $C_{\alpha}$ -RMSD versus all-atom energy are shown in Fig. 3, G to K, and details on each of the predictions are provided in the figure legend.

For 8 of the remaining 11 proteins, the lowest energy round 1 or round 2 structure (six cases) or one of the centers of the five largest clusters of low-energy models (seven cases) were topologically correct, with  $C_{\alpha}$ -RMSDs ranging from 1.5 to 5.0 Å (Table 1, columns 5 to 7), but the native side-chain packing was not captured to the extent shown in Fig. 3 (fig. S3, A to C). In one of these cases, the second-lowest energy model (fig. S3D) is quite accurate ( $C_{\alpha}$ -RMSD 1.1 Å). For seven of these eight cases (13), and for all three of the remaining cases where topologically correct predictions were not achieved,

the failure to achieve high-quality models is due to inadequate conformational sampling. The worst of the predictions (Fig. 3F) illustrates this sampling problem: Although refined native structures have lower energies than the de novo models (Fig. 3L), there is no sampling in the native basin and a false minimum is selected.

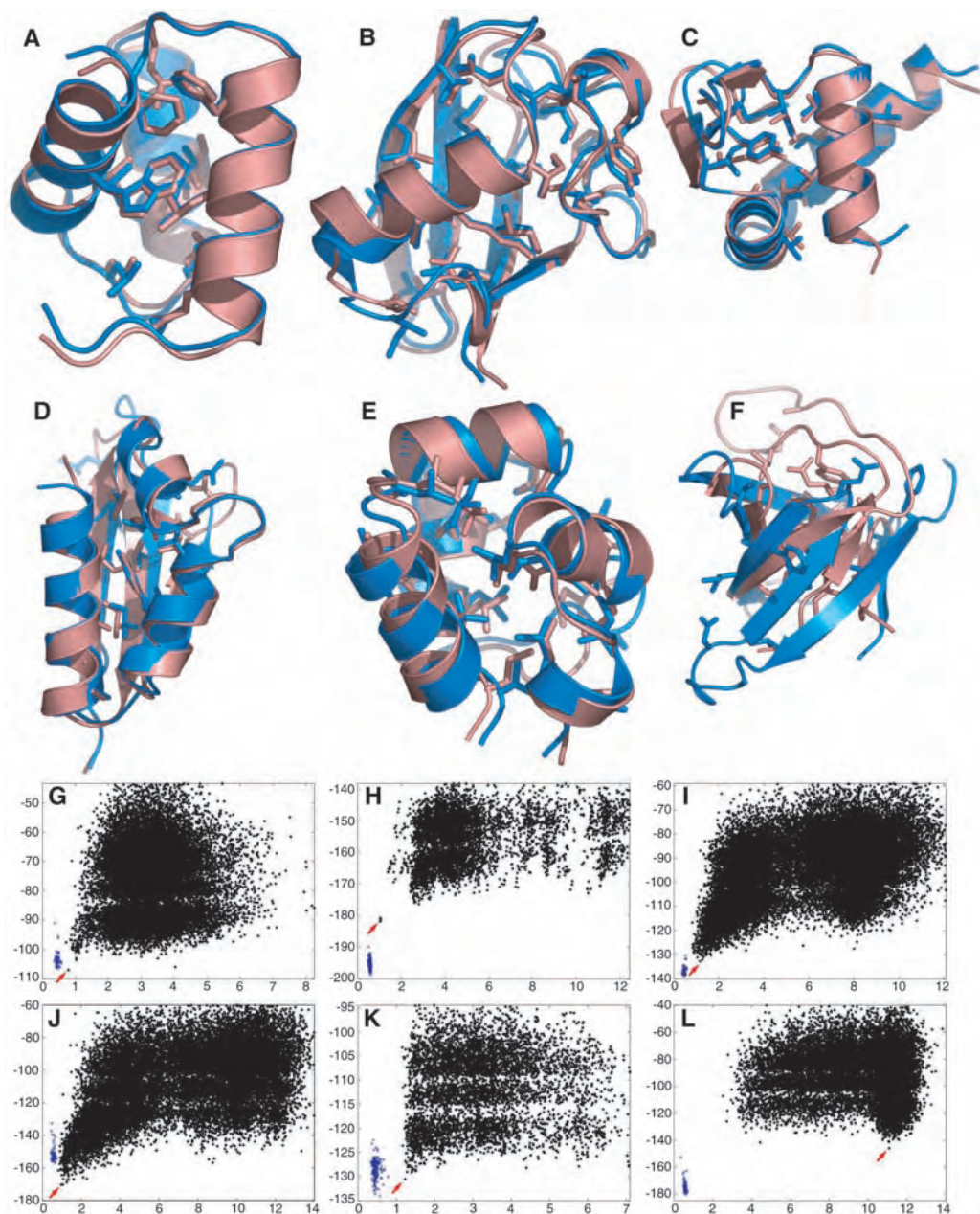
The high accuracy of the models shown in Fig. 3, A to E, is encouraging and, along with recent success in protein design and protein-protein docking (4, 14–16), suggests that the Rosetta all-atom potential may capture the key forces contributing to the stability of small, globular proteins. In particular, the emphasis on van der Waals interactions and hydrogen

bonding and the neglect of long-range electrostatics support the view that conformational specificity is provided in large part by short-range interactions, primarily the jigsaw puzzle-like complementary packing in the protein core. The free-energy landscapes in Figs. 1 and 3, together with the ability to make predictions with  $C_{\alpha}$ -RMSDs under 1 Å, suggest that conformational sampling in solution in the protein core may be restricted to a narrow ensemble centered near the crystal structure.

On the other hand, because high-accuracy models were selected for only a third of the proteins in the test set, further improvements in both the sampling methodology and the free-

energy function are clearly necessary for consistent and reliable de novo structure prediction of small proteins. Conformational sampling remains the primary stumbling block, as highlighted by the lack of models with  $C_{\alpha}$ -RMSDs <2.5 Å for most of the failures in our test set and the fact that the refined natives (blue points in Figs. 1 and 3 and figs. S1, S2, S4, and S5) generally have lower energies than the vast majority of de novo generated models. Improvements in sampling that reduce overconvergence in the low-resolution search should also eliminate the dependence on simulations with homologous sequences to adequately cover conformational space.

**Fig. 3.** High-resolution de novo structure predictions. (A to F) Superposition of low-energy models (blue) with experimental structures (red) showing core side chains. (G to L) Plots of  $C_{\alpha}$ -RMSD (x axis) against all-atom energy (y axis) for refined natives (blue points) and the de novo models (black points). Red arrows indicate the lowest energy de novo models, shown in [(A) to (F)]. [(A) and (G)] Hox-B1. In the lowest energy model (A) from round 1, the aromatic side chains, particularly the central phenylalanine, overlay almost perfectly. The all-atom refinement step reduced the model  $C_{\alpha}$ -RMSD to the native structure from 1.5 Å to 0.8 Å. [(B) and (H)] Ubiquitin. In the lowest energy model (B) from round 2, almost all of the core side chains overlay well, including the central partially buried lysine. [(C) and (I)] RecA. The lowest energy model from round 1 (C) has nearly all the core side chains in place; the RMSD versus energy plot (I) exhibits a broad funnel. [(D) and (J)] KH domain of Nova-2. A loop for which density is missing in three of four monomers in the crystal structure of the tetramer packs more closely on the rest of the protein in the low RMSD models than in the native monomer, in which the density was interpretable, and is responsible for the lower than native energy of models in the native basin (J). The lowest energy model after round 1 (D) has a  $C_{\alpha}$ -RMSD to native of 1.0 Å with the omission of this loop, which is involved in RNA binding. [(E) and (K)] 434 repressor. The lowest energy model after round 2 (E) has a  $C_{\alpha}$ -RMSD of 1.3 Å despite consistent errors in the population in one of the loops. The lowest energy models for the remaining 11 proteins in our test set were much less accurate, with side-chain packing and, in some cases, the fold incorrect. The lowest energy round 1 structure (F) for the Fyn Tyrosine kinase replaces the native diverging turn with an additional hairpin ( $C_{\alpha}$ -RMSD 11.1Å); de novo models fail to sample the deep energy minimum near the native structure (L). [(A) to (F)] were created in PyMOL (23) and [(G) to (L)] with gnuplot (www.gnuplot.info).



What are the prospects for high-resolution protein structure prediction more generally? First, protein core prediction may be a fundamentally easier problem than prediction of the detailed structures of functionally relevant parts of proteins, such as active sites where buried charged and polar interactions are more common (17). Second, the computational cost of high-resolution refinement is expected to increase dramatically with chain length, and hence the refinement of models of large proteins is likely to require orders of magnitude more computing power than the ~150 CPU days required for each of the predictions in this paper. Although our results are encouraging, consistent and reliable high-resolution modeling of protein structure remains a formidable challenge.

#### References and Notes

1. C. B. Anfinsen, E. Haber, M. Sela, F. H. White Jr., *Proc. Natl. Acad. Sci. U.S.A.* **47**, 1309 (1961).
2. C. Levinthal, *J. Chim. Phys.* **65**, 44 (1968).
3. J. Moulton, K. Fidelis, A. Zemla, T. Hubbard, *Proteins* **53** (Suppl 6), 334 (2003).
4. B. Kuhlman *et al.*, *Science* **302**, 1364 (2003).
5. J. Tsai *et al.*, *Proteins* **53**, 76 (2003).
6. K. M. S. Misura, D. Baker, *Proteins* **59**, 15 (2005).
7. Z. Li, H. A. Scheraga, *Proc. Natl. Acad. Sci. U.S.A.* **84**, 6611 (1987).

8. B. Kuhlman, D. Baker, *Proc. Natl. Acad. Sci. U.S.A.* **97**, 10383 (2000).
9. R. L. Dunbrack Jr., F. E. Cohen, *Protein Sci.* **6**, 1661 (1997).
10. Materials and methods are available as supporting material on Science Online.
11. Inspection of the multiple sequence alignment revealed that the target sequence had several hydrophobic residues at exposed beta-sheet positions in this topology that were replaced by polar residues in other members of the alignment, which offers a possible explanation for the absence of this topology in target-sequence models.
12. C. A. Rohl, C. E. Strauss, D. Chivian, D. Baker, *Proteins* **55**, 656 (2004).
13. The single case where non-native models had lower energies than the native is a domain of a larger protein that has a quite hydrophobic interface and may not be stable in isolation.
14. G. Dantas, B. Kuhlman, D. Callender, M. Wong, D. Baker, *J. Mol. Biol.* **332**, 449 (2003).
15. J. J. Gray *et al.*, *J. Mol. Biol.* **331**, 281 (2003).
16. C. Wang, O. Schueler-Furman, D. Baker, *Protein Sci.* **14**, 1328 (2005).
17. The physical chemistry of the packing of nonpolar atoms is considerably easier to model than the subtle trade-offs between desolvation of polar groups and the formation of buried polar interactions. Accurate modeling of functional sites may further require inclusion of explicit solvent molecules, modeling of protonation states and interactions with ligands, and polarizable electrostatics treatments. Together with the increase in the cost of refinement with chain length, this has implications for structural genomics efforts: The refinement to high resolution of comparative models of large

proteins (>400 amino acids) based on ~30% sequence identity, with many buried polar and charged residues, may be a harder problem than the de novo prediction of the structures of small proteins.

18. H. M. Berman *et al.*, *Nucleic Acids Res.* **28**, 235 (2000).
19. A. G. Murzin, S. E. Brenner, T. Hubbard, C. Chothia, *J. Mol. Biol.* **247**, 536 (1995).
20. To conserve computational resources, no round 2 modeling was done for Glucose Permease IIBC because the native topology was never sampled during fragment assembly. Secondary structure predictions for all 50 homologs predicted an alpha helix in place of the N-terminal beta strand in the native structure.
21. Core residues are defined as those with <20% solvent-accessible surface area compared with an extended G-X-G peptide.
22. W. L. Delano (DeLano Scientific, San Carlos, CA, USA, 2002).
23. We thank L. Malmström for computational assistance and K. Laidig for flawless administration of the computing resources necessary for these calculations. We gratefully acknowledge support from the Howard Hughes Medical Institute (P.B. and D.B.) and the Helen Hay Whitney Foundation (K.M.S.M.).

#### Supporting Online Material

[www.sciencemag.org/cgi/content/full/309/5742/1868/DC1](http://www.sciencemag.org/cgi/content/full/309/5742/1868/DC1)

Materials and Methods

Figs. S1 to S5

References

20 April 2005; accepted 15 August 2005  
10.1126/science.1113801

## Azathioprine and UVA Light Generate Mutagenic Oxidative DNA Damage

Peter O'Donovan,<sup>1</sup> Conal M. Perrett,<sup>1,3</sup> Xiaohong Zhang,<sup>1,2</sup> Beatriz Montaner,<sup>1</sup> Yao-Zhong Xu,<sup>2</sup> Catherine A. Harwood,<sup>3</sup> Jane M. McGregor,<sup>3</sup> Susan L. Walker,<sup>4</sup> Fumio Hanaoka,<sup>5</sup> Peter Karran<sup>1\*</sup>

Oxidative stress and mutagenic DNA lesions formed by reactive oxygen species (ROS) are linked to human malignancy. Clinical treatments inducing chronic oxidative stress may therefore carry a risk of therapy-related cancer. We suggest that immunosuppression by azathioprine (Aza) may be one such treatment. Aza causes the accumulation of 6-thioguanine (6-TG) in patients' DNA. Here we demonstrate that biologically relevant doses of ultraviolet A (UVA) generate ROS in cultured cells with 6-TG-substituted DNA and that 6-TG and UVA are synergistically mutagenic. A replication-blocking DNA 6-TG photoproduct, guanine sulfonate, was bypassed by error-prone, Y-family DNA polymerases in vitro. A preliminary analysis revealed that in five of five cases, Aza treatment was associated with a selective UVA photosensitivity. These findings may partly explain the prevalence of skin cancer in long-term survivors of organ transplantation.

The thiopurines azathioprine (Aza), 6-mercaptopurine (6-MP), and 6-thioguanine (6-TG) are cancer therapeutic and immunosuppressive agents. They are all prodrugs (compounds that the body converts into active drugs) requiring metabolic activation into the thioguanine nucleotides (TGNs) that are precursors for 6-TG incorporation into DNA (1). Experimentally, 6-TG is a surrogate for Aza because it by-

passes many of the activation steps and is directly converted to TGN. The normal DNA bases do not absorb significantly at ultraviolet A (UVA) wavelengths (320 to 400 nm), whereas thiopurines do, and 6-TG has an absorbance maximum at 342 nm. 6-MP generates ROS when exposed to UVA (2). ROS are pernicious DNA-damaging agents (3), and although cells are equipped to deal with them, abrupt

increases in ROS cause oxidative stress and produce mutagenic DNA lesions (4). The possibility that DNA 6-TG might act as an endogenous UVA chromophore and provide a source of promutagenic oxidative DNA damage prompted us to investigate the photochemical properties of 6-TG and the biological consequences of the interaction between DNA 6-TG and UVA.

HCT116 human colorectal carcinoma cells are mismatch repair-defective and tolerant of high levels of DNA 6-TG (5). We found that UVA generated intracellular ROS in 6-TG-treated HCT116 cells in which 6-TG replaced approximately 0.2% of DNA guanine. After uptake of CM-H2DCFDA dye and irradiation with UVA (3 kJ/m<sup>2</sup>) [approximately equivalent to 1 to 2 min of exposure around noon in England at midsummer (6)], the cells emitted a green fluorescence indicating the formation of ROS. This was detected by fluorescence-activated cell sorting and by microscopy (Fig. 1A). Because ROS are highly unstable, they

<sup>1</sup>Cancer Research UK London Research Institute, Clare Hall Laboratories, South Mimms, Hertfordshire EN6 3LD, UK. <sup>2</sup>Department of Chemistry, The Open University, Walton Hall, Milton Keynes MK7 6AA, UK. <sup>3</sup>Centre for Cutaneous Research, Institute of Cell and Molecular Science, Barts and The London Queen Mary's School of Medicine and Dentistry, 4, Newark Street, London, E1 2AT, UK. <sup>4</sup>Department of Photobiology, Guy's, King's and St Thomas' School of Medicine, St. John's Institute of Dermatology, King's College, London SE1 7EH, UK. <sup>5</sup>RIKEN Discovery Research Institute, Wako-shi, Saitama 351-0198 Japan.

\*To whom correspondence should be addressed. E-mail: peter.karran@cancer.org.uk

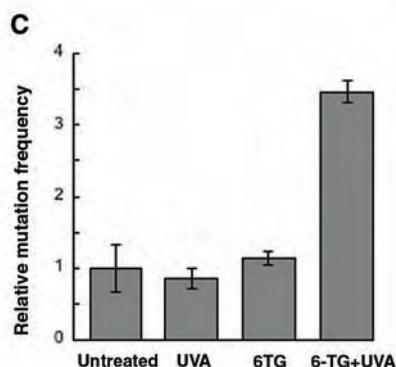
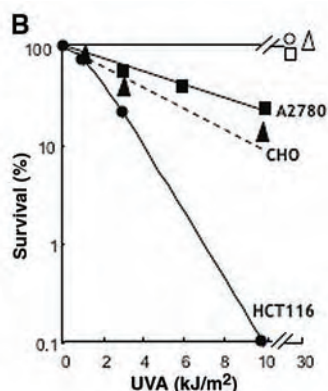
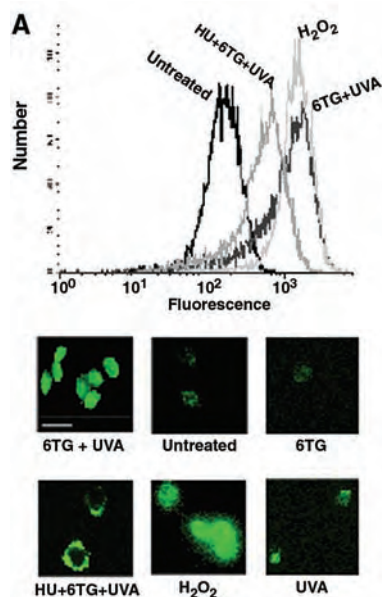


**Fig. 1.** Biological consequences of UVA irradiation of DNA 6-TG. (A) UVA generates intracellular ROS in cells with DNA 6-TG. HCT116 cells were grown for 24 hours in medium containing 1  $\mu$ M 6-TG in the presence or absence of 10 mM HU. 6-TG replaced approximately 0.2% of DNA guanine. After thorough washing with phosphate-buffered saline, 6-TG-treated cells were incubated with CM-H2DCFDA and irradiated with 3  $\text{kJ/m}^2$  of UVA as described (25). Green fluorescence generated by the reaction between CM-H2DCFDA and oxygen free radicals was analyzed by FACS or fluorescence microscopy. HCT116 cells grown without 6-TG and treated with  $\text{H}_2\text{O}_2$  served as a control for ROS generation. Representative photomicrographs of fluorescent cells are shown. Scale bar, 20  $\mu$ m. Note the absence of nuclear fluorescence in cells treated with HU. (B) 6-TG sensitizes cells to UVA. HCT116 (circles), A2780 (squares), or CHOD422 (triangles) cells were grown for 48 hours in medium containing 1, 0.1, or 0.1  $\mu$ M 6-TG, respectively. Treated cells were irradiated with the UVA doses shown and replated in medium without 6-TG. Clonal survival was determined after 10 days. Open symbols: Survival after 30  $\text{kJ/m}^2$  of UVA administered to the same cells grown in the absence of 6-TG. (C) Mutagenesis by 6-TG/UVA. CHOD422

cells were grown for 48 hours in 0.1  $\mu$ M 6-TG, washed, and irradiated with 1  $\text{kJ/m}^2$  of UVA. The *aprt* mutation frequency was calculated by determining the number of 8-azaadenine-resistant colonies (26). Results are the means of five independent determinations  $\pm$  SD. The mean spontaneous mutation frequency was  $4.1 \times 10^{-6}$  (range:  $2.1 \times 10^{-6}$  to  $6.0 \times 10^{-6}$ ), and the mean for 6-TG+UVA was  $12.6 \times 10^{-6}$  (range:  $7.1 \times 10^{-6}$  to  $19.4 \times 10^{-6}$ ).

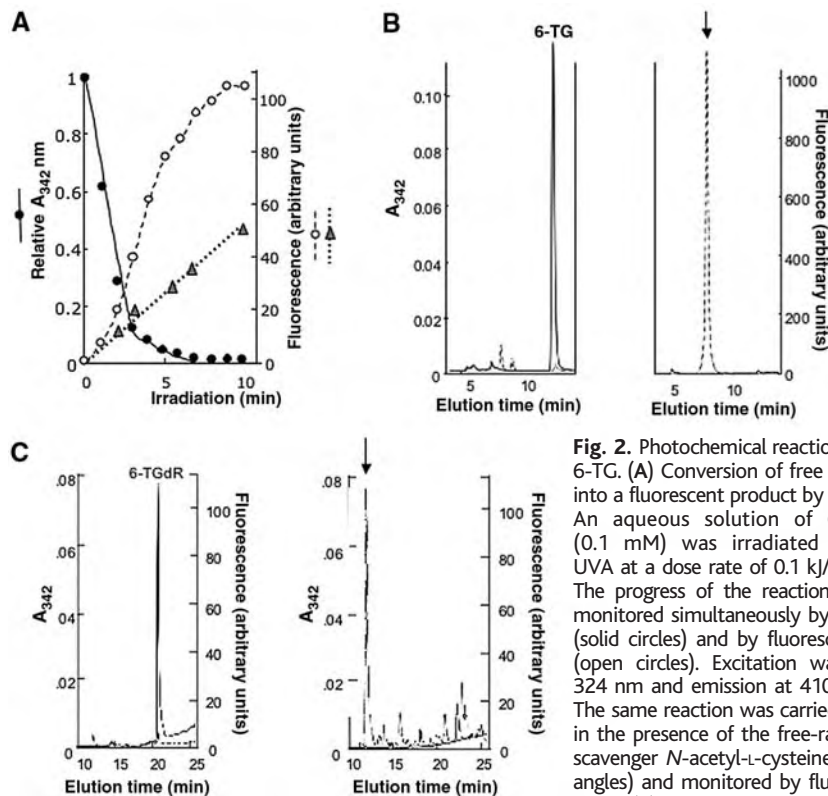


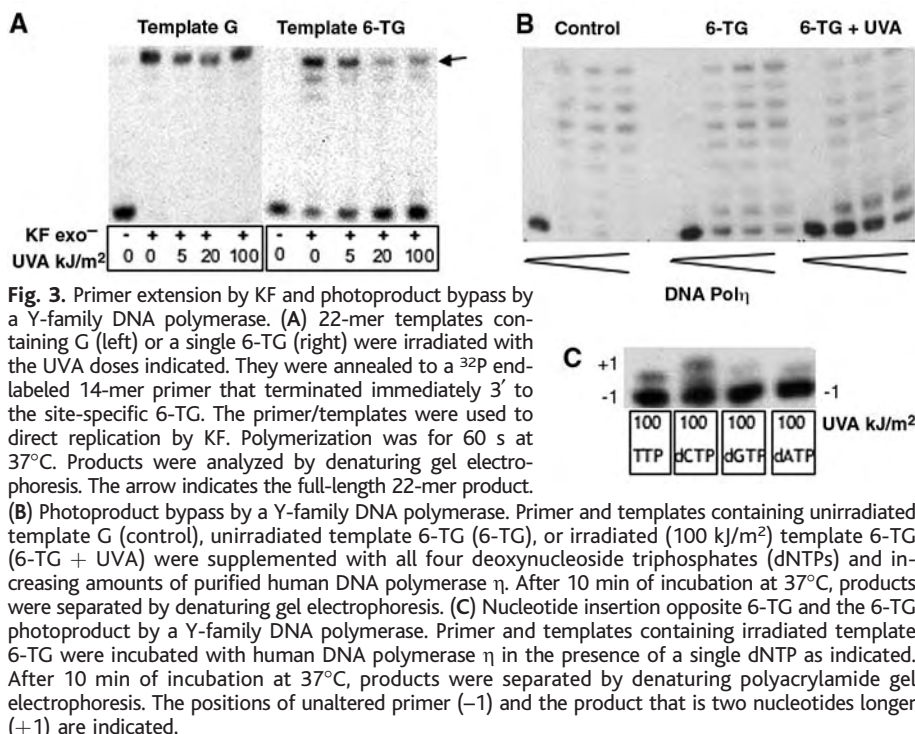
**Fig. 2.** Photochemical reactions of 6-TG. (A) Conversion of free 6-TG into a fluorescent product by UVA. An aqueous solution of 6-TG (0.1 mM) was irradiated with UVA at a dose rate of 0.1  $\text{kJ/m}^2/\text{s}$ . The progress of the reaction was monitored simultaneously by  $A_{342}$  (solid circles) and by fluorescence (open circles). Excitation was at 324 nm and emission at 410 nm. The same reaction was carried out in the presence of the free-radical scavenger *N*-acetyl-L-cysteine (triangles) and monitored by fluorescence. (B) UVA irradiation converts 6-TG into a fluorescent product. 6-TG was irradiated in solution with 10  $\text{kJ/m}^2$  of UVA, and the products were analyzed by reverse-phase HPLC. Column eluates were monitored simultaneously by  $A_{342}$  (left panel) and fluorescence (right panel). 6-TG is converted from a UVA-absorbing highly fluorescent compound with minimal fluorescence into an earlier-eluting highly fluorescent product (arrowed) that does not absorb at 342 nm. (solid line, unirradiated; dashed line, irradiated). (C) The fluorescent 6-TG photoproduct is also formed in DNA. Unirradiated (left panel) or UVA-irradiated (50  $\text{kJ/m}^2$ , right panel) 18-mer oligonucleotides that contained a single 6-TG were digested to deoxynucleosides with P1 nuclease and acid phosphatase. These were separated by HPLC. Eluates were monitored by  $A_{342}$  and fluorescence at 410 nm. (Left) In digests of unirradiated oligonucleotides, 6-TGdR elutes at 21 min. It is detected by  $A_{342}$  but has minimal fluorescence. (Right) After irradiation, no 342-nm-absorbing material is detectable, and a major fluorescent product elutes coincident with the fluorescent UVA photoproduct of authentic 6-TGdR (fig. S2) at 12 min (arrow). (solid line, unirradiated; dashed line, irradiated).

tend to react close to their site of formation. When the thiopurine was selectively excluded from DNA by carrying out 6-TG treatment in the presence of the DNA replication inhibitor hydroxyurea (HU), UVA-induced fluorescence was markedly reduced and nuclear fluorescence was abolished (Fig. 1A). This indicates that DNA 6-TG is a major source of intracellular ROS, and DNA is likely to be a significant target for oxidative damage. 6-TG-treated HCT116 cells were killed by the UVA doses that generated ROS (Fig. 1B), consistent with the formation of lethal DNA damage. UVA was also cytotoxic to 6-TG-treated, mismatch repair-proficient, A2780 human ovarian carcinoma (7) and CHOD422 cells (Fig. 1B). These cells are not tolerant of 6-TG but grow normally when 6-TG replaces  $\sim$ 0.05% of DNA guanine.

To investigate whether 6-TG plus UVA was mutagenic, we examined induction of adenine phosphoribosyltransferase (*aprt*) mutations in CHOD422 cells. In cells containing  $\sim$ 0.01% DNA 6-TG irradiated with a nontoxic UVA dose of 1  $\text{kJ/m}^2$ , there was a threefold ( $P < 0.005$ ) increase in *aprt* mutation frequency (Fig. 1C). Neither 6-TG nor UVA alone was detectably mutagenic. Without 6-TG treatment, 500  $\text{kJ/m}^2$  of UVA was required to induce a similar increase in CHO *aprt* mutation frequency (8). The susceptibility of 6-TG-treated cells to UVA-induced mutation and killing reveals DNA 6-TG to be a potent photosensitizer that increases the biological effectiveness of UVA by two orders of magnitude.

We also examined the photochemical properties of 6-TG both as a free base and in DNA. Like 6-MP (2), free 6-TG was destroyed by UVA in an oxygen-dependent reaction that





generated free radicals (Fig. 2A). 6-TG was converted into a single fluorescent product (excitation maximum 324 nm, emission maximum 410 nm) that was resolved from the parent compound by reverse-phase high-pressure liquid chromatography (HPLC) (Fig. 2B). The same fluorescent photoproduct was formed in irradiated DNA. It was acid-labile and was destroyed under the conditions used for DNA depurination, but was recovered as the deoxynucleoside after enzymatic digestion (Fig. 2C). The fluorescent 6-TG photoproduct was identified as 2-aminopurine-6-sulfonate [guanine-6-sulphonate (G-6-SO<sub>3</sub>)] (fig. S1). Its absorbance and fluorescence spectra and acid lability were identical to G-6-SO<sub>3</sub> prepared by alkaline permanganate treatment of 6-TG (9-11) and authenticated by <sup>1</sup>H nuclear magnetic resonance and mass spectroscopy [see supporting online material (SOM)]. This authentic G-6-SO<sub>3</sub> also coeluted with the fluorescent 6-TG photoproduct on HPLC. In addition, the fluorescent deoxynucleoside from digests of UVA-irradiated 6-TG DNA coeluted with the single fluorescent photoproduct of UVA-treated 6-TGdR (fig. S2).

To examine the effects of UVA 6-TG photoproducts on DNA replication, we carried out *in vitro* primer extension assays with Klenow fragment (KF). A 22-mer oligonucleotide containing a single 6-TG (fig. S3A) was irradiated with 5, 20, or 100 kJ/m<sup>2</sup> of UVA. HPLC analysis indicated that the lowest dose converted around 70% of the 6-TG to G-6-SO<sub>3</sub>. At 20 and 100 kJ/m<sup>2</sup>, ≥90% of the 6-TG was destroyed. Irradiated oligonucleotides were used as templates for KF-mediated extension of a 14-mer

primer that terminated immediately 3' to the 6-TG. An irradiated 22-mer oligonucleotide in which G replaced 6-TG was used as a control.

With the control or UVA-irradiated G template, KF extended all primer molecules to full-length 22-mers within 60 s (Fig. 3A). As reported (12), 6-TG slightly inhibited replication. In contrast, UVA-irradiated 6-TG was a powerful replication block. Thus, 5 kJ/m<sup>2</sup> significantly impaired primer elongation, and inhibition was almost complete (≥90%) at the higher UVA doses (Fig. 3A). The inhibitory effects were targeted to the photoproduct, and no other polymerase arrest or pause sites were evident. Thus, although KF replicated unmodified 6-TG with reasonable facility in this assay, it did not bypass G-6-SO<sub>3</sub> efficiently.

Y-family DNA polymerases bypass replication-blocking lesions in a DNA damage tolerance strategy. This process is potentially mutagenic owing to their low replication fidelity (13). We found that two representative Y-family DNA polymerases, human DNA polymerase η (14) and Sso P2Y1 polymerase (SsoY1pol) of *Sulfolobus solfataricus*, a hyperthermophilic archaeon (15), replicated a heavily UVA-irradiated (100 kJ/m<sup>2</sup>) 6-TG template (Fig. 3B and fig. S3B). Coding by the photoproduct was ambiguous; both DNA polymerase η and SsoY1pol inserted T or C opposite the lesion with about equal frequency (Fig. 3C and fig. S3C). Thus, *in vitro*, Y-family DNA polymerases overcome the G-6-SO<sub>3</sub> replication block in a potentially mutagenic manner.

To extend these findings to a clinical setting, we measured the amount of 6-TG in DNA

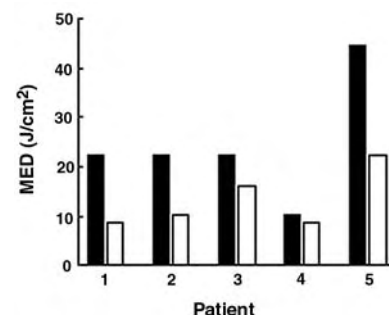


**Fig. 4. Skin photosensitivity in patients treated with Aza.** The MED for UVA was determined in five patients who were about to begin a course of Aza treatment for polymorphic light eruption, Crohn's disease, ulcerative colitis, pemphigus vulgaris, or recurrent erythema multiforme. MED measurements were repeated 3 months after beginning Aza treatment (1 to 2 mg/kg/day). Before treatment, black bars; during treatment, white bars.

extracted from the normal skin of three Aza-treated [1 to 2 mg per kilogram of body weight (mg/kg) daily] patients undergoing surgical excision of squamous cell skin carcinoma (SCC). All three samples contained 6-TG representing around 0.02% substitution of DNA guanine (table S1). Similar levels are present in lymphocyte DNA of thiopurine-treated patients (16, 17). As expected, no 6-TG was detected in skin DNA of patients who were not taking Aza. In a further five patients, we measured the effect of 1 to 2 mg/kg daily Aza on the minimal erythema dose (MED). This is the lowest dose of radiation required to produce just perceptible erythema 24 hours after the irradiation of skin not normally exposed to sunlight. In each patient, Aza treatment caused a significant reduction in the MED for UVA ( $P = 0.025$  by paired *t* test as compared to the pretreatment value) (Fig. 4). The MED for solar-simulating radiation was also reduced, but there was no concomitant sensitization to UVB (fig. S4, A and B). Erythema is associated with replication- and transcription-blocking DNA photodamage in mouse skin models (18) and is regarded as a surrogate indicator of persistent DNA damage in human skin (19). The selective UVA sensitivity associated with Aza treatment is consistent with the production of 6-TG DNA photoproducts.

Our findings indicate that normal exposure to sunlight may induce chronic oxidative stress and increase the levels of oxidative DNA lesions in the skin of patients taking Aza. A defect in processing the highly mutagenic oxidation products of normal DNA bases is associated with human cancer (20). Sustained generation of ROS-induced DNA lesions might represent a similar carcinogenic hazard. The susceptibility of DNA 6-TG itself to oxidation and the formation of DNA G-6-SO<sub>3</sub> has additional implications. Bypass of replication-blocking G-6-SO<sub>3</sub> by error-prone Y-family DNA polymerases represents another potential source of mutation.

The photochemical reactions of DNA 6-TG have implications for skin cancer. In a clinical setting, DNA 6-TG and UVA are likely to interact in the skin of organ transplant patients. Around 25,000 solid organ transplants are performed annually throughout Europe and in North America. SCC is 50 to 250 times more common among transplant patients than in the general population (21, 22), and 20 years after transplant, between 60 and 90% of patients are affected (23). Transplant-related SCC develops primarily on chronically sun-exposed skin, and sunlight plus the duration of treatment with immunosuppressive drugs are acknowledged risk factors. Until recently, most transplant patients have been treated with Aza. UVA is the major component of solar radiation, and a high fraction of incident UVA penetrates to the basal layers of the skin containing the stem cells. To date, epidemiological studies have not identified the contributions of individual immunosuppressive agents to transplant-related SCC (23, 24). The photochemical properties of DNA 6-TG described here indicate how UVA and an immunosuppressive drug might contribute to post-transplant SCC: a significant cause of morbidity in this group of patients.

References and Notes

1. M. V. Relling, T. Derieux, *Nat. Rev. Cancer* **1**, 99 (2001).
2. V. J. Hemmens, D. E. Moore, *Photochem. Photobiol.* **43**, 247 (1986).
3. J. Cadet, T. Douki, D. Gasparutto, J.-L. Ravanat, *Mutat. Res.* **531**, 5 (2003).
4. D. E. Barnes, T. Lindahl, *Annu. Rev. Genet.* **38**, 445 (2004).
5. P. Karran, *Carcinogenesis* **22**, 1931 (2001).
6. C. M. H. Driscoll et al., *Solar Radiation Measurements at the Network of Six Sites in the UK, January-December 2001* (National Radiological Protection Board, Oxford, UK, 2002).
7. P. Branch, M. Masson, G. Aquilina, M. Bignami, P. Karran, *Oncogene* **19**, 3138 (2000).
8. E. A. Drobetsky, J. Turcotte, A. Chateaufneuf, *Proc. Natl. Acad. Sci. U.S.A.* **92**, 2350 (1995).
9. I. L. Doerr, I. Wempfen, D. A. Clarke, J. J. Fox, *J. Org. Chem.* **26**, 3401 (1961).
10. H.-R. Rackwitz, K.-H. Scheit, *Chem. Ber.* **107**, 2284 (1974).
11. J. M. Finkel, *J. Pharm. Sci.* **64**, 121 (1975).
12. H. P. Rappaport, *Biochemistry* **32**, 3047 (1993).
13. A. R. Lehmann, *Mutat. Res.* **509**, 23 (2002).
14. C. Masutani et al., *Nature* **399**, 700 (1999).
15. P. Gruz et al., *J. Biol. Chem.* **276**, 47394 (2001).
16. D. J. Warren, A. Andersen, L. Slordal, *Cancer Res.* **55**, 1670 (1995).
17. C. Cuffari, D. Y. Li, J. Mahoney, J. Y. Barnes, T. M. Bayless, *Dig. Dis. Sci.* **49**, 133 (2004).
18. R. J. Berg, H. J. Ruven, A. T. Sands, F. R. deGrujil, L. H. Mullenders, *J. Invest. Dermatol.* **110**, 405 (1998).
19. A. R. Young, J. M. Sheehan, C. A. Chadwick, C. S. Potten, *J. Invest. Dermatol.* **115**, 37 (2000).
20. N. Al-Tassan et al., *Nat. Genet.* **30**, 227 (2002).

21. B. Lindelof, B. Sigurgeirsson, H. Gabel, R. S. Stern, *Br. J. Dermatol.* **143**, 513 (2000).
22. S. Euvrard, J. Kanitakis, A. Claudy, *N. Engl. J. Med.* **348**, 1681 (2003).
23. H. M. Ramsay, A. A. Fryer, C. M. Hawley, A. G. Smith, P. N. Harden, *Br. J. Dermatol.* **147**, 950 (2002).
24. M. T. Glover, J. J. Deeks, M. J. Raftery, J. Cunningham, I. M. Leigh, *Lancet* **349**, 398 (1997).
25. A. Massey, Y.-Z. Xu, P. Karran, *Curr. Biol.* **11**, 1142 (2001).
26. G. Phear, W. Armstrong, M. Meuth, *J. Mol. Biol.* **209**, 577 (1989).
27. We thank M. Yamada for her kind gift of the SspP2Y1 DNA polymerase and the staff of the Oligonucleotide Synthesis Laboratory, Cancer Research UK, for oligonucleotides. The work was supported in part by a Royal Society K. C. Wong Fellowship to X.Z. while on leave from Shanghai Jiao Tong University. We also acknowledge support from the Spanish Ministerio de Educacion y Ciencia (to B.M.) and from the Association for International Cancer Research. All studies involving patients were carried out with prior local ethics committee approval. The procedures involved and their implications were fully explained to the patients who gave informed consent.

Supporting Online Material

www.sciencemag.org/cgi/content/full/309/5742/1871/DC1

Materials and Methods  
SOM Text  
Figs. S1 to S4  
Table S1  
References

29 April 2005; accepted 4 August 2005  
10.1126/science.1114233

## Extensive Diversity of Ig-Superfamily Proteins in the Immune System of Insects

Fiona L. Watson,\* Roland Püttmann-Holgado,\*  
Franziska Thomas,† David L. Lamar,‡ Michael Hughes,  
Masahiro Kondo, Vivienne I. Rebel,§ Dietmar Schmucker||

The extensive somatic diversification of immune receptors is a hallmark of higher vertebrates. However, whether molecular diversity contributes to immune protection in invertebrates is unknown. We present evidence that *Drosophila* immune-competent cells have the potential to express more than 18,000 isoforms of the immunoglobulin (Ig)-superfamily receptor Down syndrome cell adhesion molecule (Dscam). Secreted protein isoforms of Dscam were detected in the hemolymph, and hemocyte-specific loss of Dscam impaired the efficiency of phagocytic uptake of bacteria, possibly due to reduced bacterial binding. Importantly, the molecular diversity of *Dscam* transcripts generated through a mechanism of alternative splicing is highly conserved across major insect orders, suggesting an unsuspected molecular complexity of the innate immune system of insects.

Immunoglobulin (Ig)-domain-containing proteins constitute the largest repertoire of surface receptors in animals and serve many functions in molecular recognition, cell adhesion, and signaling. Most striking is the exceptional diversity of antigen-specific receptors of the adaptive immune system in higher vertebrates, which depends on somatic gene rearrangement and clonal selection. However, somatic rearrangement of highly diverse immune receptors has been considered to exist in a relatively

small number of animal species restricted to the jawed vertebrates (1, 2).

We previously identified a single *Drosophila* *Dscam* gene as a member of the Ig superfamily and initially characterized its essential function in neuronal wiring (3). Gene organization of *Dscam* comprises clusters of variable exons flanked by constant exons (Fig. 1A) (3). Although mechanistically entirely different from somatic rearrangements, alternative splicing of the *Dscam* gene combines constant and var-

iable exons by mutually exclusive splicing and potentially generates as many as 19,008 different extracellular domains. Therefore, it is conceivable that a large protein isoform repertoire with the potential for recognizing diverse ligands and epitopes could be generated (3). To explore this, we undertook a comparative and functional analysis of *Dscam* expression in immune-competent cells of flies and other insects.

Fat body cells and hemocytes (i.e., insect blood cells) constitute important cells of the insect immune system (4-6). Most proteins in insect hemolymph, the insect equivalent of blood serum, are produced in fat body cells, which also secrete antimicrobial peptides that constitute an important component of the humoral immune defense (7). In contrast, hemocytes are involved in cellular defense strategies such as phagocytosis and wound repair (8).

In situ hybridization of tissue from third instar *Drosophila* larvae with a *Dscam*-specific probe (9) revealed *Dscam* expression in fat

Department of Cancer Biology, Dana Farber Cancer Institute, Department of Neurobiology, Harvard Medical School, Boston, MA 02115, USA.

\*These authors contributed equally to this work.

†Present address: Boehringer Ingelheim Pharma KG, 88397 Biberach, Germany.

‡Present address: Department of Medicine, Emory University School of Medicine, Atlanta, GA 30322, USA.

§Present address: Children's Cancer Research Institute, University of Texas Health Science Center, San Antonio, TX 78229, USA.

||To whom correspondence should be addressed. E-mail: dietmar\_schmucker@dfci.harvard.edu

body cells (fig. S1). For a comparison of Dscam expression in immune and neural tissue we isolated mRNA from larval hemocytes, fat body and brain tissue (9). Hemocyte-specific green fluorescent protein (GFP) expression allowed for the purification of hemocytes by fluorescence activated cell sorting (FACS) (fig. S3) (9). Reverse transcription polymerase chain reaction (RT-PCR) analysis and sequencing of ~50 cDNAs revealed that the majority of Dscam mRNAs in hemocytes, fat body, and brain contain unique exon 4 to 6 combinations (table S1) (9).

For a global assessment of alternative splicing in different cell types we used custom-made oligo-arrays (9). Microarrays contained specific 50-mer oligo-probes for all alternatively spliced exons. Dscam mRNA sequences were amplified by RT-PCR, and cDNAs were fluorescently labeled and hybridized to the microarrays (9) (Fig. 1, B to D). We found that 59 of the 60 alternative exon 4 and exon 6 sequences were expressed in all three cell types. In brain tissue, 32 exon 9 sequences were expressed (Fig. 1D). However, only a subset (total of 14) was expressed in fat body cells and a slightly different subset (total of 15) was expressed in hemocytes (Fig. 1D). On the basis of relative expression amounts, we estimate that 80 to 90% of all Dscam mRNAs in hemocytes and fat body contain exon 9, 9.6, 9.9, 9.13, 9.30, or 9.31, demonstrating that exon 9 splice variants in fat body cells and hemocytes are distinct from those found in brain (Fig. 1D and fig. S2B). Considering all of the alternative exons detected (12 for exon 4, 47 for exon 6, 16 for exon 9, and 2 for exon 17), we calculate that this potentially allows for the generation of more than 18,000 diverse receptor isoforms in fat body cells and hemocytes (Fig. 1) (9).

We raised antibodies against extracellular (D-ex1, D-ex2) and intracellular (D-cy) domains of Dscam (Fig. 2A) (9). All antibodies recognized an ~210-kD endogenous form of Dscam in extracts from cultured S2 cells (Fig. 2, B to D), a cell line thought to be derived from embryonic hemocytes and shown to share many characteristics with hemocytes (10, 11). A 210-kD form of Dscam was also confirmed in purified larval hemocytes (Fig. 2, C and D, and fig. S3) (9), fat body tissue, and at comparatively high amounts in brain (Fig. 2, D and E).

Immunoprecipitations from fat body extracts revealed three Dscam forms (Fig. 2E), possibly representing truncated forms generated by proteolytic cleavage. Unexpectedly, we found that S2 cell-conditioned medium contained a soluble Dscam protein of ~160 kD (Fig. 2F) and that a secreted Dscam protein of the same molecular weight was also present in hemolymph serum (Fig. 2G).

Liquid chromatography and tandem mass spectrometry (LC-MS/MS) directly confirmed

that S2 cells secrete Dscam isoforms (9) (table S2 and fig. S4). Coverage of the secreted forms by the identified peptides amounts to more than 50% of the entire extracellular part of Dscam (fig. S4A). Importantly, some of the identified peptides confirmed the presence of alternatively spliced sequences, including five Ig2 sequences and at least 12 Ig3 sequences (table S2 and fig. S4, B and C). In agreement with the expression profiling of exon 9 (Ig7) sequences (Fig. 1), we identified three distinct Ig7 domains (i.e., Ig7<sup>6</sup>, Ig7<sup>9</sup>, and Ig7<sup>13</sup>), which correspond to the most abundantly expressed exon 9 sequences (Fig. 1 and fig. S2B).

Considering the protein sequencing results (table S2 and fig. S4), the presence of secreted Dscam in hemolymph (Fig. 2), and the large pool of diverse Dscam mRNAs in fat body cells or hemocytes (Fig. 1D), it is possible that thousands of Dscam isoforms circulate in the hemolymph of *Drosophila*.

**Fig. 1.** Dscam isoform expression in hemocytes and fat body tissue. (A) Gene and protein structure of *Drosophila* Dscam. Mutually exclusive alternative splicing occurs for exon clusters 4, 6, 9, and 17 (3). (B and C) Alternative exon expressions in brain and hemocytes (B) or brain and fat body cells (C). Microarrays were hybridized with Cy3- and Cy5-labeled cDNA (9), and one representative array from slides that contain triplicate arrays is shown. Spots corresponding to exon 9 sequences are indicated by a box (white line) and reveal predominant expression in brain tissue. (D) Summary of expression data for all alternative exons. Every exon is represented by a single colored square: moderate to high expression (green), low expression (yellow), and very low or no expression (red). For quantitative evaluation and definition of thresholds, see (9). Four experiments for hemocytes or fat body cells and eight for brain tissue were analyzed and presented as adjacent columns. Average values are listed separately in last column (marked by asterisks). Total number of exons expressed is given at bottom. Restricted usage of exon 9 is consistent with expression profiling studies comparing different neuronal cell types (12) as well as photoreceptor neurons and S2 cells (24).

We next sought to determine whether Dscam proteins are functionally required in immune-competent cells. However, because animals with homozygous amorphic mutations in *Dscam* die as embryos (3, 12), it was not possible to directly test this in null mutant animals. Nevertheless, we were able to purify GFP-labeled hemocytes from *Dscam* mutant larvae that carry a transallelic combination of hypomorphic (*Dscam*<sup>39</sup>) and amorphic (*Dscam*<sup>20</sup>) mutations (13). Immunoblotting showed that *Dscam*<sup>20</sup>/*Dscam*<sup>39</sup> animals have a strong overall reduction in protein concentration (Fig. 3A). One important function of hemocytes is the ingestion of bacterial pathogens by phagocytosis (8). We therefore challenged wild-type and *Dscam*-deficient hemocytes with heat-killed fluorescently labeled *Escherichia coli* and determined the number of hemocytes containing fluorescent bacteria [phagocytic index (Fig. 3B and fig. S5)] (9). Normal

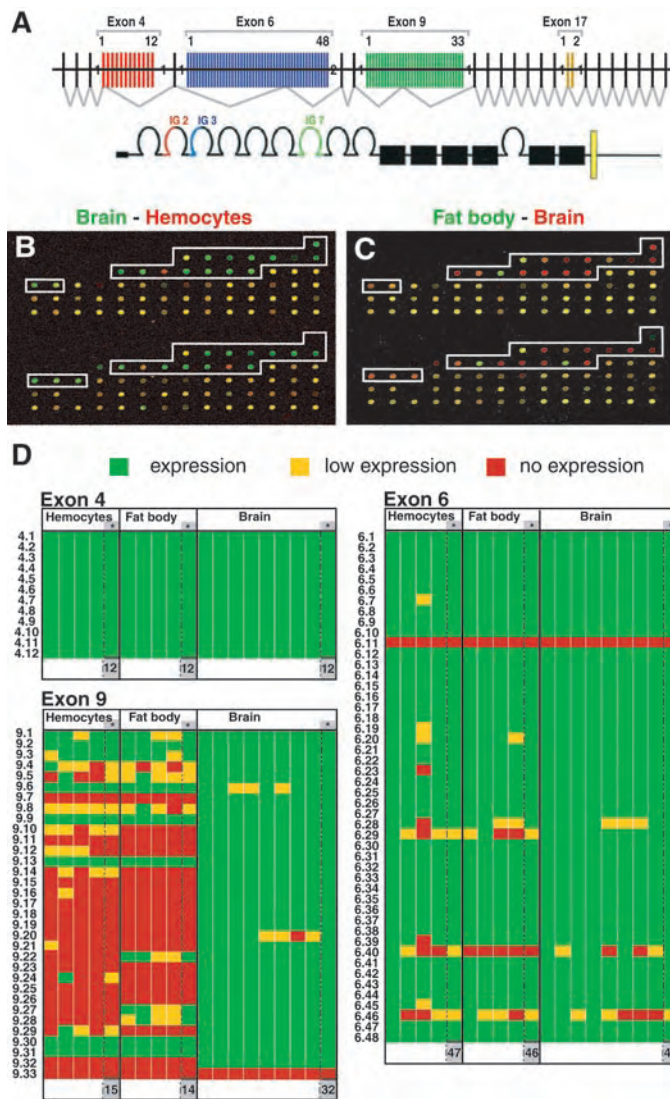
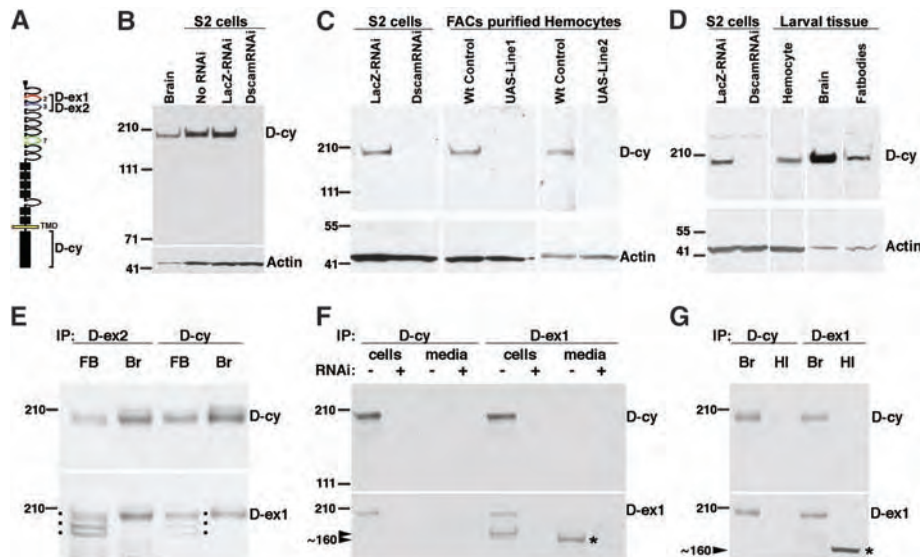


**Fig. 2.** Dscam protein is expressed in immune-competent cells. (A) Proteins recognized by antibodies to Dscam D-cy, D-ex-1, and D-ex-2. (B) Dscam protein ~210 kD in S2 cells and in brain tissue (Brain) lysates. RNAi treatment (DscamRNAi) in S2 cells selectively depletes expression of the 210-kD band compared with untreated (no RNAi) or control-treated (LacZ-RNAi) cells. (C) Hemocytes isolated from independent transgenic lines (UAS-Line1 and UAS-Line2) of larvae that express dsDscam-RNA(9) (RNAi knock-down) have strongly reduced Dscam protein amounts compared with control (Wt Control, lanes 3 and 5). (D) Full-length Dscam protein (~210 kD) is present in fat bodies (three fat bodies per lane), purified hemocytes ( $3 \times 10^4$  cells per lane) (9), and brain (one brain per lane). S2 cells ( $1 \times 10^4$  cells per lane) treated with control dsRNA (LacZ-RNAi) or Dscam dsRNA (DscamRNAi) show specificity of Dscam detection. (E) Dscam protein was immunoprecipitated (IP) from fat body (FB) or brain (Br) by using D-ex2 or D-cy. Western blot analysis detects 3 Dscam protein forms (\*) in fat bodies (9). (F) Dscam protein IP from lysates of S2 cells (cells) or conditioned media (media) using D-cy (top) or D-ex1 (bottom) indicates presence of shorter protein forms in S2 cells (lane 5). The smaller ~170-kD band (top arrowhead) likely represents a Dscam protein lacking a cytoplasmic domain. A truncated Dscam protein of ~160 kD (bottom arrowhead) is only detected in S2 cell-conditioned media lane



7, marked with asterisk). Dscam RNAi-treated samples (+) and LacZ RNAi-treated control samples (-) served as controls. (G) Brain tissue (Br) or larval hemolymph (Hl) were immunoprecipitated with D-ex1 or D-cy. Western blot analysis reveals a truncated Dscam protein of ~160-kD in hemolymph (lane 4, marked with asterisk) not detected with D-cy (lane 2).

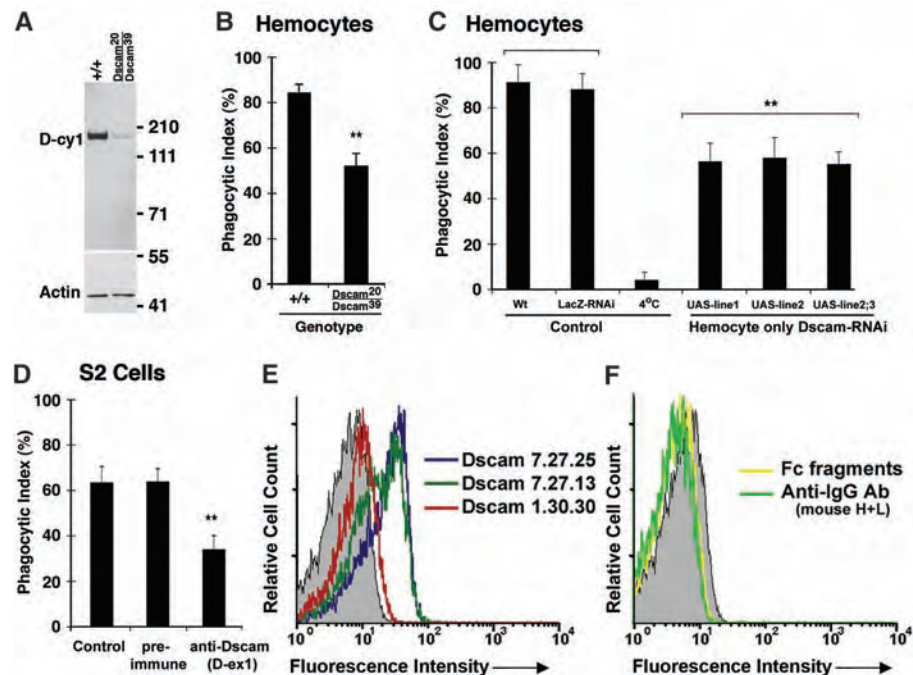


**Fig. 3.** Dscam is required in hemocytes for efficient phagocytosis and binds to *E. coli*. (A) Western blot analysis of larval brain tissue from control (+/+) or Dscam<sup>39</sup>/Dscam<sup>20</sup> larvae reveals strong reduction of Dscam protein concentration. (B) Phagocytosis assays (9) were performed on hemocytes isolated from Dscam<sup>39</sup>/Dscam<sup>20</sup> mutant larvae. Significant reduction (marked by double asterisks) in phagocytosis was found in Dscam-deficient hemocytes but not wild-type (+/+) hemocytes. (C) Assays performed on Dscam-deficient hemocytes (Dscam-RNAi). Hemocytes from three independent UAS lines showed a significant reduction ( $P < 0.01$ ) compared with wild-type (Wt) or ds-LacZ RNA-treated hemocytes (LacZ-RNAi) (9). (D) Treatment of S2 cells with neutralizing antibody to Dscam significantly ( $P < 0.01$ ) decreases phagocytosis. S2 cell treatment with either Schneider media vehicle control (control) or the pre-immune serum (pre-immune) served as controls. Error bars in (B) to (D) indicate SEM. (E and F) Dscam isoforms show binding to *E. coli* bacteria (DH5 $\alpha$  strain). Binding of Fc-tagged recombinant proteins (E) or control antibodies (F) was detected by FACS (9) using Alexa-Fluor (Molecular Probes, Eugene, OR) 488 conjugated to protein A. (E) Dscam-7.27.25 isoform (blue) and Dscam-7.27.13 isoform (green) show binding when compared with the control sample incubated with protein A Alexa-Fluor 488-conjugated only (gray). Dscam-1.30.30 (red) shows no binding above background. (F) Fc peptides (yellow) and an unrelated mouse antibody (Anti-IgG, green) exhibited no binding and were used as negative controls.

hemocytes exhibited highly efficient phagocytosis, and 85 to 90% had taken up bacteria after 10 min (Fig. 3B). In contrast, only 55% of Dscam mutant cells had taken up bacteria (Fig. 3B).

To investigate more directly the possible role of Dscam in immune defenses, we addressed three questions: First, is Dscam cell autonomously required for phagocytosis in hemocytes? Second, can antibodies that specifically bind extracellular Ig domains of Dscam acutely interfere with phagocytosis? Third, can Dscam isoforms directly bind to pathogens?

We used expression of double-stranded RNA [i.e., RNA interference (RNAi)] to suppress Dscam expression in transgenic flies (9) (Fig. 3C). A *hemolymph* promoter region-GAL4 fusion, termed Hml-GAL4, was used for activating expression exclusively in embryonic and larval hemocytes (14, 15). Hemocytes with Dscam-specific knock-down showed a substantially reduced rate of phagocytosis, with less than 60% of the cells containing bacteria (Fig. 3C). This partial inhibition may reflect RNAi-mediated knock-down in only a subset of the highly heterogeneous cell population of larval hemocytes (8, 16). We therefore examined S2 cells, which represent a less heterogeneous cell population also capable of phagocytosis (Fig. 3D), and used antibodies to Dscam to block Dscam function (9). We reasoned that the short application of antibodies against Dscam, in contrast to continuous RNAi, may be less likely to influence general hemocyte characteristics or development (8, 16). Treatment of S2 cells with polyclonal  $\alpha$ -Dscam serum D-ex1 resulted in a 30% decrease in the phagocytic index (Fig. 3D). It is possible that the  $\alpha$ -Dscam antibody

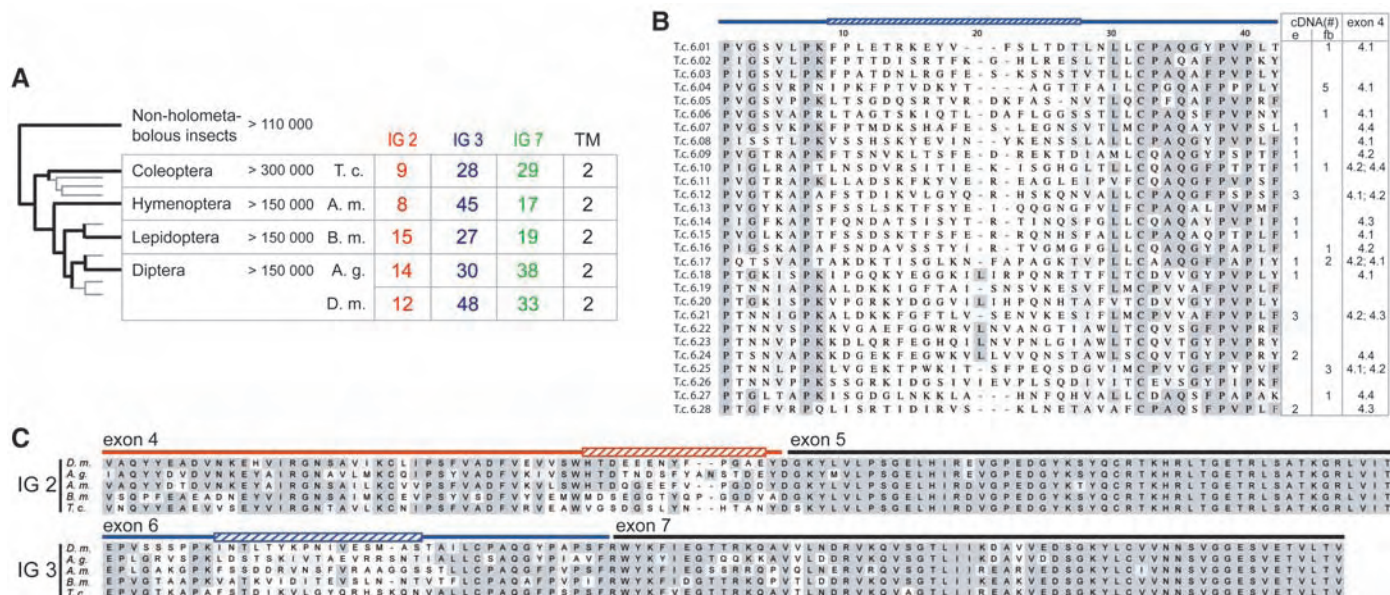


**Fig. 4.** Conservation of Dscam diversity in insects. (A) Simplified phylogenetic tree indicating estimated number of species. Orders with less than 7000 species are indicated by gray lines (18). Alternative splicing is present in all holometabolous insect orders. Abbreviations are as follows: *T. castaneum*, T.c.; *Apis mellifera*, A.m.; *Bombyx mori*, B.m.; *Anopheles gambiae*, A.g.; and *D. melanogaster*, D.m. Table lists number of exons identified. (B) Alignment (25) of Ig3 sequences (N-terminal half) of *Tribolium*. Twenty-eight alternative exons are predicted to encode Ig3 sequences or verified by RT-PCR from embryonic (e) or fat body (fb) tissues (9). Numbers of cDNAs are listed on right side. Gray shading indicates conserved amino acids. (C) Sequence alignment of the Ig domains 2 and 3 of *D. melanogaster*, *Anopheles gambiae*, *B. mori*, *Apis mellifera*, and *T. castaneum*. Despite the

large evolutionary distances, C-terminal halves of Ig2 and Ig3 are nearly identical. A highly conserved Ig-domain scaffold embeds alternatively spliced sequences, which are species-specific and show little conservation. Variable N-terminal half of Ig2 and Ig3 reveal distinct high variability regions (hatched rectangles). Location of variability hot spots is conserved across species. Note that the locations of sequence variability in Dscam Ig domains is distinctly different from variability in complementary determining regions of V-type Ig domains of mammalian immune receptors. Ig2 domains are most variable at the end of exon 4, likely to correspond to the C' strand of the Ig-fold. Ig3 domains are most variable at the middle of exon 6, possibly corresponding to the A and A' strands, similar to *Amphioxus* VCBP sequence variability (20).

may not directly block Dscam-bacteria interactions or may have additional indirect influences on the process of phagocytosis. However, the reduction of phagocytosis is consistent with the loss-of-function in vivo analysis (Fig. 3, B and C) and in vitro binding studies presented below. Taken together, partial but significant reduction in phagocytosis could be achieved by genetic inhibition of expression in hemocytes and by blocking Dscam protein interactions.

We next tested by flow cytometry whether different Dscam isoforms are capable of binding directly to bacteria. Validity of a standard binding assay was tested by using a polyclonal antibody that specifically recognizes *E. coli* epitopes (fig. S6) (9), and the same assay was used to test binding of different recombinant Dscam isoforms (Fig. 3, E and F, and fig. S6). All isoforms contained C-terminal Fc tags (9), which were used for detection with fluorescently labeled protein A (9). Isoforms are designated by the combination of alternative variable Ig domains (9). Dscam-1.30.30-Fc and Dscam-7.27.25-Fc contain all of the extracellular domains, whereas Dscam-7.27.13-Fc contains only the N-terminal 9 Ig plus the first FNIII domain. We found that Dscam-7.27.25-Fc and Dscam-7.27.13-Fc could bind to live DH5α *E. coli* bacteria (Fig. 3E and fig. S6). Binding of Dscam-7.27.13-Fc to *E. coli*

(Fig. 3E) suggests that the 10 N-terminal domains containing all three variable Ig domains are sufficient for binding. In contrast, binding of isoform Dscam-1.30.30-Fc to *E. coli* is barely detectable (Fig. 3E and fig. S6) and therefore similar to Fc peptides alone or control Ig domains containing antibodies to heavy chain (mouse) (Fig. 3F). It is possible that lack of binding of Dscam-1.30.30-Fc is unique to just this isoform and may not generally reflect the presence of distinct pools of binding and nonbinding isoforms. Therefore, it remains an important task to examine in future studies binding properties of other isoforms. Importantly, the molecular basis of Dscam binding to bacteria is presently unknown, and an assessment of binding specificity will crucially depend on the identification of potentially distinct epitopes on bacteria.

Although we do not know the detailed molecular basis of Dscam function in immune-competent cells, our results are consistent with the possibility that Dscam acts as a signaling receptor or co-receptor during phagocytosis. In addition, binding of Dscam isoforms to bacteria may reflect the possibility that diverse secreted Dscam isoforms are involved in opsonizing invading pathogens in the hemolymph.

Comparative genomic analysis of Dscam-like sequences show high conservation of

orthologous Dscam genes in Diptera and Hymenoptera orders (17). To explore Dscam expression and alternative splicing in other insect orders, we examined Dscam gene structure and expression in the flour beetle *Tribolium castaneum* (Coleoptera) and the silk moth *Bombyx mori* (Lepidoptera) (18). Orthologous genes were identified in both species (9), and all Dscam-like domains were found to be highly conserved (Fig. 4 and fig. S7). We confirmed the expression of alternative Dscam isoforms by cloning and characterizing 32 cDNAs from *Tribolium* RNA (*Tr-Dscam*) (Fig. 4B) (9). Alternatively spliced mRNA segments of *Tr-Dscam* matched corresponding Ig2, Ig3, and Ig7 segments of *Drosophila* Dscam (Fig. 4). RT-PCR and sequencing of Dscam mRNA extracted from fat body tissue of *Tribolium* larvae (9) revealed nine different isoform sequences (out of 16 cDNAs) (Fig. 4B). These results suggest that expression of diverse Dscam isoforms in immune-competent fat body cells is conserved among highly diverged insect species.

Our study provides evidence for a potentially extensive repertoire of thousands of Ig-domain-containing proteins in immune-competent cells of insects, which represent an estimated 60% of metazoan species (19). Recently, novel and diverse receptor sequences have been identified in jawless vertebrates

(lamprey), protochordates (*Amphioxus*), and mollusks (freshwater snail) (20–22). It has also been reported that a large class of scavenger receptors (with an estimated 1200 scavenger receptor cysteine-rich domains) are expressed in putative immune effector cells (coelomocytes) of echinoderms (19). Similarly, immune responses of crustaceans apparently use an extensive set of diverse antimicrobial peptides (23). Although most animals have not acquired adaptive immunity, this apparently broad conservation of receptor diversity strongly suggests important functions, and future studies will have to further address whether the presence of diverse immune receptors in invertebrates increases the effectiveness of immune responses of individual animals. Alternatively, given the relative short life span of many invertebrates, it may be that immune receptor diversity is less important ontogenetically but rather enhances the adaptive potential of animal populations to changing environmental and pathogenic threats.

**References and Notes**

1. K. Azumi *et al.*, *Immunogenetics* **55**, 570 (2003).
2. L. Du Pasquier, I. Zucchetti, R. De Santis, *Immunol. Rev.* **198**, 233 (2004).
3. D. Schmucker *et al.*, *Cell* **101**, 671 (2000).

4. P. Tzou, E. De Gregorio, B. Lemaitre, *Curr. Opin. Microbiol.* **5**, 102 (2002).
5. *Innate Immunity*, A. Ezekowitz, J. Hoffmann, Eds. (Humana, Totowa, NJ, 2003).
6. M. Ramet, P. Manfruelli, A. Pearson, B. Mathey-Prevot, R. A. Ezekowitz, *Nature* **416**, 644 (2002).
7. M. Meister, B. Lemaitre, J. A. Hoffmann, *Bioessays* **19**, 1019 (1997).
8. M. Meister, *Curr. Opin. Immunol.* **16**, 10 (2004).
9. See supporting materials and methods on Science Online.
10. C. Samakovlis, D. A. Kimbrell, P. Kylsten, A. Engstrom, D. Hultmark, *EMBO J.* **9**, 2969 (1990).
11. M. Ramet *et al.*, *Immunity* **15**, 1027 (2001).
12. T. Hummel *et al.*, *Neuron* **37**, 221 (2003).
13. X. L. Zhan *et al.*, *Neuron* **43**, 673 (2004).
14. A. Goto *et al.*, *Biochem. J.* **359**, 99 (2001).
15. H. Agaisse, U. M. Petersen, M. Boutros, B. Mathey-Prevot, N. Perrimon, *Dev. Cell* **5**, 441 (2003).
16. A. Holz, B. Bossinger, T. Strasser, W. Janning, R. Klapper, *Development* **130**, 4955 (2003).
17. B. R. Graveley *et al.*, *RNA* **10**, 1499 (2004).
18. *Introduction to Insect Biology and Diversity*, H. V. Daly, J. T. Doyen, A. H. Purcell III, Eds. (Oxford Univ. Press, New York, 1998).
19. Z. Pancer, *Proc. Natl. Acad. Sci. U.S.A.* **97**, 13156 (2000).
20. J. P. Cannon, R. N. Haire, N. Schnitker, M. G. Mueller, G. W. Litman, *Curr. Biol.* **14**, R465 (2004).
21. Z. Pancer *et al.*, *Nature* **430**, 174 (2004).
22. S. M. Zhang, C. M. Adema, T. B. Kepler, E. S. Loker, *Science* **305**, 251 (2004).
23. B. J. Cuthbertson, E. F. Shepard, R. W. Chapman, P. S. Gross, *Immunogenetics* **54**, 442 (2002).
24. G. Neves, J. Zucker, M. Daly, A. Chess, *Nat. Genet.* **36**, 240 (2004).
25. Single-letter abbreviations for the amino acid resi-

dues are as follows: A, Ala; C, Cys; D, Asp; E, Glu; F, Phe; G, Gly; H, His; I, Ile; K, Lys; L, Leu; M, Met; N, Asn; P, Pro; Q, Gln; R, Arg; S, Ser; T, Thr; V, Val; W, Trp; and Y, Tyr.

26. We thank S. Sinenko and B. Mathey-Prevot for Hml-GAL4 flies and important advice; H. Agaisse and N. Perrimon for S2 cells, UAS-dslacZ flies, and insightful discussions; S. Brown, Kansas State University, for embryonic RNA from *Tribolium*; and S. Lewis, Tufts University, for *Tribolium* animals; members of Dana-Farber Core Facility and the Mass-Spec Facility at Harvard Medical School (Boston, MA) for the help during LC-MS/MS analysis; W. Wojtowicz, J. Clemens, and L. Zipursky for kindly providing the Dscam-Fc expression constructs; E. Tanner, A. Wakabayashi, and M. Sackal for excellent technical assistance; and C. Weitz, C. Stiles, N. Perrimon, H. Agaisse, B. Mathey-Prevot, J. Green, Q. Ma, and B. Chen for critical reading of the manuscript. This research was supported by a Medical Foundation Award (D.S.), a Pew Scholars Program Award (D.S.), and a John Merck Fund Award (D.S.). Work on the Dscam expression analysis was supported by NIH grant 1R01-NS46747-01 (D.S.). Sequences have been deposited at GenBank (accession number DQ157471).

**Supporting Online Material**

www.sciencemag.org/cgi/content/full/1116887/DC1  
 Materials and Methods  
 Figs. S1 to S7  
 Tables S1 and S2  
 References and Notes

4 July 2005; accepted 8 August 2005  
 Published online 18 August 2005;  
 10.1126/science.1116887  
 Include this information when citing this paper.

# Science sets the pace

online manuscript submission

**MANUSCRIPTS**

[www.submit2science.org](http://www.submit2science.org)

Science can now receive and review all manuscripts electronically

online letter submission

**LETTERS**

[www.letter2science.org](http://www.letter2science.org)

Have your voice be heard immediately



**speed submission**

## Discovery Workstation

The CodeQuest discovery workstation now offers the almaKnowl-edgeServer (AKS) text mining system as an add-on module. This integration combines visual bioinformatics pipeline development, computational processing, and intuitive scientific literature mining. CodeQuest with AKS enables rapid exploration of the relationships between gene and protein sequences, published literature, disease pathways, and target compounds.

**Active Motif** For information 760-431-1263 [www.activemotif.com](http://www.activemotif.com)

## Cellular Function Assays

Scientists in drug discovery and oncology research have four new options for assessing cellular function, including mitochondrial membrane potential, cellular proliferation, and activation of caspase 3/7 or 8 enzymes. Designed for the Guava EasyCyte benchtop microcytometry system, the four new assays expand Guava's suite of assays for assessing cellular function in cancer-related areas of research and will have important applications in other areas as well.

**Guava Technologies** For information 510-576-1427  
[www.guavatechnologies.com](http://www.guavatechnologies.com)

## Wet Sample Microscope Capsules

Quantomix QX Capsules completely isolate wet samples from the vacuum in a microscope chamber. These capsules offer direct imaging of wet samples; compositional analysis of wet samples by X-ray analysis; ability to image unstained or unfixed cells and tissues; imaging of both adherent and non-adherent cells; high-resolution histopathology; imaging of the entire cell surface; excellent preservation and imaging of lipid structures; and easy-to-automate sample processing and imaging.

**Electron Microscopy Sciences** For information 215-412-8400  
[www.emsdiasum.com](http://www.emsdiasum.com)

## Digital Fluorescence Microscopy

The Axio Imager is an innovative, modular microscope platform for fluorescence microscopy. The new system enables users to meet the increasing challenges in the life sciences, from high-end routine to research applications, from widefield imaging to confocal microscopy. New Infinity Contrast and Color-corrected System optics guarantee image quality and maximum contrast in all techniques, while ensuring optimum transmission, contrast, and working distance. The optimized differential interference contrast provides high-contrast, homogeneous illumination. Brilliant darkfield from 2.5x to 100x oil (ultra-darkfield) can be combined with brightfield in one condenser. The apochromatic fluorescence beam path is designed for optimum color correction over the entire wavelength range. Fluorescence filters with an improved signal-to-noise ratio are available, reducing exposure times by up to 50% thanks to their excitation intensity, which can be up to 70% higher than normal. Higher contrast is achieved by active stray light minimization. Fast, motorized reflector turrets, for either six or ten filter modules, enable high-speed fluorescence examinations.

**Zeiss** For information 800-233-2343 [www.zeiss.com/micro](http://www.zeiss.com/micro)

## Genetic Analysis System

The GenomeLab GeXP Genetic Analysis System provides high-throughput, quantitative gene expression via scalable, multiplexed polymerase chain reaction (PCR). The system's patented priming strategy overcomes the biases that limit standard multiplexed PCR analysis to just a few genes at a time. GenomeLab GeXP delivers more genes per reaction and more samples per run, removing bottlenecks in gene expression studies for drug discovery and developmental research. The system can run two

96-well plates in 24 hours, and cost effectively look at the expression of 20 to 35 genes in a single reaction per well. Suitable for applications working with smaller gene sets that can provide key information relating to biological state or response, GenomeLab GeXP operates at a fraction of the cost of a standard reverse transcription-PCR system. The system delivers accurate quantitative results for hundreds or even thousands of samples using very small amounts of total RNA. It is designed to provide an alternative to expensive, low-throughput real-time PCR.

Beckman Coulter For information 800-742-2345 [www.beckmancoulter.com](http://www.beckmancoulter.com)



Beckman Coulter For information 800-742-2345 [www.beckmancoulter.com](http://www.beckmancoulter.com)

## Bubble Trap

The redesigned, inert Bubble Trap attaches to laboratory tubing to provide an effective, time-saving, and cost-efficient method for removing air bubbles that often interfere with the flow system and produce errors or cause columns to run dry. The fully mechanical Bubble Trap requires no physical interaction to operate and requires only a quick and easy membrane replacement, making it suitable for use in flow analysis systems, as a guard in liquid chromatography, for enzyme reactors, and for flow-through biosensors.

**Bio-Chem Valve and Omnifit** For information 973-263-3001 [www.bio-chemvalve.com](http://www.bio-chemvalve.com)

## Literature

*Pierce Applications Handbook and Catalog* is a 576-page compendium with technical information on protein-related products. It is divided into application-specific sections, each of which contains a comprehensive technical section followed by product information. Sections include protein/gene expression, protein purification, protein detection, protein structure, protein function, protein interactions, antibody production and purification, and gas chromatography and other reagents.

**Pierce** For information 800-874-3723 [www.piercenet.com](http://www.piercenet.com)

Newly offered instrumentation, apparatus, and laboratory materials of interest to researchers in all disciplines in academic, industrial, and government organizations are featured in this space. Emphasis is given to purpose, chief characteristics, and availability of products and materials. Endorsement by *Science* or AAAS of any products or materials mentioned is not implied. Additional information may be obtained from the manufacturer or supplier by visiting [www.science.labvelocity.com](http://www.science.labvelocity.com) on the Web, where you can request that the information be sent to you by e-mail, fax, mail, or telephone.

For more information visit **GetInfo**,  
Science's new online product index at  
<http://science.labvelocity.com>

From the pages of GetInfo, you can:

- Quickly find and request free information on products and services found in the pages of *Science*.
- Ask vendors to contact you with more information.
- Link directly to vendors' Web sites.